Particle physics and Cosmology beyond the Standard Model : Inflation, Dark Matter and Flavour

Lucien Heurtier

École Polytechnique - Université Paris-Saclay

Thèse de Doctorat

Spécialité : *Physique Théorique*

Particle physics and Cosmology beyond the Standard Model :

Inflation, Dark Matter and Flavour

Thèse présentée par

Lucien Heurtier

pour obtenir le grade de

Docteur de l'École Polytechnique

Soutenue le 24 juin 2015 devant le jury composé de :

Pierre Binétruy	Examinateur
Emilian Dudas	Directeur de Thèse
Arthur Hebecker	Rapporteur
Stéphane Lavignac	Examinateur
Michel Tytgat	Rapporteur
Fabio Zwirner	Examinateur

Abstract

This thesis has been focusing on beyond the Standard Model aspects of particle physics and their implication in cosmology. From the early times of the universe evolution, to current low energy supersymmetry and colliders phenomenology, various works have been achieved using mostly an effective, low energy formulation, at several different periods of the Universe History.

Namely, models of Inflation are presented as effective single field theories arising from supergravity, string inspired UV completion models. Furthermore, models of dark matter including a mediator particle are studied with the use of effective higher dimensional operators that are generated explicitly from microscopic underlying theories. Such models were able to produce interesting results for explaining recent measurements on the X-rays spectrum of galaxy clusters. Finally, the study of flavour changing processes in the Dirac gaugino supersymmetric extensions of the Standard Model was explored in details, predicting some challenging signatures that are to be searched for at the next run of the LHC.

Résumé

Cette thèse se concentre sur l'étude des aspects de la physique au delà du modèle standard et de ses applications à la cosmologie. Depuis les temps reculés de l'évolution de l'Univers, jusqu'à la supersymétrie de basse énergie et à la phénoménologie des accélerateurs, des travaux variés ont été réalisés utilisant pour la majeure partie une formulation de basse énergie, et ce à des stades différents de l'Histoire de l'Univers.

En effet, des modèles d'inflation sont présentés sous l'angle de théories effectives (à un champs) provenant de théories de hautes énergies issues de la supergravité et de la théorie des cordes. De plus, des modèles de matière noire incluant la présence d'une particule médiatrice sont étudiés à l'aide d'opérateurs effectifs de dimensions supérieures, générés explicitement à partir d'une théorie microscopique sous jacente. De tels modèles semblent pour expliquer de récentes mesures du spectre de rayons X mesuré dans certains cluster de galaxies. Enfin l'étude des changements de saveurs dans l'extension super-symétrique incluant des jauginos de Dirac du modèle standard prédit des signatures expérimentales qui seront très probablement recherchées lors des prochaines acquisitions du LHC.

Dédicace

À mon père, qui m'a depuis toujours donné attention et respect, ainsi que l'amour et la force d'apprendre, de découvrir, de questionner et à qui je dédie ce travail.

À Stéphanie et à mes frères et sœur, qui ont été à mes côtés tout au long de mes études et dont l'affection et le respect ont également largement contribué à l'aboutissement de ce doctorat.

À mes amis, qui se reconnaîtront sans hésiter, qui ont contribué sans aucun doute à mon dynamisme et ma bonne humeur durant toutes ces années.

À Mathieu Chamaillard et aux nombreuses discussions d'ordre scientifique, philosophique et politique que nous avons eues et qui n'ont cessé de stimuler mon esprit.

À mes collègues et amis Valentina Pozzoli, Valentin Verschinin et Jakob Gath, qui m'ont soutenu dans le quotidien.

À Jérôme Perez, Iosif Bena, Marco Caldarelli, Marc Simon et Ronald Mac Carroll, qui m'ont, au long de mon parcours porté intérêt et soutien et qui m'ont fait découvrir de la meilleure manière possible, la physique fondamentale et théorique.

À mes différents collaborateurs, pour leur patience et le respect avec lequel ils m'ont traité et bien sûr pour tout ce qu'ils m'ont apporté au travers de nos travaux communs.

À Yann Mambrini qui m'a, tout au long du doctorat, sollicité avec respect comme collaborateur et soutenu comme il l'aurait fait avec son propre étudiant.

Enfin, à Emilian Dudas qui m'a toujours montré, en tant que professeur puis directeur de thèse, à la fois disponibilité, pédagogie, respect, intérêt et sympathie tout en m'entraînant perpétuellement sur des thématiques variées et à qui je dois pour majeure partie le bagage de physique des particules qui m'accompagnera dans mes recherches à venir.

Contents

1 Introduction

Cosmology has been, across History, one of the most appealing subject of thought and research for humanity. Inspiring from the oldest ages many mythological scenarios, involving divinities under various forms, it finally led the philosophers of Antiquity to interpret it through induction and scientific investigations. Indeed, coming back to 400 B.C., the Greek civilization began to propose scientific models for explaining the movement of celestial bodies. Eudoxe ($\sim$ 400 B.C.), followed by Aristotle ($\sim$ 350 B.C.), built some fascinating models of homocentric rotating spherical trajectories of stars, reproducing fancy trajectory shapes by pure scientific arguments. Of course, the arguments and building blocks of the different theories remained naive (spherical trajectories, placing the earth at the center of the universe, ...), but for the first time of the History, Science was putting religion aside, to try to explain our Universe evolution. These first attempts got more and more evolved with time, Aristarchus ($\sim$ 250 B.C.) suggested to build an heliocentric model, Eratosthenes ($\sim$ 200 B.C.) and Hipparchus ($\sim$ 150 B.C.) released amazing celestial measurements and catalogs of stars and Ptolemy ($\sim$ 150 AD) proposed more complex trajectory structures. The quest for understanding the cosmos behavior continued after the end of the Antic period and the destruction of the library of Alexandria, with the arising of the Arabic scientific community. In A.D. 800, Haroun Al Rashid ordered the building of a *house of astronomy* in Bagdad and his grand son Al Ma'mun continued promoting the research works released there by attracting famous translators, major ancient textbooks, space observers, rehearsing up to its ancient glorious status the science of astronomy. Many different techniques were developed for mapping up the sky, building celestial calendars and the science of astronomy were pursued until the european Renaissance and the XVIth century when Copernic ($\sim$ 1550), Galileo Galilei ($\sim$ 1610) and Giordano Bruno ($\sim$ 1600) re-affirmed the idea of heliocentrism. The advent of the Newtonian description of gravitational laws (1687, *Philosophiæ Naturalis Principia Mathematica*) states the beginning of the mathematization of cosmology and astronomy. The inductive feature of astronomy hence turns into an incredible power of prediction. Neptune was thus discovered after the predictions of Le Verrier in 1846. The discovery of General Relativity by Einstein (1915), reinforced this huge power of mathematics in modeling the Universe dynamics. The twentieth century saw many fascinating observational measurement arise that, on one hand confirmed on many aspects – Perihelion precession of Mercury, deflection of light, gravitational redshift, ... – the validity of General Relativity and on the other hand showed many unexplained behavior of the universe dynamics – rotation curves of the galaxies, accelerated expansion, inhomogeneities of the CMB spectrum,... – that remain to be fully explained by the cosmological theories.

As an inextricable piece of the cosmological puzzle that the scientific community aims to unscramble, particle physics represents a key point of the understanding of the Universe evolution. Indeed the particle content of the latter, thanks to Einstein's theory of gravitation, is intimately related to its geometrical shape and dynamics. Thus our learning about particle physics can have strong implications with respect to our Universe behavior. Although the Higgs boson has been recently discovered at the Large Hadron Collider in Geneva [1, 2] as the keystone

of the Standard Model of particle physics, many aspects of particle physics remain obscure. In particular, the number of free parameters that are present in the Standard Model and the origin of their hierarchical distribution over the parameter space stand as open questions for the scientific community. The requirement from cosmological observations for the presence of obscure forms of matter and energy is also something which is still not contained in such a theory. More generally, in a will to unify the presence of four peculiarly different forces in a single theory, the standard model turns out to be far incomplete and should be embedded in a more fundamental theory such as String Theory.

In the Big Bang theory of cosmology, that we will review in the first part of this work, the History of our Universe evolution constitutes a gigantic laboratory for testing particle physics theories on highly different energy scales. Indeed one can observe today, with an impressive accuracy that our universe is in a permanent state of expansion. Its matter content hence turns out to be more and more diluted in the increasing vacuum of our cosmos, which sees its global temperature dramatically decrease with time. Looking further and further in space – meaning watching stars, constellations, galaxies, clusters of galaxies at more and more ancient times in the Universe evolution timeline – thus provides us more and more informations on the Universe dynamics at a period where the latter was incredibly more hot and energetic than it is today. We aim in this thesis to plunge back at the most early times that the Big Bang theory can imagine and attempt to describe the particle content of our spacetime at different periods and energy scales, following the expanding evolution of our Universe.

At the very first moment of the Universe evolution, after the presupposed Big Bang, it is commonly admitted that, due to a huge energy density the light was interacting all the time and not able to propagate, like it would be during a very foggy day : The Universe was at a point where it was completely dark. Hence the information one can get about this period while simply looking at the sky is very much reduced. However, the observation of the first flash of light happening at a point of the universe expansion where light had finally enough freedom to propagate – called the Cosmic Microwave Background (CMB) and measured today with high accuracy – provides us a precious piece of information concerning the dynamics of our spacetime. At this point, the standard theories of both Big Bang and particle physics combined together fails to explain the structure of the CMB measurement and requires additional ingredients to explain the quasi homogeneity of the Universe, on scales that are not supposed to have ever been able to communicate with each other. Inflation is one of the most appealing answer to such a puzzle, and requires usually the addition of a new heavy particle to the standard model, provoking an acceleration of the universe expansion at its very early stages. This new particle – called the *inflaton* – is supposed to fill the whole universe, driving the dynamics of its expansion, before producing after a while the standard particles that our world is made of today.

Yet the particle physics model that we have at our disposal to describe nature today – called the *Standard Model* (SM) of particle physics – remains, as we mentioned above, incomplete. Formal descriptions have been proposed in the past decades to include the Standard Model into larger theories which could contain additional components of undiscovered matter – in particular dark matter, but equally other possibly existing forms of matter – that are for instance String Theory, Supersymmetry, or simpler extensions of the Standard Model itself. Enlarging the initial Standard Model is usually achieved by adding to our description of physics extra symmetries that would not be visible at the low energy scale of our present world. Supersymmetry predicts for instance the existence of many new particles – called superpartners – that remain to be observed in the collider experiments. Saying that these additional degrees of free-

dom are unobserved today – which is equivalent to say that additional symmetries should be broken at low energies – tells us that enlarging the existing models should in addition contain a mechanism to explain why such extension is not visible at low energies.

In the first part of this thesis, after reviewing the theoretical and phenomenological aspects of both the Big Bang theory and the theory of Inflation we will study in detail how describing Inflation in a high energy supersymmetric theory while explicitly providing the model a mechanism of supersymmetry breaking can be difficult to handle. We will in particular see on one hand how phenomenological constraints on the inflation observables can translate into constraints on the scale of supersymmetry breaking, and on the other hand how this mechanism can in some situation be required to be the major source of the inflation process.

Another source of puzzle in cosmology comes from the strong discrepancy which exists between the amount of matter that one can estimate by looking at the sky and counting the stars and the amount of matter which is required, according to general relativity, for maintaining the galaxies stable in the Universe. A solution for this puzzle, as it will be properly described in the second part of the thesis is to assume the presence of an obscure form of matter, surrounding our galaxy and maintaining the large structures of the Universe while interacting so weakly with our visible world that it would have been almost completely invisible to any observation device up to now. We here propose to study phenomenological aspects of simple models, extending the present Standard Model with simple abelian symmetries, by assuming the constituent of dark matter would be able to exchange information with the visible sector by the help of a *mediator* particle. We study in particular possible interactions of heavy or light dark matter with respectively the strong and the electroweak sectors of the Standard Model. Our models are strongly constrained of course by experiments. On one hand such interactions must be very weak not to produce too important excesses in accelerators – which would have been already detected in the past experiments – and on the other hand they can be made sufficiently important to be visible in future collider measurements and to explain eventual astrophysical signals that are already observed.

The third part of the this work will be dedicated to a different aspect of beyond Standard Model theories, that is the treatment of the flavour changing processes of particle physics. As a matter of fact, the zoo of fundamental particle constituents of matter is indeed distributed among three different generations of fermions, each generation being assimilated to a particular flavour. Yet flavour appeared to be a feature which is not invariant through the different particle physics processes that one can observe in nature. However the structure of such *flavour oscillation* remains not fully understood, and most of the time treated – in particular in supersymmetric theories – in a rather guileless manner. The Minimal Supersymmetric Standard Model (MSSM), as one of these possible enlargement of the Standard Model, introduces new processes of flavour changing that are highly constrained by experiment, and, contrarily to the standard model not naturally suppressed from the theoretical point of view. Hence we present some works in which we consider the possibility of adding so called *Dirac Gauginos* to the MSSM to render flavour changing weaker in the theory, and propose different flavour patterns that the standard *mass insertion approximation* used in many supersymmetric theories to see how experimental constraints differ depending on the latter pattern choice. We formulate in addition phenomenological signatures that may be visible in future accelerators measurements.

From the formulation of supersymmetry breaking at scales approaching the Planck mass to low energy supersymmetry flavour changing processes, we hence go through the Universe History studying beyond standard model physics at very different scales, relating constantly

the constraints coming from accelerator measurements to theoretical considerations and astrophysical observations about cosmology. A link which is of great importance to maybe better understand, one day, what our Universe is truly constituted of.

Part I

Inflationary Cosmology

2 The theory of Big Bang

2.1 A brief History of the Universe

This thesis aims to sail through the History of the Universe from the Big Bang early time to our present, cold, low energetic Universe. We will present in this section a brief review of how this evolution is sketched in the theory of Big Bang.

Let us first sketch the qualitative picture of the History of our Universe in the Big Bang theory framework. As a general feature and a consequence of the observation that our Universe is expanding around us, the story of the Big Bang starts at an initial time $t = 0$ corresponding to a singular point of infinite energy density (or temperature). Beginning from this obscure starting point, the evolution of the spacetime is, as we will see in more technical details in what follows, characterized by a permanent cooling of the matter thermal bath it contains.

A Short Universe Timeline

- $t \sim 10^{-30} - 10^{-10}$s ($10^{12}$GeV $- T \sim 100$GeV) : Physics beyond the Standard Model is dynamically present at high energy scales before symmetries breaks down to the Standard Model gauge group as energy decreases. The Higgs vacuum expectation value forms and all the Standard Model particles become massive.
- $t \sim 10^{-5}$s ($T \sim 200$MeV) : Quarks get confined into hadrons and baryons.
- $t \sim 0.2$s ($T \sim 1 - 2$MeV) : Neutrinos decouple from the thermal bath. The ratio of densities of protons with respect to neutrons gets frozen.
- $t \sim 1$s ($T \sim 0.5$MeV) : Electrons and positrons begin to annihilate into photons.
- $t \sim 200 - 300$s ($T \sim 0.05$MeV) : Nuclear reactions become efficient giving birth from protons and neutrons to first helium and light atoms.
- $t \sim 10^{11}$s ($T \sim$ eV) : The quantity of matter equals the amount of radiation in the Universe.
- $t \sim 10^{12} - 10^{13}$s ($T \sim 0.1$eV): All electrons and protons combine to form stable atoms. Light has now freedom to propagate on large distances. A flash of light characterizes this period, namely emitting the Cosmic Microwave Background which is detected nowadays.
- $t \sim 10^{16} - 10^{17}$s : The galaxies form, creating the large structures in which we lie today.

2.2 Geometrical Formulation of the Universe Evolution

The astrophysical observations teach us that our Universe is both homogeneous and isotropic on scales larger than 100 Mpc. This can be observed all over the 3000 Mpc that constitutes

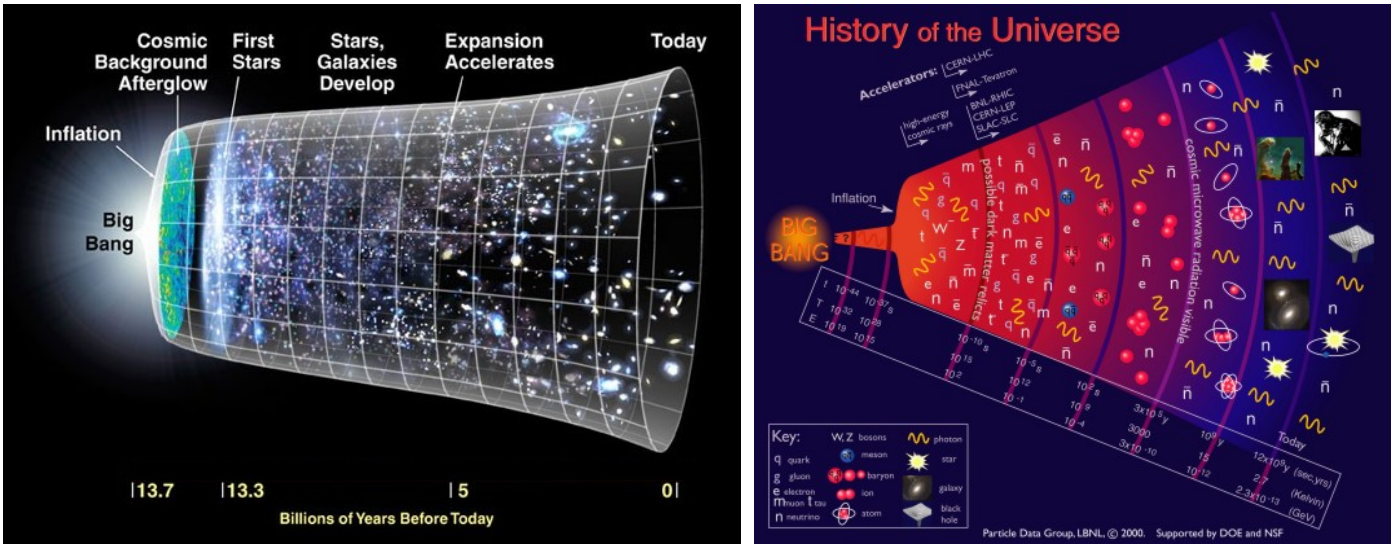

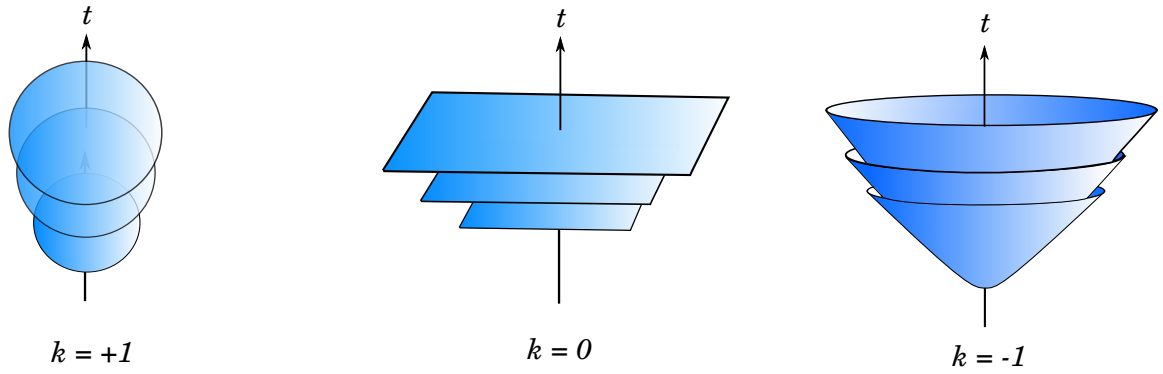

Figure 1: Depending on the curvature k, the spacelike slices of spacetime get spherical, planar or hyperbolic geometry.

our *observable Universe*. Of course this does not guarantee that our spacetime is entirely homogeneous, but it shows at least that our Hubble piece of accessible universe is smooth. Under such –well motivated – postulate, the geometry can be described on this patch by a metric of the form

$$\mathrm{d}s^2 = -\,\mathrm{d}t^2 + a^2(t)\left(\frac{\mathrm{d}r^2}{1-kr^2} + r^2(\,\mathrm{d}\theta^2 + \sin^2\theta\,\mathrm{d}\phi^2)\right)\,, \tag{2.2.1}$$

where $a(t)$ is an expansion factor and $k = -1, 0, +1$ is the spacelike curvature, giving respectively spherical, flat or hyperbolic geometries, as depicted in Fig. 1

It is often convenient to define the *conformal time* τ so that the whole spacetime scales with the expansion factor $a(\tau)$

$$\mathrm{d}s^2 = a^2(\tau)\left(-\,\mathrm{d}\tau^2 + \frac{\mathrm{d}r^2}{1-kr^2} + r^2(\,\mathrm{d}\theta^2 + \sin^2\theta\,\mathrm{d}\phi^2)\right)\,. \tag{2.2.2}$$

The dynamics of such spacetime geometry is well known to be described by the Einstein equations

$$G_{\mu\nu} \equiv R_{\mu\nu} - \frac{1}{2}Rg_{\mu\nu} = 8\pi G T_{\mu\nu} + \Lambda g_{\mu\nu} \tag{2.2.3}$$

where R and $R_{\mu\nu}$ are the curvature scalar and Ricci tensor built from the metric $\mathrm{d}s^2 \equiv g_{\mu\nu}\,\mathrm{d}x^\mu\,\mathrm{d}x^\nu$. The stress energy tensor $T_{\mu\nu}$ is generically assumed to be the one of a perfect fluid, which is of the form

$$T^\mu_\nu = \mathrm{diag}(\rho, -p, -p, -p)\,, \tag{2.2.4}$$

satisfying the equation of state

$$p = \omega\rho\,. \tag{2.2.5}$$

The radiation dominated era is then characterized by $\omega = 1/3$ while the matter dominated era, assimilating the matter content of the Universe to dust corresponds to $\omega = 0$. The case of a cosmological constant can be seen as the effect of a perfect fluid whose equation of state is defined by $\omega = -1$. An important quantity to define for cosmology is the Hubble parameter

$$H \equiv \frac{\dot{a}}{a} \tag{2.2.6}$$

which has unit of inverse time and is negative for collapsing universe but positive for an expanding spacetime, with which one can express the Einstein equations (called Friedmann equations in this particular case)

$$H^2 = \frac{\rho}{3} - \frac{k}{a^2}\,, \tag{2.2.7}$$

and

$$\dot{H} + H^2 = \frac{\ddot{a}}{a} = -\frac{\rho + 3p}{6}\,, \tag{2.2.8}$$

where over dots represent the derivative with respect to the physical time t. One can notice that (2.2.8) implies, in an expanding universe containing ordinary matter, that $\ddot{a} < 0$. Such standard Universe content would then force the expansion to decelerate. Furthermore, equations (2.2.7) and (2.2.8) can be combined to obtain

$$\frac{\mathrm{d}\ln\rho}{\mathrm{d}\ln a} = -3(1+\omega)\,. \tag{2.2.9}$$

Solving this equation and integrating (2.2.7) over time provides

$$a(t) \propto \begin{cases} t^{\frac{2}{3}(1+\omega)} & \text{if } \omega \neq -1\,, \\ e^{Ht} & \text{if } \omega = -1\,. \end{cases} \tag{2.2.10}$$

In the case where the Universe is composed of different kind of particles (baryons, photons, neutrinos, dark matter, dark energy, etc.), the associated pressures and energy densities sum up to give

$$\rho = \sum_i \rho_i \qquad \text{and} \qquad p = \sum_i p_i\,. \tag{2.2.11}$$

The respective contributions to the energy today are usually described by the ratios

$$\Omega_i \equiv \frac{\rho_i^0}{\rho_c}\,, \tag{2.2.12}$$

where $\rho_c = 3H_0^2 M_p^2$. Staring for a few seconds at equation (2.2.7), one can interpret the curvature term as a contribution to the energy density with ratio

$$\Omega_k = -\frac{k}{a_0^2 H_0^2}\,, \tag{2.2.13}$$

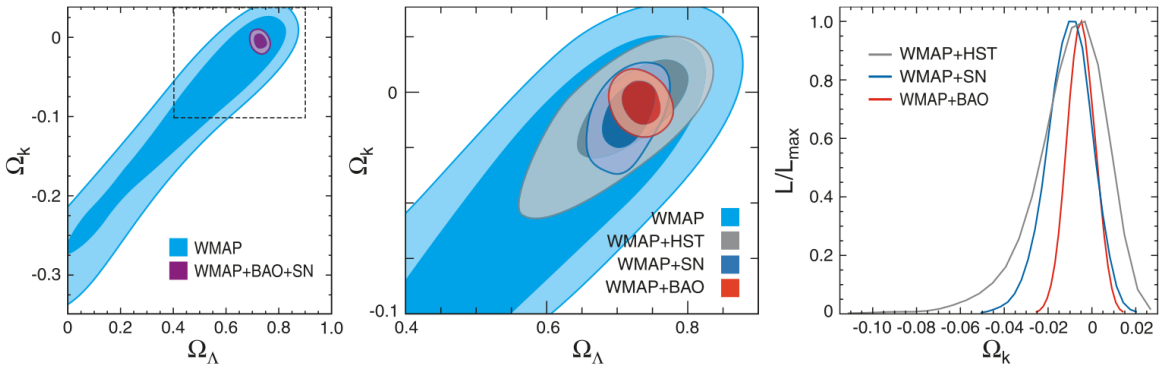

Figure 2: Combination of the CMB and LSS observations shows that the spatial geometry of the universe is essentially flat [3].

so that

$$\sum_i \Omega_i + \Omega_k = 1\,. \tag{2.2.14}$$

The second Friedmann equation, setting $a(t_0) = 1$, can the be written

$$\frac{1}{a_0 H_0^2}\frac{\mathrm{d}^2 a}{\mathrm{d}t^2} = -\frac{1}{2}\sum_i \Omega_i(1+3\omega_i)\,. \tag{2.2.15}$$

Experimental Data Such model has been tested by observations with great precision, and many precise data have been furnished concerning the ratios Ω_i and Ω_k. The WMAP collaboration reported [3] for instance (see Fig. 2) that the contribution of curvature is almost exactly vanishing

$$\Omega_k \sim 0\,, \tag{2.2.16}$$

whereas it is composed of 4% baryons ("b"), 23% dark matter ("DM") and 73% dark energy (Λ) (see Fig. 3 and Fig. 4):

$$\Omega_{DM} \sim 0.23\,, \quad \Omega_b \sim 0.04\,, \quad \Omega_\Lambda \sim 0.72\,, \tag{2.2.17}$$

with $\omega_\Lambda \approx -1$

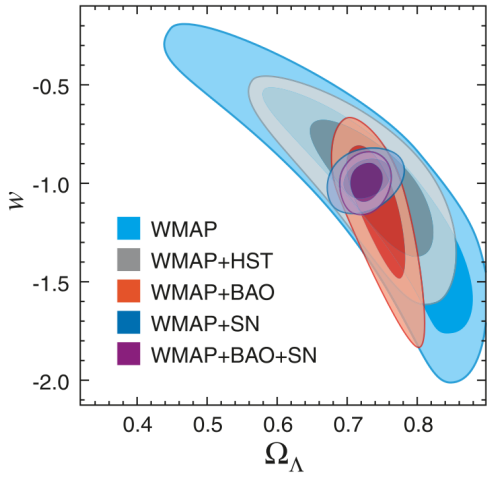

Figure 3: The energy contribution of dark energy is shown to be very close to the one of a cosmological constant with $\omega_\Lambda \approx -1$ [3].

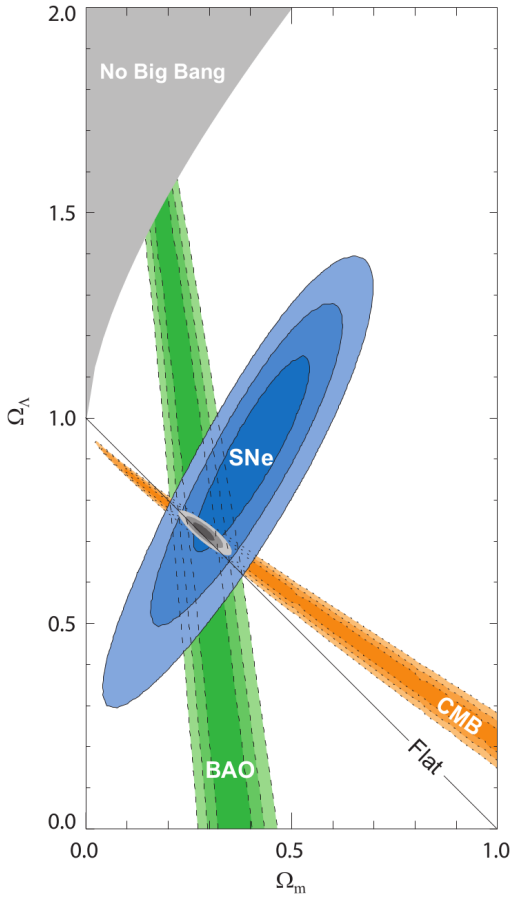

Figure 4: Contributions of dark energy and matter, measured from the Supernova Cosmology Project [4].

3 Inflation

3.1 Horizon and Flatness problems

As we saw in the previous chapter, the Big Bang theory aims to extrapolate, running back in time, what happened at early stages of the universe evolution. In particular, one can estimate to which extent certain regions of the sky were, closer to initial time, causally connected or not. In this picture, the number of causally disconnected patches contained in the region from which the CMB that we measure today was emitted is of order 10^4. This would mean that two different points in the CMB map whose respective distance to each other would exceed two degrees would never have been in causal contact since the Big Bang initial time. However such regions are observed to have extremely similar temperatures although they could not have communicated at all from the very beginning of the Universe History. This problem is called the *Horizon problem* and was first mentioned by Misner in 1969 [5] where, noticing that point, he was proposing alternative proposals of geometries, such as the (type- I) Kasner [6] Universe or the Bianchi type-IX [7] Universe. In such chaotic and so-called *Mixmaster Universe*, the expansion factor a is added two form factors that can make the universe either contract or expand during certain periods of time and possibly explain the dissolution of anisotropies of the CMB. The beauty of the Inflation theory yet led later on the community not to study too seriously this hypothesis. To illustrate this puzzle in detail, let us write again the Friedman-Lemaître-Robertson-Walker flat metric

$$\mathrm{d}s^2 \;=\; -\mathrm{d}t^2 + a^2(t)\left[\mathrm{d}r^2 + r^2\mathrm{d}\Omega^2\right] . \tag{3.1.1}$$

The form of the latter geometry tells us that the spatial size of the universe between planckian time t_i and present time t_0 scales like a_i/a_0 compared to time. As a consequence, one causal patch at the present time, whose size is given by

$$l_0^c \sim ct_0 \sim 10^{28}\,\mathrm{cm} \tag{3.1.2}$$

turns out to contain a volume of the spacetime, which, at planckian time t_i, had a size of

$$l_i \sim l_0 \frac{a_i}{a_0} . \tag{3.1.3}$$

However, the size of a causal region at that early time was

$$l_i^c \sim ct_i , \tag{3.1.4}$$

and one can estimate the ratio between these two quantities to be

$$\frac{l_i}{l_i^c} \sim \frac{t_0}{t_i}\frac{a_i}{a_0} \sim \frac{10^{17}}{10^{-43}} 10^{-32} \sim 10^{28} . \tag{3.1.5}$$

In other words, the volume of spacetime corresponding to one, possibly observable, causal patch today, would roughly correspond to $(l_i/l_i^c)^3 \sim 10^{84}$ causally disconnected patches at the planckian time. Yet, the fluctuations of the CMB spectrum temperature is of order

$$\frac{\delta\epsilon}{\epsilon} \sim 10^{-4}\,, \tag{3.1.6}$$

which would required a huge fine tuning at initial time to be released in our Universe. This can be reformulated, using a very useful quantity of cosmology, that is the *co-moving Hubble radius*. Indeed, the radial propagation of light is described by the metric

$$\mathrm{d}s^2 = a^2(\tau)(-\,\mathrm{d}\tau^2 + \,\mathrm{d}r^2) \tag{3.1.7}$$

with τ being the conformal time, and the null geodesics are described by the equations

$$r = \pm\tau + \text{Const.}\,. \tag{3.1.8}$$

The maximal distance through which light can propagate during a certain amount of time turns out to be

$$\Delta r = \Delta\tau = \int_{t_i}^{t} \frac{dt'}{a(t')}\,. \tag{3.1.9}$$

Taking $t_i = 0$ to be the starting point of the Big Bang, one can define the so called *co-moving particle horizon* (the maximal distance any particle can ever have gone, or exchanged information through)

$$r_p(t) = \int_0^t \frac{dt'}{a(t')} = \int_{a=0}^{a(t)} (aH)^{-1}\,\mathrm{d}\ln a\,, \tag{3.1.10}$$

and the *co-moving Hubble radius* (the radius over which one cannot communicate at a given time) to be

$$r_H = (aH)^{-1}\,. \tag{3.1.11}$$

Note that we are here working in units of $\ln a$, also called *e-folds* in what follows. The size of a causal region hence depends directly on the evolution of the co-moving Hubble radius. The latter can be expressed in the standard case of a perfect fluid where $p = \omega\rho$

$$r_H \propto a^{\frac{1}{2}(1+3\omega)}\,, \tag{3.1.12}$$

which, for both radiation ($\omega = 1/3$) and dust ($\omega = 0$) gives an increasing function of time. The horizon problem is represented in Fig. 1 where the CMB map is shown to contain points that were causally disconnected at the initial time.

The *flatness problem* is another puzzle of the Big Bang theory that was first described by Robert Dicke in 1969 in a lecture, according to Guth. Let us write the Friedmann equations in the case of a curved spacetime

$$H^2 = \frac{\rho}{3M_P^2} - \frac{k}{a^2}\,, \tag{3.1.13}$$

where k is the curvature of the spacelike foliation. One immediately gets by dividing both sides by the Hubble parameter that

$$1 - \Omega(a) = -\frac{k}{(aH)^2}\,, \tag{3.1.14}$$

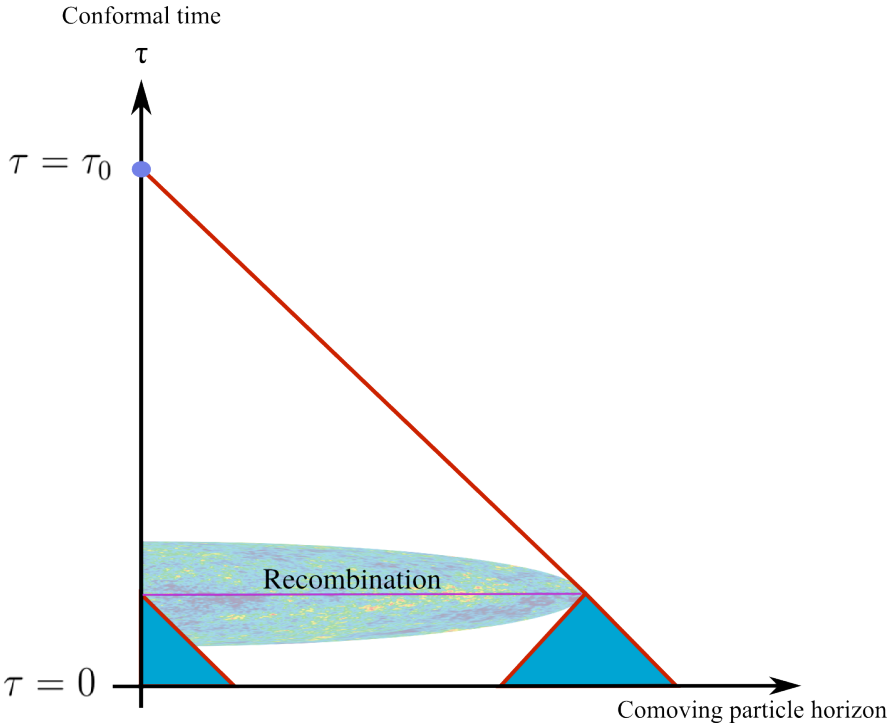

Figure 1: Evolution of the particle horizon with conformal time. The intersection between the conformal time of recombination and the past timelike cone of our present point is in the future light cone of several disconnected patches at initial time.

where

$$\Omega(a) \equiv \frac{\rho(a)}{\rho_c} \quad \text{and} \quad \rho_c = 3H^2 M_P^2 \,. \tag{3.1.15}$$

Equation (3.1.14) hence suggests that if the curvature of space is non vanishing at some early time of the Universe History, and if $(aH)^{-1}$ keeps growing with time, thus the quantity $|1-\Omega(a)|$ should explode with time. However the latter is strongly constrained by experiment and we observe that today

$$|1-\Omega(a_0)| \lesssim 0.01 \,. \tag{3.1.16}$$

Such constraint hence turns out to be even more stringent while running back in time and one should have, at the energies of baryogenesis, Grand Unification and Planck mass, the following constraints

$$\begin{aligned} |1-\Omega(a_{BBN})| &\lesssim \mathcal{O}\left(10^{-16}\right) , \\ |1-\Omega(a_{GUT})| &\lesssim \mathcal{O}\left(10^{-55}\right) , \\ |1-\Omega(a_P)| &\lesssim \mathcal{O}\left(10^{-61}\right) , \end{aligned} \tag{3.1.17}$$

which would require an enormous fine tuning at initial time to satisfy the experimental constraints we obtain nowadays... The flatness problem can also be formulated in terms of fine tuning required between kinetic and potential energy in our Universe (which defines local curvature of the spacetime) not to get the universe collapse nor expand too fast compared to what we measure today. In this sense, the flatness problem can be seen as a required fine tuning of the initial velocities that characterize the Cauchy problem that is the expansion of our Universe.

As a conclusion of this section, the main source of puzzle that arises from the homogeneity and flatness of the Universe stand mainly in the fact that with a standard matter content, the co-moving Hubble radius $(aH)^{-1}$ increases with time. We will see in the next section how Inflation is an elegant solution to circumvent this problem.

3.2 Inflation : General idea

As mentioned above, a possibility to escape the puzzles that are the horizon and flatness problems is to introduce in the Universe History a period of time where the co-moving Hubble radius shrinks, instead of growing.

$$\frac{\mathrm{d}}{\mathrm{d}t}(aH)^{-1} < 0\,. \tag{3.2.1}$$

Such requirement is equivalent to ask, in the case of a perfect fluid content (3.1.12), that the *Strong Energy Condition* is violated during a period called Inflation

$$1 + 3\omega < 0\,, \tag{3.2.2}$$

or equivalently, that the expansion is accelerated

$$\ddot{a} > 0\,. \tag{3.2.3}$$

In this case the conformal time would scale like

$$\tau \propto \frac{2}{1+3\omega} a^{\frac{1}{2}(1+3\omega)}\,, \tag{3.2.4}$$

and be sent to highly negative values while a would go to zero. This enlarges considerably the representation depicted in Fig. 1 by pushing the initial time downward to negative values, and the light cones that had no intersection at initial time in the previous situation can now – at least for some of them – be causally connected at the time of the Big Bang, as represented in Fig 2. Recalling the definition of the co-moving particle horizon

$$r_p(t) = \int_{a=0}^{a(t)} (aH)^{-1}\,\mathrm{d}\ln a\,, \tag{3.2.5}$$

one can understand how the horizon problem is solved by Inflation, through the following consideration :

- Two particles separated by $r_p(t)$ have never been able to talk to each other;
- Two particles separated by $r_H = (aH)^{-1}$ are not able to exchange information at the time t;

Hence, it is possible that today the co-moving particle horizon is much larger than the Hubble radius, so that regions that are not causally connected today can have been in causal contact before, when the co-moving Hubble radius was taking higher values. The Hubble radius can indeed be very large at early times, decrease, thanks to Inflation, and fall under the radius of a co-moving patch of spacetime where the Universe is roughly homogeneous (we will call it a smooth patch). When Inflation ends, the Hubble radius would reach its minimal value and

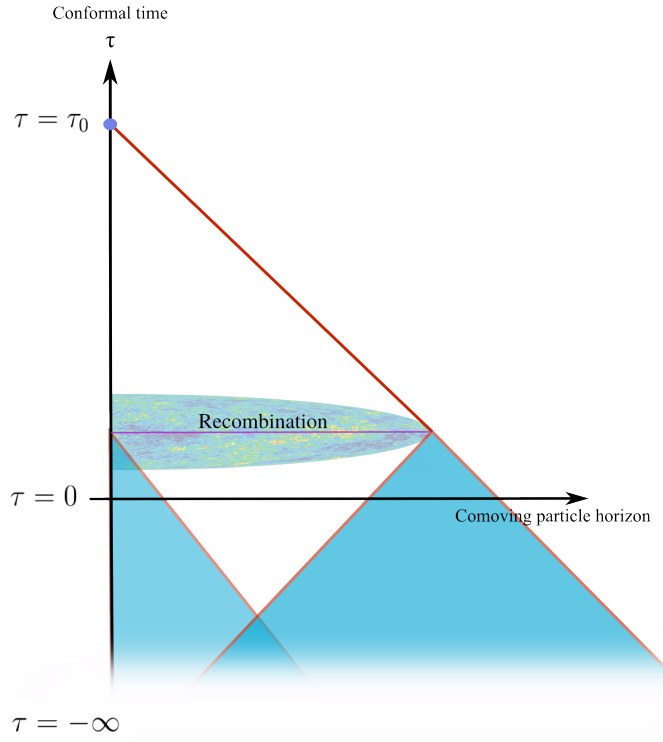

Figure 2: Schematic representation of the Inflation idea. Past timelike cones that were initially not in causal contact are pushed down to negative values of conformal time, such that it dilutes inhomogeneities sufficiently in the CMB.

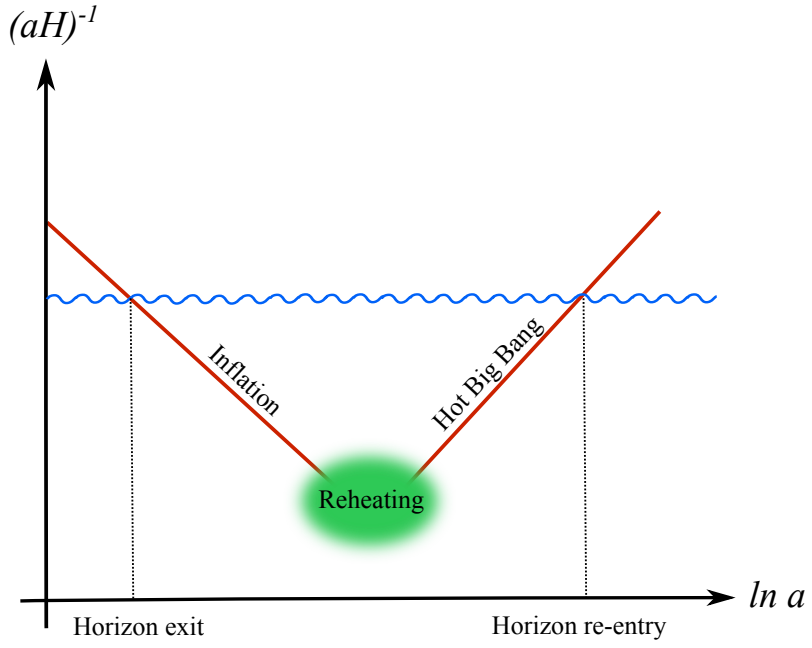

Figure 3: blablabla

start growing again until now, where the Hubble radius is still contained in a smooth region of the Universe.

The duration of Inflation, necessary to dilute sufficiently the inhomogeneities, can be expressed in a so called *number of e-folds*

$$N(t) = \ln\left(\frac{a(t_{end})}{a(t)}\right) , \tag{3.2.6}$$

where t_{end} denotes the time where Inflation ends. This Number of e-folds is measured to lie roughly between 50 and 60.

3.2.1 Inflation slow roll parameter

As we just explained, the main idea of Inflation is to make the spacetime expansion accelerate, so that it dilutes simultaneously homogeneity and curvature of our Universe, accordingly to the experimental measurement of the CMB spectrum. This condition can be expressed in terms of what will be named the *slow-roll parameter* in what follows

$$\epsilon \equiv -\frac{\dot{H}}{H^2} = -\frac{\mathrm{d}\ln H}{\mathrm{d}N} , \tag{3.2.7}$$

requiring that, during Inflation,

$$\ddot{a} > 0 \Leftrightarrow 0 \leqslant \epsilon < 1 . \tag{3.2.8}$$

This requirement will be of strong importance in the next sections.

3.3 Scalar field Inflation

As we saw above, a necessary condition for inflation to be released is to make the co-moving Hubble radius decrease for ~ 60 e-folds, meaning that the perfect fluid content of the Universe should have the feature that its equation of state satisfies

$$\omega < -\frac{1}{3} . \tag{3.3.1}$$

In order to get so, the simplest models of Inflation investigate the possibility that the Universe expansion is driven by the presence of a scalar field ϕ called *Inflaton*, evolving in a potential $V(\phi)$, in which it falls and finally oscillate at its minimum, as depicted in Fig. 4. This can be formally expressed with the simple action

$$S = \int \mathrm{d}^4x\sqrt{-g}\left[\frac{1}{2}R + \frac{1}{2}g^{\mu\nu}\partial_\mu\phi\partial_\nu\phi - V(\phi)\right] = S_{EH} + S_\phi , \tag{3.3.2}$$

S_{EH} denoting the gravitational Einstein-Hilbert action and $g \equiv \det(g^{\mu\nu})$ the determinant of the spacetime metric. The stress energy tensor can be derived from the latter action as follows

$$T^{(\phi)}_{\mu\nu} \equiv -\frac{2}{\sqrt{-g}}\frac{\delta S_\phi}{\delta g^{\mu\nu}} = \partial_\mu\phi\partial_\nu\phi - g_{\mu\nu}\left(\frac{1}{2}\partial^\sigma\phi\partial_\sigma\phi - V(\phi)\right) , \tag{3.3.3}$$

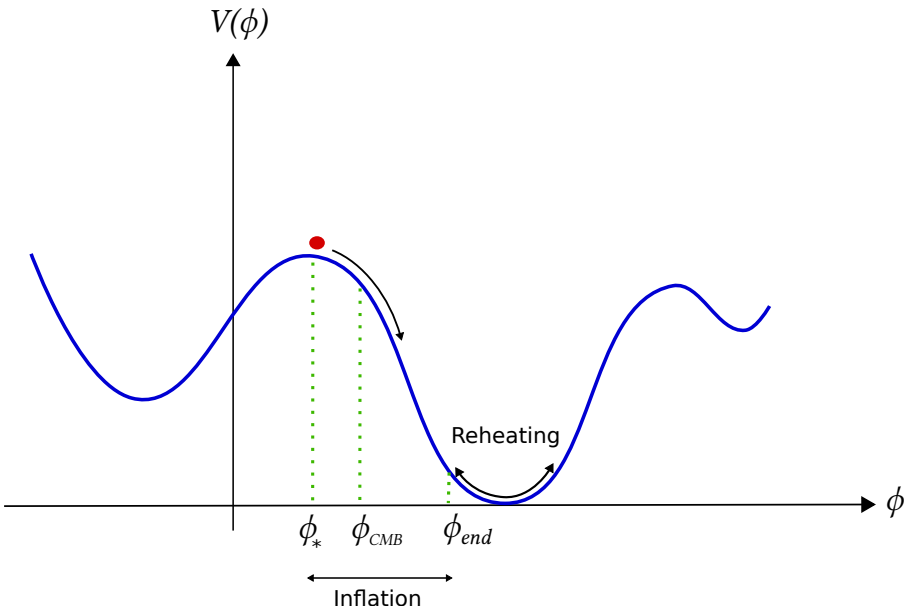

Figure 4: Generic picture of the scalar inflation scenario. The Inflaton falls along its potential releasing 60 e-folds of inflation before oscillating around its minimum, reheating the Universe.

and the equations of motion for ϕ is

$$\frac{\delta S_\phi}{\delta \phi} = 0 \Leftrightarrow \frac{1}{\sqrt{-g}}\partial_\mu \left(\sqrt{-g}\partial^\mu \phi\right) + V_{,\phi} = 0\,, \tag{3.3.4}$$

where $V_{,\phi}$ denotes the derivative with respect to ϕ. These equations can be applied to the case of an homogeneous scalar field $\phi(\mathbf{x}, t) = \phi(t)$ living in the Friedman-Lemaître-Robertson-Walker metric (2.2.1), giving rise to the following pressure and energy density

$$p_\phi = \frac{1}{2}\dot{\phi}^2 - V(\phi)\,, \tag{3.3.5}$$

$$\rho_\phi = \frac{1}{2}\dot{\phi}^2 + V(\phi)\,. \tag{3.3.6}$$

The condition (3.3.1) thus turns into

$$\omega_\phi = \frac{\frac{1}{2}\dot{\phi}^2 - V(\phi)}{\frac{1}{2}\dot{\phi}^2 + V(\phi)} < -\frac{1}{3}\,, \tag{3.3.7}$$

and is equivalent to

$$V(\phi) > \frac{1}{2}\dot{\phi}^2\,. \tag{3.3.8}$$

The latter condition can be released for a convenient choice of potential and initial conditions.

The equation of motion for ϕ (3.3.4) become

$$\ddot{\phi} + 3H\dot{\phi} + V_{,\phi} = 0\,, \tag{3.3.9}$$

where the Hubble constant H is defined by

$$H^2 = \frac{1}{3}\left(\frac{1}{2}\dot{\phi}^2 + V(\phi)\right)\,. \tag{3.3.10}$$

Note that the term $3H\dot{\phi}$ present in (3.3.9) can be interpreted as a friction term. For the time when the inflaton will be away from the vacuum, the potential will take large values ($V > \frac{1}{2}\dot{\phi}^2$), thus the Hubble constant and the latter friction term will be very large either. If the friction is large enough, inflation will settle in a slow roll regime during 60 e-folds that are necessary to dilute inhomogeneities and curvature.

The slow roll parameter ϵ can be expressed under the form

$$\epsilon \equiv \frac{3}{2}(\omega_\phi + 1) = \frac{1}{2}\frac{\dot{\phi}^2}{H^2}\,, \tag{3.3.11}$$

and the de Sitter, $p_\phi \approx -\rho_\phi$, corresponds to the limit where $\dot{\phi}^2 \ll V(\phi)$, or equivalently where $\epsilon \to 0$. The first slow roll equation thus reads

$$H^2 \simeq \frac{V(\phi)}{3}\,. \tag{3.3.12}$$

A second condition, which is necessary for inflation to last for a sufficient number of e-folds, is, as we mentioned earlier, that the friction term $3\dot{\phi}H$ dominates over the second derivative of the field $\ddot{\phi}$ so that the dynamics remains frozen for a while. This can be equivalently formulated by demanding that

$$\frac{\dot{\epsilon}}{H\epsilon} = 2\frac{\ddot{\phi}}{H\dot{\phi}} + 2\epsilon \ll 1\,, \tag{3.3.13}$$

namely asking that the variation of ϵ is negligible compared to the co-moving value of ϵ itself, or by simply imposing that the friction term is large enough

$$-\frac{\ddot{\phi}}{H\dot{\phi}} \equiv \eta \ll 1\,, \tag{3.3.14}$$

where we introduced the *second slow roll parameter* η. Necessary conditions for inflation to be released for a sufficiently long time are then summarized in

$$\epsilon \ll 1\,, \tag{3.3.15}$$

$$\eta \ll 1\,. \tag{3.3.16}$$

It can sometimes be convenient to express these conditions in a form depending only on the shape of the scalar potential, using an alternative choice of slow roll parameters, that are

$$\epsilon_V \equiv \frac{M_p^2}{2}\left(\frac{V_{,\phi}}{V}\right)^2 < 1\,, \tag{3.3.17}$$

$$|\eta_V| \equiv \left|M_p^2\frac{V_{,\phi\phi}}{V}\right| < 1\,. \tag{3.3.18}$$

Note that this set of parameters can be matched to the initial one in the slow roll regime

$$\epsilon \approx \epsilon_V\,, \tag{3.3.19}$$

$$\eta \approx \eta_V - \epsilon_V\,. \tag{3.3.20}$$

To put this discussion in a nutshell, the slow roll regime period is mainly characterized by

$$H^2 \approx \frac{V(\phi)}{3} \approx const., \tag{3.3.21}$$

$$\dot{\phi} \approx -\frac{V_{,\phi}}{3H}. \tag{3.3.22}$$

During this period, the expansion of the Universe is approximately de Sitter, namely

$$a(t) \sim e^{Ht}. \tag{3.3.23}$$

The end of inflation is finally reached when

$$\epsilon(\phi_{end}) \equiv 1, \quad \epsilon_V(\phi_{end}) \approx 1, \tag{3.3.24}$$

and one can estimate the number of inflation e-folds between an arbitrary value of ϕ and the ending point ϕ_{end}

$$N(\phi) \equiv \ln\left(\frac{a_{end}}{a}\right), \tag{3.3.25}$$

$$= \int_t^{t_{end}} H\,\mathrm{d}t = \int_\phi^{\phi_{end}} \frac{H}{\dot{\phi}}\,\mathrm{d}\phi = -\int_\phi^{\phi_{end}} \frac{\mathrm{d}\phi}{\sqrt{2\epsilon}}, \tag{3.3.26}$$

which can be expressed using the slow roll approximation (3.3.21) - (3.3.22) as

$$N(\phi) \approx -\int_\phi^{\phi_{end}} \frac{V}{V_{,\phi}}\,\mathrm{d}\phi \approx -\int_\phi^{\phi_{end}} \frac{\mathrm{d}\phi}{\sqrt{2\epsilon_V}}. \tag{3.3.27}$$

In order to solve both the horizon and the flatness problem, the total number of inflationary e-folds has to exceed

$$N_{tot} = \ln\left(\frac{a_{end}}{a_{start}}\right) \geqslant 60. \tag{3.3.28}$$

Furthermore, the number of e-folds that may separate the time of the CMB emission and the end of Inflation should seat between $N_{CMB} \sim 40-60$, depending on the details involved during the pre-heating and reheating episode. Finally we obtained

$$\boxed{N_{CMB} = -\int_\phi^{\phi_{end}} \frac{\mathrm{d}\phi}{\sqrt{2\epsilon}} \approx -\int_\phi^{\phi_{end}} \frac{\mathrm{d}\phi}{\sqrt{2\epsilon_V}} \sim 40-60.} \tag{3.3.29}$$

3.3.1 Models of Single Field Inflation

The simplest model of inflation, introduced in 1983 by A. Linde [8], is the so called *chaotic* inflation where the scalar potential is chosen to be harmonic

$$V(\phi) = \frac{m^2}{2}\phi^2. \tag{3.3.30}$$

In this case, the slow roll parameters become

$$\epsilon_V(\phi) = \eta_V(\phi) = \frac{2M_p^2}{\phi^2}. \tag{3.3.31}$$

One can then immediately notice that imposing the slow roll conditions (3.3.17) - (3.3.18) leads to values of the field of the order

$$\phi \gtrsim \sqrt{2} M_p \equiv \phi_{end} \,. \tag{3.3.32}$$

The number of e-folds becomes

$$N(\phi) = \frac{\phi^2}{4M_p^2} - \frac{1}{2} \,, \tag{3.3.33}$$

and one can get an estimation for ϕ_{CMB} by inverting the condition (3.3.29)

$$\phi_{CMB} = 2\sqrt{N_{CMB}} M_p \sim 15 M_p \,. \tag{3.3.34}$$

These two last results show that – in the chaotic inflation scenario – inflation must happen at a time where the inflaton field was actually having a vev larger than the Planck scale. This is a particular case of a class of *large field* inflation models. Other models in this class can be cited, among which stands the more general class of monomials

$$V(\phi) = \lambda_p \phi^p \,. \tag{3.3.35}$$

Another famous model is the so called *natural inflation* scenario [9], in which the inflaton rolls down from a hill potential of the form

$$V(\phi) = V_0 \left(\cos\left(\frac{\phi}{f}\right) + 1 \right) \,. \tag{3.3.36}$$

This potential usually arises if the inflaton field is taken to be an axionic field. The parameter f has to be larger than the planck mass in order to get a slow roll regime of inflation. Super-planckian values $f \gg M_p$ are a challenging issue, but natural inflation for large-field variations turns out to be quite appealing in the case of axions since the latter can be provided a shift symmetry protecting the potential from correction terms even over large field ranges.

Models can also be constructed in a setup where the value of the field stays sub-planckian during inflation. One can cite for instance the Higgs like potential

$$V(\phi) = V_0 \left[1 - \left(\frac{\phi}{\mu}\right)^2 \right]^2 \,, \tag{3.3.37}$$

which can be generalized to

$$V(\phi) = V_0 \left[1 - \left(\frac{\phi}{\mu}\right)^p \right] + \dots \,. \tag{3.3.38}$$

Another quite popular model for radiatively-induced symmetry breaking in electroweak and grand unified theories is the Coleman-Weinberg potential

$$V(\phi) = V_0 \left[\left(\frac{\phi}{\mu}\right)^4 \ln\left(\left(\frac{\phi}{\mu}\right) - \frac{1}{4} \right) + \frac{1}{4} \right] \,, \tag{3.3.39}$$

despite the fact that the parameters V_0 and μ, if compatible with the small amplitude of inflationary fluctuations cannot really be based on an $SU(5)$ or GUT theory.

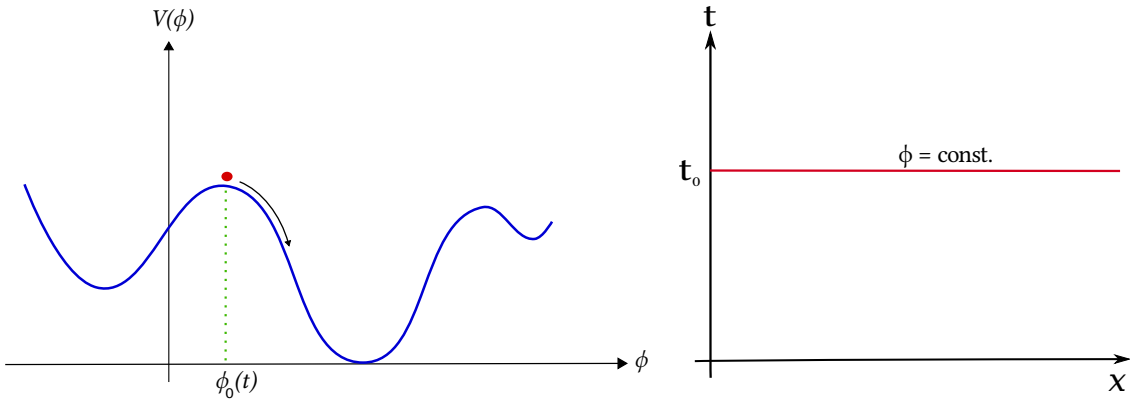

Figure 5: Classical picture : the inflaton is represented by an homogeneous scalar field.

3.4 Perturbation Theory : Observables for Inflation

In the previous sections, the reader may have noticed that we were constantly using a classical picture to explain the process of Inflation, using a classical field ϕ as the ingredient for diluting the curvature and energy density inhomogeneities. In what follows we will consider the case where the field ϕ is allowed to fluctuate around its classical value. This will slightly retire or advance the fall of the inflaton into its potential minimum, creating inhomogeneities in the energy spectrum. We will furthermore derive all the observables that are – presently or in the future – measured by experimental devices.

As described earlier, let us assume that the spacetime is entirely filled by the inflaton field at the primordial time. In the case where the field is classical, it can be described by an homogeneous time dependent field $\phi_0(t)$. In this case, the hypersurface define by $t = t_0$ coincides with one plan $\phi(t) = const$, as depicted in Fig. 5.

In the case where quantum fluctuations are allowed, the field ϕ is added a perturbation of the form

$$\phi = \phi_0(t) + \delta\phi(\mathbf{x}, t)\,. \tag{3.4.1}$$

Depending on the location in space, this perturbation can be seen as if the inflaton local time is advanced or retired. This can be seen by the fact that the hypersurface $\phi(t) = const.$ is fluctuating around the plan $t = const.$ with which it does not coincide anymore, as depicted in Fig. 6. Thus, from one place to another, at a fixed time t_0 the field ϕ will oscillate around the background classical field $\phi_0(t_0)$.

However, we will see that such perturbations can actually be absorbed by a metric coordinate transformation, seeing then the perturbation of the field as metric perturbations and local curvature of the spacetime. Such perturbations of the geometry can anyway exist and will hence mix up with the inflaton perturbations.

Let us first write the FLRW metric (2.2.1) introducing metric perturbations as follows

$$\mathrm{d}s^2 = -(1+2\Phi)\,\mathrm{d}t^2 + 2B_i\,\mathrm{d}x^i\,\mathrm{d}t + a^2(t)\left[\delta_{ij} + C_{ij}\right]\,\mathrm{d}x^i\,\mathrm{d}x^j\,, \tag{3.4.2}$$

where we introduced 10 entries, that are one scalar field Φ, 1 vector B_i and one tensor C_{ij}. It is possible to see, at the linear order of perturbations, that the Fourier modes of the perturbations do not interact together, meaning they can be studied independently. Hence, for any

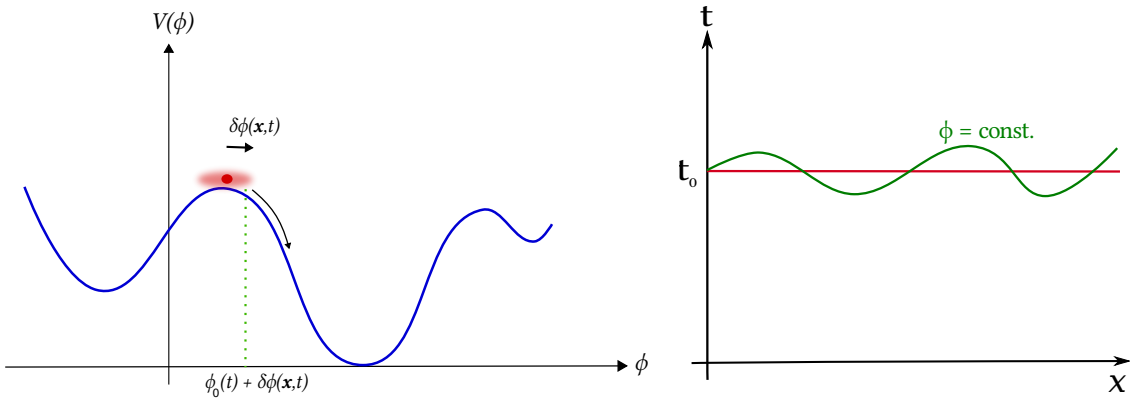

Figure 6: Quantum picture : the classical field background is added a spacetime-dependent perturbation.

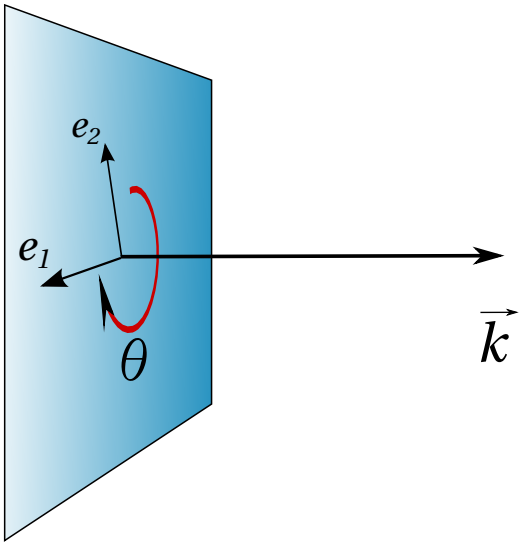

Figure 7: Rotation of angle θ in the plane (e_1, e_2) around the vector $\vec{k}$ discriminating between scalar, vector and tensor components of the perturbations.

perturbation $X(\mathbf{x}, t)$

$$X = \int \frac{\mathrm{d}k^3}{(2\pi)^3} X_{\vec{k}}(t) e^{i\vec{k}\cdot\vec{x}} \,, \tag{3.4.3}$$

and focusing on the study of one Fourier mode $X_{\vec{k}}$, one can decompose it in terms of components that behave like scalars, vector or tensor under rotation of axis $\vec{k}$ (*SVT decomposition*). One can show in particular that the perturbation B_i decomposes like

$$B_i = \partial_i B + B_i^V \,, \tag{3.4.4}$$

giving in the Fourier space

$$B_i = i\hat{k} B + e_i^a B_a^V \,, \tag{3.4.5}$$

where $\hat{k} \equiv \frac{\vec{k}}{||\vec{k}||}$ and the vectors e_i's form a basis of the plan orthogonal to the direction $\vec{k}$ as depicted in Fig. 7. The first component doesn't transform under rotation around $\vec{k}$, B being a

	Metric	Inflaton	Reduction	Total d.o.f.
Scalars	4	1	-2 -2	1
Vectors	2	0	-1 -1	0
Tensors	1	0		1

Table 3.1: Number of scalar, vector and tensor components after diffeomorphism reduction and Einstein's equation constraints. The resulting degrees of freedom are one scalar and tensor mode.

scalar component, whereas B_i^V transforms with helicity 1

$$B_a^V \to e^{i\theta} B_a^V \,. \tag{3.4.6}$$

Similarly the matrix C_{ij} can written under the form

$$C_{ij} = 2\delta_{ij}\Psi + 2\hat{k}_i\hat{k}_j E + 2\left(\hat{k}_i e_j^a E_a^V + \hat{k}_j e_i^a E_a^V\right) + \gamma_{ij}\,, \tag{3.4.7}$$

where one can work in a basis in which the tensor γ_{ij} is traceless and divergence free

$$\gamma_i^i = \partial_i \gamma_j^i = 0\,. \tag{3.4.8}$$

Thus the matrix C contains two scalar components, one vector and one tensor. Furthermore, the use of diffeomorphisms of the form

$$\left\{ \begin{array}{rcl} t & \to & t + \xi^0\,, \\ x^i & \to & x^i + \xi^i = x^i + \partial^i \xi^S + \xi^{iV} \end{array} \right. \tag{3.4.9}$$

where ξ^0, ξ^S are scalar components and ξ^V is a vector one, allows to get rid of two scalars and one vector component in the theory. In addition to this, Einstein's equations

$$G_{00} = 8\pi G T_{00} \quad \text{and} \quad G_{0i} = 8\pi G T_{0i}\,, \tag{3.4.10}$$

fix two scalar components and one vector. The number of scalars, vectors and tensors present in the theory are summarized in Tab. 3.1. It turns out that the degrees of freedom that remain after elimination of the extra components are composed of one scalar and one tensor mode. Depending on the point of view, one has the possibility to work in different gauges. In the *flat* gauge, the metric is assumed to remain flat, Ψ and E being set to zero, which provides perturbations to the inflaton field. On the opposite, one can assume that the inflaton does not get perturbed while the metric sees its curvature fluctuate. Note that the term "flat" can be used since the spacelike curvature $R^{(3)}$ is related to the perturbation components E and Ψ through the formula

$$R^{(3)} = 4\frac{\nabla^2}{a^2}\left(\Psi + \frac{1}{3}\nabla E\right)\,. \tag{3.4.11}$$

This freedom in the choice of gauge should yet not modify the physics of perturbations which can indeed be described in terms of a gauge invariant quantity, called the *curvature perturbation*

$$\zeta \equiv -\Psi - H\frac{\delta\phi}{\dot{\phi}}\,. \tag{3.4.12}$$

This invariant will provide in what follows a gauge independent tool for describing the scalar perturbations of the metric.

Scalar Perturbations from Inflation

In the flat gauge (where Ψ is assumed to be zero) one can write the scalar field action (3.3.2) at the second order in the correction $\delta\phi$, giving

$$S^{(2)} = \int \mathrm{d}t\, \mathrm{d}^3x\ a^2 \left[\frac{\dot{\delta\phi}^2}{2} - \frac{(\delta\phi)^2}{2a^2} - \frac{1}{2}V''\delta\phi^2 - \frac{1}{a^3}(a^3\epsilon H)\delta\phi^2 \right] . \tag{3.4.13}$$

The first two terms constitute the free test field action

$$S^{(2)}_{free} = \int \mathrm{d}t\, \mathrm{d}^3x\ a^2 \left[\frac{\dot{\delta\phi}^2}{2} - \frac{(\delta\phi)^2}{2a^2} \right] , \tag{3.4.14}$$

and the additional terms behave like corrections of subleading order in the slow roll parameters $\mathcal{O}(\epsilon, \eta)$

$$S^{(2)} = \int \mathrm{d}t\, \mathrm{d}^3x\ a^2 \left[\frac{\dot{\delta\phi}^2}{2} - \frac{(\delta\phi)^2}{2a^2} + \mathcal{O}(\epsilon, \eta)\, H^2\delta\phi^2 \right] . \tag{3.4.15}$$

The dynamics of the inflaton perturbation will hence be described at leading order on super-horizon scales ($k \ll aH$) by the one of a free field in a de Sitter spacetime. Writing the latter action (3.4.13) in a gauge invariant formulation provides the exact expression

$$\int \mathrm{d}t\, \mathrm{d}^3x \frac{a^3\dot{\phi}_0}{2H^2} \left[\dot{\zeta}^2 - \frac{1}{a^2}(\partial_i\zeta)^2 \right] . \tag{3.4.16}$$

whose Fourier modes will be described by a power spectrum of the form

$$\langle \zeta_{\vec{k}}\zeta_{\vec{k'}} \rangle = (2\pi)^3\delta(\vec{k} + \vec{k'})P_\zeta(\vec{k}) , \qquad \left(\frac{k}{aH} \ll 1 \right) . \tag{3.4.17}$$

A detailed study of the quantization of (3.4.16) shows that the power spectrum of the spectral curvature is given by

$$P_\zeta(\vec{k}) = \frac{1}{2k^3}\frac{H^4_\star}{\dot{\phi}^2_\star} , \tag{3.4.18}$$

where $H_\star$ and $\dot{\phi}_\star$ are quantities defined at the horizon crossing $k = aH$. Using the slow roll parameters definition (3.3.11) gives equivalently

$$P_\zeta(\vec{k}) = \frac{1}{2k^3}\frac{H^2_\star}{M^2_p}\frac{1}{2\epsilon_\star} , \tag{3.4.19}$$

and has been measured with a great precision by COBE [10] – giving the name *COBE normalization* to the associated constraint – and more recently by the PLANCK experiment [11]

$$\frac{k^3P_\zeta}{2\pi} = 2.198^{+0.076}_{-0.085} \times 10^{-9} . \qquad (k_\star \approx 0.002Mpc) \tag{3.4.20}$$

The spectral dependency of the scalar perturbations is then usually described by a *spectral index* n_s defined by

$$n_s - 1 \equiv \frac{\mathrm{d}\ln(k^3P_\zeta(k))}{\ln k} . \tag{3.4.21}$$

Using that $a \sim e^{Ht}$ and the slow roll conditions, one can relate the spectral index to the slow roll parameters at horizon crossing

$$n_s \approx -6\epsilon_{V\star} + 2\eta_{V\star} \approx -4\epsilon_\star + 2\eta_\star \,. \tag{3.4.22}$$

The Planck collaboration was able to measure with very good accuracy [11] the spectral index, which, as we will see represent one of the main constraints for inflation model building, namely

$$n_s = 0.968 \pm 0.006 \,. \tag{3.4.23}$$

Tensor Perturbations from Inflation

Similarly to the scalar perturbations, we saw that the spacetime perturbations contain one tensor mode, that can also be detected by experiment. In the same manner than the scalar perturbations, the second order action of the tensor perturbation can be written

$$S_T^{(2)} = \frac{M_p^2}{8} \int \mathrm{d}x^3 \, \mathrm{d}t a^3 \left[\dot{\gamma}_{ij}^2 - \frac{1}{a^2} (\partial \gamma_{ij})^2 \right] , \tag{3.4.24}$$

and the polarization modes behave like free fields in a de Sitter background. Two point functions of the latter modes can be shown to take the form

$$\langle \gamma_{\vec{k}}^s \gamma_{\vec{k}'}^{s'} \rangle = \frac{4}{M_p^2} \frac{H^3}{2k^3} (2\pi)^3 \delta(\vec{k} + \vec{k}') \delta^{ss'} \equiv \frac{P_T(\vec{k})}{2} (2\pi)^3 \delta(\vec{k} + \vec{k}') \delta^{ss'} \,. \tag{3.4.25}$$

where s, s' denote the polarizations of the modes. From these formula, one can define the so called *tensor-to-scalar ratio* r by

$$r \equiv \frac{P_T}{P_\zeta} = 16\epsilon \,. \tag{3.4.26}$$

This quantity is of crucial importance while trying to build a viable model of Inflation, since the shape of the chosen potential will influence directly the value of the latter. Furthermore it appears to be severely constrained by experiment. Indeed, a combined analysis from PLANCK and BICEP2 collaborations found out an upper bound on r, that is

$$r < 0.09 \quad (95\% CL) \,. \tag{3.4.27}$$

A more precise information on the exact value of r would be a very important clue, if different from zero, of the existence of tensor modes. A point that can appear to be puzzling from the theoretical viewpoint is that there seems to exist a intriguing coincidence between the energy scale of Inflation and the scale of grand unification. Indeed, it appears that these scales are related by

$$V_{inf}^{1/4} = \left(\frac{r}{0.12} \right)^{1/4} \times 2 \cdot 10^{16} \mathrm{GeV} \,. \tag{3.4.28}$$

There is no *a priori* strong reason for such a matching of scales. Another important feature of single field inflation model phenomenology, is that one can relate the value of the tensor-to-scalar ratio r to the total variation of the field. Using (3.3.29) one can indeed show [12] that

$$\frac{\Delta\phi}{M_p} \sim \mathcal{O}(1) \left(\frac{r}{0.01} \right)^{1/2} , \qquad \text{(Lyth Bound, '96)} \tag{3.4.29}$$

meaning that if the tensor-to-scalar ratio was experimentally detectable, the inflaton field would generically run over scales larger than the Planck mass.

Spectral Dependence of the Tensor Fluctuations
As it is defined for the scalar perturbations, the spectral behavior of the tensor perturbations can be described by a spectral index n_T related to the power spectrum factor by the relation

$$n_T \equiv \frac{\mathrm{d}\ln H^2}{\mathrm{d}\ln k} = 2\frac{\dot{H}}{H^2} = -2\epsilon\,. \tag{3.4.30}$$

Using Eq. (3.4.26), a consistency relation for inflation to be valid can be written under the form

$$n_T = -\frac{1}{8}r\,. \tag{3.4.31}$$

The measurement of a negative tensor perturbation spectral index would hence be a very strong piece of evidence that the theory of Inflation is a good description of our Universe evolution. Indeed, speculations on the tensor-to-scalar value, even if the latter is measured to be different from zero, would not be sufficient to claim that the observed gravitational waves would come from an inflationary period...

3.4.1 Some Alternatives to Single Field Inflation

Although very popular because of its simple formulation, we saw that single field inflation has peculiar features which make it either undetectable or involving field variations over super-planckian energy scales. As an alternative to this elegant approach, theories including several fields can produce a collective contribution to the inflation energy density while fields run over reasonable energy scales, as in N-flation [13] where the potential is assumed to be of the form

$$V(\phi_1,\ldots,\phi_N) = \sum_{i=1}^{N} V_i(\phi_i)\,. \tag{3.4.32}$$

Another appealing class of models is the one of so called Starobinsky-like potentials coming from modified versions of the Einstein-Hilbert action [14, 15, 16]. Indeed, writing an action of the sort

$$S = \int \mathrm{d}^4x\sqrt{-g}\left[\frac{1}{2}R + \frac{R^2}{12M^2}\right]\,, \tag{3.4.33}$$

where $M \ll M_p$ can be shown to be conformally equivalent to having canonical gravity plus a scalar field, going back in the Einstein frame by performing fields redefinition

$$\tilde{g}_{\mu\nu} = (1+\phi/3M^2)g_{\mu\nu}\,, \tag{3.4.34}$$

$$\varphi = \sqrt{\frac{3}{2}}\ln(1+\phi/3M^2)\,, \tag{3.4.35}$$

and providing the potential

$$V(\varphi) = \frac{3M^2}{4}\left(1-e^{-\sqrt{2/3}\varphi}\right)^2\,. \tag{3.4.36}$$

Such potential presents a plateau, on which the inflaton can slow roll before falling into its minimum, while producing observables of order

$$n_s = 1-2/N_e\,, \qquad r = 12/N_e^2\,, \tag{3.4.37}$$

making the predictions for r in particular very small by requiring that $N_e \sim 60$ e-folds ($r \sim 0.003$).

One should also mention that non minimal coupling of scalar field to gravity can equally lead to viable inflation model [17, 18, 19, 20, 21, 22]. The Standard Model Higgs boson was thus imagined to couple non minimally to gravity in so called Higgs Inflation models [23].

3.5 Inflation in Supergravity

As we have seen along the description of Inflation, and through several examples, there exist a large class of inflationary models where the inflaton field is taking large, trans-planckian vacuum expectation values during the slow roll period. For this reason the contributions of Planck-scale suppressed higher-dimensional, non renormalizable operators to the inflationary potential, of the form

$$V_{eff} = V_0 \sum_n \frac{(\bar{\phi}\phi)^n}{M_p^{2n}}\,, \tag{3.5.1}$$

are generically relevant. It is therefore crucial to embed large-field inflation within the framework of an ultraviolet completion, for which string theory is the one of the most appealing candidate, described by supergravity in its low-energy limit.

However, such corrections to the vacuum energy V_0 can easily destroy the inflationary scenario by contributing too much to the inflation energy scale. Indeed, already the first term ($n = 1$) of the series would lead to a second derivative of the potential of order $V'' \sim V_0$, pushing the second slow roll parameter η to values of order unity, preventing inflation to enter any slow roll period. This so called *η-problem* appears typically in supergravity [24, 25], where all the fields involved naturally interact through gravitational forces, and couple to the vacuum energy density, thus producing large effective contribution to the scalar potential

$$V_F \sim \left(1 + \frac{\bar{\phi}\phi}{M_p^2} + \dots\right) V_0\,. \tag{3.5.2}$$

More technically, this can be formulated by noting that a minimal Kähler potential containing the inflaton

$$K = \phi\bar{\phi} + \dots\,, \tag{3.5.3}$$

would enter an exponential factor while writing the scalar F-term potential in supergravity

$$V_F = e^K \left(|\partial_\phi W + K_{,\phi} W|^2 - 3|W|^2\right)\,, \tag{3.5.4}$$

which would render the inflation potential obviously far too step to release 60 e-folds of inflation as required to solve the flatness and homogeneity cosmological problems. It is important to note also that the η-problem can arise in all possible picture of inflation while trying to embed any model in supergravity, including small field inflation where $\phi \lesssim M_p$, since the argument exposed above doesn't make any assumption on the value of the inflaton field. Large field inflation models thus encounter even stringent problems making the η-problem a complete catastrophe, since the series (3.5.1) would not even be summable in such case. For these important reasons, several possibilities have been developed to circumvent such obstacles.

A first way to evade the η-problem is to make the inflation energy scale be sourced by D-terms rather than F-terms [26, 27, 28] in order to escape the presence of the latter exponential

factor (which is not present in the D-term scalar potential). In this case the η-problem is then simply not present.

While using F-term inflation, there appears to be mainly two ways to avoid the η-problem : On one hand, one can write the most generic minimal Kähler potential, involving all the fields present in the theory [29, 30, 31]

$$K = \phi_i^* \phi^i + \sum_{n \geqslant 2} \kappa_i^{(n)} \frac{(\phi_i^* \phi^i)^n}{M_p^{2n-2}} + \sum_{k=m+n} \kappa_{ij}^{(k)} \frac{(\phi_i^* \phi^i)^n (\phi_j^* \phi^j)^m}{M_p^{2k-2}} + \dots , \tag{3.5.5}$$

and tune the parameters $\kappa_i^{(n)}, \kappa_{ij}^{(k)}, \dots$ such that off diagonal terms appearing in the Kähler metric render the potential sufficiently flat to release slow roll inflation.

On the other hand, it is possible to evade the η-problem by providing the Kähler potential a approximate symmetry, preventing non renormalizable operators (3.5.1) to arise in the theory. This can be released by making the Kähler potential depend only on a quantity invariant under such symmetry ρ,

$$K = k(\rho) \, , \tag{3.5.6}$$

which does not contain the inflaton degree of freedom, protecting the latter from getting large supergravity mass corrections.

The simplest candidate symmetry which can be used in this aim is the *shift symmetry* [32, 33, 34] under which the complex scalar field containing the inflaton degree of freedom transforms like

$$\phi \longrightarrow \phi + ic \, , \tag{3.5.7}$$

where c denotes any real constant. To render the Kähler potential invariant under shift symmetry, the latter can thus be made depending only on the combination

$$\rho = \phi + \bar{\phi} = 2\mathrm{Re}(\phi) \, . \tag{3.5.8}$$

The degree of freedom which is hence not contained in this invariant quantity is the imaginary part of the scalar field ϕ which turns out to be a good candidate for playing the role of the inflaton

$$\varphi = \sqrt{2}\, \mathrm{Im}(\phi) \, . \tag{3.5.9}$$

Indeed the inflaton does not appear, in such circumstances, in the exponential factor, protecting its mass to be affected by large, non renormalizable operators. This simple option for solving the η-problem will be used in all the works presented in this chapter.

Another feature of supergravity models is that it usually mix up, in the F-term scalar potential, several scalar fields altogether, which renders the shape of the effective inflationary potential much more difficult to predict once one has written a given lagrangian. The inverse problem, which would consist to build a supergravity lagrangian in order to embed a given quantum field theory of inflation within SUGRA can then be sometimes very challenging. Indeed one has to write explicitly the complete scalar potential, check that the inflaton is really the lightest degree of freedom in the theory – hence the one contributing mostly to the inflation energy density – and test the stability of the inflationary trajectory.

3.5.1 Chaotic Inflation in Supergravity

As a simple example we will detail in this section how chaotic inflation can be properly embedded in supergravity. For the reasons aforementioned, the naive choice of a lagrangian of the form

$$\begin{cases} \mathcal{K} &= \phi\bar{\phi} + \dots , \\ \mathcal{W} &= \frac{m}{2}\phi^2 + \dots , \end{cases} \tag{3.5.10}$$

would obviously suffer from the η-problem and need to be provided a protecting symmetry to escape the latter. The shift symmetry can therefore be illustrated here by modifying the Kähler potential to be

$$\mathcal{K} = \frac{(\phi + \bar{\phi})^2}{2} + \dots . \tag{3.5.11}$$

Yet this trick does not suffice to produce a nice, chaotic inflationary scenario. Indeed, the cautious reader might have noticed the presence of a significant negative term in the potential (3.5.4). In the case of a simple quadratic superpotential, the latter has a dramatic effect on the shape of the scalar potential for large values of the inflaton field $\varphi = \sqrt{2}\,\mathrm{Im}(\phi)$. As a matter of fact, the potential behaves for $\varphi \gg 1$ like

$$V(\varphi) \sim -3m^2\varphi^4 , \tag{3.5.12}$$

that makes the latter unbounded from below. A solution to this auxiliary problem of SUGRA chaotic inflation was proposed in 2000 by Kawasaki *et al.* [32] who introduced in the model a *stabilizer* field S appearing simply in the lagrangian as follows

$$\begin{cases} \mathcal{K} &= \frac{|\phi+\bar{\phi}|^2}{2} + |S|^2 - \xi(S\bar{S})^2 , \\ \mathcal{W} &= mS\phi . \end{cases} \tag{3.5.13}$$

Up to higher-dimensional terms in the Kähler potential the model is determined by an R-symmetry : $R(\phi) = 0$, $R(S) = 2$, and a $\mathbb{Z}_2$-symmetry : $(\phi, S) \to \pm(\phi, S)$. The inflation trajectory appears in this case to stand in the direction $S = \mathrm{Re}\phi = 0$ and the effective inflation potential is

$$V_{eff}(\varphi) = \frac{m^2}{2}\varphi^2 = V_{chaotic} . \tag{3.5.14}$$

Here the presence of a quartic term in the Kähler potential is one possible option to stabilize the field S along the inflationary direction. S is rendere heavy enough during inflation for $\xi \gtrsim 10$. One can motivate the presence of such term in the Kähler potential by assuming that the latter stems from couplings of heavy modes to S, i.e. from

$$W_{\text{heavy}} \supset \lambda S\psi^2 + \text{mass terms} , \tag{3.5.15}$$

where ψ denotes heavy modes of mass M. Then a quartic term for S in K is generated by one-loop quantum corrections of the Coleman-Weinberg type,

$$K_{\text{1-loop}} \simeq S\bar{S}\left[1 - \frac{\lambda^2}{16\pi^2}\log\left(1 + \frac{\lambda^2 S\bar{S}}{M^2}\right)\right] \simeq S\bar{S} - \frac{\lambda^4}{16\pi^2 M^2}(S\bar{S})^2 , \tag{3.5.16}$$

as discussed in [35]. Thus, in the generic case $\lambda \sim \mathcal{O}(1)$ the parameter ξ is related to the mass scale M as follows,

$$\xi \sim \frac{1}{16\pi^2 M^2}\,. \tag{3.5.17}$$

Since the heavy degrees of freedom should be integrated out above the energy scale during inflation, $M \gtrsim \rho_{\rm inf} \sim M_{\rm GUT} \simeq 0.01$, but below the Planck scale, one can roughly assume

$$\xi \simeq 10 \tag{3.5.18}$$

to be reasonable values for the coefficient. Note that quartic terms in the Kähler potential could also arise from α' corrections in string theory. In such a setup the coefficients would rather be $\xi \sim \frac{1}{M_{\rm s}^2}$, where $M_{\rm s}$ denotes the string scale. In order for string modes to decouple, $M_{\rm s}$ would have to be larger than the energy scale during inflation, but smaller than the Planck scale. Due to the absence of the loop suppression factor $16\pi^2$, this could result in larger coefficients.

3.5.2 Generalization of the Stabilizer Approach

In a more general set up, one can construct models where the superpotential has the form [36, 37]

$$\mathcal{W} = S f(\phi)\,. \tag{3.5.19}$$

In this case the Kähler potential can have a generic form

$$\mathcal{K}(|\phi + \bar{\phi}|^2, S\bar{S})\,, \tag{3.5.20}$$

and the effective potential for the inflaton degree of freedom turns out to be (for $S = 0$)

$$V(\varphi) = \left| f\left(\frac{\varphi}{\sqrt{2}}\right)\right|^2 . \tag{3.5.21}$$

Hence the full generality of the function f introduced here may provide this simple class of models the ability to reproduce any potential $V(\varphi)$. A simple extension of the *chaotic* case ($f = m\phi$) is the situation when one adds one correction with parameter $a \ll 1$

$$f(\phi) = m\phi(1 - a\phi)\,. \tag{3.5.22}$$

A change of variable of the form $\phi \to \phi + \frac{1}{2a}$ makes this choice equivalent to the function $\tilde{f} = -ma\left(\phi^2 - \frac{1}{(2a)^2}\right)$ and the effective inflation potential has the shape of the mexican hat-like, Higgs potential

$$V(\varphi) = \frac{\lambda}{4}\left(\phi^2 - v^2\right)^2 , \tag{3.5.23}$$

where $\lambda = m^2a^2$ and $v = 1/(\sqrt{2}a)$. This potential has been explored in [36, 38, 39] and can lead, in the case where $v \gg 1$ to reasonable observables in two different cases that can be visualized in Fig. 8 :

- The inflaton starts from very large values. In this case the scenario is somehow similar to the chaotic picture and leads to large values of r.
- The inflaton starts from small values, producing observables similar to the *natural inflation* scenario [40, 9].

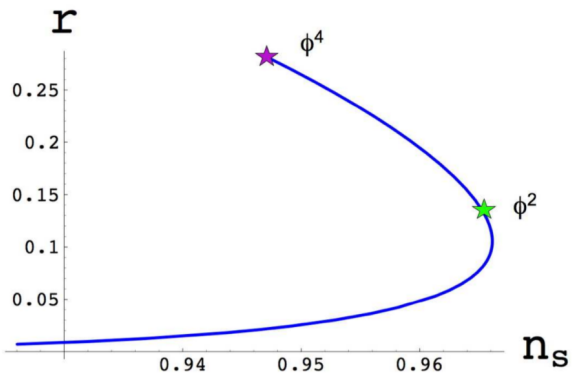

Figure 8: Figure extracted from [38] where observables are computed with the potential (3.5.23) defining *New Inflation*. When the fields starts rolling down from large values, the situation is similar to standard chaotic inflation (the star stands for the chaotic set up) and leads to large values of r (upper part of the curve), while the case where the Inflaton starts falling from $\phi \approx 0$ is somehow similar to natural inflation (lower part of the curve).

3.6 Interplay with Supersymmetry Breaking

Although being an incredibly appealing formulation of quantum field theory from many theoretical viewpoints, supersymmetry requires, from a particle physics phenomenological viewpoint, to be spontaneously broken in order to provide large masses to all the super-partners that have at the moment not been produced and observed at the LHC. However, although chaotic inflation and many of its variants have been extensively studied in the literature, its connection to supersymmetry breaking was not as closely investigated. Indeed F-term and D-term Inflation are usually using supersymmetry breaking to drive inflation by providing a sufficient energy density during 60 efolds. However it is worth to ask the question whether it is possible to produce a model were supersymmetry is spontaneously broken at the end of inflation. As we will see, this is not free of constraints. Indeed supersymmetry breaking will have a strong influence on the shape of the inflaton potential, and hence be severely constrained by observables.

Simplest setups to achieve F-term supersymmetry breaking are the O'Raifeartaigh model [41] and the Polonyi model [42]. Our first goal will thus be to explore to which point these models can contain or be added an inflationary sector and how the supersymmetry breaking scale is constrained by experiment in this peculiar case. Coupling the inflaton sector to a supersymmetry breaking sector turns out to be more difficult than expected. In the simplest working scenarios we find that the gravitino mass is bounded from above, which, as we will see in more generality in the next sections, is a strong result of chaotic inflation in supergravity when using a stabilizer field. This study has given rise to a publication in collaboration with W. Buchmuller, E. Dudas and C. Wieck [43].

3.6.1 SUSY Breaking Safari : Our Strategy

In the sections that will follow, we will study in full detail different models of Inflation including at least one stabilizer field to produce a chaotic-like potential in supergravity and breaking supersymmetry in the vacuum. Our approach will be similar in the different situations and we

recall here its different steps :

1. Write a lagrangian containing at least an Inflaton field and a stabilizer.
2. Choose the superpotential and a set of fields such that supersymmetry is broken in the ground state.
3. Study the vacuum at the end of Inflation :
   - Tune the parameters to cancel the cosmological constant,
   - Compute the gravitino mass in terms of these parameters.
4. Study the inflation trajectory :
   - Work out how the fields are stabilized, by imposing the condition of having a single field inflation,
   - Check that the Inflaton is the lightest degree of freedom and that other fields have masses larger than the Hubble scale, not to contribute too much the energy density during inflation and hence perturb the latter,
   - Eventually check numerically that these heavy fields stabilize quickly during inflation,
   - Integrate out the latter to write the effective inflation potential,
   - Find out in which range of values the gravitino mass can stand in order to predict observables in agreement with experimental constraint aforementioned.

3.6.2 Minimal chaotic inflation with a Polonyi field

A minimal way to implement supersymmetry breaking after chaotic inflation is specified by the superpotential[1]

$$W = mS\phi + fX + W_0\,, \tag{3.6.1}$$

i.e., by adding a Polonyi-like sector with a chiral superfield X to the inflation model. Thus, the two sectors decouple except for gravitational-strength interactions. By field redefinitions and a Kähler transformation m, f, and W_0 can be chosen to be real; they have mass dimension one, two, and three, respectively. Similar to the superpotential, a suitable Kähler potential is obtained by adding the contributions from the inflation and supersymmetry breaking sectors, i.e.,

$$K = \frac{1}{2}(\phi + \bar{\phi})^2 + S\bar{S} + X\bar{X} - \xi_1(X\bar{X})^2 - \xi_2(S\bar{S})^2\,. \tag{3.6.2}$$

As we mentioned in Section 3.5.1, in the absence of the term proportional to ξ_2, the stabilizing scalar S gets no Hubble-scale contributions to its mass. Will see in the next sections that this

[1]Notice that this form of superpotential has been studied, in slightly different contexts, in [44, 45].

is actually a more general result and applies to any model with or without supersymmetry breaking and a Lagrangian of the type

$$\begin{aligned} K &= K_{a\bar{b}}\chi_a\bar{\chi}_{\bar{b}} + S\bar{S} + K(\phi+\bar{\phi}) + \dots\,, \\ W &= W_0 + W_1(\chi_a, S) + mS\phi\,, \end{aligned} \tag{3.6.3}$$

where $\dots$ denotes higher-order terms in the fields χ_a, and $K(\phi+\bar{\phi})$ has at least a quadratic term in an expansion of its argument. On the other hand, the quartic term in the supersymmetry breaking field X is needed to stabilize the corresponding scalar in the true vacuum and circumvent the Polonyi problem. Thus, the terms proportional to ξ_1 and ξ_2 are necessary to ensure stability of all directions during inflation and in the ground state. Both terms may result from integrating out heavy degrees of freedom at the quantum level. Since X gets a Hubble-scale mass during inflation, we often neglect the term involving ξ_1 in our discussion of inflation.

Vacuum after inflation

In this combined model, if f is small compared to all other scales in the theory, m still corresponds to the inflaton mass, f denotes the scale of supersymmetry breaking after inflation, and W_0 is chosen such that the vacuum energy vanishes after inflation. The latter is achieved by imposing

$$W_0 \simeq \frac{f}{\sqrt{3}}\,, \tag{3.6.4}$$

at leading order in f. After inflation the vacuum of the system is found to lie at

$$\langle\phi\rangle = \langle S\rangle = 0\,, \qquad \langle X\rangle \simeq \frac{1}{2\sqrt{3}\xi_1}\,. \tag{3.6.5}$$

In this vacuum the gravitino mass is given by

$$m_{3/2} \equiv e^{K/2}|W| \simeq W_0 \simeq \frac{f}{\sqrt{3}}\,. \tag{3.6.6}$$

However, as will become clear in what follows, this vacuum structure is altered if f is chosen to be larger than m. Starting from the full scalar potential

$$V = e^K\left\{|mS + (\phi+\bar{\phi})W|^2 + K^{-1}_{S\bar{S}}|m\phi + K_S W|^2 + K^{-1}_{X\bar{X}}|f + K_X W|^2 - 3|W|^2\right\}\,, \tag{3.6.7}$$

with

$$K_X = \bar{X}(1-2\xi_1|X|^2)\,, \quad K_{X\bar{X}} = 1 - 4\xi_1|X|^2\,, \tag{3.6.8}$$

$$K_S = \bar{S}(1-2\xi_2|S|^2)\,, \qquad K_{S\bar{S}} = 1 - 4\xi_2|S|^2\,, \tag{3.6.9}$$

we expand V up to second order in all real scalars and obtain

$$\begin{aligned} V = {} & f^2 - 3W_0^2 - 2\sqrt{2}fW_0\,\alpha + 2mW_0\,\varphi\chi + \frac{1}{2}f^2\left(2\zeta^2+\chi^2+\psi^2\right) \\ & - W_0^2\left(\alpha^2+\beta^2+\zeta^2+\chi^2+\psi^2\right) + \frac{1}{2}m^2\left(\zeta^2+\chi^2+\psi^2+\varphi^2\right) \\ & + 2f^2\xi_1\left(\alpha^2+\beta^2\right)\,, \end{aligned} \tag{3.6.10}$$

with

$$S = \frac{\psi + i\chi}{\sqrt{2}}\,, \quad X = \frac{\alpha + i\beta}{\sqrt{2}}\,, \quad \phi = \frac{\zeta + i\varphi}{\sqrt{2}}\,. \tag{3.6.11}$$

From the mass matrix of this system it is evident that assuming $W_0 = \frac{f}{\sqrt{3}}$ leads to a tachyonic direction close to the origin of the potential if

$$f > m\,. \tag{3.6.12}$$

Specifically, only for $f < m$ there is a stable vacuum at $\langle\phi\rangle = \langle S\rangle = 0$ and $f^2 = 3W_0^2$ cancels the cosmological constant. For larger f a linear combination of ϕ and S obtains a vev and cosmological constant cancellation is ensured by

$$\langle V\rangle = f^2 - 3W_0^2 + \frac{m^2\left(f^2 - 6W_0^2\right)}{256\left(f^2 - 2W_0^2\right)^4\left(f^2 - W_0^2 + 2\xi_2\left(f^2 - 3W_0^2\right)\right)} = 0\,, \tag{3.6.13}$$

at leading order in m. This effect, although small, is taken into account in our analysis of the inflaton dynamics.

Interaction during inflation

During inflation all fields in the combined system defined by Eq. (3.6.1) and Eq. (3.6.2) must be stabilized with large masses, i.e., masses larger than the Hubble scale during inflation, so they can be integrated out. Considering the scalar potential in Eq. (3.6.7) it is evident that all real scalar degrees of freedom are stabilized at the origin with large masses, except for the inflaton $\varphi = \sqrt{2}\,\mathrm{Im}\,\phi$ and the imaginary part of the stabilizer field $\chi = \sqrt{2}\,\mathrm{Im}\,S$. Due to the presence of the additional scale f and the constant W_0, χ is shifted from its original minimum at $\langle\chi\rangle = 0$. Assuming that $\chi \ll 1$, we can expand the potential Eq. (3.6.7) up to second order around $\chi = 0$. The result reads

$$V = f^2 - 3W_0^2 + \frac{1}{2}m^2\varphi^2 + 2mW_0\varphi\chi + \frac{1}{2}\left(f^2 - 2W_0^2 + m^2 + 2m^2\varphi^2\xi_2\right)\chi^2\,, \tag{3.6.14}$$

neglecting the non-zero vev of X. Minimizing this expression with respect to χ we find

$$\chi \simeq -\frac{2mW_0\varphi}{f^2 - 2W_0^2 + m^2 + 2m^2\varphi^2\xi_2}\,, \tag{3.6.15}$$

during inflation. Notice that Eq. (3.6.15) depends on f and W_0, as well as on φ, and that only the imaginary part of S receives a shift.

Numerical simulations

Using a numerical analysis we can verify that S indeed remains stabilized in its new minimum for the entire inflationary epoch. While the inflaton slowly rolls down its quadratic potential the stabilizer field trails its inflaton-dependent minimum near-instantly, see Fig. 9.

Therefore, S can still be treated as a heavy degree of freedom and can be integrated out at its shifted vev given by Eq. (3.6.15). This yields an effective potential for the inflaton direction which reads

$$V(\varphi) = f^2 - 3W_0^2 + \frac{1}{2}m^2\varphi^2\left(1 - \frac{4W_0^2}{f^2 - 2W_0^2 + m^2 + 2m^2\varphi^2\xi_2}\right)\,. \tag{3.6.16}$$

Evidently, depending on the magnitude of f and hence the gravitino mass, the correction resulting from integrating out S may severely alter the predictions of chaotic inflation.

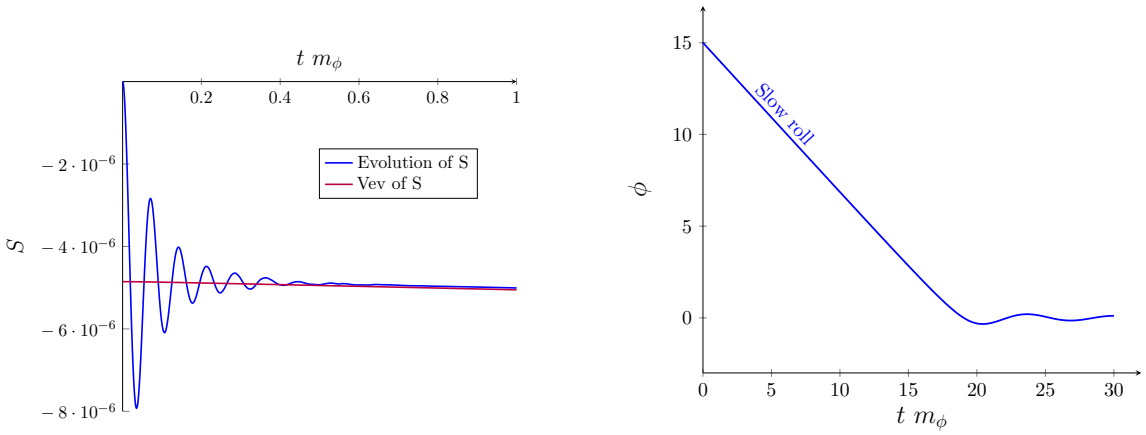

(a) (b)

Figure 9: Evolution of the canonically normalized imaginary part of S (a) and the inflaton φ (b) during inflation, for $\xi_1 = \xi_2 = 10$ and $f = 10^{-8}$. In this case, since $f < m$, cancellation of the cosmological constant implies $W_0^2 = \frac{f^2}{3}$. Depending on its initial value the stabilizer field settles in its shifted minimum very early and remains stabilized for the rest of the inflationary epoch and beyond (notice the different time scales in the plots). Due to its inflaton-dependence, the vev of S evolves with time.

Bounds on the gravitino mass

Considering the effective inflaton potential Eq. (3.6.16), alteration of the CMB observables, in particular the scalar spectral index n_s and the tensor-to-scalar ratio r, is to be expected at $f \gtrsim m$. One can expect that increasing f even further will make inflation unfeasible at a value which satisfies

$$3m^2 \lesssim f^2 \lesssim 2m^2\varphi^2\xi_2\,, \tag{3.6.17}$$

neglecting the correction to W_0 in Eq. (3.6.13). Since m is fixed by observations to be $m \simeq 6 \times 10^{-6}$ in Planck units, it is necessary to specify realistic values of ξ_2 to obtain a meaningful upper bound on the gravitino mass. As we already showed in Section 3.5.1 we can assume that the Kähler potential terms involving ξ_1 and ξ_2 stem from couplings of heavy modes ψ_i to S and X,

$$W_{\text{heavy}} \supset \lambda_1 S\psi_1^2 + \lambda_2 X\psi_2^2 + \text{mass terms}\,, \tag{3.6.18}$$

and hence assume natural values for these parameters to of order

$$\xi_1 \simeq \xi_2 \simeq 10\,. \tag{3.6.19}$$

Evidently, above a value of $f \simeq 8 \times 10^{-5}$ the tensor-to-scalar ratio increases above 0.2 and n_s drops below 0.94, a point at which the model is essentially ruled out by observation. This translates into a bound on the gravitino mass,

$$\boxed{m_{3/2} \lesssim 10^{14}\,\text{GeV}}\,. \tag{3.6.20}$$

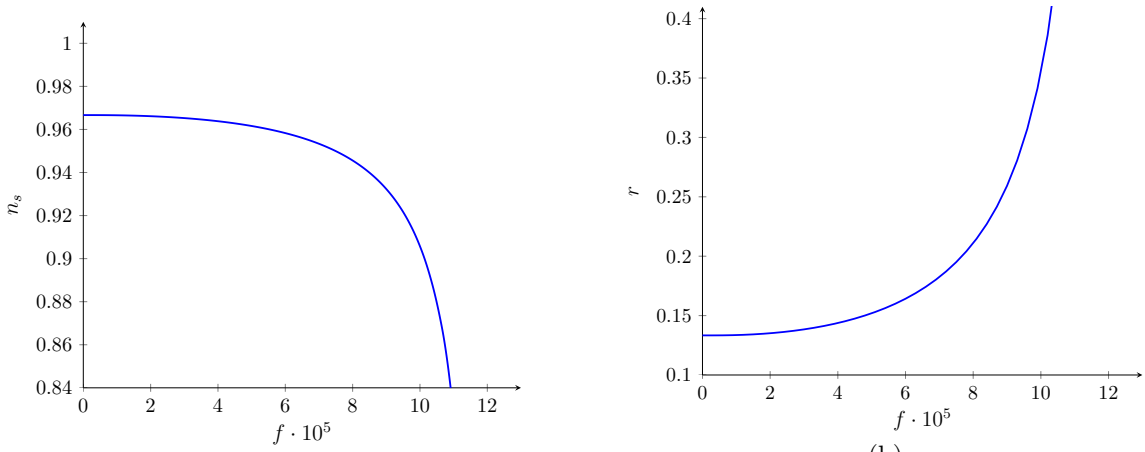

(a) (b)

Figure 10: n_s and r as a function of the supersymmetry breaking scale f. Clearly, the model is ruled out by observation at values of f quite below 10^{-4}.

Therefore, the most minimal way of achieving supersymmetry breaking in chaotic inflation excludes the possibility $m_{3/2} \gtrsim H$, when releasing inflation with the use of a stabilizer field. This may have interesting implications for setups with string-inspired supersymmetry breaking in which the supersymmetry breaking scale is usually very high, as recently investigated in [46, 47, 48].

3.6.3 Effects of additional interactions

As an attempt to relax the gravitino mass bound (3.6.20) it is possible to extend the previous minimal model by a coupling between X and ϕ in the superpotential which preserves the R-symmetry,

$$W = mS\phi + MX\phi + fX + W_0\,. \tag{3.6.21}$$

The new mass scale M contributes, together with m, to the mass of the inflaton, i.e.,

$$V = \frac{1}{2}m^2\varphi^2 \longrightarrow V = \frac{1}{2}(m^2 + M^2)\varphi^2\,, \tag{3.6.22}$$

in the absence of supersymmetry breaking. The associated Kähler potential can be written as

$$K = \frac{1}{2}(\phi + \bar{\phi})^2 + S\bar{S} + X\bar{X} - \xi_1(X\bar{X})^2\,. \tag{3.6.23}$$

Notice that no quartic term in S is needed to stabilize the corresponding scalars in this setup. As before, we can always choose W_0, f, and m to be real, but the mass M is generically complex. For simplicity, we take it to be real in what follows.

Vacuum after inflation

In this framework, the fields are stabilized at different vevs in the vacuum, and the constant W_0

consequently takes a different value to cancel the cosmological constant. Specifically, writing the complex scalars in terms of their real components

$$S = \frac{\psi + i\chi}{\sqrt{2}}\,, \quad X = \frac{\alpha + i\beta}{\sqrt{2}}\,, \quad \phi = \frac{\zeta + i\varphi}{\sqrt{2}}\,, \tag{3.6.24}$$

the associated vacuum expectation values after inflation are given by

$$\langle\varphi\rangle = \langle\chi\rangle = \langle\beta\rangle = 0\,, \quad \langle\zeta\rangle \simeq -\sqrt{2}\frac{Mf}{m^2+M^2}\,, \quad \langle\alpha\rangle \simeq \frac{1}{\sqrt{6}\,\xi_1}\frac{m}{\sqrt{m^2+M^2}}\,, \tag{3.6.25}$$

and

$$\langle\psi\rangle \simeq \frac{M}{(m^2+M^2)^{3/2}}\frac{f^2\,(m^2+3M^2) - 3m^2\,(m^2+M^2)}{3\sqrt{6}\;\xi_1\;m^2}\,, \tag{3.6.26}$$

at leading order in f and $1/\xi_1$. The gravitino mass in the true vacuum is given by

$$m_{3/2} \simeq W_0 \simeq \frac{m}{\sqrt{m^2+M^2}}\frac{f}{\sqrt{3}}\,. \tag{3.6.27}$$

Notice that, as in the model discussed in Section 3.6.2, this vacuum will be corrected for large values of f. The corrections will, however, not alter our conclusions about the allowed gravitino mass by much. Therefore, in what follows we use the value of W_0 stated in Eq. (3.6.27) as a leading-order approximation.

Interaction during inflation

As in the decoupled model discussed in Section 3.6.2, the supersymmetry breaking scale f induces a shift of the imaginary part of S during inflation. In fact, some of the other real scalars are shifted as well, but their vevs are suppressed compared to that of χ and will therefore be neglected in what follows. A numerical analysis once more confirms that all vevs are reached quickly and that all fields, except the inflaton φ, remain stabilized during inflation. In the same manner as in the previous section, expanding up to second order in χ and integrating out the field gives a leading-order effective potential for the inflaton. The result reads

$$\begin{aligned} V(\varphi) \;=\; & \frac{1}{2}(1+\delta^2)m^2\varphi^2\left(1 - \frac{8f^2}{f^2(2+8\delta^2+6\delta^4) + 3m^2(1+\delta^2)^2(2+\delta^2\varphi^2)}\right) \\ & + f^2\left(1 - \frac{1}{1+\delta^2}\right)\,, \end{aligned} \tag{3.6.28}$$

where we have introduced the dimensionless parameter

$$\delta = \frac{M}{m}\,. \tag{3.6.29}$$

Notice that, in the limit $\delta \to 0$, Eq. (3.6.28) reduces to the effective potential of the minimal model in Section 3.6.2, given by Eq. (3.6.16). The only difference is that in the present setup $\xi_2 = 0$. Again, it appears that in this model chaotic inflation is not possible for arbitrarily large values of f.

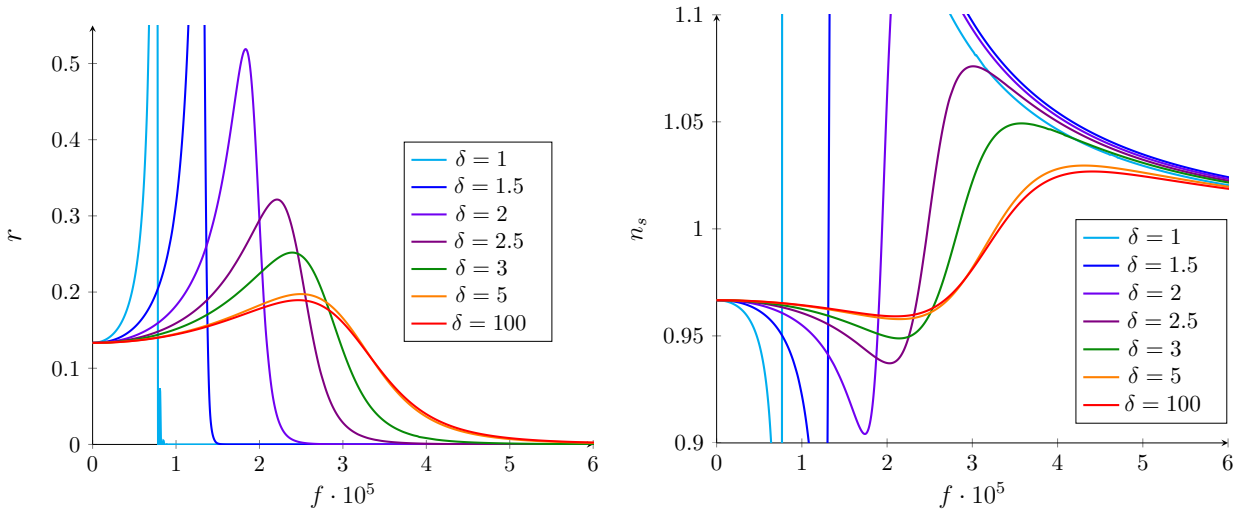

Figure 11: CMB observables as functions of the supersymmetry breaking scale f, for different values of δ and $m = 6 \times 10^{-6}$, $\xi_1 = 10$ in Planck units.

Bounds on the gravitino mass

In fact, it turns out there is a more stringent upper bound on the gravitino mass. The region of parameter space where the model reduces to a single-field inflation model is $\delta > \mathcal{O}(1)$. In this case, there is again a bound stemming from the alteration of the CMB observables due to the presence of f.

To visualize this bound, and how it scales with δ, the observables n_s and r are depicted in Fig. 11 as functions of f. For small values of δ, there is a bound from demanding that r does not surpass 0.2 and n_s does not drop below 0.94, analogous to Section 3.6.2. For larger values of δ, however, these requirements are always fulfilled and a bound on f arises from demanding that n_s does not surpass ~ 0.98. Although increasing δ pushes the bound to slightly higher values of f, this effect saturates at roughly $\delta \sim 10$. However, since for $\delta \gg 1$ the gravitino mass can be written as

$$m_{3/2} = \frac{1}{\sqrt{1+\delta^2}} \frac{f}{\sqrt{3}} \simeq \frac{1}{\delta} \frac{f}{\sqrt{3}}\,, \tag{3.6.30}$$

increasing δ will, at a certain point, actually make the upper bound on $m_{3/2}$ more stringent. It turns out that the least severe upper bound on $m_{3/2}$ is obtained for $\delta \simeq 4$, in which case

$$f \lesssim 3 \times 10^{-5} \quad \Rightarrow \quad m_{3/2} \lesssim 8 \times 10^{12}\,\text{GeV}\,. \tag{3.6.31}$$

Clearly the attempt to relax the bound obtained in the decoupled model of Section 3.6.2 was not successful, since now $m_{3/2} \lesssim 0.1\,H$. One may suspect that this is due to the absence of the large stabilizing term proportional to ξ_2. Indeed, including this term in the present setup trivially reproduces the mass bound Eq. (3.6.20) in the limit $\delta \to 0$. Whenever M, and thus δ, is non-zero, however, the additional coupling will make the bound more severe. In particular, in the regime $\delta \sim \mathcal{O}(1)$ the upper bound on $m_{3/2}$ is very close to the bound obtained using $\xi_2 = 0$.

3.6.4 Supersymmetry breaking in the O'Raifeartaigh model

A minimal way to incorporate chaotic inflation and supersymmetry breaking seems to be contained in the O'Raifeartaigh model, without the addition of extra fields or couplings. In particular, writing the superpotential of [41] as

$$W = X(f + \frac{1}{2}hS^2) + mS\phi + W_0\,, \tag{3.6.32}$$

where the stabilizer S and the inflaton ϕ take up the roles of the two - usually heavy - "O'Raifeartons" and the F-term of X breaks supersymmetry. If ϕ is protected by a shift symmetry, as in the cases studied before, the tree-level Kähler potential takes the form

$$K = \frac{1}{2}(\phi + \bar{\phi})^2 + S\bar{S} + X\bar{X}\,. \tag{3.6.33}$$

Again we can choose W_0, f, and m to be real, in which case the Yukawa coupling h can be complex. For simplicity, we take it to be real in what follows. In this setup, inflation should be possible in the direction of the imaginary part of ϕ. After inflation, ϕ is stabilized at the origin and supersymmetry is broken by X as in the Polonyi model.

However, upon closer inspection the model turns out to be problematic due to tachyonic instabilities during inflation. The F-term of S induces contributions in the scalar potential of the form

$$V \supset m\varphi\, X\bar{S} + \text{c.c.}\,, \tag{3.6.34}$$

i.e., there are mass eigenstates with squared mass

$$m^2_{\text{tach}} \sim -m\varphi \sim -H\,. \tag{3.6.35}$$

Considering the original O'Raifeartaigh model and the discussion involving Eq. (3.5.16) one may hope that quantum corrections from integrating out S can lift these tachyonic directions, but they can not. In order to induce a loop-generated mass term of a size comparable to $\sqrt{H} \sim M_{\text{GUT}}$, heavy modes would have to be integrated out far below the GUT scale. In other words, the coefficient ξ in Eq. (3.5.17) would have to be larger than allowed by the effective field theory if the new states are heavy enough to not perturb the single-field inflation dynamics.

There are two notable ways out to make an O'Raifeartaigh model interacting with the inflaton viable. The first one is invoking microscopic (string theory) contributions to the Kähler potential of the form $(1/\Lambda^2_{\text{UV}})|S|^4$, with a UV cut-off $\Lambda_{\text{UV}} \lesssim M_{\text{GUT}}$. During inflation, these would generate large mass terms for S which would cure the tachyonic contributions. A string theory with $M_{\text{s}} \sim M_{\text{GUT}}$ and α'-corrections to the Kähler potential, plus some additional assumptions on the origin of S, could be responsible for the existence of such terms.

A second solution could be to add a term of the type $\xi_1|X|^4$ with a very large coefficient ξ_1. This would decouple the sgoldstino scalar and again could cure the problem. Technically, this is equivalent to working with a constrained goldstino superfield $X^2 = 0$. The solution is

$$X = \frac{\psi_X\psi_X}{2F_X} + \sqrt{2}\theta\psi_X + \theta^2 F_X\,, \tag{3.6.36}$$

and leads to a non-linearly realized supersymmetry which was discussed in other inflationary contexts in [49, 50, 51, 52, 53]. In our case, the effective action is described by

$$\begin{aligned} K &= \frac{1}{2}(\phi+\bar{\phi})^2 + S\bar{S} + X\bar{X} - \xi|S|^4\,, \\ W &= X\left(f + \frac{1}{2}hS^2\right) + mS\phi + W_0\,, \quad \text{and} \quad X^2 = 0\,. \end{aligned} \tag{3.6.37}$$

Since the superfield X contains no scalar, the dynamics simplifies. As in the previous examples, the only relevant fields during inflation are the inflaton φ and $\mathrm{Im}S = \chi/\sqrt{2}$. At all orders in the inflaton and quadratic order in S, the scalar potential is

$$V \simeq f^2 - 3W_0^2 + \frac{1}{2}m^2\varphi^2 + 2mW_0\varphi\chi + \frac{1}{2}\left(f^2 - 2W_0^2 - hf + m^2 + 2m^2\varphi^2\xi\right)\chi^2\,. \tag{3.6.38}$$

As in the simpler models before, the field χ will track the inflaton trajectory, with a value given by

$$\chi = -\frac{2mW_0\varphi}{f^2 - 2W_0^2 - hf + m^2 + 2m^2\varphi^2\xi}\,. \tag{3.6.39}$$

Since the tracking is very fast, we can write down an effective inflaton potential by inserting Eq. (3.6.39) into the scalar potential Eq. (3.6.38). The result reads

$$V(\varphi) = f^2 - 3W_0^2 + \frac{1}{2}m^2\varphi^2\left(1 - \frac{4W_0^2}{f^2 - 2W_0^2 - hf + m^2 + 2\xi m^2\varphi^2}\right)\,. \tag{3.6.40}$$

Notice that, as in Section 2.2, we neglect the sub-leading correction stemming from the modified cosmological constant cancellation condition for large f.

As is well-known, the O'Raifeartaigh model has two vacua's, depending on the values of the parameters:

- $|hf| > m^2$
  In this case, either the imaginary or the real part of S has a non-zero vev in the ground state in the rigid supersymmetric limit, equal to $\sqrt{2(|hf| - m^2)}/h$. Cancellation of the cosmological constant at leading order is in this case ensured by

  $$m^2(2|hf| - m^2) \simeq 3h^2|W_0|^2\,. \tag{3.6.41}$$

  The gravitino mass in the ground state is given by

  $$m_{3/2} \simeq \frac{m}{\sqrt{3}h}\sqrt{2|hf| - m^2}\,, \tag{3.6.42}$$

  which, for $h \sim O(1)$, is bounded by

  $$m_{3/2} < m\,. \tag{3.6.43}$$

  However, even if h is chosen to be very small to avoid this bound, we expect the CMB observables to receive similar corrections as in the model discussed in Section 2.1, as soon as $f \gtrsim m$.

- $|hf| < m^2$
  In this case, all fields are stabilized at the origin in the true vacuum and $W_0 = \frac{f}{\sqrt{3}}$ cancels the cosmological constant. Again, as can be deduced from the similarity of the effective inflaton potentials, the analysis of Section 2.1 applies to good approximation. Therefore, we expect a bound on the gravitino mass of

$$m_{3/2} \lesssim H \,. \tag{3.6.44}$$

In summary, in the O'Raifeartaigh model with non-linear supersymmetry, imposed by the constraint $X^2 = 0$, the outcome is again an upper bound on the gravitino mass which is similar to the ones obtained in the previously discussed models.

We have proposed here two solutions to make an O'Raifeartaigh model coupled non-trivially to the inflaton viable from the chaotic inflation perspective. The simplest option, however, is clearly to decouple the supersymmetry breaking sector containing the fields χ_i from the inflaton sector containing the inflaton ϕ and the stabilizer S, like for example in models with a superpotential

$$W = W_{\text{O'R}}(\chi_i) + mS\phi \,. \tag{3.6.45}$$

The model of Section 3.6.2 is probably the simplest example of this type.

3.7 Intermediate Conclusions

In this section, we have studied in detail the interplay between large-field inflation and supersymmetry breaking reinforcing the models with small value of the superpotential during inflation, among which we studied models with a 'stabilizer' field coupled to the inflaton and a supersymmetry breaking sector. We found that models with renormalizable couplings of non-gravitational origin between the inflaton and the supersymmetry breaking sector are very constrained and difficult to construct. Therefore, the simplest viable models turn out to be the ones in which the coupling between the two sectors is purely gravitational. In all the cases presented above, we found an upper bound on the supersymmetry breaking scale and consequently on the gravitino mass. The precise bound is model-dependent but parametrically of the order of the inflaton mass. Therefore, chaotic inflation is challenged in scenarios like KKLT moduli stabilization, where usually $m_{3/2} > H$ is required. Let us stress that models with "strong moduli stabilization" [54, 55, 56, 57] with a light gravitino, $m_{3/2} \ll m$, were constructed some time ago and are perfectly viable from our perspective, in particular with regard to low-energy supersymmetry or mini-split models. Our results merely emphasize that the complementary high-mass region $m_{3/2} > m$, interesting in some string constructions, is more problematic for chaotic inflation, again in the models with "stabilizer". Our results imply non-trivial constraints on high-scale supersymmetry breaking scenarios, if the inflationary dynamics is of large-field, chaotic type. Models with moderately small (compared to the inflaton mass) scale of supersymmetry breaking [54, 55, 56, 57] are therefore preferable from this viewpoint.

3.8 Moduli Stabilization and Inflation

String Theory is probably one of the most exciting and popular model of unification, assembling all together the different interactions of nature in a single mathematical formulation. Yet it

requires a tedious treatment, after compactifying extra dimensions that one cannot see in our 4D world, so that higher dimensional objects present in the 10D or 11D formulation of M-Theory do not destroy our experimentally constrained four dimensional phenomenology of physics.

One challenging goal for String Theory and Supergravity is to construct a theoretical model of compactification in which our 4D world arises to be a de Sitter vacuum (as it was indicated by experimental data [58, 59]). For theoretical reasons [60, 61, 62] the latter cannot be achieved at the leading order action of either 10D or 11D formulation of M-Theory, in a g_s and α' expansion. Yet it was proposed by Kachru, Kallosh, Linde and Trivedi in 2003 [63] to use quantum α' corrections and extended objects like D-branes to build a dS solution of String Theory. We will first review this model and its implication in a first section before entering a more general discussion on the role of supersymmetry breaking in achieving both moduli stabilization and a proper inflationary scenario. This work has been published in [64] in collaboration with W. Buchmuller, E. Dudas, A. Westphal, C. Wieck and M. Winkler.

3.8.1 Introduction to String Inspired Models : the KKLT proposal

Working in type IIB string theory, compactified on a Calabi Yau (CY) manifold in the presence of fluxes, one can assume that the complex structure moduli and the dilaton are fixed [65] and deal with stabilizing the remaining Kähler moduli (assuming the compactification overall volume is the only remaining Kähler modulus). At leading order in α' and g_s the latter is not fixed, due to a no-scale structure, and one will need to include corrections breaking the no-scale structure of the lagrangian to do so.

In particular, in the presence of non zero flux, one gets for the Calabi Yau moduli [66, 67, 68] a superpotential of the form

$$\mathcal{W} = \int_{\mathcal{M}} G_3 \wedge \Omega \,, \tag{3.8.1}$$

where $G_3 = F_3 - \tau H_3$ with τ being the axio-dilaton, Ω the $(3,0)$ holomorphic form, and F_3, G_3 being the three-form fluxes in type IIB arising from NS and RR sectors respectively.

The tree level Kähler potential reads in this case

$$\mathcal{K} = -3\ln\left[T+\bar{T}\right] - \ln\left[S+\bar{S}\right] - \ln\left[-i\int_{\mathcal{M}} \Omega\wedge\bar{\Omega}\right] \,, \tag{3.8.2}$$

where T is the single overall volume modulus.

One can show that, by a suitable choice of H_3, F_3, the complex structure moduli, the dilaton and the moduli of D7 branes (in type IIB language) are completely fixed, with masses at the scale – rendered arbitrarily large by the latter choice –

$$m \sim \frac{\alpha'}{R^3} \,, \tag{3.8.3}$$

R being the radius of the compactification manifold $\mathcal{M}$, and that the only remaining dynamical fields are Kähler moduli, in particular the overall volume T

For stabilizing the latter, it was proposed in [63] to include D3 branes [69] or stacks of N_c D7 branes wrapping four-cycles on the compactification manifold. In the second case, gluino condensation under the $\mathcal{N}=1$ supersymmetric $SU(N_c)$ arising in the low energy theory leads to write a superpotential of the form

$$\mathcal{W}_{gauge} = Ae^{-\frac{2\pi T}{N_c}} \equiv Ae^{-aT} \,, \tag{3.8.4}$$

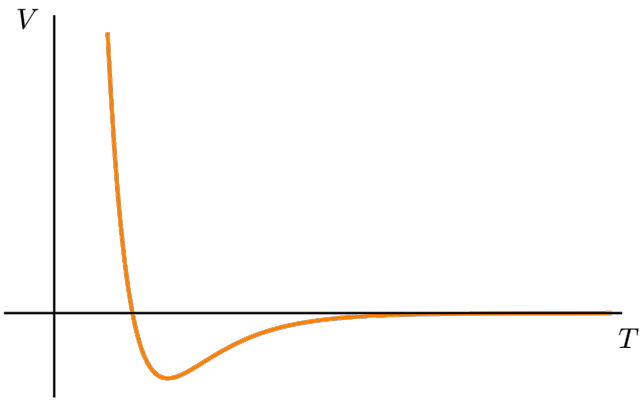

Figure 12: Schematic representation of the supersymmetric AdS vacuum obtained in the unlifted version of the KKLT model.

where A is determined by the energy scale under which the associated $SQCD$ theory is valid.

The so called $KKLT$ model, thus proposes to study the moduli stabilization with the lagrangian

$$\begin{cases} \mathcal{K} &= -3\ln\left[T+\bar{T}\right] , \\ \mathcal{W} &= Ae^{-aT}+W_0 , \end{cases} \tag{3.8.5}$$

W_0 being the tree level contribution generated by the fluxes.

Such lagrangian was studied and shown to produce an AdS supersymmetric vacuum, as depicted in Fig. 12. To construct a dS solution, it was argued in [63] that the presence of anti $\overline{\text{D3}}$ branes transverse to the compactification manifold would contribute to the energy density – breaking slightly supersymmetry – through the uplift

$$\delta V \sim \frac{1}{(T+\bar{T})^2} , \tag{3.8.6}$$

where D depends on the number of $\overline{\text{D3}}$ branes involved[2]. The value of the minimum of T appears to be in this case almost identical to the previous AdS minimum location and the mass of the latter field arises to be very large compared to the tuned cosmological constant. The potential ends up with the shape represented in Fig. 13 where one can of course notice the presence of a *runaway* vacuum at infinity. The finite dS vacuum turns hence out to be metastable, and a possible destabilization of the modulus would have dramatical consequences since it would de-compactify the Calabi Yau manifold.

The AdS vacuum being supersymmetric, one can estimate the depth of the minimum in Fig. 12 to be of order

$$V_{AdS} = -3e^{\mathcal{K}}|\mathcal{W}|^2 = -3m_{3/2}^2 . \tag{3.8.7}$$

One can in addition translate this result in the presence of the uplift (3.8.6) showing that in this case $D_T\mathcal{W}(T_0^{dS}) \ll \mathcal{W}(T_0^{dS})$ and hence

$$m_{3/2}^2 \approx \frac{V_{AdS}}{3} \approx \frac{V_{barrier}}{3} . \tag{3.8.8}$$

[2]More generally, the uplift can take the form $\delta V \sim (T+\bar{T})^{-n}$ where $n=2$ in the case of anti D3 branes and $n=3$ in the case of an F-term uplift.

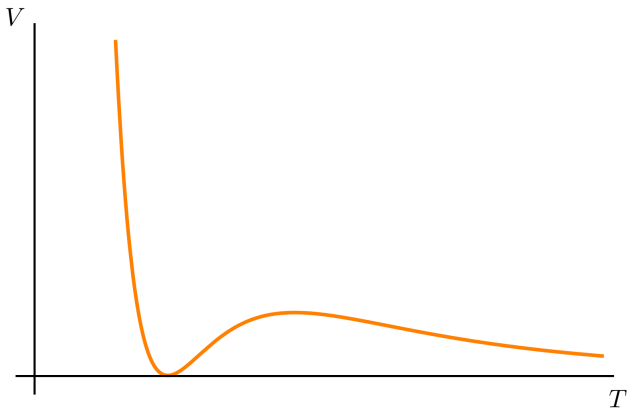

Figure 13: Schematic representation of the dS vacuum obtained after uplifting of the AdS vacuum obtained in the KKLT model.

As we will see in what follows, this has strong consequences while trying to couple gravitationally an inflationary sector to the KKLT model of moduli stabilization. Indeed, a typical energy scale during inflation has a dependence[3] in ρ and ϕ of the sort

$$V_{tot}^{infl.} \approx V_{KKLT}(T) + \frac{V(\phi)}{(T+\bar{T})^n} \,. \tag{3.8.9}$$

Consequently, such term destabilize the potential for $V^{infl.} \gg V_{barrier} \sim m_{3/2}$, see Fig. 14. Since during inflation $V_{infl.} = \frac{H^2}{3}$ this condition requires that the gravitino mass satisfies

$$H \lesssim m_{3/2} \,. \tag{3.8.10}$$

We will illustrate this bound in more detailed analysis in what follows. Alternatively, one can reconcile a small value of the gravitino mass by using different kinds of stabilization for pulling up the potential and obtain a dS vacuum. This was proposed in [54, 70] using a *racetrack-type* superpotential with two exponents

$$\mathcal{W} = W_0 + Ae^{-a\rho} + Be^{-b\rho} \,. \tag{3.8.11}$$

In this case, the addition of two extra parameters allows a fine-tuning such that one can get (see Fig. 15) either one Minkowski and one AdS vacuum either two different AdS vacua's, as well as a barrier whose height is independent on the gravitino mass and can be rendered – by an appropriate choice of parameters – arbitrarily large, while the gravitino can be tuned to be very small

$$H \gg m_{3/2} \,. \tag{3.8.12}$$

The case of two AdS minima can further be uplifted by adding an O'Raifeartaigh sector giving rise to the O'KKLT model [35] that we will not describe in detail in this work.

In the following sections we will investigate in more details, how one can embed quadratic inflation into supergravity including a moduli stabilization sector. As we will see, this will lead to modifications such that quadratic inflation could remain a viable possibility from the experimental constraints viewpoint.

[3]Note that we have redefine ρ such that $-i(\rho - \bar{\rho}) \to (\rho + \bar{\rho})$, notation to which we will stick for convenience in the rest of the thesis.

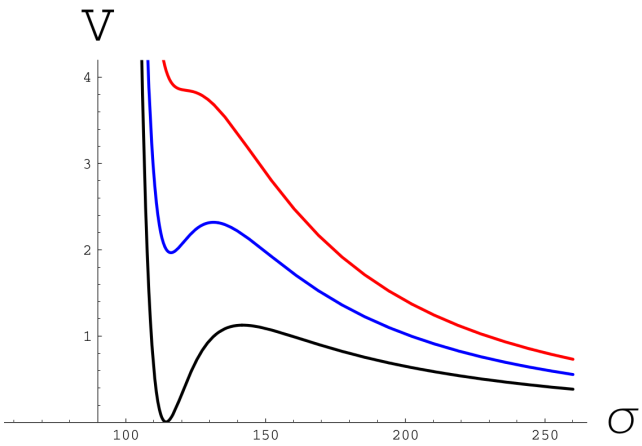

Figure 14: Figure extracted from [54]. The lowest curve stands for the one of the standard KKLT model. The second one describes, e.g., the inflationary potential with the term $V_{infl.} = \frac{V(\phi)}{(\rho+\bar{\rho})^3}$ added to the KKLT potential. The top curve shows that when the inflationary potential becomes too large, the barrier disappears, and the internal space de- compactifies.

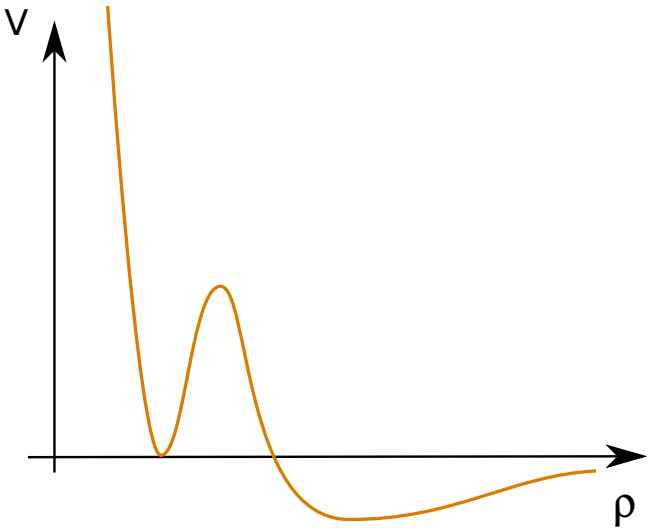

Figure 15: Schematic form of the KL potential in the case of one minkowski vacuum and one Ads minimum.

3.8.2 Non Decoupling Effects of Moduli Stabilization : A Roadmap

In Section 3.6 we have seen how the interplay between a SUSY breaking sector and chaotic inflation with the use of a stabilizer field leads through several examples to a bound which is contrary to the one we just discussed in the light of the KKLT model, that is one requires on the contrary that

$$m_{3/2} \lesssim H \,. \tag{3.8.13}$$

As we will see, setting an upper bound for the gravitino mass is a generic feature of the chaotic inflation implementation with a stabilizer field while one wants to stabilize all the heavy fields present in the theory, including moduli.

Yet, there has been substantial progress in implementing chaotic inflation without a stabilizer, and related models, in string theory. For recent discussions, cf. [47, 71, 48, 72, 73, 74, 75, 76, 77]. In particular, the authors of [74, 75] have analyzed the effects of moduli stabilization in F-term axion monodromy inflation. A general supergravity analysis comparing the scale of inflation and the gravitino mass has been performed in [78, 79]. On the other hand, it has proven difficult to implement the model proposed in [32] in explicit string constructions. For recent treatments, cf.[71, 80], and for a different approach, cf. [81].

As we saw in the previous section, string compactification usually involves many scalar fields that have to be stabilized during and after inflation. We saw how the KKLT model was one proposal for achieving this task, and that supersymmetry breaking may be strongly constrained by this requirement. From the point of view of releasing inflation without a stabilizer field, one may ask whether some of these heavy moduli fields can mitigate the problems of the quadratic inflation model without a stabilizer field that was reviewed in Section 3.5.1. In particular, it may be possible that in no-scale supergravity setups involving moduli fields the negative term which makes V unbounded from below is canceled. In what follows we consider models which only contain Kähler moduli, assuming all other moduli to be stabilized supersymmetrically.

We will make clear in the next section many important points about moduli stabilization. First we will demonstrate that this no-scale cancellation can only happen when the moduli break supersymmetry. In the absence of supersymmetry breaking, fields heavier than the Hubble scale will indeed – which is not that much surprising – completely decouple from the dynamics of inflation, as discussed in [82] and, for the case of chaotic inflation without a stabilizer field, in [43].

On the contrary, we will see that supersymmetry breaking generically induces effects which do not decouple, in particular soft-breaking terms. Therefore, moduli stabilization with broken supersymmetry affects inflation even if the involved fields are heavy and can be integrated out. One can then divide moduli stabilization schemes in two classes.

1. The stabilization of moduli does not (or almost not) induce supersymmetry breaking. This means that the moduli masses and the inflaton mass are much bigger than the scale of supersymmetry breaking, given by the gravitino mass $m_{3/2}$. In this case, the moduli can decouple with little effects on the dynamics of inflation, cf. [82]. Examples in this class are those with "strong moduli stabilization", treated in [54, 56], as well as stabilization via world-sheet instanton couplings as discussed in [27]. In models of this class chaotic inflation without a stabilizer does not work because the inflaton potential remains unbounded from below for $\varphi \gtrsim 1$.

2. The stabilization of moduli spontaneously breaks supersymmetry such that the scale of supersymmetry breaking is larger than the inflaton mass. In this case, integrating out the heavy moduli results in substantial effects on the dynamics of inflation. This class is what we will study in detail in this section. Indeed we will investigate how supersymmetry breaking interplays with chaotic inflation different models that are the KKLT model [63] and the Large Volume Scenario [83]. We will see that in all three examples inflation is possible if the gravitino mass is larger than the Hubble scale. Many of the details are, however, different in the three cases. Note that the considered models of moduli stabilization are hardly compatible with the alternative inflation model of [32] which requires the gravitino mass to be parametrically smaller than the inflaton mass [43].

We will finally see that, despite the differences in detail, all considered models reduce to an effective single-field inflaton potential of remarkable universality. The moduli backreact on the inflaton, and the flattened effective potential in all models is of the form

$$V = \frac{1}{2} m_\varphi^2 \, \varphi^2 \left(1 - \frac{\varphi^2}{2\varphi_{\rm M}^2}\right) . \tag{3.8.14}$$

This potential is characterized by the inflaton mass m setting the scale of the potential and position $\varphi_{\rm M}$ of a local maximum induced by the negative quartic terms stemming from integrating out the moduli. Hence, all the setups exposed will be shown to share universal predictions for the CMB observables, in particular $r \gtrsim 0.05$, after imposing the Planck constraints.

3.9 Integrating out Heavy Moduli : General Results

3.9.1 The Generic Picture

In a similar way we proceeded in the last sections, we are interested in supergravity models in which the inflaton field φ is the imaginary part of a complex scalar field $\phi = \frac{1}{\sqrt{2}}(\chi + i\varphi)$ and interacts with heavy moduli and supersymmetry breaking fields, collectively denoted by T_α. Yet in this section we will focus on models without "stabilizer field", that is, the effective action is generically defined by

$$K = K_0(T_\alpha, \overline{T}_{\bar\alpha}) + \frac{1}{2} K_1(T_\alpha, \overline{T}_{\bar\alpha})(\phi + \bar\phi)^2 , \tag{3.9.1}$$

$$W = W_{\rm mod}(T_\alpha) + \frac{1}{2} m \phi^2 , \tag{3.9.2}$$

where the T_α's denote arbitrary moduli fields, much heavier than the inflaton, that one wants to get stabilized, and integrated out during inflation. As already mentioned earlier, these moduli can be integrated out either in a supersymmetric vacuum or breaking supersymmetry at their minimum of potential. We will hence investigate whether both these picture can produce an acceptable inflation scenario in this general framework of chaotic inflation *without* stabilizer.

Supersymmetric decoupling

Let us first have a glance at the simplest chaotic inflation model in supergravity without stabilizer field, including the effect of supersymmetry breaking. The simplest model of this type

is described by

$$K = \frac{1}{2}(\phi + \bar{\phi})^2 + X\bar{X} - \xi_1(X\bar{X})^2\,,$$
$$W_{\rm inf} = \frac{1}{2}m\phi^2 + fX + W_0\,. \tag{3.9.3}$$

Note that we have included here a polonyi field sector to break supersymmetry, compared to the generic form we wrote in Eq. (3.9.1), but this will not change the conclusion of the discussion. However, this model suffers from the same instability problem as in the absence of supersymmetry breaking, as mentioned in Section 3.5.1. This becomes evident to see by inspecting the scalar potential,

$$V = e^K\Bigg\{\left|m\phi\left[1+\frac{1}{2}\phi(\phi+\bar{\phi})\right] + (fX+W_0)(\phi+\bar{\phi})\right|^2 + K^{-1}_{X\bar{X}}\left|f + K_X\left(\frac{1}{2}m\phi^2 + fX + W_0\right)\right|^2 - 3\left|\frac{m\phi^2}{2} + fX + W_0\right|^2\Bigg\}\,. \tag{3.9.4}$$

Indeed, we recover a potential unbounded from below for large ϕ. Since the origin of the problem is the negative supergravity contribution to the potential, at first sight, the presence of a supersymmetrically stabilized modulus ρ can solve the problem via a no-scale cancellation. Note that the effects of stabilized Kähler moduli on similar models of chaotic inflation have been previously studied in [84, 44, 82]. Starting from the Kähler potential

$$K = -3\log(\rho+\bar{\rho}) + \frac{1}{2}(\phi+\bar{\phi})^2 + X\bar{X} - \xi_1(X\bar{X})^2\,, \tag{3.9.5}$$

and superpotential

$$W = W_{\rm mod}(\rho) + W_{\rm inf}(\phi, X)\,, \tag{3.9.6}$$
$$W_{\rm inf}(\phi, X) = \frac{1}{2}m\phi^2 + fX + W_0\,, \tag{3.9.7}$$

the scalar potential reads

$$V = e^K\left\{\frac{(\rho+\bar{\rho})^2}{3}|\partial_\rho W|^2 - (\rho+\bar{\rho})(\partial_\rho W\overline{W} + \overline{\partial_\rho W}W) + K^{\alpha\bar{\alpha}}D_\alpha W D_{\bar{\alpha}}\overline{W}\right\}\,, \tag{3.9.8}$$

where $\alpha = \phi, X$. Thus, the dangerous negative term indeed seems to be canceled due to the no-scale structure of the model.

However, upon closer inspection this cancellation does not occur. During inflation, there is a non-trivial interaction between the inflaton and the modulus field. The modulus vev is shifted by an amount $\delta\rho$, which can be evaluated in an inverse expansion of the modulus mass [82], assuming it is heavy enough. Similar setups with heavy Kähler moduli have been previously studied in [54, 55, 56, 57]. We assume that $W_{\rm mod}$ is such that the scalar potential has a local minimum at $\rho_0 = \bar{\rho}_0 \equiv \sigma_0$ which is supersymmetric and Minkowski,

$$D_\rho W_{\rm mod}(\sigma_0) = W_{\rm mod}(\sigma_0) = 0\,. \tag{3.9.9}$$

The mass of the modulus in the ground state is given by

$$m_\rho = \frac{\sqrt{2\sigma_0}}{3}\, W''_{\rm mod}(\sigma_0)\,, \tag{3.9.10}$$

where primes denote derivatives with respect to ρ. Notice that this stabilization scheme differs from the original proposal by KKLT, in the sense that m_ρ and $m_{3/2}$ are uncorrelated and the modulus can be much heavier than the gravitino.

We want now to visualize how the inflaton potential changes when the modulus is integrated out and taken to be very heavy. Hence, for $m_\rho > H$, in order to guarantee single-field inflation, the shift of the modulus vev $\delta\rho$ can be expanded in powers of H/m_ρ and is given, at leading order, by

$$\delta\rho \simeq \frac{W_{\rm inf}}{\sqrt{2\sigma_0} m_\rho}\,, \tag{3.9.11}$$

which is small, $\delta\rho \leq \sigma_0$, if $m_\rho > \frac{W_{\rm inf}}{(2\sigma_0)^{3/2}}$.

As demonstrated in [82], once the modulus is integrated out at its shifted vev the inflaton potential is corrected by terms which can be expanded in powers of H/m_ρ. The modified inflaton potential reads

$$V = \frac{V_{\rm inf}(\phi_\alpha)}{(2\sigma_0)^3} - \frac{3}{2(2\sigma_0)^{9/2}\, m_\rho}\Big\{ W_{\rm inf}\Big[V_{\rm inf}(\phi_\alpha) + e^K K^{\alpha\bar\alpha}\partial_\alpha W_{\rm inf} D_{\bar\alpha}\overline{W}_{\rm inf}\Big] + \text{ c.c.}\Big\}\,, \tag{3.9.12}$$

at leading order in H/m_ρ. Here $V_{\rm inf}(\phi_\alpha)$ denotes the inflationary potential in the absence of a modulus sector. But this is precisely the potential before the addition of the modulus, Eq. (3.9.30), which is unbounded from below. The leading order correction in Eq. (3.9.12) may be sizable, depending on m_ρ, but cannot solve the problem of unboundedness from below! Therefore, after integrating out ρ at its true minimum **the no-scale cancellation is not effective** since the modulus minimizes its F-term, including the contribution from the inflaton sector.

Coming back to our generic framework (3.9.1), we just saw in this example that for a single heavy modulus T with $K_0(T,\overline{T}) = -3\ln\left(T+\overline{T}\right)$ and $K_1(T,\overline{T}) = 1$ the effects on the dynamics of inflation can be expressed as

$$\begin{aligned} V \approx{}& \frac{V_{\rm inf}(\phi_\alpha)}{(2T_0)^3} - \frac{3}{2(2T_0)^{9/2}\, m_T}\Big\{ W_{\rm inf}\Big[V_{\rm inf}(\phi_\alpha) + e^K K^{\alpha\bar\alpha}\partial_\alpha W_{\rm inf} D_{\bar\alpha}\overline{W}_{\rm inf}\Big] + \text{ c.c.}\Big\} \\ & - \frac{3e^K}{(2T_0)^6\, m_T^2}\Big| K^{\alpha\bar\alpha} D_\alpha W_{\rm inf}\partial_{\bar\alpha}\overline{W}_{\rm inf}\Big|^2\,, \end{aligned} \tag{3.9.13}$$

up to terms suppressed by higher powers of the modulus mass m_T. Evidently, all corrections stemming from integrating out the heavy modulus disappear in the limit $m_T \to \infty$. Of course the study could be held for a more general lagrangian, but we will see in what follows that the discussion would be unchanged.

This conclusion is actually to be expected: if the modulus does not break supersymmetry and is heavy enough to not perturb the single-field chaotic inflation, it will decouple from the inflationary dynamics at leading order. Then the leading-order scalar potential can be obtained in the limit $m_\rho \to \infty$ which results in the original model defined by Eq. (3.9.29). A lighter modulus can certainly change the situation, but for $m_\rho < H$ the model turns into a much more complicated multi-field inflation model.

Effects of supersymmetry breaking
Another solution to this problem is to stabilize the modulus non-supersymmetrically. If the modulus ρ studied earlier would have had a non-vanishing F-term during inflation, it may indeed have canceled the dangerous $-3|W|^2$ term by virtue of the no-scale structure. A similar setup has recently been discussed in [48], where the modulus is stabilized non-supersymmetrically in a Large Volume Scenario.

In the generic framework, if any of the fields T_α was breaking supersymmetry the picture would change. In this case, there are well-known effects that do not decouple from inflation. In the context of low-energy supersymmetric models these lead to soft-breaking terms whose size is controlled by the gravitino mass. In particular, considering spontaneous supersymmetry breaking we expect the effective inflaton potential to be of the form

$$V = V_{\text{SUGRA}} + \frac{c}{2}\tilde{m}m_{3/2}\varphi^2 + \dots \,, \tag{3.9.14}$$

where c is a model-dependent real constant and V_{SUGRA} is to be computed using

$$K = \frac{1}{2}\left(\phi + \bar{\phi}\right)^2 \,, \qquad W = \frac{1}{2}\tilde{m}\phi^2 \,, \tag{3.9.15}$$

with $\tilde{m} = K_1^{-1} e^{\frac{1}{2}K_0(T_0,\overline{T}_0)} m$ and the wave-function normalization $\phi \to K_1^{-1/2}\phi$ to match the notation of Eq. (3.9.2). Notice that in Eq. (3.9.14) a term proportional to $m_{3/2}^2\varphi^2$ is absent due to the shift symmetry $\phi \to \phi + i\alpha$, which is broken softly by the mass term in the superpotential. Computing V_{SUGRA} from Eqs. (3.9.15) while imposing cancellation of the cosmological constant at the end of inflation, $\varphi = 0$, and setting the heavy real scalar $\chi \equiv \sqrt{2}\,\text{Re}(\phi)$ to its minimum at $\langle\chi\rangle = 0$, we find

$$V = \frac{1}{2}\tilde{m}^2\varphi^2 + \frac{c}{2}\tilde{m}m_{3/2}\varphi^2 - \frac{3}{16}\tilde{m}^2\varphi^4 + \dots \,. \tag{3.9.16}$$

Apparently, the second term only decouples from inflation if $m_{3/2} \ll \tilde{m}$. The dots in Eqs. (3.9.14) and (5.1.1) denote sub-leading terms and higher powers in φ, for example terms of order $\mathcal{O}(\tilde{m}m_{3/2}\varphi^4)$. Usually, such terms can be discarded easily. In large-field inflation, however, super-Planckian excursions of φ can make corrections relevant. Therefore, in the following we systematically calculate corrections to the leading-order potential in Eq. (5.1.1). We are curious to find out if corrections from the modulus sector can cancel the third term in the effective potential, which makes V unbounded from below. Furthermore, if the modulus sector has an approximate no-scale symmetry we expect a cancellation of the bilinear soft mass term, i.e., $c \ll 1$. We wish to discuss if, in this situation, chaotic inflation can proceed via the supersymmetric mass term of φ without spoiling the stabilization of moduli.

3.9.2 Integrating out heavy moduli

In the following, we would like to generalize the results of [82], in particular Eq. (3.9.13), to more general supergravity Lagrangians. Starting from Eqs. (3.9.2) we find for the Kähler metric and its inverse

$$K_{I\bar{J}} = \begin{pmatrix} K_{0,\alpha\bar{\beta}} & 0 \\ 0 & K_1 \end{pmatrix} \,, \qquad K^{I\bar{J}} = \begin{pmatrix} K_0^{\alpha\bar{\beta}} & 0 \\ 0 & K_1^{-1} \end{pmatrix} \,. \tag{3.9.17}$$

The indices I and J run over the T_α and ϕ. Accordingly, the scalar potential is given by

$$V = e^{K_0}\Bigg\{ K_0^{\alpha\bar{\beta}}\left[W_\alpha + K_{0,\alpha}\left(W_{\rm mod}(T_\alpha) + \frac{1}{2}m\phi^2\right)\right]\left[\overline{W}_{\bar{\beta}} + K_{0,\bar{\beta}}\left(\overline{W}_{\rm mod}(\overline{T}_{\bar{\alpha}}) + \frac{1}{2}m\bar{\phi}^2\right)\right] + K_1^{-1}m^2|\phi|^2 - 3\left|W_{\rm mod}(T_\alpha) + \frac{1}{2}m\phi^2\right|^2\Bigg\}. \tag{3.9.18}$$

Assuming the cosmological constant to be canceled at $\phi = 0$, i.e., after inflation has ended, means

$$K_0^{\alpha\bar{\beta}}\left[W_\alpha + K_{0,\alpha}W_{\rm mod}\right]\left[\overline{W}_{\bar{\beta}} + K_{0,\bar{\beta}}\overline{W}_{\rm mod}\right] = 3\left|W_{\rm mod}(T_{\alpha,0})\right|^2 . \tag{3.9.19}$$

Furthermore, we assume that the moduli fields adiabatically trace the minimum of their potential during inflation. This is justified as long as their masses are larger than the Hubble scale. We can now integrate out the heavy fields T_α to obtain an effective scalar potential for the inflaton φ. Using Eq. (3.9.19) and using that χ is heavy due to its soft mass and stabilized at the origin we can expand V in powers of the inflaton field,

$$V = e^{K_0}\Bigg\{ K_0^{\alpha\bar{\beta}}\left[W_\alpha + K_{0,\alpha}\left(W_{\rm mod}(T_\alpha) - \frac{1}{4}m\varphi^2\right)\right]\left[\overline{W}_{\bar{\beta}} + K_{0,\bar{\beta}}\left(\overline{W}_{\rm mod}(\overline{T}_{\bar{\alpha}}) - \frac{1}{4}m\varphi^2\right)\right] + \frac{1}{2}K_1^{-1}m^2\varphi^2 - 3\left|W_{\rm mod}(T_\alpha) - \frac{1}{4}m\varphi^2\right|^2\Bigg\} \tag{3.9.20}$$

which can be put under the form

$$V = V_0(T_\alpha, \overline{T}_{\bar{\alpha}}) + \frac{1}{2}V_1(T_\alpha, \overline{T}_{\bar{\alpha}})m\varphi^2 + \frac{1}{4}V_2(T_\alpha, \overline{T}_{\bar{\alpha}})m^2\varphi^4 . \tag{3.9.21}$$

The explicit coefficients V_0, V_1, and V_2 and other details of the computation can be found in the Appendix of [64]. During inflation the fields T_α are displaced from their minima,

$$T_\alpha \;=\; T_{\alpha,0} + \delta T_\alpha . \tag{3.9.22}$$

We can expand the coefficients V_i of Eq. (3.9.21) at leading order in δT_α as long as $|\delta T_\alpha| \ll |T_{\alpha,0}|$ (condition which can be verified a posteriori). Introducing $\rho_\alpha = (T_\alpha, \overline{T}_{\bar{\alpha}})$ this can be written as

$$V = \frac{1}{2}\delta\rho_\alpha M^2_{\alpha\beta}\delta\rho_\beta + \frac{1}{2}\left(V_1 + \frac{\partial V_1}{\partial\rho_\alpha}\delta\rho_\alpha\right)m\varphi^2 + \frac{1}{4}V_2m^2\varphi^4 + \dots , \tag{3.9.23}$$

where $M^2_{\alpha\beta}$ denotes the un-normalized mass matrix of the ρ_α. Again, detail computations can be found in [64]. Minimizing this expression with respect to $\delta\rho_\alpha$ gives,

$$\delta\rho_\alpha = -\frac{1}{2}(M^{-2})^{\alpha\beta}\frac{\partial V_1}{\partial\rho_\beta}m\varphi^2 . \tag{3.9.24}$$

Plugging this back into Eq. (3.9.23) one obtains the effective potential in its most general form,

$$\begin{aligned} V = &\frac{1}{2}V_1\left(T_{\alpha,0}, \overline{T}_{\bar{\alpha},0}\right) m\varphi^2 + \frac{1}{4}V_2\left(T_{\alpha,0}, \overline{T}_{\bar{\alpha},0}\right) m^2\varphi^4 \\ &- \frac{1}{2}\begin{pmatrix} \frac{\partial V_1}{\partial T_\alpha} & \frac{\partial V_1}{\partial \overline{T}_{\bar{\alpha}}} \end{pmatrix} \begin{pmatrix} (m^{-2})^{\alpha\bar{\beta}} & (m^{-2})^{\alpha\beta} \\ (m^{-2})^{\bar{\alpha}\bar{\beta}} & (m^{-2})^{\bar{\alpha}\beta} \end{pmatrix} \begin{pmatrix} \frac{\partial V_1}{\partial \overline{T}_{\bar{\beta}}} \\ \frac{\partial V_1}{\partial T_\beta} \end{pmatrix} m^2\varphi^4 + \dots \,. \end{aligned} \tag{3.9.25}$$

To simplify this expression it is useful to consider a limit in which supersymmetry is weakly broken. This is the case when the supersymmetric mass, i.e., the mass of the fermions associated with the scalars T_α, is much larger than the gravitino mass (With the exception of the goldstino, of course). Specifically, when

$$\text{Eigenvalues}\left[(m_F)_{\alpha\beta}\right] = \text{Eigenvalues}\left[e^{G/2}\left(\nabla_\alpha G_\beta + \frac{1}{3}G_\alpha G_\beta\right)\right] \gg m_{3/2}\,. \tag{3.9.26}$$

Alternatively, one may consider the case where the supersymmetry breaking scale is large but the supersymmetry breaking sector decouples from moduli stabilization. An example for this is supersymmetry breaking in the O'Raifeartaigh model with a very heavy Polonyi field. For both of these possibilities the effective inflaton potential can be expanded to finally obtain the expression

$$\begin{aligned} V \approx &\frac{m\varphi^2}{2}e^{K_0}\left\{-\frac{1}{2}K_0^{\alpha\bar{\beta}}\left(K_{0,\bar{\beta}}D_\alpha W_{\text{mod}} + K_{0,\alpha}\overline{D}_{\bar{\beta}}\overline{W}_{\text{mod}}\right) + mK_1^{-1} + \frac{3}{2}(W_{\text{mod}} + \overline{W}_{\text{mod}})\right\} \\ &+ \frac{m^2\varphi^4}{16}e^{K_0}\Bigg\{-3 + e^{K_0/2}\Big[K_\delta\left(m_F^{-1}\right)^{\beta\delta}\Big[-K_0^{\epsilon\bar{\epsilon}}(K_{\beta\epsilon} + K_\beta K_\epsilon - \Gamma^\gamma_{\beta\epsilon}K_\gamma)\overline{D}_{\bar{\epsilon}}\overline{W}_{\text{mod}} \\ &\qquad + 2D_\beta W_{\text{mod}} + 3K_\beta\overline{W}_{\text{mod}} + 2mK_1^{-2}\left(K_{0,\beta}K_1 - K_{1,\beta}\right)\Big] + \text{h.c.}\Big]\Bigg\}\,, \end{aligned} \tag{3.9.27}$$

which is the desired generalization of Eq. (3.9.13). Notice, however, that the quadratic term is independent of the small-supersymmetry breaking approximation. It is simply the total mass – supersymmetric and soft mass – of the inflaton in the true vacuum, computed from the effective action defined by (3.9.2). Indeed, using the definition of the inflaton $\text{Im}\,\phi = \varphi/\sqrt{2}$ and the supergravity scalar masses in Eqs. (3.6.3), we find that the inflaton mass is

$$m_\varphi^2 = m_{\phi\bar{\phi}}^2 - \frac{1}{2}\left(m_{\phi\phi}^2 + m_{\bar{\phi}\bar{\phi}}^2\right)\,. \tag{3.9.28}$$

It is a straight-forward, though non-trivial exercise to prove that Eq. (3.9.28) equals the mass term in the first line of Eq. (3.9.27).

Using this result we can, in principle, calculate the effective potential with corrections for any model of moduli stabilization described by the ansatz Eqs. (3.9.2). In practice, however, the approximation outlined above to obtain Eq. (3.9.27) – more precisely, the quartic term, as explained above – is not always applicable. In that case, either a more general expression for the effective potential can be used, given by Eq. (3.9.25), or the calculation can be significantly simplified by expanding in small parameters while performing the above analysis. Before demonstrating this in three popular examples of moduli stabilization with spontaneously broken supersymmetry, we give a short remark on chaotic inflation with a stabilizer field.

3.9.3 Chaotic inflation with a stabilizer field

Although we will concentrate in the next sections on simple chaotic inflation model with a quadratic superpotential, we will here make a couple of remarks about the scenario with a stabilizer field. This model has been intensively studied in the literature, and its interplay with supersymmetric moduli stabilization has been treated in [84, 44, 82]. A generalization of the results in [82] can be found analogously to the above analysis.

As a starting point we can consider

$$\begin{aligned} K &= K_0(T_\alpha, \overline{T}_{\bar{\alpha}}) + \frac{1}{2}K_1(T_\alpha, \overline{T}_{\bar{\alpha}})(\phi+\bar{\phi})^2 + K_{S\bar{S}}|S|^2 + \frac{1}{4}K_{S\bar{S}S\bar{S}}|S|^4 + \dots\,, \\ W &= W_{\rm mod}(T_\alpha) + mS\phi\,. \end{aligned} \tag{3.9.29}$$

As before, for simplicity we assume the superpotentials of the moduli sector and inflation sector to be decoupled. The canonically normalized inflaton is $\varphi = \sqrt{2}\mathrm{Im}\,\phi$, and $\psi = \sqrt{2}\mathrm{Im}\,S$. The real parts of ϕ and S are assumed to be stabilized at the origin. The scalar potential is given by

$$\begin{aligned} V = e^K\Big\{ & K_0^{\alpha\bar{\beta}}\left[W_\alpha + K_{0,\alpha}(W_{\rm mod}+mS\phi)\right]\left[\overline{W}_{\bar{\beta}} + K_{0,\bar{\beta}}(\overline{W}_{\rm mod} + \overline{mS\phi})\right] + \; K_1^{-1}m^2|S|^2 \\ & + \frac{1}{K_{S\bar{S}} + K_{S\bar{S}S\bar{S}}|S|^2}\left|\left(1+K_{S\bar{S}}|S|^2\right)m\phi + K_{S\bar{S}}\bar{S}W_{\rm mod}\right|^2 - 3\left|W_{\rm mod}+mS\phi\right|^2\Big\}\,. \end{aligned} \tag{3.9.30}$$

Imposing cancellation of the cosmological constant, Eq. (3.9.19), and stabilization of all T_α and S during inflation, we can again integrate out the heavy T_α and do a similar analysis than we did in the previous section to find, in the near-supersymmetric limit outlined above, the effective inflaton potential

$$\begin{aligned} V \approx \frac{1}{2}m^2\varphi^2\left(K_{S\bar{S}}^{-1}e^{K_0} - \frac{V_1^2}{m_S^2}\right) - \frac{V_1^2 e^{K_0}}{4m_S^4}m^4\varphi^4\Bigg\{ & \frac{K_{S\bar{S}S\bar{S}}}{K_{S\bar{S}}^2} + e^{K_0/2}\Big[K_\delta(m_F^{-1})^{\beta\delta} \\ & \times\left[K_0^{\epsilon\bar{\epsilon}}(K_{\beta\epsilon}+K_\beta K_\epsilon - \Gamma^\gamma_{\beta\epsilon}K_\gamma)\overline{D}_{\bar{\epsilon}}\overline{W}_{\rm mod} - D_\beta W_{\rm mod} - \frac{1}{2}K_\beta\overline{W}_{\rm mod}\right] + \text{h.c.}\Big]\Bigg\}\,, \end{aligned} \tag{3.9.31}$$

where

$$V_1 = V_1\Big|_{S=0} = -\frac{1}{2}e^K\left\{K_0^{\alpha\bar{\beta}}\left(K_{0,\bar{\beta}}D_\alpha W_{\rm mod} + K_{0,\alpha}\overline{D}_{\bar{\beta}}\overline{W}_{\rm mod}\right) - 2(W_{\rm mod}+\overline{W}_{\rm mod})\right\}\,. \tag{3.9.32}$$

Analogous to the case without stabilizer the quadratic term in φ is independent of the small-supersymmetry breaking approximation.

Let us compare this result to the the case without stabilizer, Eq. (3.9.27). Since $V_1 \sim m_{3/2}$ and $m_S^2 \sim \tilde{m}^2 + m_{3/2}^2$, the corrections to the chaotic scalar potential $\frac{1}{2}\tilde{m}^2\varphi^2$, with $\tilde{m} = me^{K_0/2}$, are negligible for $m_{3/2} \ll \tilde{m}$. For large gravitino masses $m_{3/2} \gtrsim \tilde{m}$, on the other hand, the quadratic inflaton term in Eq. (3.9.31) becomes negative and stops inflation. Simultaneously, the quartic term becomes sizeable. Thus, these generic results fit nicely with the explicit analysis performed in [43]. However, remember that Eq. (3.9.31) is only valid in the near-supersymmetric limit. If the supersymmetry-breaking T_α can not be completely decoupled in the fermion mass

matrix, a more general result can be found in [64] concerning the appropriate quartic term in the scalar potential. Since all moduli stabilization schemes with supersymmetry breaking that we consider require a large gravitino mass, it is difficult to reconcile these schemes with chaotic inflation with a stabilizer. Therefore, in the examples treated in the following sections we restrict ourselves to the more interesting models with no stabilizer field.

3.10 Chaotic inflation with KKLT moduli stabilization

As a first example we discuss stabilization of a single Kähler modulus T by the mechanism of KKLT[63] and its interaction with chaotic inflation. Before treating the coupled Lagrangian we discuss important properties of the original KKLT vacuum and its uplift. Many of these are well-known facts, nonetheless it is instructive to review them before discussing the interaction with inflation.

3.10.1 KKLT moduli stabilization and uplift

The possibly simplest setup to stabilize Kähler moduli via non-perturbative effects was proposed in [63]. The original model assumes all complex structure moduli of a compact CY manifold and the dilaton to be stabilized by fluxes, as first developed in [65]. The remaining effective theory contains a single lightest Kähler modulus, in the following denoted by T, which parameterizes the volume of the compact manifold. T then has the following tree-level Kähler potential,

$$K = -3\ln\left(T+\overline{T}\right), \tag{3.10.1}$$

and does not appear in the flux superpotential, W_0, responsible for stabilizing the complex structure and the dilaton. Therefore, T is massless at perturbative tree-level and must be stabilized to avoid a series of well-known problems. This is achieved by employing non-perturbative corrections to the superpotential, so that W takes the form

$$W = W_0 + Ae^{-aT}. \tag{3.10.2}$$

We treat W_0 and A as constants determined by fluxes and vacuum expectation values of complex structure moduli. They are assumed to be real in what follows. A relative phase between A and W_0 can always be compensated by a field redefinition. Depending on whether the non-perturbative term stems from a Euclidean D3 instanton or from a gaugino condensate on a stack of D7 branes, a can be 2π or $\frac{2\pi}{N}$, where N is the rank of the condensing gauge group. The scalar potential

$$V = e^K\left(K^{T\overline{T}}D_T W\overline{D_T W} - 3|W|^2\right), \tag{3.10.3}$$

has two extrema, $\partial_T V = 0$, corresponding to

$$D_T W = 0\,. \tag{3.10.4}$$

One extremum lies at $T=\infty$, where the potential vanishes. In addition there is a supersymmetric AdS vacuum at $\tilde{T_0}$ which is determined by

$$W_0 = -Ae^{-a\tilde{T_0}}\left(1+\frac{2}{3}a\tilde{T_0}\right). \tag{3.10.5}$$

For real parameters of the superpotential $\tilde{T}_0$ is real. $\mathrm{Im}\, T$ is stabilized at the origin at the same mass scale as $\mathrm{Re}\, T$.

To uplift the AdS vacuum to a Minkowski vacuum the authors of [63] introduced an anti-D3 brane. To avoid explicit supersymmetry breaking[4] we resort to uplifting via the F-term of a Polonyi field X, with

$$K_{\rm up} = k\big(|X|^2\big)\ , \qquad W_{\rm up} = fX\,. \tag{3.10.6}$$

Uplifting of AdS vacua's via F-terms of matter fields was first discussed in [86]. We assume that the function k contains a quartic term so that X is stabilized close to the origin at a high scale, and thus the field completely decouples from the dynamics of moduli stabilization and inflation. Such a quartic term may effectively arise from couplings to heavy fields, cf. [41].[5] The only contribution of the Polonyi field to V is then its F-term,

$$V_{\rm up} = e^K f^2\,, \tag{3.10.7}$$

which can be used to cancel the cosmological constant in the true vacuum defined by Eq. (3.10.5).

In addition to the extremum at $T=\infty$ corresponding to $D_T W = 0$, the uplifted scalar potential has two further extrema which are determined by

$$D_T W = -\frac{3W}{4T}\left(1 \pm \sqrt{1 - \frac{2f^2}{(aT+2)W^2}}\right)\,. \tag{3.10.8}$$

The negative sign yields the uplifted AdS minimum,

$$D_T W = -\frac{3f^2}{4aT_0^2\, W|_{T_0}} + \mathcal{O}(T_0^{-3})\,, \tag{3.10.9}$$

where the value of the modulus T is shifted to $T_0 = \tilde{T}_0 + \delta T_{\rm up}$. The shift in T is easily obtained by expanding $D_T W$ in $\delta T_{\rm up}$,

$$\begin{aligned} D_T W|_{\tilde{T}_0} &\approx D_T W|_{T_0} - \delta T_{\rm up}\, \partial_T D_T W|_{T_0} \\ &\approx D_T W|_{T_0} - \delta T_{\rm up}\left((-a + K_T)\, D_T W|_{T_0} + ((a - K_T)\, K_T + \partial_T K_T)\, W|_{T_0}\right)\,. \end{aligned} \tag{3.10.10}$$

Using Eqs. (3.10.4) and (3.10.9) we find

$$\frac{\delta T_{\rm up}}{T_0} \approx \frac{f^2}{2a^2 T_0 W_0^2} + \mathcal{O}(T_0^{-2})\,, \tag{3.10.11}$$

where we have used $W|_{T_0} \approx W_0$. Using Eqs. (3.10.3), (3.10.7), and (3.10.9) one finds that the cosmological constant of the AdS vacuum is canceled by tuning f to

$$f = \sqrt{3} W_0 \left(1 - \frac{3}{2aT_0} + \mathcal{O}(T_0^{-2})\right)\,. \tag{3.10.12}$$

[4] See, however, [85] for a very recent treatment of this issue.

[5] For a more thorough treatment of the dynamics linking supersymmetry breaking and chaotic inflation, cf. [44, 43].

Note that there is a sub-leading contribution of the modulus to supersymmetry breaking,

$$\langle F_T\rangle = e^{K/2}\sqrt{K^{T\overline{T}}}D_T W\Big|_{T_0} \approx -\frac{3\sqrt{3}W_0}{a(2T_0)^{5/2}} \approx -\frac{3\langle F_X\rangle}{4aT_0}\,. \tag{3.10.13}$$

Since $aT_0 \gg 1$ for consistency of the single-instanton approximation, the dominant contribution to supersymmetry breaking stems from the Polonyi field. The gravitino mass in the Minkowski vacuum is given by

$$m_{3/2} = e^{K/2}W = \frac{W_0}{(2T_0)^{3/2}}\left(1 - \frac{3}{2aT_0} + \mathcal{O}(aT_0)^{-2}\right) \approx \frac{W_0}{(2T_0)^{3/2}}\,. \tag{3.10.14}$$

It is closely related to the mass of the canonically normalized modulus,

$$m_T \approx 2aT_0 m_{3/2}\,. \tag{3.10.15}$$

The uplifted Minkowski vacuum is protected by a barrier from the run-away vacuum at $T = \infty$. The height of the barrier can be found by choosing the positive sign in the expression (3.10.8) for the covariant derivative, corresponding to the local maximum in the scalar potential. For the field value of the modulus at the position of the barrier, $T_{\rm B}$, we find

$$V_{\rm B} = V\Big|_{T_{\rm B}} \approx \frac{f^2}{(2T_{\rm B})^3} \sim 3m_{3/2}^2\,. \tag{3.10.16}$$

We are now ready to analyze the effect of chaotic inflation on the uplifted KKLT vacuum. Since the F-term of T does not vanish, one may hope that it can cure the problem of unboundedness which plagues the simplest variant of chaotic inflation. To analyze the two-field system defined by the modulus and the inflaton, it is instructive to use both an analytic and a numerical approach.

3.10.2 KKLT and chaotic inflation: analytic approach

Treating the interaction between the modulus and inflaton sectors in the simplest way, we assume that their superpotentials and Kähler potentials completely decouple. Thus, the theory is defined by

$$W = W_0 + Ae^{-aT} + fX + \frac{1}{2}m\phi^2\,, \tag{3.10.17a}$$

$$K = -3\ln\left(T+\overline{T}\right) + k\left(|X|^2\right) + \frac{1}{2}\left(\phi+\bar{\phi}\right)^2\,. \tag{3.10.17b}$$

In particular, in the notation of Sec. 3.9 we choose

$$W_{\rm mod}(T_\alpha) = W_0 + Ae^{-aT} + fX\,, \tag{3.10.18}$$

$$K_0(T_\alpha, \overline{T}_{\bar{\alpha}}) = -3\ln\left(T+\overline{T}\right) + k\left(|X|^2\right) \tag{3.10.19}$$

$$K_1(T_\alpha, \overline{T}_{\bar{\alpha}}) = 1\,. \tag{3.10.20}$$

Note that the relative phase between W_0 and m is physical. In the following we choose all superpotential parameters to be real, so that only the real part of T is affected by inflation.

Therefore, we set $T = \overline{T}$ in the following discussion. Our results do not change qualitatively if we allow for m and/or W_0 to be complex. Moreover, the Polonyi field X is treated in the way discussed in Sec. 3.10.1. The canonically normalized inflaton field is $\sqrt{2}\mathrm{Im}\,\phi \equiv \varphi$, which does not appear in the Kähler potential. On the inflationary trajectory the superpotential reads

$$W = W_0 + Ae^{-aT} - \frac{1}{4}m\varphi^2 \,. \tag{3.10.21}$$

A natural question to ask is the following: can the effective theory of inflation defined by Eqs. (3.10.17) resemble chaotic inflation, after integrating out T at a high scale?

Leading-order effective potential

To answer this question we solve the equation of motion for T during inflation, $\partial_T V = 0$, which yields for the covariant derivative

$$D_T W = -\frac{3W}{4T}\left[1 \pm \sqrt{1 - \frac{2}{(aT+2)W^2}\left(f^2 + \frac{1}{2}m^2\varphi^2\right)}\right] , \tag{3.10.22}$$

which implicitly determines T as function of φ. In addition, there is the extremum at $T = \infty$ with $D_T W = V = 0$. The negative sign in Eq. (3.10.22) again yields the uplifted AdS minimum,

$$D_T W = -\frac{3}{4aT^2}\frac{f^2 + \frac{1}{2}m^2\varphi^2}{W} + \mathcal{O}(T^{-3}) \,. \tag{3.10.23}$$

Using Eqs. (3.10.21) and (3.10.23) we obtain for the effective inflaton potential

$$\begin{aligned} V(\varphi) &= \frac{1}{(2T)^3}\left(f^2 + \frac{1}{2}m^2\varphi^2 - 3W^2 + \mathcal{O}(T^{-2})\right) \\ &= \frac{1}{2}\tilde{m}^2\varphi^2 + \frac{3}{2}\tilde{m}m_{3/2}\varphi^2 - \frac{3}{16}\tilde{m}^2\varphi^4 + \mathcal{O}\left(\frac{\delta T}{T_0}\right) , \end{aligned} \tag{3.10.24}$$

with $\tilde{m} = \frac{m}{(2T_0)^{3/2}}$ and $m_{3/2}$ given by Eq. (3.10.14). The corrections of order $\delta T/T_0$ are due to the φ-dependent shift of the modulus, $\delta T(\varphi) = T(\varphi) - T_0$. Thus, it seems that after integrating out T the negative definite term proportional to $\tilde{m}^2\varphi^4$ still appears in the potential, making it unbounded from below. This is related to the fact that the modulus is only a sub-leading source of supersymmetry breaking. Notice that this way of obtaining the leading-order potential is equivalent to the naive treatment outlined in Sec. 3.9.1, which resulted in Eq. (5.1.1).

However, things are not quite as they seem by merely studying the result Eq. (3.10.24). For large values of φ, i.e., when the quartic term in the effective potential dominates, the modulus can be destabilized by the potential energy of φ. In this case, the inflationary trajectory becomes tachyonic and the modulus can no longer be integrated out. To see when this point is reached, it suffices to consider the structure of Eq. (3.10.22). A necessary condition for the existence of real solutions for $D_T W$ is clearly $W^2 \gtrsim 0$. For $W^2 \approx 0$, the uplifted AdS minimum and the maximum merge in a saddle point. Using Eq. (3.10.21) we then obtain an upper bound on allowed values of φ,

$$\tilde{m}\varphi^2 \lesssim 4m_{3/2} \,. \tag{3.10.25}$$

This is the well-known bound $H < m_{3/2}$ stressed in [54], as will become more clear in our numerical example in Sec. 3.10.3. There, a more detailed analysis reveals that the modulus is destabilized slightly before the above bound is saturated. In fact, the local maximum of the effective inflaton potential Eq. (3.10.24) is never reached while the modulus is stabilized.[6]

Corrections to the effective potential

The corrections to the effective potential are determined by the shift of the modulus field $\delta T(\varphi) = T(\varphi) - T_0$.[7] Expanding the covariant derivative in δT and φ^2, analogous to Eq. (3.10.10), we find

$$\frac{\delta T}{T_0} = \frac{\tilde{m}\varphi^2}{4aT_0 m_{3/2}} + \mathcal{O}(T_0^{-2})\,. \tag{3.10.26}$$

With this, the effective inflaton potential including the leading-order correction becomes, at quartic order in φ and leading order in $(aT_0)^{-1}$ and $\tilde{m}/m_{3/2}$

$$V(\varphi) = \frac{1}{2}\tilde{m}^2\varphi^2 + \frac{3}{2}\tilde{m}m_{3/2}\varphi^2 - \frac{3}{16}\tilde{m}^2\varphi^4 - \frac{3}{4aT_0}\left(3\tilde{m}m_{3/2}\varphi^2 + \frac{3}{4}\tilde{m}^2\varphi^4\right) + \dots\,. \tag{3.10.27}$$

To obtain higher-order corrections to the potential, the potential must be expanded to higher orders in δT, and δT must be computed up to higher powers in T_0^{-1}.

So far we have analyzed the deformation of the Minkowski vacuum due to the inflaton field starting from the covariant derivative. Alternatively, on can directly find the shift $\delta T(\varphi)$ by minimizing the scalar potential,

$$V = V|_{T_0} + (\partial_T V)|_{T_0}\delta T + \frac{1}{2}(\partial_T^2 V)|_{T_0}\delta T^2 + \mathcal{O}(\delta T^3)\,, \tag{3.10.28}$$

along the lines of the general analysis in Sec. 3.9.2. One then expects that the shift δT is inversely proportional to the modulus mass, cf. Eq. (3.9.24). Eq. (3.10.26) can indeed be rewritten in this form,

$$\frac{\delta T}{T_0} = \frac{\tilde{m}\varphi^2}{2m_T} + \mathcal{O}(T_0^{-2})\,. \tag{3.10.29}$$

In a manner similar to integrating out T, it is possible to verify that the displacement δX of the Polonyi field during inflation gives negligible contributions to the inflaton potential. For the particular choice

$$k\left(|X|^2\right) = |X|^2 - \frac{|X|^4}{\Lambda^2}\,, \tag{3.10.30}$$

for example, the displacement of X is at leading order

$$\delta X = \Lambda^2 \delta T\,. \tag{3.10.31}$$

Since $\Lambda \ll 1$ to stabilize X at a high scale with a small vacuum expectation value, the contribution of integrating out X at Eq. (3.10.31) is clearly negligible.

Among other things, this means that the sector which dominates supersymmetry breaking can be completely decoupled from the dynamics of inflation. In this case, it is possible to obtain the effective potential Eq. (3.10.27) essentially by applying the general expression Eq. (3.9.27).

[6] In fact, the full potential defined by Eqs. (3.10.17) is bounded from below at all points in field space.

[7] Notice that for real superpotential parameters the displacement of T is real as well.

3.10.3 A numerical example

Let us now study whether 60 e-folds of inflation can be realized with the effective inflaton potential Eq. (3.10.27), and if the resulting predictions for the CMB observables resemble those of chaotic inflation. It is worth noting that in the parameter regime where T is stabilized, i.e., when $m_{3/2}$ is very large, the bilinear term proportional to $\tilde{m}m_{3/2}$ actually dominates in V and drives inflation. In this case, the relevant terms in the inflaton potential are

$$V(\varphi) \approx \frac{3}{2}\tilde{m}m_{3/2}\varphi^2\left(1-\frac{1}{8}\frac{\tilde{m}}{m_{3/2}}\varphi^2\right) . \tag{3.10.32}$$

Consequently, inflation is only possible if $\tilde{m}$ and $m_{3/2}$ have the same sign. With Eq. (3.10.16) the corrections can be interpreted as a power series in $\frac{H^2}{V_{\rm B}}$, the squared Hubble scale divided by the barrier height of the modulus potential. This is a natural expansion parameter because the modulus is destabilized when the vacuum energy of φ lifts the modulus over the barrier, cf. the bound found in Eq. (3.10.25). Neglecting order-one coefficients, COBE normalization imposes $\sqrt{|\tilde{m}m_{3/2}|} \sim 3\times 10^{-6}$. This puts a lower bound on the gravitino mass, i.e.,

$$m_{3/2} > \sqrt{|\tilde{m}m_{3/2}|}\,\varphi_\star \sim 5\times 10^{-5} \sim H\,, \tag{3.10.33}$$

where $\varphi_\star \approx 15$ denotes the inflaton field value at the beginning of the last 60 e-folds of inflation. This means that the gravitino must be very heavy and there is a moderate hierarchy between the gravitino and inflaton mass for 60 e-folds of chaotic inflation to be possible. This is illustrated in Fig. 16 for a suitable set of parameters.

Indeed, 60 e-folds of inflation can take place starting at $\varphi_\star \approx 15$. The CMB observables in our example are found to be

$$\begin{aligned} n_{\rm s} &= 0.966\,, \\ r &= 0.106\,, \end{aligned} \tag{3.10.34}$$

which are slightly below the predictions of pure quadratic inflation. This is due to the flattening of the quadratic potential by the negative quartic term. Notice that the modulus is destabilized and the inflaton trajectory becomes tachyonic at the critical value $\varphi_{\rm c} \approx 24$, corresponding to the bound in (3.10.25). Therefore, Eq. (3.10.32) and the dashed line in Fig. 16 are only meaningful up to this point.

Moreover, the interplay between inflaton and modulus can be illustrated by means of the full scalar potential as a function of T and φ, depicted in Fig. 17. The minimum in the modulus direction is uplifted as φ increases, until the point where it disappears at $\varphi_{\rm c} \approx 24$.

3.11 Chaotic inflation and the Large Volume Scenario

3.11.1 LVS moduli stabilization and uplift

Another well-known example of moduli stabilization with spontaneously broken supersymmetry is the Large Volume Scenario developed in [83]. It is based on the observation that, for certain types of CY compactifications with multiple Kähler moduli, the scalar potential may have a non-supersymmetric AdS minimum at exponentially large volume. A particularly simple

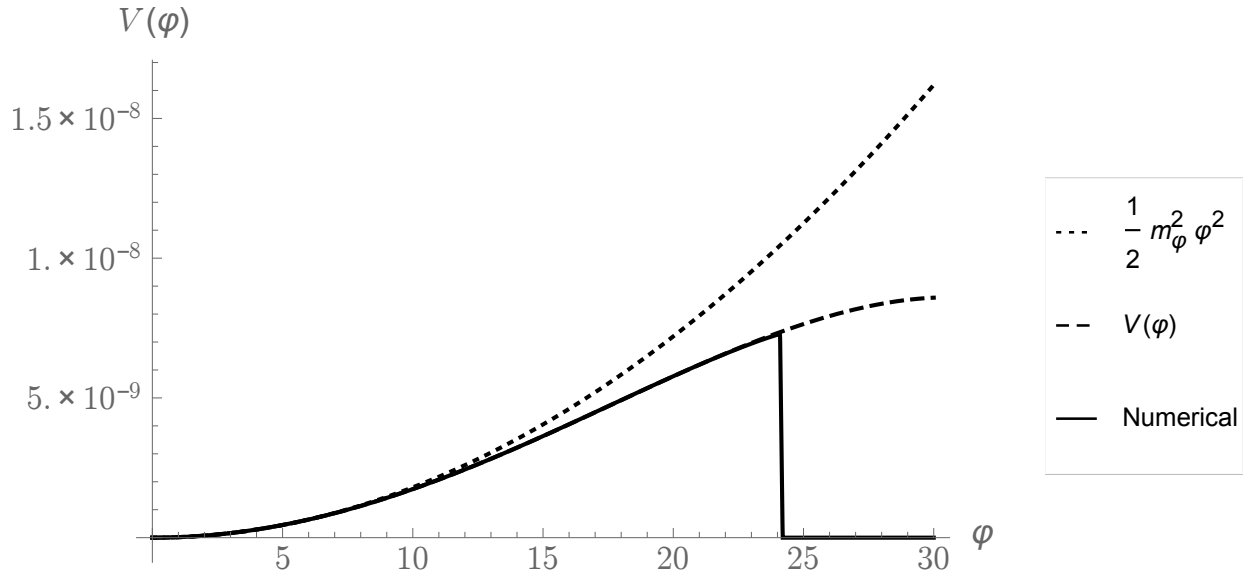

Figure 16: Effective inflaton potential in KKLT for $W_0 = 0.009$, $A = -0.75$, $a = \frac{2\pi}{10}$, and $m = 1.67 \times 10^{-5}$. With these parameters we find $T_0 = 10$ and $m_{3/2} = 10^{-4}$. The dotted line denotes a purely quadratic potential with $m_\varphi = 6 \times 10^{-6}$ imposed by COBE normalization. The dashed line is the effective potential Eq. (3.10.27) evaluated at all orders in $(aT_0)^{-1}$. This potential is valid only as long as the modulus remains stabilized. The solid line is obtained numerically by setting the modulus to its minimum value at each value of φ. Evidently, above the critical value $\varphi_c \approx 24$ the modulus is destabilized towards the run-away minimum at $T = \infty$ and the theory can not be described by Eq. (3.10.27) any longer.

example of this type is given by a "swiss-cheese" CY manifold with a single "hole", i.e., a manifold whose volume is parameterized by

$$\mathcal{V} = (T_\mathrm{b} + \overline{T}_\mathrm{b})^{3/2} - (T_\mathrm{s} + \overline{T}_\mathrm{s})^{3/2}\,, \tag{3.11.1}$$

where T_b is the Kähler modulus of some big four-cycle, i.e., the "cheese", and T_s controls the volume of a small four-cycle, the "hole". The simplest setup for a Large Volume Scenario is then described by

$$W = W_0 + Ae^{-aT_\mathrm{s}}\,, \tag{3.11.2}$$

and

$$K = -2\ln(\mathcal{V} + \xi)\,, \tag{3.11.3}$$

with $\xi = -\frac{\zeta(3)}{4(2\pi)^3}\chi\langle \mathrm{Re}\, S\rangle^{3/2}$ where χ denotes the Euler number of the compactification manifold and S denotes the dilaton. Throughout this work we assume the dilaton to be stabilized supersymmetrically at a high scale so that ξ can be treated as a constant. As in the previous examples we consider real superpotential parameters, and hence restrict our attention to the real parts of the moduli, i.e., we set $T_\mathrm{b,s} = \overline{T}_\mathrm{b,s}$ in the following.

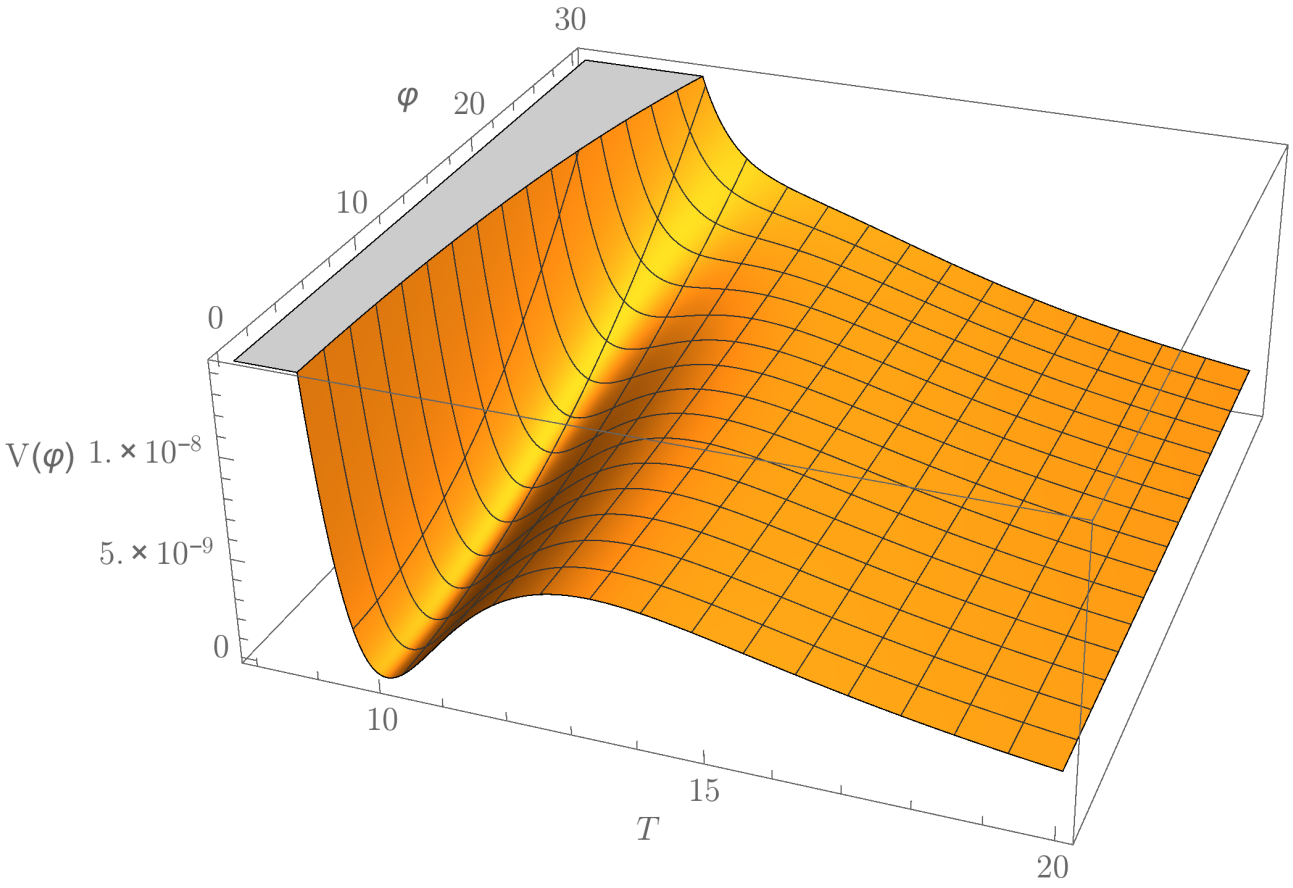

Figure 17: Scalar potential as defined by Eqs. (3.10.17) as a function of T and φ, for the same parameter example as in Fig. 16. Apparently, a minimum for the modulus exists for $\varphi \lesssim \varphi_c \approx 24$. Beyond this point the modulus runs away towards $T = \infty$ and can no longer be integrated out. For $\varphi < \varphi_c$ inflation may take place in the valley of the uplifted modulus minimum.

The extrema of the potential satisfy the two equations $\partial_{T_b} V = \partial_{T_s} V = 0$. Since the superpotential does not depend on T_b, they lead to two quadratic equations for $D_{T_s} W$ which can be rewritten as

$$D_{T_s} W = \tilde{Y} W \,, \qquad \tilde{Z}_i = 0 \,. \tag{3.11.4}$$

The functions $\tilde{Y}$ and $\tilde{Z}_i$ are functions of a and various derivatives of the Kähler that can be found in [64]. Assuming that $\mathcal{V}$ is large and expanding K_{T_s} and $\tilde{Y}$ in powers of $\mathcal{V}^{-1}$, the equation for $D_{T_s} W$ yields

$$\partial_{T_s} W|_{T_0} = aAe^{-aT_0} \approx \frac{3(2T_0)^{1/2}}{2\mathcal{V}_0} W_0 \,. \tag{3.11.5}$$

Eq. (3.11.5) determines the volume in terms of T_0,

$$\mathcal{V}_0 \approx \frac{3\sqrt{T_0} e^{aT_0} W_0}{\sqrt{2} aA} \left(1 - \frac{3}{4aT_0}\right) , \tag{3.11.6}$$

at next-to-leading order in $(aT_0)^{-1}$. The second equation in (3.11.4) determines the value of T_s. Using the large volume expansions for the functions $\tilde{Z}_i$ one finds

$$T_0 \approx \frac{\xi^{2/3}}{2}\left(1+\frac{2}{3a\xi^{2/3}}\right)+\mathcal{O}\left((a\xi^{2/3})^{-2}\right)\,. \tag{3.11.7}$$

At leading order in $\mathcal{V}^{-1}$, T_0 only depends on ξ and a. Eqs. (3.11.6) and (3.11.7) can also be obtained by considering the scalar potential in the large volume limit,

$$V \approx \frac{2\sqrt{2}\,a^2A^2\sqrt{T_\mathrm{s}}\,e^{-2aT_\mathrm{s}}}{3\mathcal{V}}-\frac{4aAW_0T_\mathrm{s}\,e^{-aT_\mathrm{s}}}{\mathcal{V}^2}+\frac{3\xi W_0^2}{2\mathcal{V}^3}\,. \tag{3.11.8}$$

To obtain this form the imaginary part of T_s has been fixed at $\langle \mathrm{Im}\, T_\mathrm{s}\rangle = \frac{\pi}{a}$. In this case, W_0 and A must have the same sign for the stabilization mechanism to work. Minimizing V with respect to $\mathcal{V}$ and T_s one finds the local AdS minimum with the values $\mathcal{V}_0$ and T_0 given above.

The depth of the AdS vacuum is

$$V_\mathrm{AdS} \sim -\frac{W_0^2}{\mathcal{V}_0^3}\,, \tag{3.11.9}$$

rather than $W_0^2/\mathcal{V}_0^2$ as one may naively expect. This is due to the approximate no-scale cancellation between F_{T_b} and W_0^2. To achieve a complete uplift to a Minkowski vacuum we employ, once more, a Polonyi field X as a toy example. Treating the uplift in the same way as in KKLT moduli stabilization, we assume that X is stabilized with a nearly-vanishing vacuum expectation value.[8] However, in the LVS scheme the quartic term in the Kähler potential is not required as X is stabilized by its soft mass term. The contribution of the Polonyi field then amounts to a term $V_\mathrm{up} = \frac{f^2}{\mathcal{V}^2}$ in the scalar potential. To cancel the cosmological constant in the vacuum, it must be

$$f^2 \approx \chi_0 W_0^2\,, \qquad \chi_0 = \frac{9\sqrt{2T_0}}{2a\mathcal{V}_0}\,, \tag{3.11.10}$$

up to terms suppressed by higher powers of $\mathcal{V}$ or aT_s. Here, $\mathcal{V}_0$ and T_0 denote the values of the two real fields in the uplifted vacuum. The expression for the volume is still given by Eq. (3.11.6), where T_0 is now the shifted modulus

$$T_0 \approx \frac{\xi^{2/3}}{2}\left(1+\frac{2}{a\xi^{2/3}}\right)+\mathcal{O}\left((a\xi^{2/3})^{-2}\right) \tag{3.11.11}$$

The F-terms of the fields in this vacuum are given by

$$F_{T_\mathrm{b}} \approx -\sqrt{3}\,\frac{W_0}{\mathcal{V}_0}\,, \qquad F_{T_\mathrm{s}} \approx \sqrt{6aT_0\chi_0}\,\frac{W_0}{\mathcal{V}_0}\,, \qquad F_X \approx \sqrt{\chi_0}\,\frac{W_0}{\mathcal{V}_0}\,. \tag{3.11.12}$$

Clearly, the dominant contribution to supersymmetry breaking comes from the volume mode. As expected, the uplift sector is important to cancel the cosmological constant but its contribution to supersymmetry breaking is suppressed in the large volume limit. The corresponding gravitino mass is, again,

$$m_{3/2} \approx \frac{W_0}{\mathcal{V}_0}\,, \tag{3.11.13}$$

[8] Indeed it is possible to verify that, once coupled to chaotic inflation, the displacement of X is again negligible compared to that of $\mathcal{V}$ and T_s.

up to terms suppressed by higher powers of the inverse volume or aT_0. The masses of the canonically normalized moduli are, schematically[9]

$$m_{T_\mathrm{b}} \sim \frac{W_0}{\mathcal{V}_0^{3/2}}\,, \qquad m_{T_\mathrm{s}} \sim \frac{W_0}{\mathcal{V}_0}\,. \tag{3.11.14}$$

The uplifted vacuum is protected by a potential barrier of height

$$V_\mathrm{B} \sim \frac{m_{3/2}^2}{\mathcal{V}_0}\,. \tag{3.11.15}$$

Although the structure of this vacuum is more complicated than in the previous two cases, the coupling of chaotic inflation works in the same way. As will become clear in the following, the results are qualitatively similar.

3.11.2 LVS and chaotic inflation

Our starting point for the coupled model is this time

$$W = W_0 + Ae^{-aT_\mathrm{s}} + fX + \frac{1}{2}m\phi^2\,, \tag{3.11.16}$$

$$K = -2\ln\left[\left(T_\mathrm{b}+\overline{T}_\mathrm{b}\right)^{3/2} - \left(T_\mathrm{s}+\overline{T}_\mathrm{s}\right)^{3/2} + \xi\right] + k\big(|X|^2\big) + \frac{1}{2}\left(\phi+\bar{\phi}\right)^2. \tag{3.11.17}$$

The uplift sector is treated as described above, since it is safe to neglect its influence on inflation. The scalar potential at leading order in $\mathcal{V}^{-1}$ reads

$$\begin{aligned} V = {} & \frac{2\sqrt{2}\,a^2A^2\sqrt{T_\mathrm{s}}\,e^{-2aT_\mathrm{s}}}{3\mathcal{V}} - \frac{16aAT_\mathrm{s}\,e^{-aT_\mathrm{s}}\left(4W_0 - m\varphi^2\right)}{\mathcal{V}^2} \\ & + \frac{3\xi\left(4W_0 - m\varphi^2\right)^2}{32\mathcal{V}^3} + \frac{\left(\mathcal{V}-2\xi\right)\left(f^2+\frac{1}{2}m^2\varphi^2\right)}{\mathcal{V}^3}\,. \end{aligned} \tag{3.11.18}$$

Comparing this expression to Eq. (3.11.8) we observe that, in principle, the contribution of the inflaton can be absorbed in a redefinition of W_0 and f. As before, we treat inflation as a perturbation of the true vacuum. Hence, we naively expect chaotic inflation to be successful in LVS as long as

$$m^2\varphi^2 \ll f^2\,, \qquad m\varphi^2 \ll W_0\,, \tag{3.11.19}$$

neglecting order-one coefficients. It will become clear in the following that these two conditions precisely guarantee that the inflaton energy density does not destabilize the moduli.

To compute the effective inflaton potential we have to take the displacements of both moduli into account. Hence, we expand the potential around

$$\delta\mathcal{V} = \mathcal{V} - \mathcal{V}_0\,, \qquad \delta T_\mathrm{s} = T_\mathrm{s} - T_0\,. \tag{3.11.20}$$

[9]Note that the axion of T_b is exactly massless and thus irrelevant during inflation. The axion of T_s is stabilized at the same mass scale as the real part of T_s.

Minimizing the result with respect to both shifts yields

$$\frac{\delta\mathcal{V}}{\mathcal{V}_0} \approx \frac{\tilde{m}^2\varphi^2}{\chi_0 m_{3/2}^2} + \frac{\tilde{m}\varphi^2}{4m_{3/2}}\,, \tag{3.11.21a}$$

$$\frac{\delta T_\mathrm{s}}{T_0} \approx \frac{\tilde{m}^2\varphi^2}{aT_0\chi_0 m_{3/2}^2} + \frac{\tilde{m}\varphi^2}{2aT_0 m_{3/2}}\,, \tag{3.11.21b}$$

up to terms suppressed by higher powers of $\mathcal{V}^{-1}$ or $(aT_0)^{-1}$. The displacement of T_s is relatively suppressed by one power of $\mathcal{V}_0$. This is to be expected because T_s is the heavier of the two moduli. Nonetheless, δT_s must be taken into account to find the correct leading-order result.

Integrating out the displacements of both moduli, we are left with the leading-order effective potential

$$V(\varphi) \approx \frac{1}{2}\tilde{m}^2\varphi^2 + \frac{\chi_0}{4}\tilde{m}m_{3/2}\varphi^2 - \frac{1}{2\chi_0}\frac{\tilde{m}^4\varphi^4}{m_{3/2}^2} - \frac{1}{4}\frac{\tilde{m}^3\varphi^4}{m_{3/2}} - \frac{\chi_0}{16aT_0}\tilde{m}^2\varphi^4\,. \tag{3.11.22}$$

We refrain from rewriting this unwieldy expression in terms of the moduli masses, but the idea is the same as in our previous examples. Some of the correction terms are suppressed by inverse powers of m_{T_b} and m_{T_s} and vanish in the limit of very heavy moduli. Others, like the supersymmetry breaking second term in Eq. (3.11.22) grow with the moduli masses, and hence do not vanish. As in the previous examples, the region where $V(\varphi)$ is unbounded from below is never reached since the moduli are destabilized at smaller values of φ.

We can now rewrite the effective potential to study inflation. In particular,

$$V(\varphi) \approx \frac{1}{2}\tilde{m}^2\varphi^2\left(1 - \frac{1}{\chi_0}\frac{\tilde{m}^2}{m_{3/2}^2}\varphi^2\right) + \frac{\chi_0}{4}\tilde{m}m_{3/2}\varphi^2\left(1 - \frac{1}{4aT_0}\frac{\tilde{m}}{m_{3/2}}\varphi^2\right)\,. \tag{3.11.23}$$

Again, $V(\varphi)$ contains a supersymmetric mass term and a bilinear soft term – suppressed by one power of χ_0 –, both with a correction proportional to $\frac{H^2}{V_\mathrm{B}}$. By requiring the barrier to be larger than the Hubble scale during inflation, the gravitino mass is generically constrained as follows,

$$m_{3/2} > H\sqrt{\mathcal{V}_0} \sim 10^{-4}\sqrt{\mathcal{V}_0}\,. \tag{3.11.24}$$

As before, this constraint is equivalent to demanding that φ is not large enough to uplift the modulus minimum to a saddle point.

3.11.3 Numerical examples

Based on the effective potential Eq. (3.11.23) we can distinguish two cases in which 60 e-folds of inflation may be realized.

The supersymmetric term dominates

If $\tilde{m} \gg \chi_0 m_{3/2} \sim m_{3/2}/\mathcal{V}_0$, in principle the supersymmetric quadratic term in Eq. (3.11.23) could dominate, yielding the leading-order potential

$$V(\varphi) \approx \frac{1}{2}\tilde{m}^2\varphi^2\left(1 - \frac{1}{\chi_0}\frac{\tilde{m}^2}{m_{3/2}^2}\varphi^2\right)\,. \tag{3.11.25}$$

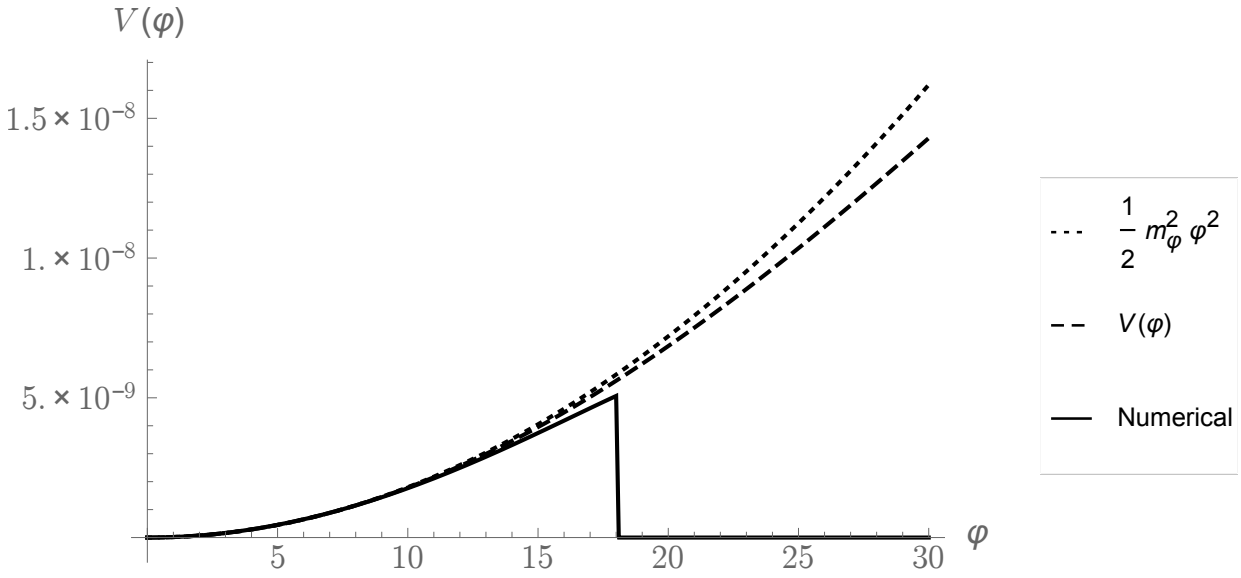

Figure 18: Effective inflaton potential in LVS for $W_0 = 1$, $A = 0.13$, $a = 2\pi$, $m = 5.8\times10^{-4}$, and $\xi = 1.25$. With these parameters we find $T_0 = 0.75$, $\mathcal{V}_0 = 200$, and $m_{3/2} = 0.005$. The dotted line denotes a purely quadratic potential with $m_\varphi = 6\times10^{-6}$ imposed by COBE normalization. The dashed line is the effective potential Eq. (3.11.22) evaluated at all orders in aT_0. The solid line is obtained numerically by setting the modulus to its minimum value at each value of φ. Since the barrier height and Hubble scale are the same as in the previous example, modulus destabilization occurs at $\varphi_c \approx 18$. Again, Eq. (3.11.22) and the dashed line are only meaningful for $\varphi < \varphi_c$. Notice that the difference between the dashed and the solid line is comparably large in this example. This is because the relatively small value of $\mathcal{V}_0$ limits the precision of the expansion in $\mathcal{V}^{-1}$.

However, this scenario is excluded by a consistency requirement of the LVS scheme. Specifically, the gravitino mass must not exceed the Kaluza-Klein scale which, as discussed in [87], means that $W_0 \ll \mathcal{V}_0^{1/3}$. Requiring the supersymmetric term to be larger than the soft term while both moduli are stabilized always violates this bound. For different effects related to the Kaluza-Klein scale, cf. [88, 89].

The bilinear soft term dominates

If, on the other hand, $\tilde{m} \ll \chi_0 m_{3/2} \sim m_{3/2}/\mathcal{V}_0$, the term proportional to $\tilde{m}m_{3/2}$ may drive inflation. In this case, the leading-order inflaton potential reads

$$V(\varphi) \approx \frac{\chi_0}{4}\tilde{m}m_{3/2}\varphi^2\left(1 - \frac{1}{4aT_0}\frac{\tilde{m}}{m_{3/2}}\varphi^2\right) . \tag{3.11.26}$$

The gravitino mass is constrained by the generic requirement (3.11.24). Interestingly, by requiring $m_{3/2} < m_{\rm KK}$ for consistency, the volume of the compactification manifold is bounded from above, $\mathcal{V}_0 \lesssim 10^3$. A numerical example for this scenario is depicted in Fig. 18.

The CMB observables in our example are found to be

$$\begin{aligned} n_{\rm s} &= 0.964\,, \\ r &= 0.116\,, \end{aligned} \tag{3.11.27}$$

at $\varphi_\star \approx 15.2$. Modulus destabilization towards the run-away minimum occurs at $\varphi_{\rm c} \approx 18$.

3.12 Universality and CMB observables

Let us consider the effective single-field inflaton potential arising in the two previous example models as well as in the general discussion of Sec. 2. We observe that a simple expression captures all models and their flattening of the inflaton potential by moduli backreaction,

$$V(\varphi) = \frac{1}{2} m_\varphi^2\, \varphi^2 - \frac{1}{4}\lambda\varphi^4\,, \qquad \lambda > 0\,. \tag{3.12.1}$$

This expression is valid at leading order in the modulus shift, and thus holds for a certain range $\varphi < \varphi_{\rm c}$ until the moduli are destabilized.

Due to the negative quartic term the potential has a local maximum at $\varphi_{\rm M} = m/\sqrt{\lambda}$. All three scenarios share the property that the moduli destabilization point occurs to the left of the maximum of the leading-order inflaton potential,

$$\varphi_{\rm c} < \varphi_{\rm M}\,. \tag{3.12.2}$$

Hence, $V(\varphi)$ is a good approximation for $\varphi < \varphi_c$. Two parameters determine the effective potential, $m/\sqrt{\lambda}$ gives the position of the maximum and m fixes the overall normalization of $V(\varphi)$. Thus, we can write the potential in terms of m and $\varphi_{\rm M}$,

$$V(\varphi) = \frac{1}{2} m_\varphi^2\, \varphi^2 \left(1 - \frac{\varphi^2}{2\varphi_{\rm M}^2}\right)\,. \tag{3.12.3}$$

As long as $\varphi_{\rm M}, \varphi_{\rm c} \gg 1$ inflation can occur to the left of the local maximum. For $\varphi_{\rm M} \to \infty$ the potential asymptotes to the pure quadratic form. In this limit, the field value $\varphi_\star$ corresponding to $N_e(\varphi_\star)$ e-folds of slow-roll before the end of inflation takes the limiting value $\varphi_\star = 2\sqrt{N_e}$, which for $N_e = 50 - 60$ is about 15.

For decreasing $\varphi_{\rm M}$ the 60 e-fold point lies increasingly close to the local maximum and the destabilization point. Thus, for $\varphi_{\rm c} \to \varphi_\star$ the inflationary dynamics changes continuously from the quadratic large-field behaviour to a nearly hill-top small-field model. Correspondingly, the scalar spectral index and r are decreased compared to pure quadratic inflation.

Inflaton potentials of this type arise in the context of non-minimally coupled quadratic inflation [39] and more recently in subcritical models of D-term hybrid inflation [90, 27, 91]. As the leading-order scalar potential is the same for all our models, the CMB observables agree as well. Reproducing the particularly simple form given in [90, 91] one finds

$$\epsilon = \frac{2}{\varphi^2}\left(\frac{1 - \frac{\varphi^2}{\varphi_{\rm M}^2}}{1 - \frac{\varphi^2}{2\varphi_{\rm M}^2}}\right)^2\,, \qquad \eta = \frac{2}{\varphi^2}\left(\frac{1 - \frac{3\varphi^2}{\varphi_{\rm M}^2}}{1 - \frac{\varphi^2}{2\varphi_{\rm M}^2}}\right)\,. \tag{3.12.4}$$

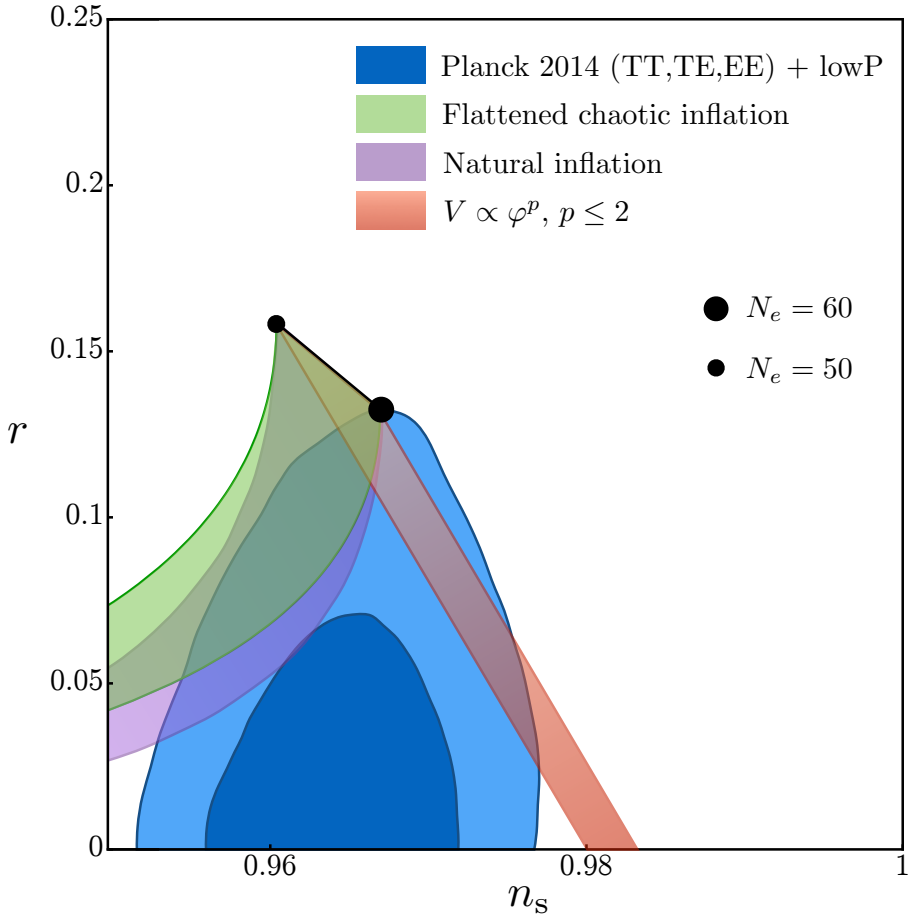

Figure 19: Prediction for the CMB observables n_s and r of the leading-order effective inflaton potential. In the limit $\varphi_\mathrm{M} \to \infty$ the observables asymptote to the predictions of pure quadratic inflation. Decreasing φ_M brings the potential increasingly into the hill-top regime. This leads to the green band of decreasing n_s and r values spanned by the 60 and 50 e-fold curves. Note, once more, that the regime of true hill-top inflation can actually never be reached because moduli destabilization occurs to the left of the would-be local maximum in $V(\varphi)$ at φ_M.

Extracting $\varphi_\star$ from $N_e = \int_{\varphi_e}^{\varphi_\star} \mathrm{d}\varphi/\sqrt{2\epsilon}$ we obtain

$$\varphi_\star^2 = 4N_e + 2 - \frac{4N_e^2}{\varphi_\mathrm{M}^2} - \frac{8N_e^3}{3\varphi_\mathrm{M}^4} + \frac{4N_e^4}{3\varphi_\mathrm{M}^6} + \ldots \tag{3.12.5}$$

where we have used the leading-order expression for the end-point of slow-roll inflation, $\varphi_\mathrm{e} = \sqrt{2} - \mathcal{O}(\varphi_\mathrm{M}^{-2})$. From this it is evident that all our models approach the quadratic inflation limit as $\varphi_\mathrm{M} \to \infty$.

Comparison with the full numerical solution for $\varphi_\star$ reveals that the analytic expression above must be given up to $\mathcal{O}(\varphi_\mathrm{M}^{-6})$ for sufficient accuracy. The terms with inverse powers of φ_M are given at leading order in N_e to allow for a compact expression. We find that for $n_\mathrm{s} \gtrsim 0.94$ this form approximates the ensuing values of n_s and r to 5% numerical accuracy compared to the exact coefficients given in [91]. Plugging back $\varphi_\star$ into the expressions for ϵ and η we can

compute the spectral parameters of the curvature and tensor perturbation power spectra

$$\begin{aligned} n_{\rm s} &= 1 - 6\epsilon(\varphi_\star) + 2\eta(\varphi_\star)\,, \\ r &= 16\epsilon(\varphi_\star)\,. \end{aligned} \tag{3.12.6}$$

at horizon exit. Doing this numerically and comparing the result with the Planck data results in the green band in Fig. 19 which is identical to the corresponding graph in [91]. Imposing the constraints on $n_{\rm s}$ and r we find a lower bound on the tensor-to-scalar ratio, $r \gtrsim 0.05$, for $N_e = 60$.

Finally, we make an interesting observation. On the one hand, our effective inflation potential arises for all three models studied here as an approximation of, for example, type IIB string theory constructions of axion monodromy inflation with an F-term supergravity description [47, 71, 48, 72, 73, 74, 75, 76, 77] as well as of models of D-term hybrid inflation [90, 27, 91]. Moreover, we found in this work that all our models show a form of polynomial flattening of the naive quadratic inflation potential by subtracting (at leading order) a higher-power monomial term in φ

$$V(\varphi) \sim \varphi^{p_0} f(\varphi)\,, \qquad f(\varphi) = 1 - c\varphi^2 + \dots\,, \qquad p_0 = 2\,. \tag{3.12.7}$$

The flattening occurs in a regime with $c \ll 1$ and small higher-oder coefficients.

On the other hand, there is a large class of models of axion monodromy inflation which feature a form of monomial flattening [92, 93, 94, 95, 96]. Some of these setups work without a supergravity embedding or with inflation from a sector with non-linearly realized supersymmetry arising from non-supersymmetric compactifications like Riemann surfaces [97, 98, 92, 99, 96] while another one involves F-term monodromy on D-branes [76]. In these constructions a quadratic or quartic inflation potential flattens by suppressing the monomial power $p < p_0$,

$$V(\varphi) \sim \varphi^{p_0} f(\varphi)\,, \qquad f(\varphi) = \varphi^{-\Delta p} \qquad p_0 = 2, 4\,. \tag{3.12.8}$$

The correlation between the two types of flattening – polynomial and monomial – may be due to the different mechanisms of volume stabilization (non-perturbative versus perturbative). In particular, polynomial flattening seems to correlate with models showing spontaneous bulk F-term supersymmetry breaking and non-perturbative volume stabilization (implying CY compactification). We may speculate here that both of these correlations hold more widely.

Moreover, the two types of flattening have quite different observational predictions, with polynomial flattening corresponding to the green band and monomial flattening yielding the red band in Fig. 19. Future CMB data may enable us to discriminate between the two types of flattening – and hence maybe even between classes of string compactifications.

3.13 Non Decoupling Effects of Moduli Stabilization : A Recap

We studied in this last section the interplay between Kähler moduli stabilization and large-field inflation in the context of string-effective supergravity models. We found that if moduli stabilization breaks supersymmetry, the modulus sector never decouples from inflation. On the one hand, supersymmetry breaking induces a bilinear soft mass term for the inflaton which

can potentially drive 60 e-folds of slow-roll inflation. On the other hand, the potential contains dangerous terms which destabilize the moduli if the inflaton field exceeds a critical value.

We have illustrated our results in two prominent models of moduli stabilization: KKLT and the simplest Large Volume Scenario. In both models we have analyzed corrections to the inflaton potential from supersymmetry breaking and from integrating out the moduli. Although the dominant source of supersymmetry breaking and the structure of vacua's differ in the three models, they share a number of common features. First, we find that both of them give rise to an effective inflaton potential of the form

$$V(\varphi) = \frac{1}{2} m_\varphi^2 \, \varphi^2 - \frac{1}{4} \lambda \varphi^4 \,,$$

after the moduli have been integrated out. Hence, they share universal predictions for the CMB observables, in particular $r \gtrsim 0.05$. Second, in all models the stability of moduli during inflation imposes a severe lower bound on the scale of supersymmetry breaking. In KKLT this is the well-known bound $m_{3/2} > H$. In the Large Volume Scenario, the moduli masses and the potential barrier are suppressed compared to $m_{3/2}$ due to an approximate no-scale symmetry. This leads to the more stringent constraint $m_{3/2} > H\sqrt{\mathcal{V}}$, where $\mathcal{V}$ denotes the volume of the compactification manifold. Unfortunately, this implies that supersymmetry can no longer protect the flatness of the inflaton potential. This is opposite to chaotic inflation with a stabilizer field, where the gravitino mass must be parametrically smaller than the inflaton mass. Third, in all considered schemes the parameter choices required by successful inflation appear unnatural from the perspective of string theory. Although our analysis is limited to specific examples we believe that this problem is characteristic for a wide class of large-field inflation models coupled to a modulus sector.

Another important caveat is that the initial conditions of inflation must be chosen very carefully. The moduli are destabilized if the energy density of the universe exceeds the barrier protecting their local minimum. In this case, the desired regime of slow-roll inflation is never reached. In this sense, the effective inflation models obtained after integrating out the moduli are no longer "chaotic".

3.14 Conclusion

Inflation is one of the most obscure but exciting phases of the History of our Universe. The flatness and horizon problems are very strong pieces of evidence that the actual content of our spacetime in insufficient to explain its complete evolution from the initial time that the Big Bang is supposed to represent. Yet the incredibly well verified predictions the theory of Big Bang has been able to produce address us a challenging question : Which kind of devil has ever been responsible for such a brutal acceleration of the Universe expansion at early time of our Universe History?

The answer to this question may stand somewhere among one of the aforementioned models of Inflation but stays at the moment unaccessible to experiment. Although the more and more stringent constraints on the tensor to scalar ratio can help discriminating between the different scenarios proposed it could be that constraints reach a critical low point ($r \lesssim 0.001$) under which B modes of tensor perturbations are supposed to convert into E modes through gravitational lensing and can in principle not be detected anymore. On the contrary, if r is measured to be

positive with good precision and the tensor spectral index to be negative and of value $-r/8$, one would be more confident that inflation is the right theory for modeling early cosmology.

In this part we have reviewed many different aspects of the role that supersymmetry breaking can play in an inflation scenario and in the process of stabilizing moduli, in the case one would try to embed the inflation scenario in a String Theory framework. Chaotic inflation, although one of the simplest model of inflation, faces several difficulties when trying to incorporate it in supergravity, and we saw how either a stabilizer field joined to a supersymmetry breaking sector with small gravitino mass can cure the problem, or models without stabilizer involving heavy moduli where on the contrary, supersymmetry breaking must be the major component driving inflation.

The latter studies turned into a quite generic formulation, even if the discussion could be of course enlarged. In particular we kept working on chaotic-like formulations of Inflation, which represents a particular class of set up for modeling Inflation. Small field inflation, models predicting small tensor to scalar ratios, or multi field inflation could be studied as well as models getting perturbed by non decoupling effects of supersymmetry breaking.

This interplay between theories modeling the very early Universe as well as the processes which let our present world with a broken supersymmetry is a crucial way to cross-constrain both edges of a global theory of the Universe and its particle content. Possible future measurement of the tensor to scalar ratio, and/or the polarization of the CMB with good accuracy could give important constraints on the gravitino mass. Reversely, a potential observation of the super-partners at the LHC during the next runs of the accelerator could provide us important information on the supersymmetric scale, and consequently discriminate between different scenarios of inflation at early time of the Universe clock.

Part II

Dark Matter Models

4 | Dark Matter : Generalities

4.1 Introduction

Is there anything out there? This question is at the heart of every dark matter search, from experimental detection, to theoretical model building and investigations. Namely, from the brilliant discovery of General Relativity by Einstein in 1915 [100], where gravitation seemed at first sight to have found a clean and smart, but incredibly powerful formulation, it appeared a few decades after that many gravitational phenomenons remained unexplained in our cosmos. Dark Energy, dark matter, the scientific community stays nowadays staring at the sky looking for the obscure components which make our Galaxy stable, our Universe accelerating, in a picture where our ordinary matter seems rather weak and insignificant. Therefore it is of great importance, for our understanding of the gravitational behavior of celestial bodies as well as for our knowledge of what particles actually compose the main part of our Universe, to be able to explain how any dark matter candidate could ever communicate with our visible world, and how one can model properly the dynamics of the Universe in the presence of the latter.

In this second part of the thesis, I will first review how dark matter remains one of the most probable piece for making the Big Bang Theory puzzle complete, introducing important tools for modeling the Universe thermodynamics. Then I will present different works all deriving dark matter models in the presence of intermediate mediators, and study how the visible sector gets altered by the presence of a dark sector, either in the electroweak or in the strong sector of particle physics. This work led to two key publications released in collaboration with Yann Mambrini, Emilian Dudas and Bryan Zaldivar [101, 102].

4.2 On the Track to Dark Matter

The first piece of evidence of an obscure form of gravitational sources in our galaxy arose in 1932 in a paper from Oort [103]. The vertical dynamics of stars around the galactic plane indeed gives a good hint to estimate the local density of the galaxy. Oort then investigated the possibility of modeling the dynamics of stars inside our galaxy as being similar to a gravitational gas of stellar bodies, and managed to formulate an estimation of the matter density present in the Solar vicinity, to notice a discrepancy of a factor 2 between his theoretical prediction and local density estimated at that time. He then suggested for the first time the possibility that some other, invisible matter could be present near the galactic disk, retaining stars from escaping transversally our galaxy.

Another crucial hint for the presence of dark matter comes from the measurement of the rotation curve $v = v(r)$ of the galaxies mass content. Decomposing the velocity of a star inside its host galaxy in terms of its radial and transverse components $v_r = \cos\theta$ and $v_t = \sin\theta$ (see Fig. 1) it is possible to measure both separately by the mean of different techniques : The position θ of the star in our sky gives information on v_r whereas the Doppler-Fizeau effect

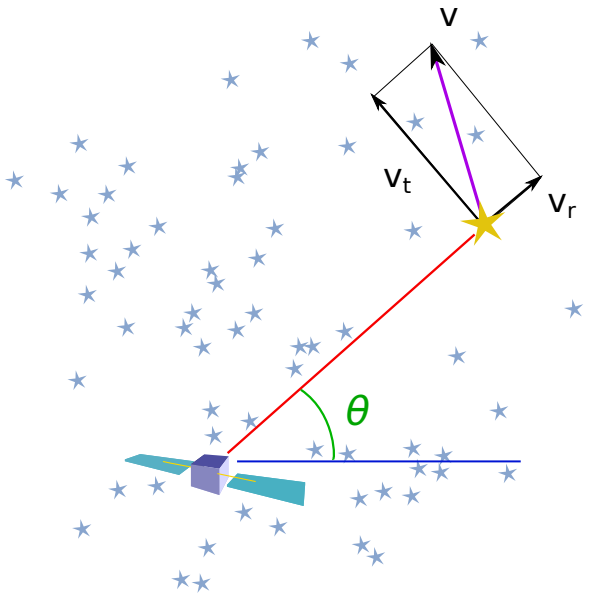

Figure 1: Parametrization of the stars velocities in term of polar coordinates.

(shifting the stellar emission spectrum towards blue or red wavelengths) provides informations on the tangential velocity v_t.

Starting from 1940, numerous measurements of the rotation curves in different spiral galaxies showed a significant anomaly in the outer regions of the latter. Indeed, whereas the velocities of stars in the central region of the galaxies are expected to behave like the one a rigid body

$$v_{center}(r) \sim r\,, \tag{4.2.1}$$

the Kepler law suggests – in the very rough approximation of a spherical mass distribution – that the stars velocities should decrease like

$$v_{outer}(r) \sim \frac{1}{\sqrt{r}} \tag{4.2.2}$$

in the outer regions. Surprisingly, observations are far different from this last prediction. Indeed, after growing like $v \sim r$ near the center, the velocity is observed to reach a plateau at large values of the radius instead of decreasing, as depicted in Fig. 2. The first measurement of the rotation curves was achieved in a first place by Ford and Rubin in 1970 [105]. To put this in a nutshell, stars which are very far from the galactic center and possessing a high velocity, keep rotating around the galaxy instead of escaping its gravitational field. This led the scientific community to conclude that either the theory of general relativity reaches its limits of application on very large scales, or there should be some additional presence of mass, retaining these outer stars, that will give rise to the concept of *Dark Matter*. The latter, in order to reproduce the observed rotation curves could be spread around the galaxies under the form of a halo, of mass density behaving like $\rho(r) \sim r^{-2}$ at large distances. Yet such a potential can be investigated but would lead to a constant velocity while r goes to infinity. As a consequence, more evolved profiles have been proposed to take the form

$$\rho_{NFW}(r) = \frac{\rho_0}{\left(\frac{r}{r_s}\right)\left(1+\frac{r}{r_s}\right)^2}\,, \tag{4.2.3}$$

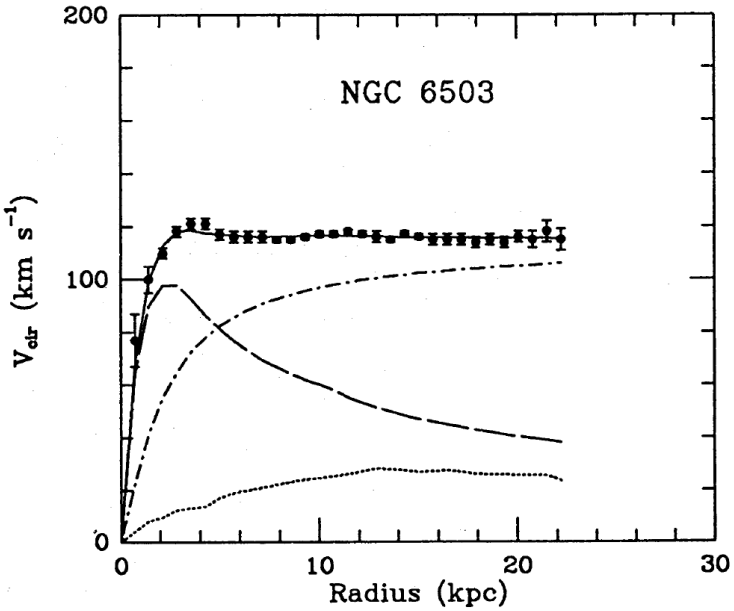

Figure 2: Experimental measurement of the rotation curve extracted from [104] for the galaxy NGC6503 decomposed among its different constituents : gas, visible disk and dark halo

r_s being a typical length scale for the halo, depending on the galaxy features, after which the velocity reaches a plateau on a scale of order $\sim r_s$ before decreasing after a while. Such profile is usually called NFW profile and was proposed by Navarro, Frenk and White in [106]. More generally, one parametrizes our ignorance on the dark matter profile shape by using the generic form of density

$$\rho_{DM}(r) = \frac{\rho_0}{\left(\frac{r}{r_s}\right)^{\alpha}\left(1+\frac{r}{r_s}\right)^{3-\alpha}}\,, \tag{4.2.4}$$

where $0 \leqslant \alpha \leqslant 3/2$.

Historically, the first person who proposed the existence of unobserved matter was Zwicky, who realized in 1933 that the measure of galaxy velocities inside the Coma cluster were much too high compared to the expectations of the virial theorem. Indeed a self interacting system of N objects of average mass m, should have kinetic and potential energy of respectively

$$E = \frac{1}{2}Nmv^2\,, \quad U = \frac{Gm^2}{r}\frac{N(N-1)}{2}\,. \tag{4.2.5}$$

The virial theorem hence predicts that

$$E = -\frac{U}{2} \Rightarrow M = Nm = \frac{2rv^2}{G}\,. \tag{4.2.6}$$

The observed mass M of a given cluster should then in principle give access to the mean velocity of the bodies it is composed of. However, it appeared that this mean velocity was dramatically underestimated :there should hence be much more matter involved ! As far as numbers are concerned, this computation was predicting the presence of 400 times more matter than it is actually observed.

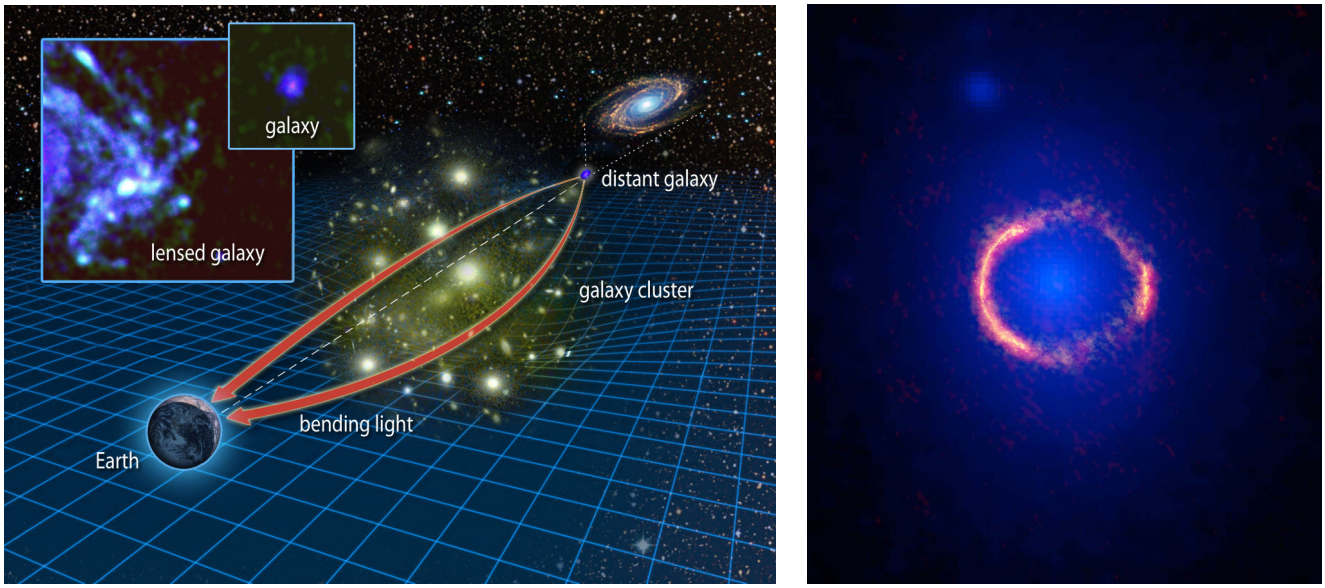

(a) (b)

Figure 3: (a) Explanation of the gravitational lensing effect. Light is deflected by entering in the gravitational field of some very massive celestial body. (b) ALMA/Hubble composite image of the gravitationally lensed galaxy SDP.81. Light rays, deflected all around the a lensing galaxy, form the structure of ring called *Einstein's ring*. Credit: ALMA (NRAO/ESO/NAOJ); B. Saxton NRAO/AUI/NSF; NASA/ESA Hubble, T. Hunter (NRAO)

Gravitational Lensing

In the theory of General Relativity, developed by Einstein in 1915 [107, 100] the spacetime is considered to behave like a geometrical manifold, locally curved by the presence of matter, and whose *timelike* and *null* geodesics represent respectively the trajectories of massive and massless bodies. In such a framework, the light propagating through our spacetime can sometime encounter very massive celestial bodies which deform significantly – by deforming the space geometry all around – its trajectory between the source of emission and the observer. The latter deformation is hence a very useful quantity to measure, in order to estimate indirectly how much matter is present in certain regions of our Universe.

The first deflection of this kind was measured in 1919 by Eddington [108] who observed for light rays entering the gravitational field of the Sun, a deflection angle of $\delta \approx 1.75''$ (See Fig. 4)

This so called "gravitational lensing" effect allows to estimate, for stars, galaxies, clusters of galaxies, what is the actual quantity of matter, only through indirect, gravitational considerations. It turns out that this measured quantity is in good agreement with the considerations made above about the virial theorem for the case of clusters. Namely, the ordinary matter represents only 20% of the matter present in the latter object !

A very appealing observation of this discrepancy between direct observation of matter and indirect measurements of mass through gravitational lensing, was the observation of the so called *Bullet Cluster* (1E 0657-558). The latter consists of two colliding clusters of galaxies at a comoving radial distance of 1.141 Gpc (3.721 Gly) and is often considered to be one of the best evidence for the existence of dark matter [109]. Indeed the famous picture presented

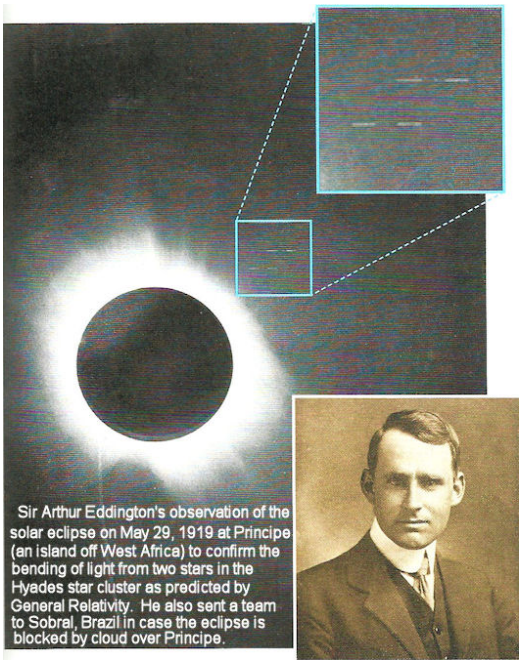

Figure 4: Picture taken by Eddington during his expedition to west Africa, measuring light deflection by observing the position of stars during an eclipse in May 1919. The light emitted by the star passes very closed to the sun and is deviated by its gravitational field.

in Fig. 5 shows in color X rays measurements released by Chandra in 2004 [110], where one can clearly see two regions of emission, coming from ordinary baryonic matter after interaction of the clusters. However one can notice in blue the regions of the sky, delimited by study of the lensing, where most of the matter is measured to be present. The separation between the visible, luminous, regions –containing ordinary matter – and the blue region of – theoretical, invisible – matter presence, suggests that nearly all of the matter is dark, and weakly interacting : the hot gas in each cluster interacts with one another and is consequently slowed down in its progression, whereas invisible, dark matter bullets pass by, almost ignoring clouds of ordinary matter and even very feebly interacting with one another.

4.2.1 Production of Dark Matter : A Thermal History

As we have seen above, anomalies in the rotation curves of galaxies, the bullet cluster observation, etc. suggest the presence of a massive matter component, which should in addition be relatively weakly interacting with ordinary matter. This enormous amount of obscure matter, often called WIMP (Weakly Interacting Massive Particle) is generally expected to be produced at the very early times of the Universe History. Dark matter production and equilibrium are hence of great importance to study in order to better understand its evolution through the ages.

Let us consider a sketch where only two stable kinds of particles, X being a dark matter candidate, and Y being a standard model constituent, interact with each other through the reaction $X\bar{X} \leftrightarrow Y\bar{Y}$.

Of course, during early times, while the temperature of the Universe was far higher than the

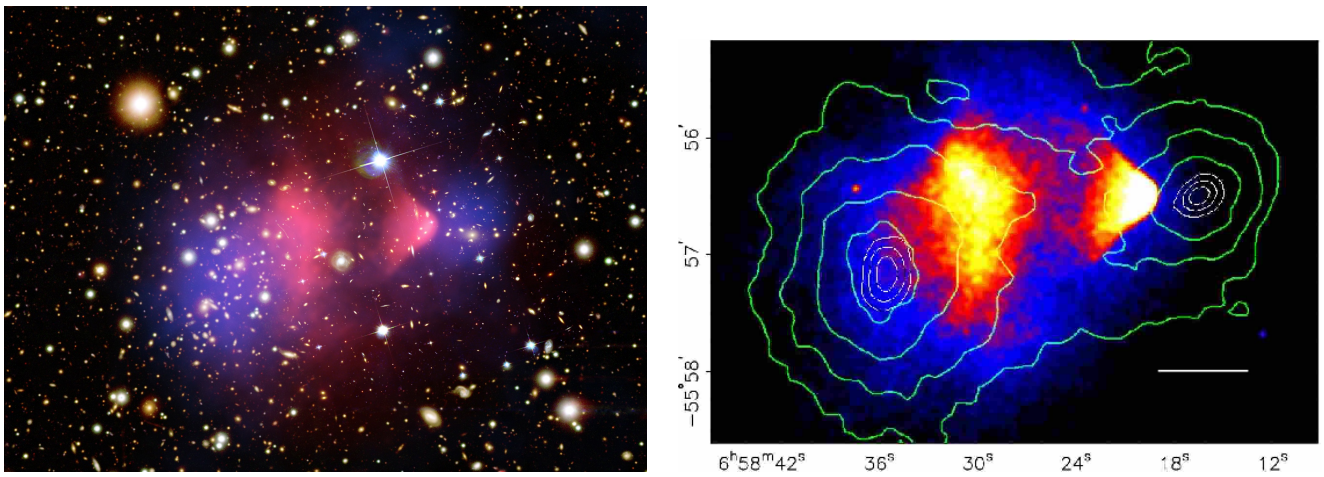

(a) (b)

Figure 5: Observations of the Bullet Cluster [109]. Pink clouds denotes the presence of detected X ray emission (a) while blue regions represent the suspected presence of mass through study of the gravitational lensing. The second picture (b) represents the X-ray measurement superimposed with the gravitational lensing isocurves (green).

dark matter mass m_X, creation and annihilation of X and Y were equivalently efficient. Thus the particle X was maintained to stand in large abundance with the standard model sector. Yet, as the temperature decreases with the expansion of the Universe, the process of creation of X becomes inefficient when $T \lesssim m_X$, while annihilation does not stop functioning. The number density of X can be computed, in the hypothesis of thermal equilibrium, to be

$$n_X^{eq} = g_X \left(\frac{m_X T}{2\pi}\right)^{3/2} e^{m_X/T}\,, \tag{4.2.7}$$

where g_X is the number of internal degrees of freedom of the particle X. However, an important effect on thermal equilibrium that has to be taken into account is the effect of the Universe Hubble expansion on the interaction process. Indeed, if particles were in thermal equilibrium indefinitely, their number density would not cease decreasing while the Universe cools down, as indicated by Eq. 4.2.7. In this case, it can be difficult to explain the presence of the remaining, so called "relic" density of dark matter which is suspected to lie around our galaxies today. A possible explanation for the existence of relic density is the competition between the self annihilation process and the Hubble expansion. Indeed, expansion of our Universe works towards a dilution of the WIMPs density whereas the annihilation rate becomes negligible. Dark matter thus can survive, expansion making annihilation inefficient. Both effects are well described by the Boltzmann equation

$$\frac{\mathrm{d}n_X}{\mathrm{d}t} + 3Hn_X = -\langle\sigma v\rangle(n_X^2 - n_X^{eq2})\,, \tag{4.2.8}$$

where n_X is the WIMPs' number density, H is the Hubble factor defined in Eq. (2.2.6) $H = \left(\frac{8\pi^3\rho}{3M_p}\right)^{1/2}$ and $\langle\sigma v\rangle$ is the averaged cross section of annihilation of X multiplied by the relative velocity of the annihilating particles.

To give a first comment, one can see in Eq. 4.2.8 that in the case where $T \gg m_X$, n_X is large and stabilized to n_X^{eq} at equilibrium, whereas when $T \ll m_X$, the number density n_X decreases and the term $3Hn_X$ becomes more and more relevant. When $\langle\sigma v\rangle n_X^2$ becomes sufficiently small, expansion dominates and the annihilation process is stopped. This is called the *thermal freeze out*.

The temperature of freeze out T_{FO} can then be computed using Eq. 4.2.8 and is usually expressed in terms of the variable$x \equiv m_X/T$, giving

$$x_{FO} \equiv \frac{m_X}{T_{FO}} \approx \ln\left[c(c+2)\sqrt{\frac{45}{8}}\frac{g_X}{2\pi^3}\frac{m_X M_p}{g_\star^{1/2} x_{FO}^{1/2}}\left(a + \frac{6\,b}{x_{FO}}\right)\right], \tag{4.2.9}$$

where $c \sim 0.5$ is a numerical factor, g_X is the number of external degrees of freedom ($g_X \sim 120$ in the Standard Model at $T \sim 1$TeV, $g_X \sim 65$ at $T \sim$ GeV) and a, b are the coefficients in the non relativistic expansion of the cross section

$$\langle\sigma v\rangle = a + bv^2 = \mathcal{O}\left(v^4\right). \tag{4.2.10}$$

This provides the WIMP density remaining in our Universe

$$\Omega_X h^2 \approx \frac{1.04 \times 10^9 \text{GeV}^-1}{M_p}\frac{x_{FO}}{g_X^{1/2}\left(a + \frac{3\,b}{x_{FO}}\right)}. \tag{4.2.11}$$

In the case of a dark matter of order GeV mass, and a weak scale cross section, the freeze out temperature turns out to be of order $x_{FO} \sim 20 - 30$, and the relic density becomes

$$\Omega_X h^2 \approx 0.1\left(\frac{x_{FO}}{20}\right)\left(\frac{g_X}{80}\right)^{-1/2}\left(\frac{a + \frac{3\,b}{x_{FO}}}{3 \cdot 10^{-26}\text{cm}^3.\text{s}^{-1}}\right)^{-1}. \tag{4.2.12}$$

This relation states surprisingly that, for a typical electroweak cross section, the relic abundance Ω_X gets a value approaching $\Omega_X \sim 0.2 - 0.3$ which is precisely the value measured by recent measurement of the Universe matter content. This coincidence, far from being a proof for the existence of a WIMP-like dark matter, is often called the *WIMP miracle* and used as a motivation suggesting that dark matter could naturally be imagined to take the form of a massive ($\sim$ GeV $-$ TeV), weakly interacting particle.

4.3 Thermodynamics of the Decoupling

Let us here clarify how statistical distributions of thermodynamics are treated while dealing with the universe particle content. First let us specify that while talking about the "Universe temperature", one always talks about the temperature of the photon thermal bath, with which, depending on the age of the universe, several other species are in thermal equilibrium. All the particles present in this bath hence follow the well known Fermi-Dirac or Bose-Einstein distribution (respectively for fermions "+" and bosons "-")

$$f(\mathbf{p}) = \frac{1}{\exp\{(E-\mu)/T\} \pm 1}. \tag{4.3.1}$$

μ is here denoting a chemical potential which could in principle differ, depending on the different species of particles in equilibrium at the time considered. The number density, energy density and pressure of the considered gas can then be expressed in terms of this distribution function as follows

$$n = g \int \frac{\mathrm{d}^3 p}{(2\pi)^3} f(\mathbf{p}) \,, \tag{4.3.2}$$

$$\rho = g \int \frac{\mathrm{d}^3 p}{(2\pi)^3} E(\mathbf{p}) f(\mathbf{p}) \,, \tag{4.3.3}$$

$$P = g \int \frac{\mathrm{d}^3 p}{(2\pi)^3} \frac{|\mathbf{p}|^2}{3E} f(\mathbf{p}) \,, \tag{4.3.4}$$

where g is the number of internal degrees of freedom of the gas considered. In the relativistic limit where $T \gg m \,, \mu$, these quantities can be derived to find

$$n = \begin{cases} g \frac{\zeta(3)}{\pi^2} T^3 & \text{(Bose)} \\ \\ g \frac{3}{4} \frac{\zeta(3)}{\pi^2} T^3 & \text{(Fermi)} \end{cases} \,, \qquad \rho = \begin{cases} g \frac{\pi^2}{30} T^4 & \text{(Bose)} \\ \\ g \frac{7}{8} \frac{\pi^2}{30} T^4 & \text{(Fermi)} \end{cases} \,, \qquad P = \frac{\rho}{3} \,. \tag{4.3.5}$$

In the non relativistic limit $m \gg T$, these formulas become

$$n = g \left(\frac{mT}{2\pi} \right) e^{-(m-\mu)/T} \,, \quad \rho = mn \,, \quad P = nT \ll \rho \,. \tag{4.3.6}$$

Here we have considered the distribution of a single gas species. Yet in the primordial Universe many different species are in thermal equilibrium. Some of them, depending on their masses, will be relativistic and some of them will not. In the latter case, energy density and pressure will be exponentially suppressed, such that the only particles contributing to the Universe energy density and pressure will be the relativistic ones, and one can define a combined number of degrees of freedom $g_\star$ by

$$g_\star \equiv \sum_{i=bosons} g_i \left(\frac{T_i}{T} \right)^4 + \frac{7}{8} \sum_{i=fermions} g_i \left(\frac{T_i}{T} \right)^4 \,, \tag{4.3.7}$$

such that these quantities express as

$$\rho = \frac{\pi^2}{30} g_\star T^4 \,, \qquad \text{and} \qquad P = \frac{\pi^2}{90} g_\star T^4 \,. \tag{4.3.8}$$

Here the T_i's stand for the respective temperature of each baths composed of one species only. The latter are in equilibrium with photons before decoupling with the thermal bath and this step function is a good approximation of the true function $g(T)$ during the Universe expansion.

A few lines of thermodynamics arguments (using mainly the first law of thermodynamics) show that the entropy density of the gas considered goes like

$$s = \frac{\rho + P}{T} \,, \tag{4.3.9}$$

that is the entropy density varies with respect to the temperature as the simple function

$$s = \frac{2\pi^2}{45} g_\star^s T^3 \,, \tag{4.3.10}$$

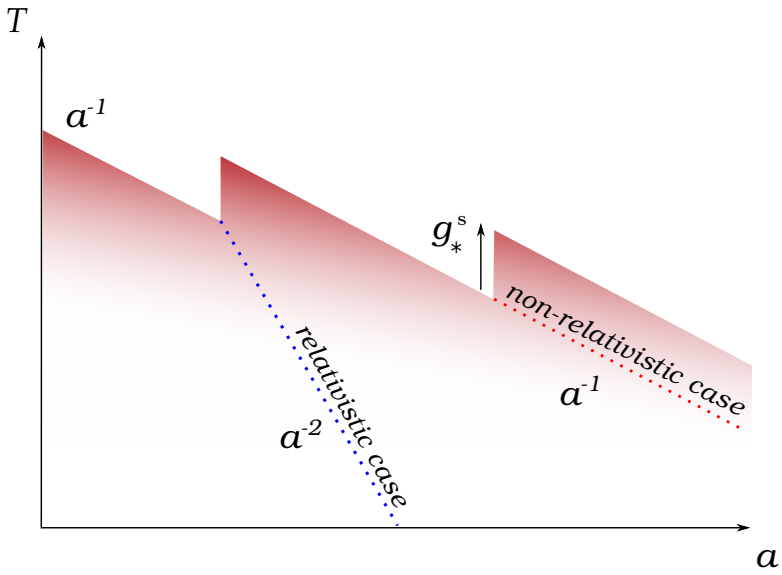

Figure 6: Evolution of the temperature of different species (relativistic and non-relativistic) after their decoupling from the thermal bath.

where

$$g_\star^s = \sum_{i=bosons} g_i \left(\frac{T_i}{T}\right)^3 + \frac{7}{8} \sum_{i=fermions} g_i \left(\frac{T_i}{T}\right)^3 . \tag{4.3.11}$$

Again, when all relativistic degrees of freedom are in thermal equilibrium, factors $\left(\frac{T_i}{T}\right)$ are set to one in the latter expressions and $g_\star = g_\star^s$ but these two numbers differ as soon as one species decouples from the thermal bath.

These results have important consequences on the evolution of the thermal bath temperature. Indeed, the constance of the entropy

$$S = a^3 s \propto (aT)^3 , \tag{4.3.12}$$

indicates that the temperature evolve like

$$T \propto a(t)^{-1} . \tag{4.3.13}$$

In addition to that, the process of decoupling is constrained to happen at constant entropy and hence makes the temperature of the thermal bath satisfy

$$T_\gamma^{after} = T_\gamma^{before} \times \left(\frac{g_s^{before}}{g_s^{after}}\right)^{1/3} . \tag{4.3.14}$$

Since the value of the number of degrees of freedom is decreasing while a species decouples, the latter relation enforces the temperature of the thermal bath to increase, reheating the Universe. After the decoupling, depending on its mass, a particle species can be frozen while still relativistic or not. Both cases will lead to different evolution of their respective own temperature, that can be shown to be

$$T_i \propto a(t)^{-1} \quad \text{(Relativistic)} \qquad T_i \propto a(t)^{-2} \quad \text{(Non-Relativistic)} . \tag{4.3.15}$$

The two kinds of evolutions are depicted in Fig. 6, where the thermal bath is reheated by the different decoupling phases, while the temperatures of each species population decreases with the aforementioned laws.

This evolution of the Universe temperature is of a crucial importance to understand the process of decoupling and how the temperature laws of the different species involved change during the different phases of the Universe History.

Now that we have seen in details how one can describe a thermal evolution of the Universe and in particular, how the addition of a dark matter sector, in thermal equilibrium at the early time of the Universe with the visible sector, can play a role in this evolution, we will investigate in what follows what a dark matter candidate can be and how it can – weakly – interact with our observable world.

5 A Simple Extension of the Standard Model : An Extra $U(1)$ Symmetry

One of the simplest possible option to enlarge the standard model is to add to the latter new abelian gauge interactions. For a recent review on the subject, see for instance [111, 112]. As we will see this has the appealing feature to provide new interactions that can be used to model the way a dark sector can talk to our visible world. In such a picture, one could for example imagine the dark matter be a fermionic component interacting, through this new $U(1)_X$ with standard model particles. This new interaction would in this case be carried by a new gauge boson, playing the role of a mediator between dark matter and visible matter that is generically called a Z' boson (or *hidden photon* in the case it is supposed very light or massless).

The most common approach to study the existence of one additional gauge boson is to couple it to the standard model fermions, analogously than it is in the usual electroweak theory. The possibility that there exists couplings of the form

$$\mathcal{L} \supset g_X(\bar{\psi}_{SM}\gamma^\mu\psi_{SM})Z_\mu\,, \tag{5.0.1}$$

is however very much constrained by direct searches and especially by FCNC processes. There exists a large amount of proposals, among which models like $B-L$ or combinations $\alpha(B-L)+\beta Y$ are the most popular, where the Z' is coupling to the SM fermions with flavor blind charges. These models are actually the only ones which contain family-independent, anomaly-free gauged symmetries commuting with the SM gauge group in case where there are no new fermions beyond the ones of the SM. Family-dependent anomaly-free models with no extra fermions were also extensively studied [113, 114, 115]. In such cases, the fact that the Z' is in direct contact with Standard Model fermions, and if the coupling g_X is not too small, the Z' should be heavy enough to escape detection. It is roughly constrained to stand in the multi-TeV mass range.

There exists also a wide literature on light $U(1)$'s of string or field theory origin with anomaly cancellation a la Green-Schwarz [116, 117, 118, 119, 120, 121, 122, 123, 124, 125, 126, 127, 128, 129, 130, 131], with low-energy anomalies canceled by axionic couplings and generalized Chern-Simons terms, or in other models with Stueckelberg realization of Z' [132, 133, 134].

There is, however another way to sketch the possible interaction of this new gauge boson with the standard model if one imagine that none of the SM fermions are charged under this $U(1)_X$ but if there exists additional heavy fermions $\Psi_{L,R}$, called "mediators" in what follows, mediating effective interactions, described by the dimension-four kinetic mixing and higher-dimensional operators between the Z' and the SM sector. This approach was adopted in 2012 by Dudas, Mambrini, Pokorski and Romagnoni [135, 136] aiming to fit the 130 GeV gamma ray line claimed to be observed by FERMI LAT at that time [137]. Indeed, a detection of significance $\gtrsim 3.2\sigma$ was claimed indicating the presence of a gamma ray line a round the galactic center, that could possibly be a smoking gun evidence for the presence of dark matter in the milky way (See Fig. 1). Yet a few years later, the significance has decreased and the signal may be not even present at all. Nevertheless, this approach for SM gauge boson coupling to a

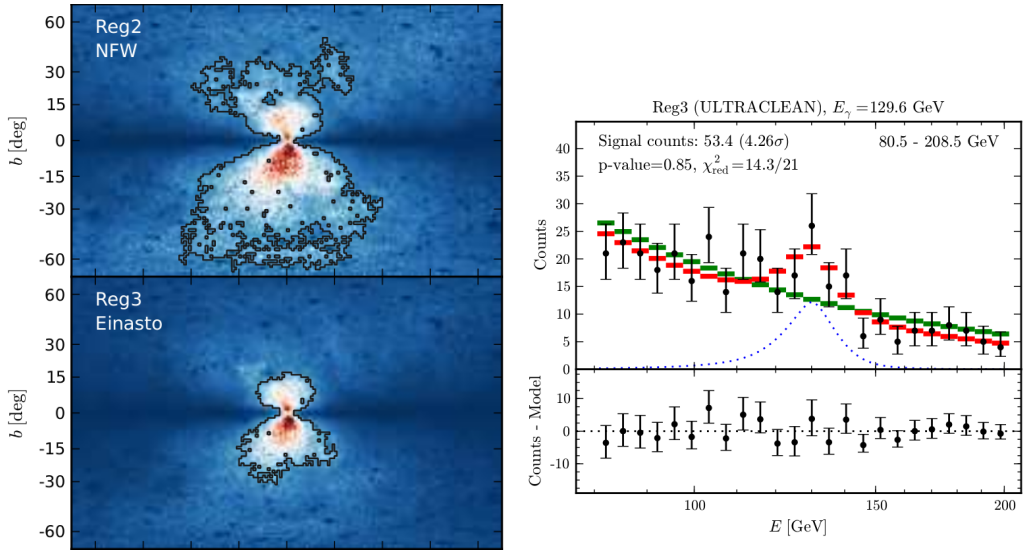

Figure 1: Plot extracted from [137]. On the left panel, distribution of the signal, red regions denoting the presence of the line in the two bubbles surrounding the galactic center. On the right panel, experimental data showing the 3.2σ excess at 130 GeV.

Z' boson through dimension 6 operators provides an elegant way to parametrize our ignorance on the underlying UV completion model but also a natural way to get very tiny interactions – thanks to a $1/\Lambda^n$ suppression – between the visible sector and the dark matter sector, which can communicate with the latter through the exchange of the Z' boson.

If one wants mediators parametrically heavier than the electroweak scale (say in the TeV range), we need, in addition to possible SM Higgs contributions, an additional source to their mass. A purely Dirac mass is of course a simple viable option. However as argued in [135, 136], because of the Furry theorem, in this case the only low-dimensional induced effective operator is the kinetic mixing, whereas the next higher-dimensional ones are of dimension eight.

A natural option to obtain dimension-six effective operators is alternatively to generate the mediator masses by the vev of some scalar field ϕ breaking spontaneously the Z' gauge symmetry (a heavy Higgs boson). The corresponding induced mediator masses, called generically M in what follows, determine the mass scale of the higher dimensional operators and also the UV cutoff of the effective theory. In principle, there could also be contributions to their mass from the SM Higgs field $m \sim \lambda\langle H\rangle = \lambda v$, but one can consider them to be smaller, such that we can expand in powers of v/M and obtain operators invariant under the SM gauge group. Such a framework was already investigated in [135, 136, 138, 139] from the viewpoint of the effective couplings of Z' to electroweak gauge bosons.

In the work we will present here, we wanted to explore the possibility that these heavy mediators could be charged under the colored $SU(3)$ gauged group of the standard model. Under such assumption, the Z' boson would naturally couple gluons through dimension six operators, suppressed by a power two in the mass scale M aforementioned providing very feeble interactions between the Z' and the colored sector of the visible sector. In what follows, we consider the kinetic mixing to be small enough (which has been actually tested to be a reasonable assumption in the parameter space allowed by the PLANCK/WMAP data). If we are interested in Z' couplings to gluons, this can be achieved for example by having colored

	ψ_{DM}	Ψ_M	ψ_{SM}
$U(1)_X$	•	•	
$U(1) \times SU(2) \times SU(3)$		•	•

Table 5.1: Summary of the gauge symmetries involved in the model. Standard model fermions are assumed to be charged only under standard model gauge group while heavy mediators Ψ_M are supposed to be charged both under the SM gauge group and the new abelian interaction. Finally, dark matter fermion ψ_{DM} is charged under $U(1)_X$ such that it can interact with the SM through a Z' exchange.

mediators with no hypercharge. We will restrict ourselves throughout this thesis to CP even couplings for simplicity.

As far as the dark matter sector is concerned, we will assume the dark matter candidate to be the lightest fermion in the dark sector and being charged under the $U(1)_X$ symmetry, such that the Z' interaction constitutes the unique portal between the visible and invisible sectors. The situation is summed up in Tab. 5.1.

5.1 Z', heavy fermion mediators and effective operators

We would like to make clear in this section, how to write an explicit model containing all the ingredients mentioned above, in a completely covariant manner. Effective operators generated by loops of heavy fermions are generically invariant under the Standard Model gauge group. As far as the $U(1)_X$ symmetry is concerned, it turns out that it can be realized non linearly, a la Stueckelberg. Indeed, if the mass of the mediators were induced by operators invariant under the whole gauge group then effective operators would be gauge invariant in the usual way. Yet heavy mediators get here their masses through the breaking of the $U(1)_X$ symmetry. The associated heavy Higgs can be hence expanded around its vacuum expectation value V, introducing the dimensionless axion field $\theta_X = \frac{a_X}{V}$

$$\Phi = \frac{1}{\sqrt{2}} (V + \phi) \exp(i\theta_X) \,. \tag{5.1.1}$$

The spontaneous breaking of the symmetry leads to an effective theory containing only the axionic field θ_X transforming non-linearly as follows

$$\delta Z'_\mu \;=\; \partial_\mu \alpha \quad , \quad \delta\theta_X \;=\; \frac{g_X}{2}\, \alpha \,. \tag{5.1.2}$$

The use of the covariant derivative

$$D_\mu \theta_X \equiv \; \partial_\mu \theta_X - \frac{g_X}{2} Z'_\mu \,, \tag{5.1.3}$$

provides an important tool for defining covariant effective operators as we will see.

The Lagrangian

We will give here the toolbox that will be explored in the following section for studying the possible interaction of dark matter with the gluons. In order to make the theory be as relevant as possible, we aim to derive in the cleanest manner a generic form for the effective operators, starting from a sufficiently general microscopic picture. The exact lagrangian that we will use, describing all the microscopic physics, including the mediator fields $\Psi_{L,R}$, is taken to be of the form

$$\begin{aligned}\mathcal{L} &= \mathcal{L}_{SM} + \bar{\Psi}^i_L \left(i\gamma^\mu D_\mu + \frac{g_X}{2} X^i_L \gamma^\mu Z'_\mu\right) \Psi^i_L + \bar{\Psi}^i_R \left(i\gamma^\mu D_\mu + \frac{g_X}{2} X^i_R \gamma^\mu Z'_\mu\right) \Psi^i_R \\ &- \left(\bar{\Psi}^i_L M_{ij} e^{\frac{i a_X (X^i_L - X^j_R)}{V}} \Psi^i_R + \text{h.c.}\right) + \frac{1}{2}(\partial_\mu a_X - M_{Z'} Z'_\mu)^2 - \frac{1}{4} F^X_{\mu\nu} F^{X\,\mu\nu} \end{aligned} \tag{5.1.4}$$

where $\mathcal{L}_{SM}$ is the Standard Model Lagrangian, D_μ's are the covariant derivatives with respect to the standard model gauge group, and where $M_{Z'} \equiv g_X V/2$. As stated above this lagrangian, being written in terms of covariant derivatives only, is invariant under (5.1.2) and hence completely gauge invariant.

For phenomenological applications, we consider here a model in which the dark matter is represented by the lightest stable fermion ψ^{DM} charged under Z' and uncharged under SM (the mass of dark matter will be denoted by m_ψ in what follows). The *mediators* $\Psi_{L,R}$ are considered to be heavy enough so that they have not been discovered yet in colliders. Assuming than they are heavier than both dark matter and the Z' boson, they can be integrated out so that we have to deal with effective operators, including new parameters. At low energy, the mediators being integrated out give rise to a new effective lagrangian

$$\mathcal{L}_{eff} = \mathcal{L}_1(\psi^{\rm DM}, Z'_\mu) + \mathcal{L}_2(A^{SM}_\mu) + \mathcal{L}_{mix}(Z'_\mu, A^{SM}_\mu) \ , \tag{5.1.5}$$

where $\mathcal{L}_2$ and $\mathcal{L}_1$ represent the new effective operators generated separately in the SM gauge sector and Z' one, whereas in $\mathcal{L}_{mix}$ we collect all the induced terms mixing Z' with the Standard Model. Notice that $\mathcal{L}_1$ also contains the DM particle (i.e. the lightest mediator) which is not integrated out.

As we explained earlier, the mediators acquire their mass after the breaking of the $U(1)_X$ symmetry, meaning their mass matrix has the symbolic form

$$M_{ij} \ \sim \ \lambda_{ij} V \ , \tag{5.1.6}$$

where V is the vev breaking the Z' gauge group $U(1)_X$. At the one-loop perturbative level, mediators generate only Z' couplings to the SM gauge fields and the SM Higgs as represented in Fig. 2 in the case of Z' coupling to gluons. Indeed, in the absence of kinetic mixing, one-loop couplings to SM fermions can be generated only if there are Yukawa couplings mixing mediators with SM fermions. We forbid such couplings in what follows[1].

As we will see in section 5.4, it is important, while building a particle physics model, not to introduce anomalies, especially while new triangle diagrams can be generated in addition to the standard model ones. If the UV complete model, describing the high-energy physics is

[1]Which can be easily achieved by imposing for instance a Z_2 parity, under which all mediator fields are odd and all SM fields are even

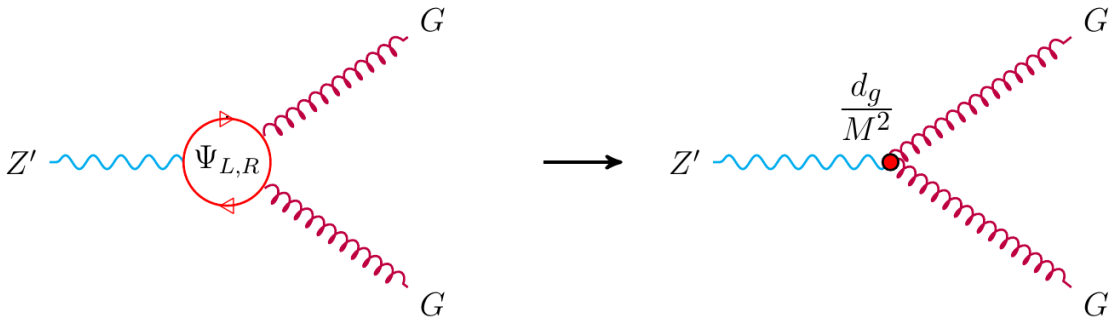

Figure 2: When heavy fermions are integrated out, they generate dimension-six effective operators of strength d_g/M^2.

anomaly-free and the SM fermions are neutral under Z', then the mediators have to form an anomaly-free set. We will consider that this is the case in what follows.

Another restriction that we will impose is the operators we introduce conserve CP for simplicity. Being given this hypothesis one has to note in addition that if the mediators are completely non-chiral, meaning they are completely vector-like both with respect to the SM and $U(1)_X$, there are no dimension-six induced operators, since the only one that can be potentially written, $\mathcal{T}r(F^X F_{SM}\tilde{F}_{SM})$ actually vanishes exactly (a demonstration can be found in Appendix C of [102]). In the case where these heavy fermions are chiral with respect to $U(1)_X$ and vector-like with respect to the SM, the induced dimension-six operators are

$$\begin{aligned}
\mathcal{L}^{(6)}_{\text{CP even}} &= \frac{1}{M^2}\Big\{ d_g \partial^\mu D_\mu \theta_X \mathcal{T}r(G\tilde{G}) + d'_g \partial^\mu D^\nu \theta_X \mathrm{Tr}(G_{\mu\rho}\tilde{G}^\rho_\nu) \\
&+ e_g D^\mu \theta_X \mathrm{Tr}(G_{\nu\rho}\mathcal{D}_\mu \tilde{G}^{\rho\nu}) + e'_g D_\mu \theta_X \mathrm{Tr}(G_{\alpha\nu}\mathcal{D}^\nu \tilde{G}^{\mu\alpha}) \Big\} \; + \\
&+ \frac{1}{M^2}\Big\{ D^\mu \theta_X \Big[i(D^\nu H)^\dagger (c_1 \tilde{F}^Y_{\mu\nu} + 2c_2 \tilde{F}^W_{\mu\nu}) H + h.c. \Big] \\
&+ \partial^m D_m \theta_X (d_1 \mathcal{T}r(F^Y \tilde{F}^Y) + 2d_2 \mathcal{T}r(F^W \tilde{F}^W)) + d'_{ew} \partial^\mu D^\nu \theta_X \mathrm{Tr}(F_{\mu\rho}\tilde{F}^\rho_\nu) \\
&+ e_{ew} D^\mu \theta_X \mathrm{Tr}(F_{\nu\rho}\mathcal{D}_\mu \tilde{F}^{\rho\nu}) + e'_{ew} D_\mu \theta_X \mathrm{Tr}(F_{\alpha\nu}\mathcal{D}^\nu \tilde{F}^{\mu\alpha}) \Big\} \;, \qquad (5.1.7)
\end{aligned}$$

where $\mathcal{D}_\mu G_{\alpha\beta}$ denotes the gluon covariant derivative, in components

$$\mathcal{D}_\mu G^a_{\alpha\beta} = \partial_\mu G^a_{\alpha\beta} + g f^{abc} G^b_\mu G^c_{\alpha\beta} \,, \qquad (5.1.8)$$

and where we defined, for notational convenience

$$\widetilde{F}_{\mu\nu} \equiv \frac{1}{2}\epsilon_{\mu\nu\rho\sigma}F^{\rho\sigma} \,, \quad \mathcal{T}r(FG) \equiv \mathrm{Tr}[F_{\mu\nu}G^{\mu\nu}] \,, \quad \mathcal{T}r(EFG) \equiv \mathrm{Tr}[E_\mu{}^\lambda F_{\lambda\nu} G^{\nu\mu}] \,, \qquad (5.1.9)$$

"Tr" taking into account a possible trace over non-abelian indices. The last three terms, indexed by "*ew*" in (5.1.7) refer to all $SU(2) \times U(1)_Y$ electroweak gauge bosons. In what follows we work in the unitary gauge where the axion is set to zero $\theta_X = 0$.

5.1.1 Microscopic Generation of Effective Couplings

After one has written down a lagrangian with the largest possible number of effective dimension six operators (see Eq. (5.1.7)), it turns out that the number of new parameters inserted to parametrize our ignorance on the underlying macroscopic theory is rather large. Since we imagined a UV complete formulation of how these operators are generated, one can try to derive explicit forms of these operators being given this high energy framework and check in particular which operators are indeed generated.

This can be achieved easily by computing the one loop triangle diagrams relating the Z' boson to a pair of gluons as depicted in Fig. 3.

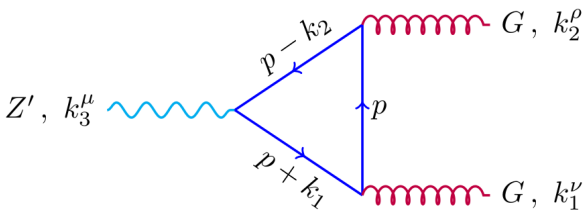

Figure 3: Integration of heavy fermions in a triangle diagram.

At the one loop order, there are several contributions to the effective vertex function $\Gamma^{\mu\nu\rho}$. The first is the triangle loop diagram without chirality flip, given by

$$\Gamma^{(1)}_{\mu\nu\rho} = \sum_i t_{iaa} \int \frac{d^4p}{(2\pi)^4} \, \mathrm{Tr}\left[\frac{\not{p} + \not{k}_2}{(p+k_2)^2 - M_i^2} \gamma_\rho \frac{\not{p}}{p^2 - M_i^2} \gamma_\nu \frac{\not{p} - \not{k}_1}{(p-k_1)^2 - M_i^2} \gamma_\mu \gamma_5 \right] . \tag{5.1.10}$$

where $t_{iaa} = \mathrm{Tr}(X_i T^a T^a)$. Using Ward identities, it is sufficient to compute this diagram in order to find the full amplitude[2]. After symmetrization among the two gluon legs, one finds

$$\Gamma^{\mathcal{O}}_{\mu\nu\rho} = -\sum_i \frac{i t_{iaa,L-R}}{12\pi^2 M_i^2} \{ [2(k_1+k_2)_\mu \epsilon_{\nu\rho\alpha\beta} - k_{1\rho}\epsilon_{\mu\nu\alpha\beta} - k_{2\nu}\epsilon_{\rho\mu\alpha\beta}] k_1^\alpha k_2^\beta + \epsilon_{\mu\nu\rho\alpha} k_1 k_2 (k_2 - k_1)^\alpha \} , \tag{5.1.11}$$

where $t_{iaa,L-R} = \mathrm{Tr}((X_L - X_R) T^a T^a)_i$ and the corresponding dimension-six operator for the triangle diagram represented in Fig. 3 turns out to be

$$\mathcal{O} = \frac{g_3^2}{24\pi^2} \sum_i \mathrm{Tr}\left(\frac{(X_L - X_R) T_a T_a}{M^2} \right)_i \left[\partial^\mu D_\mu \theta_X \mathcal{T}r(G\tilde{G}) - 2 D_\mu \theta_X \mathrm{Tr}(G_{\alpha\nu} \mathcal{D}^\nu \tilde{G}^{\mu\alpha}) \right] , \tag{5.1.12}$$

where g_3 is the QCD strong coupling.

On the other hand, it can be shown (see Appendix C of [102]) that the antisymmetric part of the amplitude in the gluonic legs is zero, which is consistent with the fact that there is no possible dimension-six operator mixing Z' to gluons, that is antisymmetric in the gluon fields. As a byproduct, we also find that the heavy mediators we are considering do not induce operators of the type

$$\frac{1}{M^2} \mathrm{Tr}(G_{\mu\nu} [G^{\nu\lambda}, \tilde{G}^\mu_\lambda]) , \tag{5.1.13}$$

[2]Find a proper demonstration in Appendix B of [102]

that are completely antisymmetric in the three gluon fields , and similar operators for electroweak gauge fields. This means that there are no constraints from purely SM dimension-six operators induced in this setup and all the phenomenological constraints come from the mixing of Z' with SM fields.

Let us come again to the expression 5.1.1. Indeed, the implication of such formula are of great importance for what will follow. As we saw, writing down an generic lagrangian, conserving the global CP symmetry, and coupling together a Z' with gluons gives rise to four different operators to which are associated four different free parameters. Among other details, what we showed here is that only two of these four operators are actually generated through loops in the quite generic picture of heavy fermions integrated out. Furthermore, the exact computation of the latter loop provides a relation between the two remaining free parameters, expressing both in terms of the heavy mediators charges and the strong coupling. As a consequence, one ends with two different effective operators providing the effective interaction lagrangian

$$\mathcal{L}_{int} = \frac{d_g}{M^2}\left[\partial^\mu D_\mu \theta_X \mathcal{T}r(G\tilde{G}) - 2D_\mu\theta_X \mathrm{Tr}(G_{\alpha\nu}\mathcal{D}^\nu \tilde{G}^{\mu\alpha})\right] , \tag{5.1.14}$$

where

$$d_g \equiv \frac{g_3^2}{24\pi^2}\sum_i \mathrm{Tr}\left[(X_L - X_R)T_a T_a\right]_i . \tag{5.1.15}$$

5.2 Dark Matter Annihilation to gluons

We just saw how one can express the interaction lagrangian of our Z' boson with a pair of gluons, generating explicitly the effective operators in terms of microscopic charges involved in the underlying high energy theory. It is yet important to notice that, with on-shell gluons in the final state, only the first operator will contribute to the amplitude. We will hence continue working with the simplified lagrangian

$$\mathcal{L}_{int} = \frac{d_g}{M^2}\left[\partial^\mu D_\mu \theta_X \mathcal{T}r(G\tilde{G})\right] . \tag{5.2.1}$$

On the side of the dark sector, we assume dark matter to couple minimally to the Z' boson as follows

$$\mathcal{L} \supset \bar{\psi}_L^{DM}\frac{g_X}{2}X_L^{DM}\gamma^\mu Z'_\mu \psi_L^{DM} + \bar{\psi}_R^{DM}\frac{g_X}{2}X_R^{DM}\gamma^\mu Z'_\mu \psi_R^{DM} , \tag{5.2.2}$$

which provides us two ways of annihilating dark matter. The first one is an *s-channel* production of an off shell Z' boson decaying to a pair of gluons. The second one is a *t-channel* process, leading to two Z' bosons, which will mostly decay into gluons. The associated Feynman diagrams are presented in Fig.4.

In the unitary gauge, rescaling for notation convenience the effective coupling d_g the Z'-gluon-gluon vertex coming from the operator d_g is

$$\frac{d_g}{M^2}\left\{g_X \partial^m Z'_m \epsilon^{\mu\nu\rho\sigma}\partial_\mu G^A_\nu \partial_\rho G^A_\sigma\right\} . \tag{5.2.3}$$

The propagator of the vector boson Z' in the unitary gauge is

$$\Delta(q) = -i\,\frac{\eta_{\mu\nu} - \frac{q_\mu q_\nu}{M^2_{Z'}}}{q^2 - M^2_{Z'} + iM_{Z'}\Gamma(Z')} , \tag{5.2.4}$$

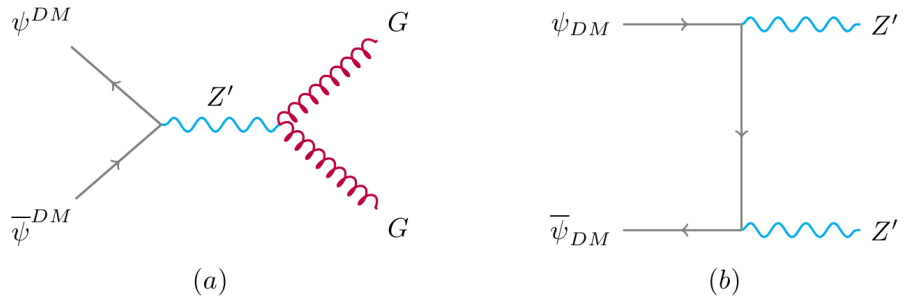

Figure 4: Gluon pair production via two different processes, that are the s-channel (a) and the t-channel Z' pair production (b), that decay subsequently into two gluons each.

For dark matter fermions of mass smaller than $M_{Z'}/2$, the main contribution to the Z' width $\Gamma(Z')$ is $\Gamma(Z' \to \psi^{DM}\overline{\psi^{DM}})$, which is computed to be

$$\Gamma(Z') = \frac{g_X^2}{384\pi M_{Z'}^2}\left[(X_L^2+X_R^2)M_{Z'}^2 - (X_L^2+X_R^2-6X_RX_L)m_\psi^2\right]\sqrt{M_{Z'}^2-4m_\psi^2}\ . \tag{5.2.5}$$

For heavier masses of dark matter, one has to consider the Z' decay width into gluons and $SU(2)$ gauge bosons. However, it can be easily checked that the detailed values of these widths do not influence much the results in what follows[3].

5.2.1 *s*-channel Cross-Section

Vector-coupling case

In the case of a vector-like coupling of DM fermion to Z' boson (no γ^5 in the coupling), one obtains the interaction lagrangian

$$\mathcal{L}_{int} = \bar{\psi}^{DM}\frac{g_X}{2}X^{DM}\gamma^\mu Z'_\mu\psi^{DM}, \quad \text{where} \qquad X^{DM} \equiv X_R^{DM} = X_L^{DM}\ . \tag{5.2.6}$$

One can then perform the tree-level diagram cross section and find out that the amplitude vanishes $\mathcal{M}=0$. Therefore, the d_g-term coupling does not contribute to the final cross section at all. Indeed, due to the effective coupling of the form $d_g\partial^m Z'_m \mathcal{T}r(G\tilde{G})$, the vertex $Z'\psi^{DM}\psi^{DM}$ gets multiplied by the virtual momentum as follows

$$q^\mu\bar{v}(p_2)\gamma_\mu u(p_1) = \bar{v}(p_2)(\not{p}_2+\not{p}_1)u(p_1) = 0\ , \tag{5.2.7}$$

after using Dirac equation for the spinors describing the wave functions of the dark matter fermions. Hence one has to write an interaction between dark matter and our new gauge boson Z' using an axial coupling.

[3]Indeed, we will see that the cross section of dark matter annihilation into gluons is suppressed for an invariant mass $\sqrt{s}$ approaching $M_{Z'}$, as a consequence of the Landau-Yang theorem [140]. In the non-relativistic approximation, this happens in the energy region closed to $s \simeq 4m_\psi^2 + m_\psi^2 v_{rel}^2 \geqslant 4m_\psi^2$. The suppression therefore occurs for a mass m_ψ significantly lower than $M_{Z'}/2$, where the decay width is essentially that of decay into two dark matter particles.

Axial-vector couplings case
Adding to the previous coupling an axial component, one can write in full generality, an axial-vector coupling

$$\mathcal{L}_{int} = \frac{g_X}{2}\left(\frac{X_R^{DM}+X_L^{DM}}{2}\right)\bar{\psi}^{DM}\gamma^\mu Z'_\mu\psi^{DM} + \frac{g_X}{2}\left(\frac{X_R^{DM}-X_L^{DM}}{2}\right)\bar{\psi}^{DM}\gamma^\mu\gamma_5 Z'_\mu\psi^{DM}\,. \quad (5.2.8)$$

The annihilation cross section of dark matter into a gluon pair takes non zero values in this case and becomes

$$\sigma_{s-channel} = \frac{d_g^2}{M^4}\frac{(-4E^2+M_{Z'}^2)^2}{(-4E^2+M_{Z'}^2)^2+M_{Z'}^2\Gamma^2(Z')}\frac{E^5 g_X^4 m_\psi^2(X_L-X_R)^2}{\pi M_{Z'}^4\sqrt{E^2-m_\psi^2}}\,. \quad (5.2.9)$$

It is worth to notice that this cross section is suppressed for energies of order $M_{Z'}/2$ due to the Landau-Yang theorem[140]. Indeed the latter states that a spin 1 massive vector boson, cannot decay into two massless spin one. There is also a helicity suppression for the case of a light dark matter, that can be understood by writing the vertex $Z'\psi^{DM}\psi^{DM}$ in this case

$$\begin{aligned}(X_L-X_R)q^\mu\bar{v}(p_2)\gamma_\mu\gamma_5 u(p_1) &= (X_L-X_R)\bar{v}(p_2)(\not{p}_2\gamma_5-\gamma_5\not{p}_1)u(p_1)\,,\\ &= -2m_\psi(X_L-X_R)\bar{v}(p_2)\gamma_5 u(p_1), \end{aligned} \quad (5.2.10)$$

by the use of Dirac equation.

This finally gives in the non-relativistic approximation $s \simeq 4m_\psi^2 + m_\psi^2 v_{rel}^2 \Leftrightarrow E \simeq m_\psi\sqrt{1+\frac{v_{rel}^2}{4}}$, with v_{rel} being the relative velocity between the two colliding dark matter fermions, the total cross section

$$\langle\sigma v\rangle_{s-channel} \simeq \frac{d_g^2}{M^4}\frac{g_X^4 m_\psi^6(X_L-X_R)^2}{\pi M_{Z'}^4}\left\{\frac{2\left(M_{Z'}^2-4m_\psi^2\right)^2}{\left(M_{Z'}^2\Gamma^2(Z')+\left(M_{Z'}^2-4m_\psi^2\right)^2\right)}\right\}+\mathcal{O}\left(v^2\right) \quad (5.2.11)$$

5.2.2 *t*-channel Cross Section

As mentioned earlier, we also have to consider a t-channel process, producing pairs of Z' bosons in dark matter annihilation for Z' mass below the dark matter mass. Considering that the only non vanishing coupling is the one in d_g, each Z' will decay into gluons; this process will then produce gluons in the final state. After expanding in powers of v^2, the cross-section in this case can be expressed as

$$\begin{aligned}\langle\sigma v\rangle_{t-channel} = &\frac{g_X^4\sqrt{m_\psi^2-M_{Z'}^2}}{128\pi^2 m_\psi M_{Z'}^2\left(2m_\psi^2-M_{Z'}^2\right)^2}\left(2m_\psi^4X_L^4-4m_\psi^4X_L^2X_R^2+2m_\psi^4X_R^4-3m_\psi^2M_{Z'}^2X_L^4\right.\\ &\left.+10m_\psi^2M_{Z'}^2X_L^2X_R^2-3m_\psi^2M_{Z'}^2X_R^4+M_{Z'}^4X_L^4-6M_{Z'}^4X_L^2X_R^2+M_{Z'}^4X_R^4\right)+\mathcal{O}\left(v^2\right)\,.\end{aligned}$$

(5.2.12)

5.3 Constraining the Model with Experimental Data

We have so far made theoretical computations, determining how dark matter could interact with gluons through an annihilation process. We aim, in this section, to constrain the parameter space to enter the recent experimental measurements error bars or excesses with respect to the standard model. A coupling $Z'GG$ can be tested in several laboratories, from direct detection experiments to indirect detection, relic abundance or LHC searches. We present in the following the constraints obtained from these different searches, before summarizing all of them at the end of the section. The reader can find a recent complementary analysis of gluonic effective couplings to dark matter in [141].

5.3.1 Relic Abundance vs Indirect Detection

We saw in section 4.2.1 that the relic abundance Ω_{DM} of dark matter, present nowadays in our universe, highly depends on the cross section of annihilation of dark matter that we computed in the previous section. Indeed, the thermal equilibrium that keeps dark matter at the same temperature than the thermal bath for a while strongly depends on its capacity to be produced, and to annihilate, before it completely decouples from the latter. As far as numbers are concerned, the PLANCK collaboration released recently its latest results concerning the composition of the Universe [142]. It confirms the results of WMAP experiment [143] obtaining for the relic abundance of non–baryonic matter $\Omega h^2 = 0.1199 \pm 0.0027$ at 68% of CL. Using the relation 4.2.12, one can hence use this high level of precision to know what reasonable parameters provide a sufficient production of dark matter from the thermal bath to respect the previous PLANCK/WMAP results.

Moreover, if dark matter is present in the galaxy and in different celestial bodies, its weak interaction with ordinary matter should produce detectable traces in the indirect detection experiments. Indeed, astrophysical constraints arise from the study of diffuse gamma ray produced indirectly by the dark matter annihilation in various astrophysical bodies, among which are the center of the Milky Way [144], the galactic halo [145], the dwarf spheroidal galaxies [146] or the radio observation of nearby galaxies like M31 [147].

These two different kinds of constraints acts on a theoretical model in opposite manners. On one hand, the cross section given by the relic abundance will set a lower bound on the theoretical cross section we predict. Indeed, knowing the amount of visible matter present in the Universe and making dark matter interact too feebly with the visible sector would predict the presence of a huge amount of dark matter, which is not observed by the Planck/WMAP measurements and would render the Universe overclose. On the other hand, indirect detection sets an upper bound on the cross section, stating, being given the amount of unexplained ray production we observe in the Universe and the expected amount of present dark matter, what can be the highest possible interaction rate.

Relic abundance

As we just saw, depending on the spectrum, two annihilation processes allow the dark matter candidate to keep thermal equilibrium with the standard model particles of the plasma: the s–channel exchange of a Z' (Eq.5.2.11) with a pair of gluons, and the t-channel production of Z' (Eq.5.2.12), as long as this channel is kinematically open. It is then possible to solve

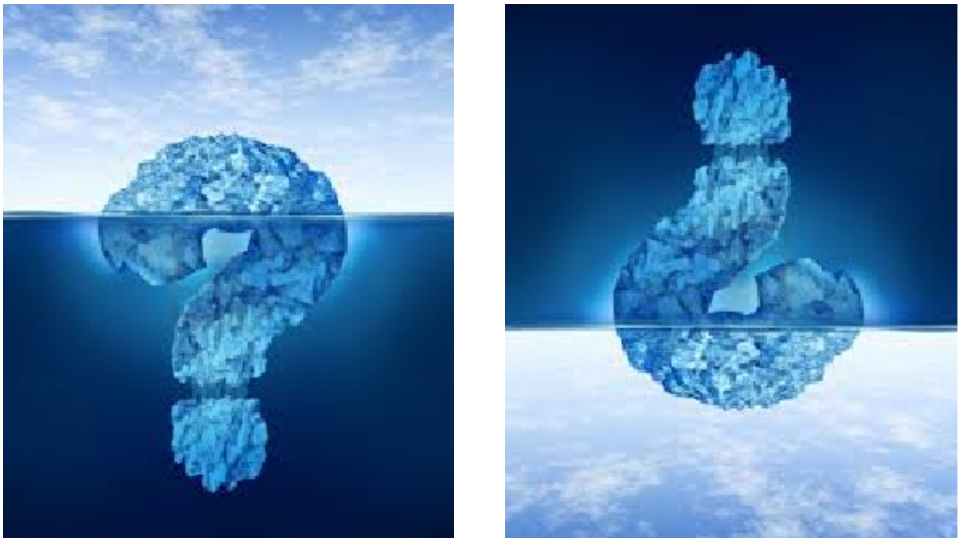

Figure 5: Different approaches to constrain the parameter space. Relic abundance is a measure of the ratio *dark matter / visible matter* present in the Universe (bound on the hidden part of the iceberg, compared to the visible one). If the cross section was too low, one would need much more dark matter to explain the amount of visible matter we actually observe. Indirect detection sets an upper bound on the visible rays in the Universe (visible part of the iceberg), setting upper limits on the annihilation cross section.

numerically the Boltzman equation 4.2.8 to compute, in our theoretical model what is the relic density for a given choice of parameters.

Adapting the public software MicrOMEGAs [148], one can easily find out from (5.2.11-5.2.12) which parameters give the right relic density. We noticed in section 5.2.1 that the coupling of the dark matter should be axial, as the vectorial part of the current coupling to Z'_μ does not gives any contribution to the process $\psi^{DM}\psi^{DM} \to Z' \to GG$. For simplicity, we will set charges $X_R = 1, X_L = 2 \;\Rightarrow\; |X_R - X_L| = 1$. Our results for a different set of charges are modified in a straightforward way. To keep our results as conservative as possible, we plotted the WMAP limits $0.087 < \Omega h^2 < 0.138$ at 5σ.

We show in Fig. 6 the parameter space allowed in the plane $(\frac{M^2}{d_g}, m_\psi)$ for different values of $M_{Z'}$ and g_X. Points *above* the red lines region would lead to an overpopulation of dark matter whereas points lying *below* the red lines would require additional dark matter candidates to respect PLANCK/WMAP constraints. We can notice several, interesting features from these results. First of all, we observe that as soon as the $Z'Z'$ final state is kinematically allowed ($m_\psi > M_{Z'}$) this annihilation channel is the dominant one as soon as g_X is sufficiently large (we checked that this happens for $g_X \gtrsim 0.3$) and mainly independent on the dark matter mass. This is easy to understand after an inspection of Eq.(5.2.12). Indeed, in the limit $m_\psi \gg M_{Z'}$, one obtains $\langle\sigma v\rangle_{Z'Z'} \simeq \frac{9g_X^4}{256\pi^2 M_{Z'}^2}$. In other words, once

$$\frac{9\ g_X^4}{256\pi^2 M_{Z'}^2} \gtrsim 2.5\times10^{-9}\ \text{GeV}^{-2} \quad\to\quad g_X \gtrsim 3\times10^{-2}\sqrt{\frac{M_{Z'}}{\text{GeV}}}\ , \tag{5.3.1}$$

then the t-channel process $\psi^{DM}\psi^{DM} \to Z'Z'$ dominates the annihilation and forbids the dark matter to overpopulate the Universe ($\Omega_\psi h^2 \lesssim 0.138$). This corresponds to $g_X \simeq 0.3$ for $M_{Z'} = 100$ GeV and $g_X \simeq 1$ for $M_{Z'} = 1$ TeV, which fits pretty accurately the numerical results we

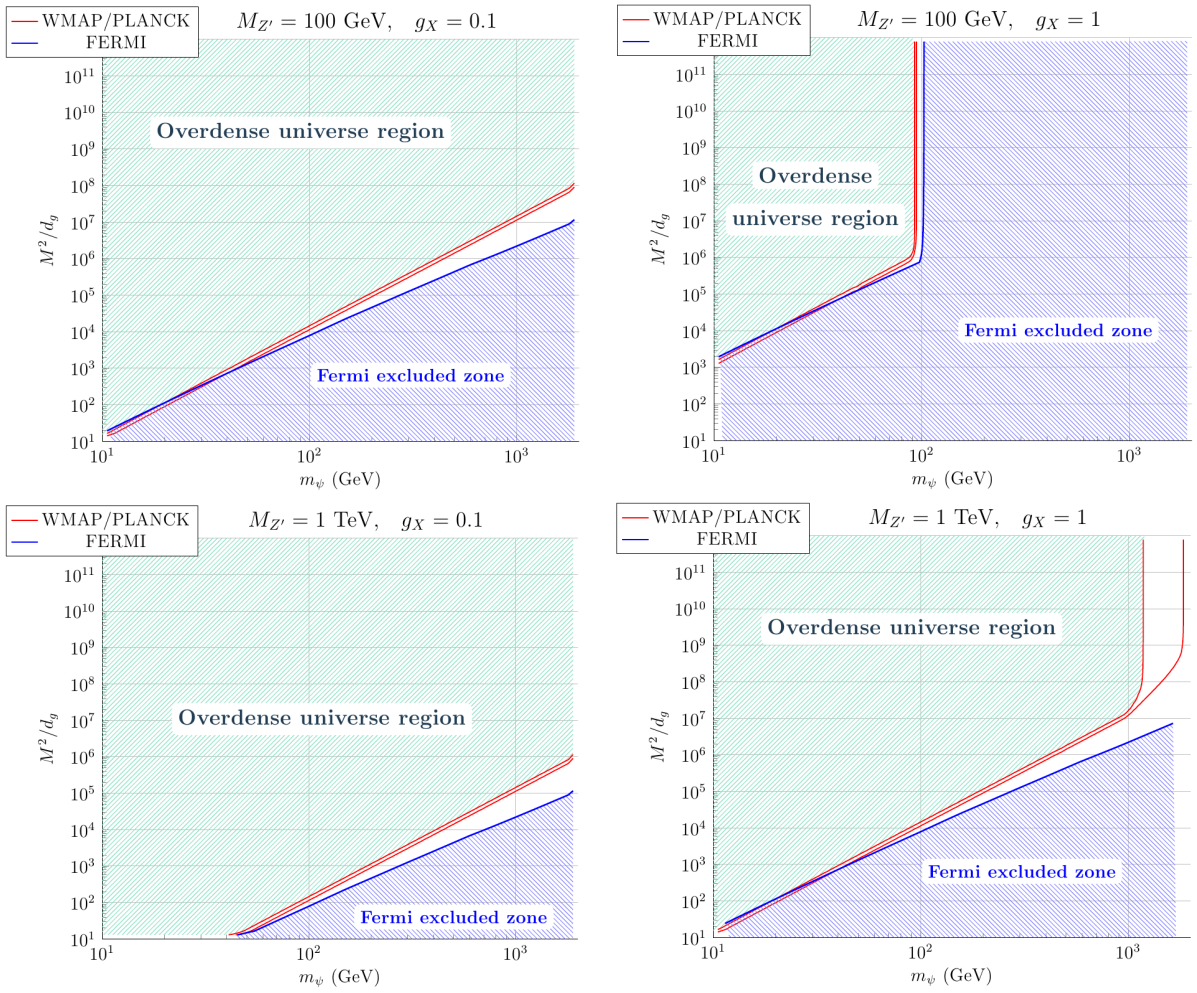

Figure 6: Constraints from WMAP/PLANCK (red line) and FERMI dSphs galaxies (blue line) in the $(\frac{M^2}{d_g}, m_\psi)$ plane for different values of g_X (0.1 on the left and 1 on the right), $M_{Z'} = 100$ GeV (up) and $M_{Z'} = 1$ TeV (down). See the text for more details.

obtained. This limit also explains why the region allowed by PLANCK/WMAP is larger for $M_{Z'} = 1$ TeV: the value $g_X = 1$ is at the border limit for the $t-$channel to dominate. From Eq.(5.3.1) we also understand why the $Z'Z'$ final state, even if kinematically allowed, has no influence on the limits set by the relic abundance for $g_X = 0.1$: the coupling is too small to give sufficient annihilation products. The dominant process is then the $s-$channel Z' exchange ($\simeq 15\%$ of $Z'Z'$ final state for $g_X = 0.1$ and $M_{Z'} = 1$ TeV.).
The linearity of the constraints coming from WMAP/Planck data when the $s-$channel is dominating can also be easily understood. Indeed, after a glance at Eq.(5.2.11), one obtains, neglecting the tiny region around the pole $M_{Z'} = 2m_\psi$,

$$\langle \sigma v \rangle \simeq \frac{d_g^2}{M^4} \frac{2g_X^4}{\pi} \frac{m_\psi^6}{M_{Z'}^4} \quad (\text{for } M_{Z'} \gg m_\psi \text{ or } M_{Z'} \ll m_\psi) \ , \tag{5.3.2}$$

implying, for constant $\langle \sigma v \rangle$,

$$\log\left(\frac{M^2}{d_g}\right) = 3 \log m_\psi + \text{const} \ , \tag{5.3.3}$$

which is exactly the behavior we observe in Fig.6.

Indirect Detection
As far as the constraints from indirect detection are concerned, we have considered the ones obtained by the observation of dwarf galaxies by the FERMI telescope [146]. Since dwarf galaxies are mainly composed of dark matter, the background is there naturally minimized.

We show the result of our analysis in Fig.6 where the points *below* and on the *right* of the blue lines are excluded by FERMI observations. As expected, the region below $m_\psi \lesssim 40 - 50$ GeV (where the curves from FERMI and WMAP/PLANCK cross) is in tension with FERMI limit, as hadronic final states are the more restricted by FERMI analysis, which seems to exclude any thermal relics below this dark matter mass. When the $Z'Z'$ final state is allowed, the annihilation cross section $\psi\psi \to Z'Z'$ is so large that it is almost automatically excluded by FERMI data. One can notice however that FERMI considers in their analysis the Z' decays into quarks only, whereas in our case it decays into gluons.

5.3.2 Direct Detection

Since our proposal is to make dark matter interact with the strong sector one could easily imagine that this model could have signatures in direct detection experiments. In order to investigate this possibility, one can integrate out the Z' gauge boson and write the corresponding dimension-eight operator connecting the dark matter with the gluons. One gets

$$\frac{d_g}{M^2 M_{Z'}^2} \ \bar{\psi}^{DM} \gamma^\mu \left(\frac{X_R + X_L}{2} + \frac{X_R - X_L}{2} \gamma_5 \right) \psi^{DM} \mathcal{T}r \ \partial_\mu (G\tilde{G}) \ . \tag{5.3.4}$$

By using the observed CP invariance of the strong interactions, we find that the only non-vanishing relevant gluonic matrix element we can write between an initial and a final nucleon state is $\langle N(p)|\text{Tr } G_\mu^\nu \tilde{G}_\nu^\lambda |N(p')\rangle = A \epsilon_\mu^{\lambda\alpha\beta} p_\alpha p'_\beta$, where A is a Lorentz invariant. As a consequence,

$$\langle N(p)| \mathcal{T}r \ \partial_\mu (G\tilde{G}) |N(p')\rangle = 0 \ . \tag{5.3.5}$$

There are therefore **no constraints on this operator from direct detection experiments**.

5.3.3 Monojet Events at the LHC

As a generic feature of dark matter models, the annihilation process should be looked upside down to be considered also from the point of view of dark matter production in accelerators. The model described in previous sections can therefore be probed at the LHC. Indeed the Z'-gluon-gluon vertex makes possible to produce a dark matter pair out of two protons, provided a Z' is produced. Typical production channels are shown in Fig. 7, where we consider a generic process:

$$p\ p \to j\ \bar{\psi}_{\rm DM}\ \psi_{\rm DM} \tag{5.3.6}$$

of a proton-proton collision giving rise to 1 jet, plus missing energy ($E_T^{\rm miss}$).

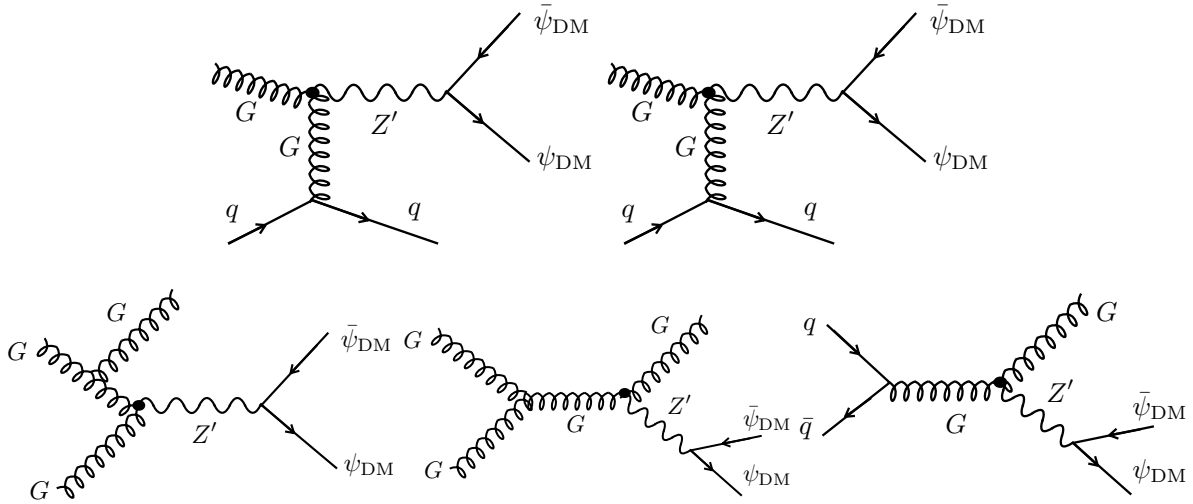

Figure 7: Dark matter production processes at the LHC (at partonic level), in association with 1 jet: $p\ p \to j\bar{\psi}_{\rm DM}\psi_{\rm DM}$.

The monojet final state was first studied using Tevatron data [149] in the framework of effective $\psi_{\rm DM}$-quark interactions of different nature. In a similar fashion, bounds to dark matter effective models have been obtained by analyzing single-photon final states using LEP [150] and LHC [151] data. An interesting complementarity between these two approaches has been analyzed in [152]. Since then, the ATLAS and CMS groups have taken the monojet signal analyses as an important direction in the search for dark matter at the LHC (see [153] and [154] for the most recent results from ATLAS and CMS, respectively).

For achieving this study we used the monojet data coming from the CMS analysis [154], which collected events using a center-of-mass energy of 8 TeV up to an integrated luminosity of 19.5/fb. The results are shown in Fig. 8, where we show the exclusion power of the monojet analysis to the model. We present the bounds for the quantity M^2/d_g as a function of the dark matter mass, for three different values of the Z' mass: 100 GeV, 500 GeV and 1 TeV.

5.3.4 Constraints Summary

All the constraints detailed above can finally be gathered in a single plot to see what are the new allowed regions in the parameter space. Superposing Fig.(6) and 8, we get a new representation of those *validity zones*, as represented in Fig.(9). As explained earlier, parameters are allowed

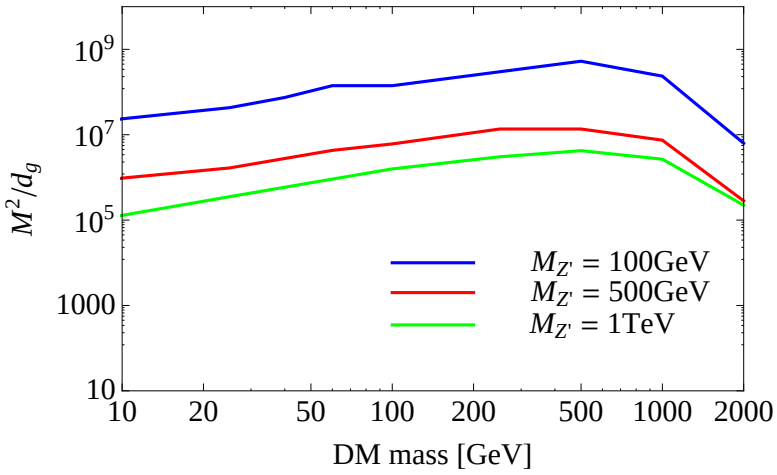

Figure 8: 90% CL lower bounds on the quantity M^2/d_g as a function of the dark matter mass, for $M_{Z'} = 100$ GeV (blue), 500 GeV (red) and 1 TeV (green). Based on the CMS analysis with collected data using a center-of-mass energy of 8 TeV and a luminosity of 19.5/fb.

to lie below the red/full lines (Overdensity of the universe), above the orange/full line (LHC bounds on monojets production). Since the whole study has been released using effective dimension six operators generated by integrating out heavy fermions loops, one has to check that the parameter range is still in the window where $M \gg m_\psi$. This is indicated on Fig.(9) where we considered natural values of d_g varying between 10^{-2} and 1 (purple and green/dashed line, respectively). Thus one can easily distinguish between the two regions $m_\psi \ll M$ (upper region) and $m_\psi \gg M$ (lower region).

In the case where $d_g \sim 10^{-2}$, it is important to notice that low values of the coupling constant g_X provide almost no validity region in the parameter space since parameters have to lie above the purple/dashed line. On the other hand, for $g_X = 1$ one can also notice that the allowed region is much larger in the case of a heavy Z'. The case $d_g \sim 1$ considerably relax the constraints since the validity zones are almost in the region where $m_\psi \ll M$ (below the green/dashed line).

The model we exposed hence appears to be viable in most of the situations explored. As a general feature it appears that the mass of dark matter should exceed the mass of the Z' boson and that the bigger the coupling g_X, the more the area of validity is open. However let us recall that in our microscopic interpretation of the non renormalizable operators, both the masses of Z' and the heavy mediators were sourced by a heavy higgs vev V as follows

$$M_{Z'} \equiv \frac{g_X}{2} V \,, \tag{5.3.7}$$

$$M \sim \lambda_{ij} V \,, \tag{5.3.8}$$

where λ_{ij} were Yukawa couplings. Hence it turns out that the relation between M and $M_{Z'}$ is not arbitrary and would lead, for similar values of the Yukawas and the coupling constant g_x to a rough estimation

$$M \sim M_{Z'} \,. \tag{5.3.9}$$

In such case, and for values of d_g of order $\mathcal{O}(0.1-1)$ the situation with a Z' of mass ~ 100GeV seems disfavored since the effective coupling d_g/M^2 is required to be lower than $\mathcal{O}(10^{-8}-10^{-7})$,

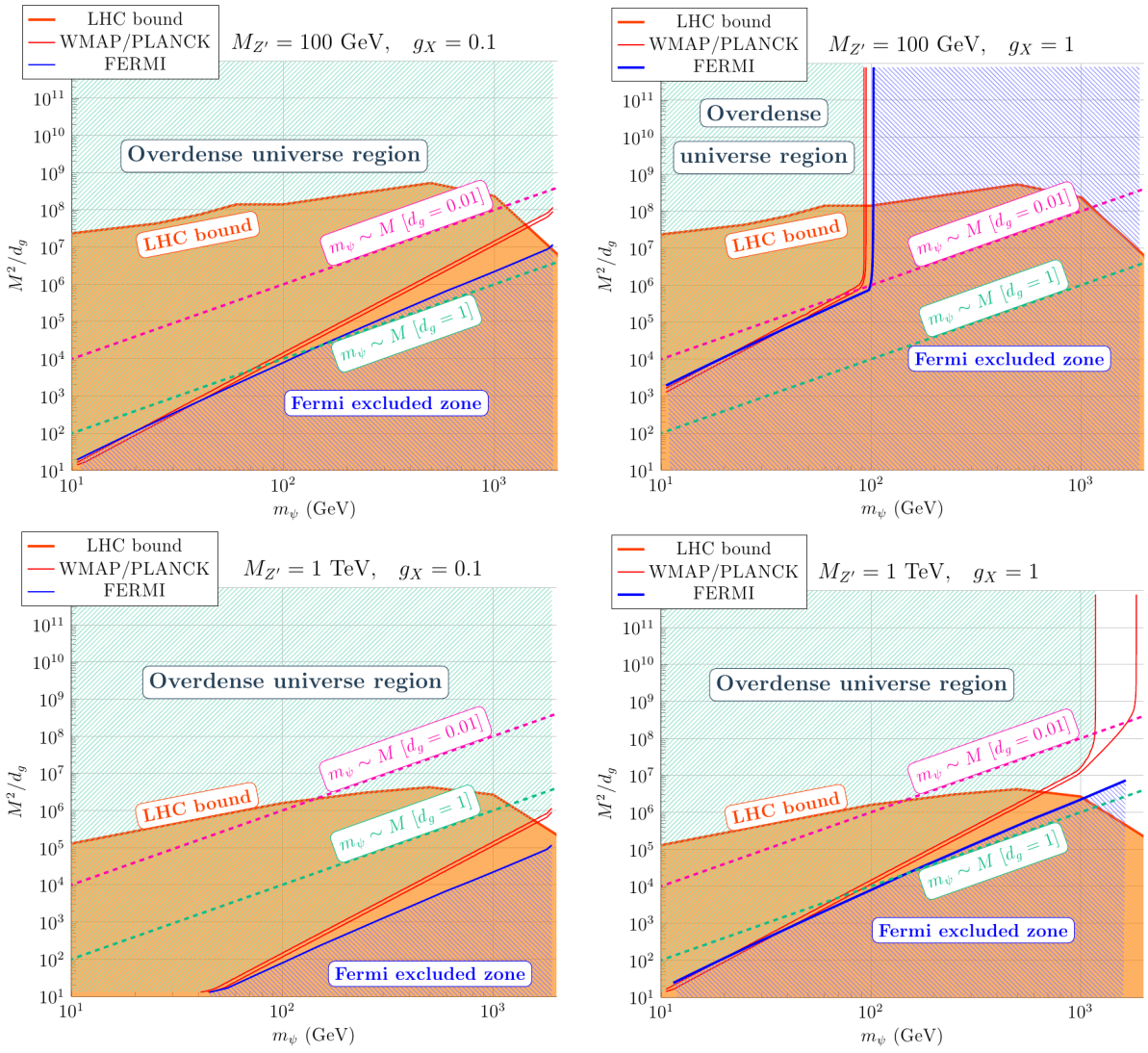

Figure 9: Experimental constraints on m_ψ and M^2/d_g parameters, including LHC and universe overdensity constraints. Below the purple/dashed line $M \ll m_\psi$ and the effective theory analysis we made is not valid.

which is difficult to release with Eq. (5.3.9) for natural choices of the microscopic parameters. It hence turns out that a Z' in a range of mass over 500GeV is then safer from the microscopic point of view.

5.4 Anomaly Cancellation

As we mentioned in section 5.1, introducing new couplings to heavy mediators can potentially produce anomalies in a quantum field theory model. After reviewing anomaly cancellation, we will present how one can imagine a model in which such a Z' boson could in principle couple even to SM quarks without introducing anomalies.

Let us consider the simplest (massive) fermionic lagrangian

$$\mathcal{L} = \bar{\psi}\left(\not{\partial} - e\not{A} - m\right)\psi\,. \tag{5.4.1}$$

In the limit where the mass m goes to zero, this lagrangian is left invariant by two global symmetries, called respectively *vector* and *axial* symmetries

$$\psi \to e^{i\alpha}\psi\,, \qquad \psi \to e^{i\beta\gamma^5}\psi\,. \tag{5.4.2}$$

The Noether currents (vector and axial currents) associated to the latter transformations can then be written

$$J_V^\mu = \bar{\psi}\gamma^\mu\psi\,, \qquad J_A^\mu = \bar{\psi}\gamma^\mu\gamma^5\psi\,, \tag{5.4.3}$$

and satisfy classically the equations of motion

$$\partial_\mu J_V^\mu = 0\,, \qquad \partial_\mu J_A^\mu = 2im\bar{\psi}\gamma^5\psi\,, \tag{5.4.4}$$

where the vector current turns out to be exactly conserved while the axial current is only conserved in the massless limit. At the quantum level, a carefull analysis of the non invariance of the effective action with the path integral shows that the axial divergence, has an additional anomalous term related to the electromagnetic background as follows

$$\left(\partial_\mu J_A^\mu\right)_{an.} = -\frac{e^2}{16\pi^2}\epsilon^{\mu\nu\rho\sigma}F_{\mu\nu}F_{\rho\sigma}\,. \tag{5.4.5}$$

To show this, one can indeed study the effect of symmetries on the functional measure in the path integral

$$\langle\mathcal{O}(x_1,x_2,...,x_n)\rangle = \frac{1}{Z[0]}\int \mathcal{D}\bar{\psi}\mathcal{D}\psi exp\left\{i\int \mathrm{d}^4x i\bar{\psi}\not{\partial}\psi\right\}\mathcal{O}(x_1,x_2,...,x_n)\,, \tag{5.4.6}$$

where $\mathcal{O}$ is an arbitrary gauge invariant operator. In what follows we will consider this operator to contain a product of currents $\mathcal{O}(x,y) = J^\mu(x)J^\nu(y)$. One can then show that invariance of this path integral under a local, vector transformation imposes that

$$\partial_\mu\langle J_V^\mu(x)\mathcal{O}(x_1,x_2,...,x_n)\rangle = 0\,, \tag{5.4.7}$$

whereas the invariance transformation under axial transformations leads to

$$\partial_\mu\langle J_A^\mu(x)\mathcal{O}(x_1,x_2,...,x_n)\rangle_{an.} = -\frac{e^2}{16\pi^2}\langle\epsilon^{\mu\nu\rho\sigma}F_{\mu\nu}(x)F_{\rho\sigma}(x)\mathcal{O}(x_1,x_2,...,x_n)\rangle\,, \tag{5.4.8}$$

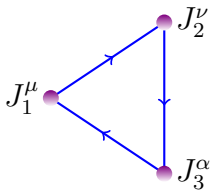

Figure 10: Triangle diagram computed with entries containing only Noether currents, providing the vertex function $M^{\mu\nu\alpha}$.

giving the result aforementioned.

This result can be recovered by computing the loop triangle diagrams in which the pion π^0 couples to photons. In the presence of the operator $\mathcal{O} = i\lambda\pi\bar{\psi}\gamma^5\psi$, the amplitude of the process takes the form

$$\mathcal{M} = \lambda\frac{e^2}{4\pi^2 m}\epsilon^{\mu\nu\sigma\rho}\epsilon_\mu^{\gamma_1}\epsilon_\nu^{\gamma_2}q_\rho^{\gamma_1}q_\sigma^{\gamma_2}\,, \tag{5.4.9}$$

which is to say that the operator to which the pion couples in an electro magnetic background takes the mean value given by Eq. 5.4.5. A major difference between the classical and the quantum theory in this case stands in the fact that this non conservation of the axial current is still true at the quantum level in the limit where $m = 0$. This discrepancy between the classical and the quantum theory while looking at the symmetries of a given lagrangian tells us that the chiral symmetry is *anomalous*.

More generically, in an arbitrary gauge theory, involving several gauge groups, anomalies can naturally arise at the one loop level through the non conservation of operators of the form

$$\mathcal{O}_{ijk}^{\mu\nu\alpha}(x,y,z) = J_i^\mu(x)J_j^\nu(y)J_k^\alpha(z)\,, \tag{5.4.10}$$

where indices i, j, k stem for the different gauge groups involved. The computation of the triangle diagrams represented in Fig. 10 will then give us direct indication on the presence of gauge anomalies in the theory.

In particular, let us consider a theory containing only one left handed Weyl fermion

$$\mathcal{L} = -\frac{1}{4}F_{\mu\nu}^2 + \bar{\psi}\left(i\not{\partial} - e\not{A}\right)P_L\psi\,, \tag{5.4.11}$$

where, as usual, $P_L \equiv \frac{1}{2}(1-\gamma^5)$. In this case the photon couples to a current $J_L^\mu = \bar{\psi}\gamma^\mu P_L\psi$ and one can denote the three point function for currents $\langle J_L^\mu J_L^\nu J_L^\alpha\rangle$ by $M_L^{\mu\nu\alpha}$

$$M_L^{\mu\nu\alpha} = \int\frac{\mathrm{d}^4k}{(2\pi)^4}\left[\frac{\mathrm{Tr}[\gamma^\mu P_L\not{k}\gamma^\nu P_L(\not{k}+\not{q}_2)\gamma^\alpha P_L(\not{k}-\not{q}_1)]}{k^2(k+q_2)^2(k-q_1^2)} + \begin{pmatrix}\mu\leftrightarrow\nu\\ 1\leftrightarrow 2\end{pmatrix}\right]. \tag{5.4.12}$$

This matrix element decomposes into one part without γ^5 (vector three point function) and one containing only one γ^5 matrix, giving

$$M_L^{\mu\nu\alpha} = \frac{1}{2}\left(M_V^{\mu\nu\alpha} - M_5^{\mu\nu\alpha}\right)\,, \tag{5.4.13}$$

where the two terms come from the current matrix elements $\langle J_V^\mu J_V^\nu J_V^\alpha\rangle$ and $\langle J_A^\mu J_V^\nu J_V^\alpha\rangle$. As we saw above, conservation of the vector current but non conservation of the axial current, shows that

$$\partial_\mu\langle J_L^\mu J_L^\nu J_L^\alpha\rangle \neq 0\,. \tag{5.4.14}$$

However in more general theories, both left and right-handed Weyl fermions can be involved with different charges Q_L and Q_R as in the following simple example

$$\mathcal{L} = -\frac{1}{4}F_{\mu\nu}^2 + \bar{\psi}\left(i\not{\partial} - Q_L e\not{A}\right) P_L\psi + \bar{\psi}\left(i\not{\partial} - Q_R e\not{A}\right) P_R\psi\,, \tag{5.4.15}$$

where the photon A_μ couples to the mixed current

$$J^\mu = Q_L\bar{\psi}\gamma^\mu P_L\psi + Q_R\bar{\psi}\gamma^\mu P_R\psi\,. \tag{5.4.16}$$

In this case, anomalies are generated by matrix elements of the form

$$\frac{1}{2}\left(Q_R^3 - Q_L^3\right) M_5^{\alpha\mu\nu}\,. \tag{5.4.17}$$

which naturally cancel if $Q_R = Q_L$. In the case of the standard model, one can compute in this manner the $U(1)_Y^3$ anomalies by writing

$$\partial_\mu J_Y^\mu = \left(\sum_{left} Y_L^3 - \sum_{right} Y_R^3\right)\frac{g'^2}{16\pi^2}\epsilon^{\mu\nu\rho\sigma}B_{\mu\nu}B_{\rho\sigma}\,, \tag{5.4.18}$$

where $B_{\mu\nu}$ is the field strength of the hypercharge $U(1)_Y$ gauge group. The summation in the standard model runs over left-handed leptons (charged leptons and neutrino), the right-handed charged leptons and (possibly existing) right-handed neutrinos, left handed quarks and their right-handed counterparts, giving the anomaly cancellation constraint

$$0 = (2Y_L^3 - Y_e^3 - Y_{\nu_R}^3) + 3(2Y_Q^3 - Y_u^3 - Y_d^3)\,. \tag{5.4.19}$$

This condition is satisfied with the choice of charges

$$Y_L = -\frac{1}{2}\,,\quad Y_e = -1\,,\quad Y_{\nu_R} = 0\,,\quad Y_Q = \frac{1}{6}\quad Y_u = \frac{2}{3}\,,\quad Y_d = -\frac{1}{3}\,. \tag{5.4.20}$$

Of course, the gauge group considered in the standard model contain non abelian factors and one has to derive a similar condition in the case of non-abelian gauge theories. Arbitrary currents can be written in this case

$$J_\mu^a = \sum_\psi \bar{\psi}_i T_{ij}^a\gamma^\mu\psi_j\,, \tag{5.4.21}$$

where the T_{ij}^a are the generators of the gauge group Lie algebra. It turns out that the key quantity arising in triangle diagrams amplitudes and generating anomalies is a trace of the generators involved in the loop of the form

$$d_{abc} = \frac{1}{2}\mathrm{Tr}[\{T_a, T_b\}T_c]\,. \tag{5.4.22}$$

We will see in the next section how this quantity can be chosen to vanish for a specific choice of charges, in the case where the Z' boson does couple to quarks taking part in the model dynamics.

5.4.1 "Anomalous" Z'

Until now we have made the important assumption that no SM fermion is charged under Z' and the only couplings arise through gauge-invariant higher-dimensional operators generated by integrating out heavy fermions forming an anomaly-free set. A more subtle option, in the spirit of [155, 121, 122, 126, 127, 128, 129, 130, 131, 135, 136, 138, 139] is to integrate-out a set of heavy fermions which do contribute to gauge anomalies. In this case there are non-decoupling effects leading to axionic couplings and eventually generalized Chern-Simons terms. Let us consider two simple examples in order to exemplify the main points.

i) Example with no colour anomalies

Field	Q_3^L	t_R	b_R
Z'charge	1	1	1

In this case, after defining the anomaly coefficients $C_a = \mathrm{Tr}(XT_a^2)_{L-R}$ and $C_X = \mathrm{Tr}(X^2Y)_{L-R}$, the low-energy effective theory has the following mixed anomalies:

$$\begin{aligned}
U(1)_X SU(3)^2 \quad &: \quad C_3 \;=\; \frac{1}{2}\times(2-1-1) = 0\;, \\
U(1)_X SU(2)^2 \quad &: \quad C_2 \;=\; \frac{1}{2}\times 3\;, \\
U(1)_X U(1)_Y^2 \quad &: \quad C_1 \;=\; 6\times\frac{1}{9} - 3\times(\frac{16}{9}+\frac{4}{9}) = -6\;, \\
U(1)_X^2 U(1)_Y \quad &: \quad C_X \;=\; 6\times\frac{1}{3} - 3\times\frac{4}{3} + 3\times\frac{2}{3} = 0\;.
\end{aligned} \tag{5.4.23}$$

i) Example with colour anomalies

Field	Q_3^L	t_R	b_R
Z'charge	1	1	0

In this case, the low-energy effective theory has the following anomalies:

$$\begin{aligned}
U(1)_X SU(3)^2 \quad &: \quad C_3 \;=\; \frac{1}{2}\times(2-1) = \frac{1}{2}\;, \\
U(1)_X SU(2)^2 \quad &: \quad C_2 \;=\; \frac{1}{2}\times 3\;, \\
U(1)_X U(1)_Y^2 \quad &: \quad C_1 \;=\; 6\times\frac{1}{9} - 3\times\frac{16}{9} = -\frac{14}{3}\;, \\
U(1)_X^2 U(1)_Y \quad &: \quad C_X \;=\; 6\times\frac{1}{3} - 3\times\frac{4}{3} = -2\;.
\end{aligned} \tag{5.4.24}$$

In such examples, the heavy-fermion spectrum has to exactly cancel the low-energy gauge anomalies. In the decoupling limit there is an axionic coupling with a coefficient exactly determined by the low-energy induced anomalies

$$\mathcal{L}_{\mathrm{ax}} \;=\; \frac{a_X(x)}{16\pi^2 V}\left[\sum_a (C_a g_a^2\;\epsilon^{\mu\nu\rho\sigma}F^a_{\mu\nu}F^a_{\rho\sigma}) \;+\; C_X\;g_X g'\epsilon^{\mu\nu\rho\sigma}F^X_{\mu\nu}F^Y_{\rho\sigma}\right]\;. \tag{5.4.25}$$

As shown in the Appendix B of [102], we can also capture the effect of these axionic couplings in the unitary gauge, where the axionic effect is encoded in the particular high-energy behaviour of the anomalous three gauge boson amplitude with light fermions in the loop. This is strictly speaking true in the large (infinite) mass limit of heavy fermions. For finite mass, there are corrections and the low-energy description in the unitary gauge with three-gauge anomalous couplings is corrected by finite mass effects.

6 Light Mediators : Fitting the 3.5 keV Line

In the previous section we exposed a model where, according to the WIMP miracle indication, a new gauge boson and our fermionic dark matter candidates were taking typical masses of order $100\text{GeV} - 1\text{TeV}$. However, even if we know quite well the cosmological abundance of dark matter [143, 142], little is known about its mass in reality. In view of recent results from both direct and indirect detection experiments, the Weakly Interacting Massive Particle paradigm begins to be severely constrained by XENON [156], LUX [157] or the FERMI satellite [158, 159, 160].

Nevertheless, several other scenarios offer much lighter [161] or heavier [162] candidates with feeble [163, 164, 165, 166, 167, 168] or very feeble [169] couplings. Their thermal histories can be relatively different (but not less motivated) from the standard freeze out one. The cases of FIMP (for Freeze In Massive Particle or Feebly Interacting Massive Particle) or WISP (for Weakly Interacting Slim Particle) are typical cases where the coupling is too weak to reach the thermal equilibrium with the standard model bath [163, 164]. The dark matter candidate can be so weakly coupled that it decoupled from the bath at the reheating epoch, like the gravitino or candidates motivated by SO(10) schemes. Other scenario proposed an even more weakly interacting particle, so weakly interacting that the dark matter is stable at the scale of the age of the universe: the decaying dark matter (see [170] for a review on the subject).

6.1 A New γ-ray Line

One of the most clean signature for attesting of the presence of dark matter in a celestial body, would be the clear detection of a monochromatic rayline which would be absolutely unexplained by the known chemical, astrophysical processes predicted by the standard model of particle physics. Yet it has been until now difficult to measure such a signal with a sufficiently

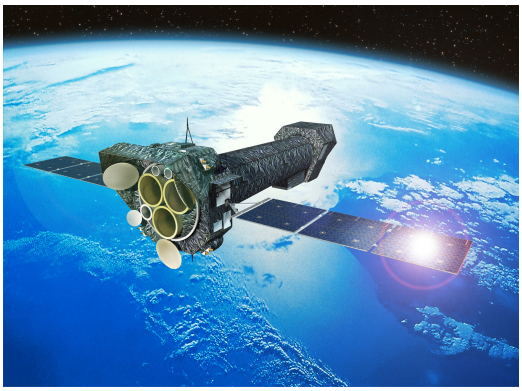

Figure 1: Picture of the XMN-Newton telescope. This satellite was the one achieving the measurements of the X-ray spectrum from which the 3.5keV signal was extracted.

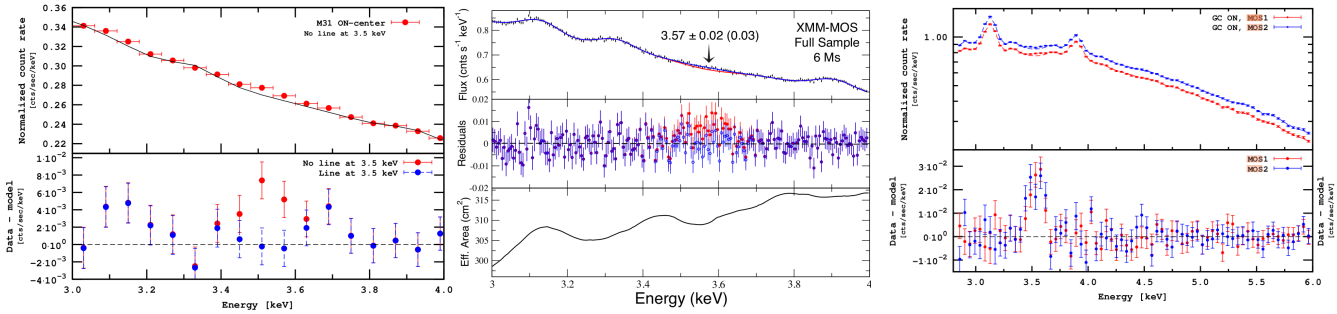

Figure 2: Detection of 3.5keV line from different analysis. The left panel is extracted from Boyarski et al. analysis [172], the central one is the analogous study from Bulbul et al. [171] and the right panel is the analysis of the signal when detected in the Milky Way, made by Boyarski et al. [173].

high significance to be able to claim for a dark matter discovery.

At the beginning of the year 2014, a 3.55 keV X-ray line has been reported in the stacks analysis of 73 galaxy clusters from the XMM-Newton telescope [171]

with a significance larger than 3σ. A similar analysis found evidence at the 4.4 σ level for a 3.52 keV line from their analysis of the X-ray spectrum of the Andromeda galaxy (M31) and the Perseus Cluster [172]. Such signal was later on measured in other regions of the sky, and most importantly measured in the center of our Galaxy [173].

Such a detection is a very sensible task to achieve since one should take into account the presence of atomic lines very close to 3.5 keV, such that the Potassium and Chlorine lines, while extracting the background. Thus the work of Boyarski et al. and Bulbul et al. were strongly controversial a few months after their initial claim [174, 175, 176, 177]. Yet the debate is still open today and seems to confirm the presence of an X-ray signal around 3.5 keV.

In both original analysis, the unidentified line was interpreted as a possible signal of sterile neutrino dark matter ν_s [178] decaying through a loop $\nu_s \to \gamma\nu$. While more conventional explanations in term of atomic physics effects are currently lacking, several works have been released in the following weeks, all focusing on a decaying dark matter candidate. Extensions with a sterile neutrino as dark matter candidate [179, 180, 181, 182, 183, 184], radiatively-induced (sterile) neutrinos decay [185], axions or ALPs [186, 187, 188, 189, 190, 191, 192], axinos [193, 194, 195], pseudo-Nambu-Goldstone bosons [196] or supersymmetric models (gravitino [197, 198, 199], sgoldstino [200]or low scale supersymmetry breaking [201]) were proposed, all relying on processes ensuring a fine tuned lifetime $\tau \simeq 10^{28}$ seconds to fit the observed line. Other more exotic candidates like decaying moduli [202], millicharged dark matter [203], dark atoms [204], magnetic dark matter [205], majoron decay [206] or multicomponent dark matter [207, 208] have been proposed. Recent works have also proposed annihilating scenarios in the context of the so called *Weinberg* model [209]. Another original model was studied in [210, 211] with an eXciting dark matter, where the photons come from the transition from an excited state down to the ground state for the dark matter particle, which in this case can be significantly heavier than 3.5 keV. Moreover, it is well known that for a warm dark matter candidate of mass $\sim$keV, free streaming produces a cutoff in the linear fluctuation power spectrum at a scale corresponding to dwarf galaxies and can fit observations for $m_s \gtrsim 1.5$ keV [212].

Most of these scenarios seemed to exclude an annihilating dark matter scenario [213]. We will indeed see how using a naive effective contact operator is indeed incompatible with the

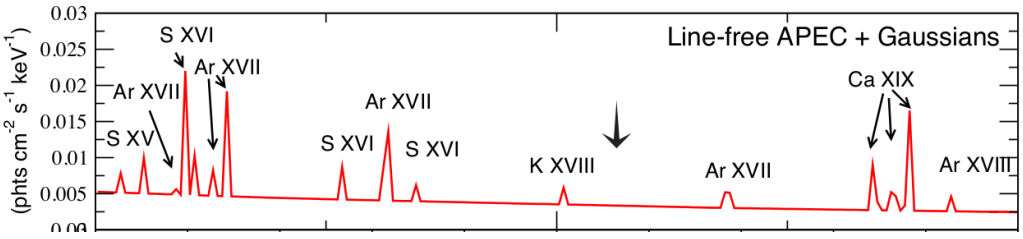

Figure 3: Presence of X-ray atomic transition lines, close to the signal of 3.5 keV detected.

experimental data we get about the flux of this ray line [171, 172]. Building an annihilating scenario moreover requires a careful study of the thermal History of the Universe in detail in order to reproduce the measured relic density, as we will see in the next sections.

However recent measurements seem to emphasize that the detection of the 3.5keV line strongly depends on the dark matter velocity distribution, which could, if confirmed, constitute a hint that the dark matter decay is actually excluded compared to the annihilating one in which such feature can naturally appear.

6.2 When Parametrization Looses Information

An old, but sometimes useful approach in particle physics for explaining a mysterious phenomena, is to introduce new interactions by parameterizing our lack of knowledge with the use of effective couplings and operators. Such operators, as we saw in the previous section can be non renormalizable and require a UV completion model, that is supposed to generate the latter as an effective theory at the energy scale of the physical processes experimentally observed. Indeed, it is rather natural to imagine that the physics beyond a measurable scale of energy is represented by heavy particles not yet produced in accelerators, but coupling to the observable sector. This is frequently used in LHC studies [214] or dark matter searches [152, 150, 215, 216].

One conclusion we can pick up from the microscopic calculations made in section 5.1.1 is that the form of the operators can be strongly dependent on the underlying microscopic theory. But more importantly the effective operator approach can become misleading when there are light mediators involved in the annihilation process, as was shown in [217]. Supersymmetric or grand unified models do not escape this rule: light stau or Z' for instance generate new processes observable at LHC and not predicted by a naive effective operators approach. This is exactly what is happening in the case of a cosmological monochromatic signal.

6.2.1 The Experimental Signal

In this section we review what are the main constraints coming from the experimental measure of the 3.55 keV line in the case of annihilating dark matter and interpret them in terms of constraints on the annihilation cross section while building a given model.

If the signal analyzed in [171, 172] is generated by dark matter annihilation to two photons $ss \to \gamma\gamma$ (with a dark matter mass of 3.5 keV) then one should fit the annihilation cross section $\langle \sigma v \rangle_{\gamma\gamma}$ with the flux measured in the vicinity of the sun. A naive estimate of the total

luminosity of Perseus can be computed using

$$L = \int_0^{R_{Pe}} 4\pi r^2 n_{DM}^2 \langle\sigma v\rangle_{\gamma\gamma} = \int_0^{R_{Pe}} 4\pi r^2 \left(\frac{\rho(r)}{m_s}\right)^2 \langle\sigma v\rangle_{\gamma\gamma} \tag{6.2.1}$$

with R_{pe} being the Perseus radius. Let us here adopt a simple picture in which the halo distribution of dark matter is simply a spherical and homogeneous distribution. One could check that the consequence of such assumption on the cross section values does not change significantly, with respect to the precision expected in the study which will follow. The Perseus observation involves a mass[1] of $M_{Pe} = 1.49 \times 10^{14} M_\odot$ in a region of $R_{Pe} = 0.25$ Mpc at a distance of $D_{Pe} = 78$ Mpc from the solar system. One can then estimate

$$\begin{aligned} n_{DM} \simeq \frac{1.49 \times 10^{14} M_\odot}{m_s} \frac{3}{4\pi R_{Pe}^3} &= 2.0 \times 10^{-37} \mathrm{GeV}^3 \\ &= 2.6 \times 10^{4} \mathrm{cm}^{-3} \ . \end{aligned} \tag{6.2.2}$$

Combining Eq.(6.2.1) and (6.2.2), it is then very easy to compute the luminosity in the Perseus cluster,

$$L \simeq 1.2 \times 10^{55} \left(\frac{3.5 \text{ keV}}{m_s}\right)^2 \left(\frac{\langle\sigma v\rangle_{\gamma\gamma}}{10^{-26}\mathrm{cm}^3\mathrm{s}^{-1}}\right) \text{ photon/s} \ , \tag{6.2.3}$$

giving a constraint on the flux $\phi_{\gamma\gamma} = L/(4\pi D_{Pe}^2)$ that one should observe on earth

$$\phi_{\gamma\gamma} = 1.7 \times 10^{-5} \left(\frac{3.5 \text{ keV}}{m_s}\right)^2 \left(\frac{\langle\sigma v\rangle_{\gamma\gamma}}{10^{-32}\mathrm{cm}^3\mathrm{s}^{-1}}\right) \ \mathrm{cm}^{-2}\mathrm{s}^{-1} \ . \tag{6.2.4}$$

According to the authors of [172, 210], one can identify a monochromatic signal arising from M31 or Perseus cluster with a flux $\phi_{\gamma\gamma} = 5.2^{+3.70}_{-2.13} \times 10^{-5}$ photons cm^{-2} per seconds at 3.56 keV with the cluster core. Taking into account also other observations like M31, we will impose in our analysis a conservative required annihilation cross section estimated as

$$\langle\sigma v\rangle_{\gamma\gamma} \simeq (2 \times 10^{-33} - 4 \times 10^{-32}) \ \mathrm{cm}^3\mathrm{s}^{-1} \ . \tag{6.2.5}$$

As one can easily imagine, inserting in the theory new – light – particles interacting with photons can have dramatical consequences on the Cosmic Microwave Background anisotropies. The authors of [218, 219] show that the corresponding condition is given by

$$\langle\sigma v\rangle_{\gamma\gamma}^{CMB} \lesssim 2.42 \times 10^{-27} \left(\frac{m_s}{1 \text{ GeV}}\right) \ \mathrm{cm}^3\mathrm{s}^{-1} \ , \tag{6.2.6}$$

which for a 3.5 keV dark matter is $\langle\sigma v\rangle_{\gamma\gamma} < 8.5 \times 10^{-33}\mathrm{cm}^3\mathrm{s}^{-1}$. *In fine* one will then restrict ourself to the parameter space allowing a monochromatic signal and respecting the CMB constraints:

$$2 \times 10^{-33}\mathrm{cm}^3\mathrm{s}^{-1} < \langle\sigma v\rangle_{\gamma\gamma} < 8.5 \times 10^{-33}\mathrm{cm}^3\mathrm{s}^{-1} \ . \tag{6.2.7}$$

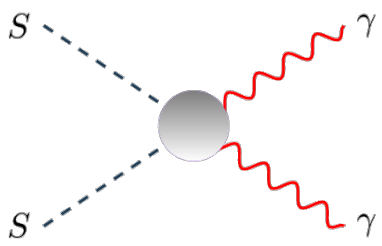

Figure 4: Effective diagram for dark matter annihilation

6.2.2 A Naive Attempt

In this section we will, as announced earlier, see how adopting a naive effective formulation of a dark matter interacting with photons, can be misleading and make people wrongly conclude that annihilation is ruled out. Indeed, in the case of a scalar particle annihilating into two photons, the CP–even effective lagrangian can be written (the cases of fermionic dark matter, CP-odd or pseudo–scalar couplings are detailed in the appendix of [101])

$$\mathcal{L}_{eff} = \frac{S^2}{\Lambda^2} F_{\mu\nu} F^{\mu\nu} \ , \tag{6.2.8}$$

with $F_{\mu\nu} = \partial_\mu A_\nu - \partial_\nu A_\mu$ being the electromagnetic field strength. The scale Λ is related to the mass of the particles running in the loops (see Fig.(4)) which , being charged under $U(1)_{em}$, should be heavier or at least of the order of TeV. A list of generic couplings of this type can be found in [141]. One obtains in this case the cross section

$$\langle \sigma v \rangle^{eff}_{\gamma\gamma} = \frac{2 m_s^2}{\pi \Lambda^4} \ . \tag{6.2.9}$$

One now has to match this formula with the value of the cross section (6.2.7) dictated by the experimental value of the experimental flux. One obtains consequently constraints on the value of the high energy scale Λ

$$10 \text{ GeV} < \Lambda < 15 \text{ GeV} \ . \tag{6.2.10}$$

This value is obviously far below any accelerator limit on charged particles. Hence, no possible interpretation of this operator in terms of heavy particle integrated in loops is possible. It seems then impossible at first sight to UV complete this operator and achieve a large enough rate.

However one can easily imagine that this effective formulation fails when additional light degrees of freedom are involved in the process. We will in the next section imagine the case where a light particle mediates the interaction between dark matter and photons, in the same manner our previous proposal of Z' boson was mediating interactions between the dark and visible sectors.

[1] See table 2 of [171]

6.3 A Natural Microscopic Approach

It is then easy to build a microscopic model and to check how observables get modified. Indeed, the presence of a keV-MeV dark matter particle here *naturally* leads to a keV scale dynamics, as the presence of GeV particles in the standard model naturally leads to GeV scale dynamics in the Higgs sector. We then can suppose the presence of a (pseudo)scalar coupling to the dark matter candidate, and generating the keV dynamics. We will consider for simplicity a scalar dark matter; other dark matter spin or couplings do not change the conclusions and are reviewed in details in the Appendix of [101].

6.3.1 Scalar Dark Matter

We present here a proposal of model for fitting the 3.55 keV line with annihilating scalar dark matter. The situation is the following : we introduce a scalar mediator ϕ, coupling directly at tree-level to dark matter, but indirectly to the standard model through loops (suppressed by a high energy scale Λ). This is a typical secluded dark matter type of model [220]. The lagrangian can then be written for a scalar dark matter

$$\mathcal{L}_{eff} \supset -\frac{m_s^2}{2}S^2 - \frac{m_\phi^2}{2}\phi^2 - \tilde{m}\phi S^2 + \frac{\phi}{\Lambda}F_{\mu\nu}F^{\mu\nu}. \tag{6.3.1}$$

We assume the parameter $\tilde{m}$ to be a free mass scale parameter. However such coupling can be explicitly generated by symmetry breaking in renormalizable models, as illustrated in section 6.5. In the latter case, $\tilde{m}$ is expected to be at most of the same order of magnitude than m_ϕ since it gets its value from the *vev* of a field $\Phi = v_\phi + \phi$ after spontaneous symmetry breaking. Furthermore this is what would be more generally expected if $\tilde{m}$ is generated by whatever dynamical mechanism involving only ϕ and the light field S. The mass scale Λ is related to the mass of heavy particles integrated in the loop. In a perturbative set up with N charged fermions running in the loop $\Lambda \sim \frac{4\pi}{N h_\phi \alpha} M_\psi$, where h_ϕ is the Yukawa coupling of ϕ to the charged fermions of mass M_ψ. Using the constraint $M_\psi \gtrsim 500$ GeV from collider searches and perturbativity one finds that the minimum natural values for Λ are $\Lambda \sim 50 - 500$ TeV, whereas $\Lambda \sim 5$ TeV can only be obtained in a strongly coupled hidden sector.

Such a lagrangian gives for the annihilation cross section (process depicted in Fig.(5)

$$\langle \sigma v \rangle_{\gamma\gamma}^{micro} = \frac{4 m_s^2 \tilde{m}^2}{\pi \Lambda^2 (4m_s^2 - m_\phi^2)^2} \ . \tag{6.3.2}$$

One can notice in the latter expression that the scale Λ now appears at the denominator to the power two only compared to the naive formulation, while $(4m_s^2 - m_\phi^2)^2$ appears in the denominator. The natural smallness of this last quantity then allows the scale Λ to take reasonably high values making the model safer with respect to experimental constraints on charged fermions from LEP. As recently emphasized by the authors of [217] for the LHC analysis of mono jet events, the effective operators approach ceases to be valid once the ultraviolet (microscopic) theory contains some light mediators, which is exactly the case here.

6.3.2 Fitting the X-ray line

Depending on the hierarchy between the masses of the mediator ϕ and the dark matter particle S, the condition (6.2.7) coming from the measurement of the emission flux leads to two kinds

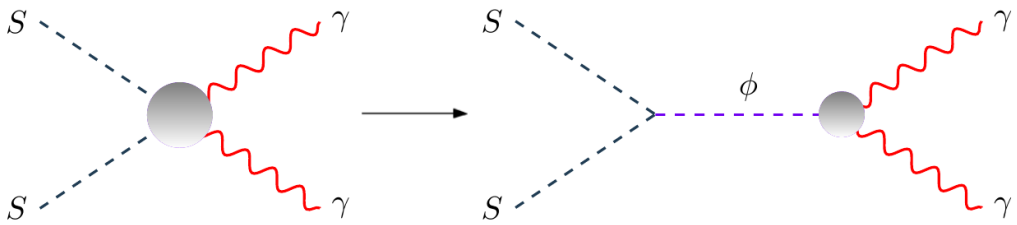

Figure 5: Microscopic diagram for dark matter annihilation

of constraints

$$\textbf{Case A} \quad : \quad m_\phi \gtrsim m_s \text{ (Heavy Mediator)},$$

$$m_\phi \simeq (12.3 \quad - \quad 17.6)\sqrt{\frac{m_s}{3.5 \text{ keV}}}\sqrt{\frac{\tilde{m}}{\Lambda}} \text{ GeV} \tag{6.3.3}$$

$$\textbf{Case B} \quad : \quad m_\phi \lesssim m_s \text{ (Light Mediator)},$$

$$\frac{\tilde{m}}{\Lambda} \quad \sim \quad (1.63 - 3.36) \times 10^{-13} \, . \tag{6.3.4}$$

Both cases could give at first sight viable results but we will see that experimental bounds on light scalar particle interactions with the electromagnetic sector (which is the main feature of the mediator ϕ we introduced) are strongly restrictive.

6.3.3 Experimental Bounds

As we just mentioned above, interactions of a light scalar, or axion-like particle (ALP) with the visible sector is very much constrained by collider data (LEP) and astrophysics. A summary of these constraints on Axion-Like Particles (ALPs) is presented in Fig. 6.

Indeed bounds on pseudoscalar particles interacting with photons (see [221]) have been studied, using LEP data from ALEPH, OPAL, L3 and DELPHI, and have shown that the coupling of the pseudoscalar with photons cannot exceed a value of $2.6 \times 10^{-4}\text{GeV}^{-1}$ for a mediator of mass $m_\phi \lesssim 50$ MeV, which means, in terms of our mass scale

$$\Lambda \gtrsim 3 \text{ TeV} \qquad [m_\phi \lesssim 50 \text{ MeV}] \, . \tag{6.3.5}$$

Furthermore, one of the most restrictive constraints on ALPs comes from the non-observation of anomalous energy loss of horizontal branch (HB) stars via a too important ALP production [222]. Indeed those constraints impose

$$\Lambda \gtrsim 10^{10} \text{ GeV} \qquad [m_\phi \lesssim 30 \text{ keV}] \, , \tag{6.3.6}$$

for a mediator mass up to $m_\phi \lesssim 30$ keV. At higher masses arise constraints coming from the CMB, BBN and Extragalactic Background Light (EBL) studies, setting lower limits on

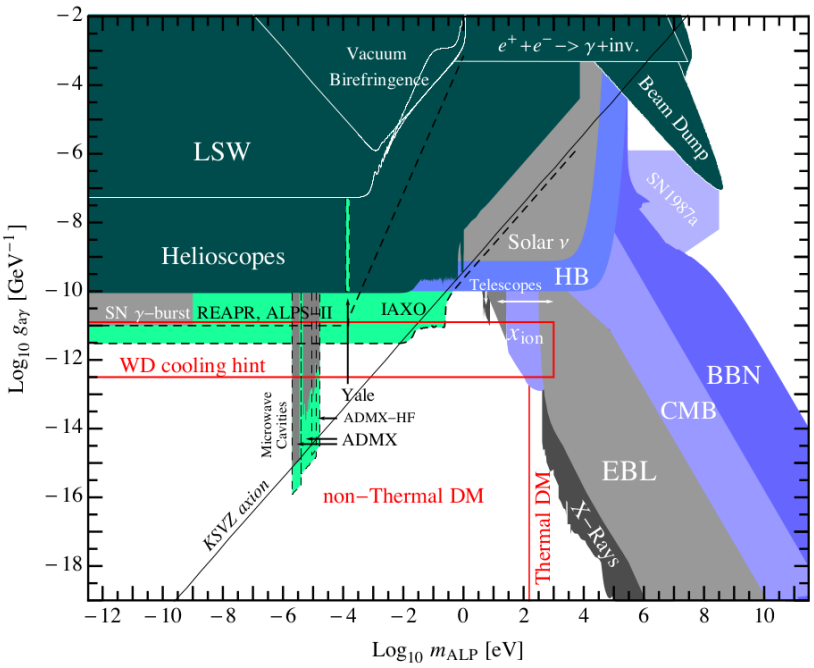

Figure 6: Experimental constraints on an ALP particle coupling to the electromagnetic field with a coupling constant $g_{a\gamma}$. Plot extracted from [221]

the coupling with photons. A nice review on the subject can be found in [223, 224]. Various astrophysical constraints on ALP masses and coupling to photons are summarized in, e.g. [223].

These constraints on our model essentially put lower bounds on Λ. Indeed, for a light mediator (Case B) HB results impose that the mass scale Λ takes very high values ($\gtrsim 10^{10}$ GeV). In this case, as indicated by Eq.(6.3.4), one would need the tri-linear coupling to be of order $\tilde{m} \gtrsim 10^{-3}$ GeV. However, in this case, since m_ϕ is assumed to be smaller than the keV scale, one would conclude that $\tilde{m}/m_\phi \gtrsim 10^3$ which is, as mentioned in the previous section, quite unnatural. We will then concentrate our study on Case A, where the mediator ϕ is assumed to be heavier than the dark matter field S.

In Case A, the discussion is a bit more subtle, as far as the experimental constraints are concerned. According to the bounds arising from CMB, BBN (see e.g. [225, 226]) and EBL [227], for mediator masses lower than a hundred keV, the mass scale Λ must reach very high values ($\gtrsim 10^{16}$ GeV) to escape experimental exclusion bounds. However, such constraints were derived assuming the ALP particle is sufficiently stable to produce significant effects on these different observables. We will see in Eq. (6.3.7) that those regions of the parameter space are anyway forbidden, even in the case of an unstable mediator ϕ, for theoretical reasons, considering together the condition $\tilde{m} \lesssim m_\phi$ and the flux condition (6.3.3), even if the mediator would be a short lived scalar particle. Still such region of the parameter space is not acceptable since it would lead to a very heavy parameter $\tilde{m}$. For higher masses of the mediator ($m_\phi \gtrsim$ 300 keV) more reasonable values of Λ are allowed, and we are left with lower bounds coming from LEP. The previous description is depicted in Fig. 7 where the different regions explored are summarized.

Different choices of Λ will then lead to different pairs of $(m_\phi, \tilde{m})$, as depicted in Fig.(8)

In order to fix ideas, and anticipating results of section 6.5, we indicated in red in the figure

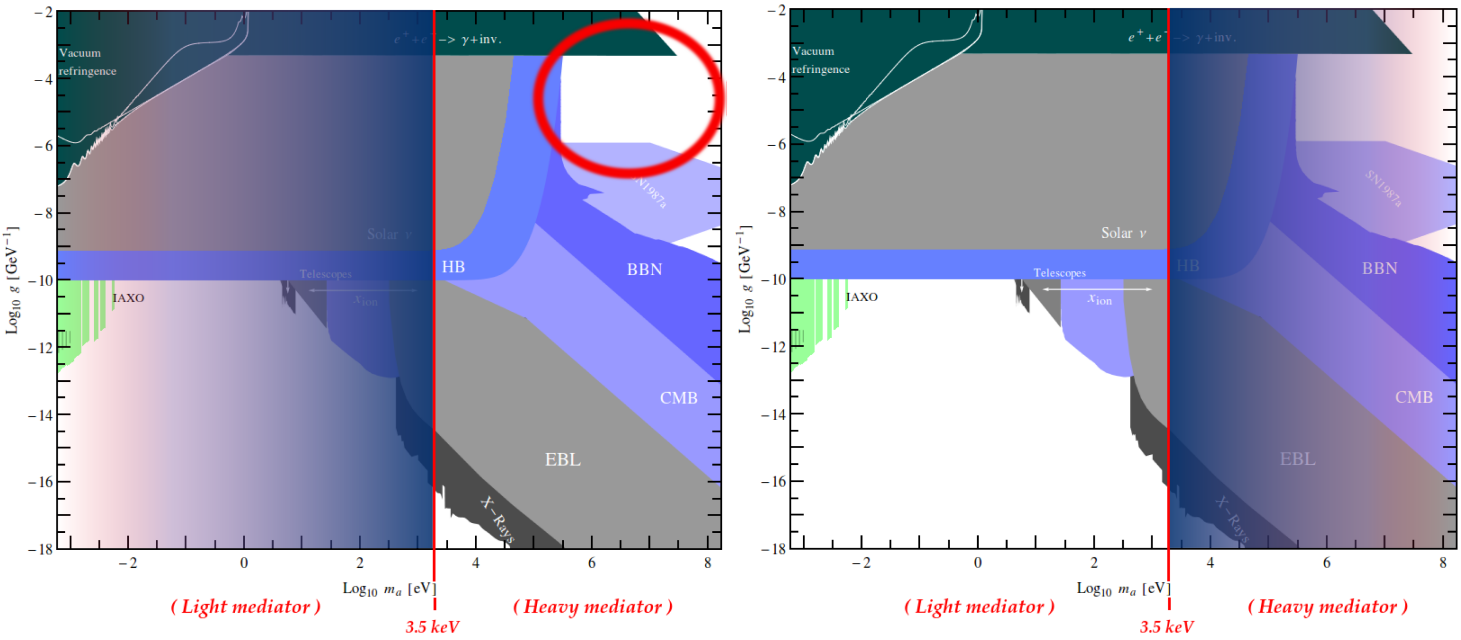

Figure 7: Experimental constraints on an ALP particle coupling to the electromagnetic field with a coupling constant $g_{a\gamma}$. The allowed region on the left panel (Case A : heavy mediator) is located below the band delimiting the LEP constraints, right to the HB bounds and above the constraints coming from supernovae. The right panel (Case B : light mediator) shows the region allowed by experiment, which is yet excluded by the theoretical requirement that $\tilde{m} \lesssim m_\phi$.

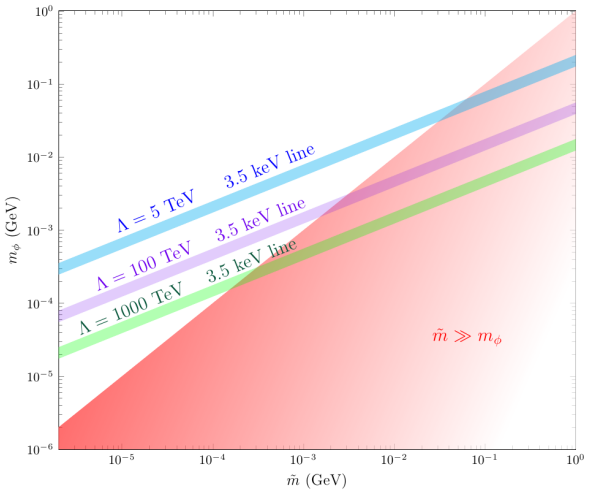

Figure 8: $(m_\phi,\tilde{m})$ parameter space allowed by the γ flux measurements in the case of a heavy mediator (Case A), for different values of Λ. The red shaded region indicates where $\tilde{m}$ is higher than m_ϕ.

the region where $\tilde{m} \gtrsim m_\phi$. This shows clearly, that imposing $m_\phi \gtrsim 300$ keV sets an upper limit for Λ, giving approximately

$$\Lambda \lesssim 1000 \text{ TeV} . \tag{6.3.7}$$

Furthermore, the lower limit $\Lambda \gtrsim 5$ TeV mentioned in section 6.3.1 – still acceptable if there is

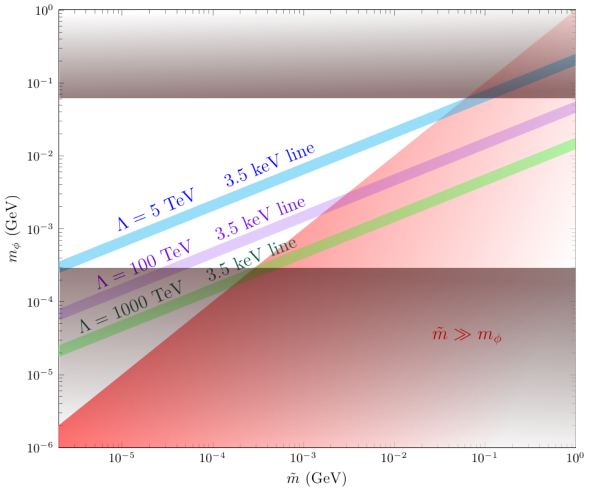

Figure 9: $(m_\phi,\tilde{m})$ parameter space allowed by the γ flux measurements in the case of a heavy mediator (Case A), for different values of Λ. Grey bands indicate here constraints coming from experiment on ALPs particles, providing a narrow mass range for the mass of the mediator ϕ.

some strongly coupled hidden sector generating the effective mass scale Λ – imposes an upper limit on the mediator mass, $m_\phi \lesssim 50$ MeV. One would thus expect from this model that the mediator mass lies in the region

$$300 \text{ keV} \lesssim m_\phi \lesssim 50 \text{ MeV} . \tag{6.3.8}$$

6.4 Relic Abundance

As we saw in section 4.2.1, building a model of annihilating dark matter has strong consequences on the thermal history of the Universe. In particular, one has to provide the dark matter candidate a sufficient annihilation cross section in order to reproduce the relic density of the Universe which is measured nowadays.

Computing the relic abundance in models with a very weak annihilation cross section and a keV dark matter particle is highly non-standard. Indeed, it is well known from the standard lore that a hot dark matter candidate leads to a relic density

$$\Omega h^2 \simeq 9.6 \times 10^{-2} \frac{g_{eff}}{g_s(x_f)} \left(\frac{m_s}{1 \text{ eV}}\right) , \tag{6.4.1}$$

where g_{eff} is the effective number of degrees of freedom of the dark matter candidate and g_s the effective number of degrees of freedom for the entropy. Eq.(6.4.1) gives $m_s \simeq 5$ eV if one wants to respect PLANCK [142] limit $\Omega_{DM} h^2 = 0.1199 \pm 0.0027$. However, this condition is valid only under the hypothesis that the dark matter is in thermal equilibrium with a common temperature

T with the thermal bath. In the case of the line signal observed in the clusters, the cross section necessary to fit the result is far below the classical thermic one $\langle\sigma v\rangle_{therm} = 3 \times 10^{-26}\text{cm}^3\text{s}^{-1}$. This had led previous studies to rule out scalar dark matter candidates lighter than $\mathcal{O}$ (MeV) [228]. In fact, the dark bath, composed of the light mediator ϕ and the dark matter S cannot be in equilibrium with the standard plasma.

There are several ways to address this issue. A first possible attempt to solve the problem, proposed in [163, 164] and [165, 166, 167, 168], is to suppose that the dark matter is produced through the *freeze in* mechanism: the interacting photons annihilate to produce the dark matter in the inverse process of Fig.(5). Yet it is not possible to get the right relic density in this way since, solving the Boltzmann equation in this case would produce too much dark matter. Indeed equilibrium dark matter density would reach quickly a value that would overclose the Universe.

Another way to solve the problem was proposed in [229, 230] where the authors noticed that the condition (6.4.1) is not valid anymore if the temperature of the hidden sector T_h is different from the one of the thermal bath T. In this case, one can compute the temperature T_h needed to obtain a 3.56 keV particle respecting the relic abundance constraint. Yet, as we will see in what follows, we still need the hidden sector content to be richer in order to provide new dark matter annihilation channels leading to the right relic abundance. This will be done adding to the model a right-handed sterile neutrino.

6.4.1 Dark matter annihilation into sterile neutrinos

One way of solving the lack of annihilation of dark matter described above is to assume that a right-handed sterile neutrino couples directly to the mediator scalar particle previously introduced. This would provide another channel for annihilating dark matter which would boost the relic density to its experimental value.

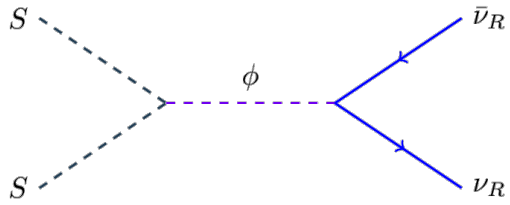

Figure 10: Microscopic model of dark matter decaying into right-handed sterile neutrinos.

In a similar fashion than we did in section 6.3.1, one can add to the usual neutrino interaction terms a Yukawa coupling between the field ϕ and the sterile neutrino ν_R, using the two-component spinor notation,

$$-\mathcal{L}_\nu = \frac{M}{2}\nu_R\nu_R + m_D\nu_L\nu_R + \lambda_\nu\phi\nu_R\nu_R + h.c.\,, \tag{6.4.2}$$

After diagonalization of the mass matrix, the sterile neutrino gets mass $m_{st} \simeq M$ while the active one obtains a mass of $m_{act} \simeq m_D^2/M$ via the seesaw mechanism.

Such interactions give the following cross section for dark matter annihilation into a pair of sterile neutrinos

$$\langle\sigma v\rangle_{\nu\nu} = \frac{\lambda_\nu^2\tilde{m}^2}{8\pi^2}\frac{(m_s^2 - M^2)}{m_s^2(4m_s^2 - m_\phi^2)^2}\sqrt{1 - \frac{M^2}{m_s^2}}\,. \tag{6.4.3}$$

Assuming that M is negligible compared to m_s leads to a cross section depending only on m_s, m_ϕ and $\tilde{m}$, λ_ν :

$$\langle \sigma v \rangle_{\nu\nu} \sim \frac{\lambda_\nu^2}{8\pi^2} \left(\frac{\tilde{m}}{m_s} \right)^2 \frac{m_s^2}{(4m_s^2 - m_\phi^2)^2} \ . \tag{6.4.4}$$

As far as experimental constraints are concerned, the mass of the sterile neutrino specie cannot be arbitrary small since it would imply a too high mixing angle $\theta \simeq m_D/M$, constrained by the BBN measurement (see e.g. [231, 232] for phenomenological and theoretical reviews). However, a sterile neutrino of mass $M \simeq 1$ keV with an active neutrino of mass $m_{act} \simeq 10^{-2}$ eV would lead to a mixing angle parameter of order $10^{-3} - 10^{-2}$ and would be still acceptable regarding the experimental bounds. As we will see in the next sections, this new channel of annihilation, being provided this new parameter λ_ν, furnishes us a way of fitting on one hand the right flux of annihilation into photons (explaining perfectly the signal at 3.5 keV) and on the other hand producing the right dark matter relic density by tuning the flux of annihilation into sterile neutrinos.

6.4.2 Cosmological Constraints on an Almost Hidden Sector

For the purpose explained above, we introduced in our model two species of very light particles that are the dark matter candidate and the sterile neutrinos, interacting together via the exchange of the mediator ϕ. In such a framework, dark matter and sterile neutrinos can be seen as living together in a – almost – *hidden* thermal bath decoupled from the visible sector. We will adopt here a formalism for modeling such a behavior, which was developed in [230, 229], where they imagined how a hidden sector could get its own thermal equilibrium and change the resolution of the Boltzmann equation.

Let us denote the temperature of this hidden bath by

$$T_h \equiv \xi(t) T \ , \tag{6.4.5}$$

where in what follows ξ will be assumed to be a constant parameter[2]. As described in [229, 230], such a point of view can have important consequences on the thermal dynamics of the hidden sector, since ξ enters into the Boltzmann equation. Indeed dark matter can decouple while still relativistic or semi-relativistic and lead to different relic densities, as the parameter ξ takes different values (See Fig.(13)). Such freedom in the temperature of the hidden sector is yet constrained by astrophysical considerations. In particular, a hidden sector dark matter can freeze out while still being relativistic. It is then important to check that its free streaming length is smaller than typical galactic length scales (typically $\lambda_{FSH} \lesssim 230$ kpc, see e.g. [233, 234]) so that it does not destroy the matter power spectrum. Another constraint, introduced by Tremaine and Gunn in [235], comes from bounding the phase-space density of structures like small dwarf galaxies by statistical quantum mechanics considerations. Both constraints are computed and summarized in the case of a ~ 3 keV dark matter in [229] and lead naturally to a relic density value different from the one of the visible thermal bath ($\langle \sigma v \rangle_0 \sim 10^{-9}$ GeV^{-2}) as depicted in Fig. 11, depending on how cold the hidden sector is. We thus get

$$0.015 \ \langle \sigma v \rangle_0 \lesssim \langle \sigma v \rangle \lesssim 0.045 \ \langle \sigma v \rangle_0, \tag{6.4.6}$$

[2]See ref. [230] for a discussion on the validity of this approximation.

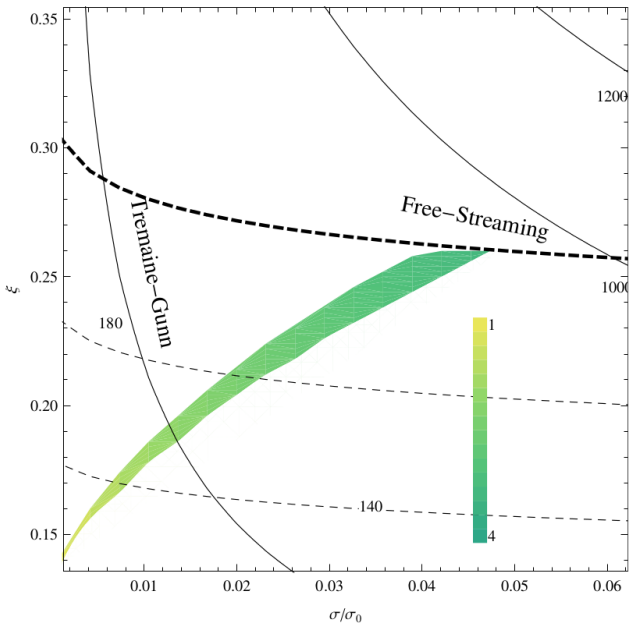

Figure 11: Plot extracted from [229], solving the Boltzmann equation in the case of a light ($\sim$ 3keV) dark matter hidden sector, decoupling while still semi relativistic. The diagram provides alternative values for the relic density cross section, constrained by astrophysical bounds that are the Tremaine-Gunn bound and the free streaming.

the upper limit corresponding to the free streaming constraint whereas the lower one to a strict Tremaine-Gunn bound.

One should also remark that the dark matter is relatively warm ($x_f = m_S/T_f \simeq 2-4$ for points respecting WMAP/PLANCK) in this case. As a warm candidate, it can elude the possible problems of cold dark matter *i.e.* the few number of galaxy mergers ($\lesssim 10\%$) or the core observed profiles compared to the cusp ones predicted by N-body simulations.

Results

In the light of section 6.3.3 and equation (6.4.4) one can now constrain couplings between the mediator ϕ to both the dark and the visible sector $\tilde{m}$ and λ_ν, taking into account that relic density can lie in the region (6.4.6) exhibited above, as well as imposing constraints on the photons flux measurement. Results are presented in Fig.(12) where we show the allowed parameter space imposing cosmological bounds [229] superimposed within the regions fitting the 3.5 keV excess, for $m_\phi = 500$ keV. As one can see, a relatively large region respects the cosmological bounds and the monochromatic excess. The values of λ_ν are also quite constrained ($\sim 10^{-7} - 10^{-5}$, depending on the mass scale Λ), leading to different values of the hidden sector temperature (as represented in Fig.(13)).

6.5 An explicit UV model

As we have shown in constraining the model with experimental data, the mediator ϕ is required to be significantly heavier than the dark matter candidate. One could argue that the implication

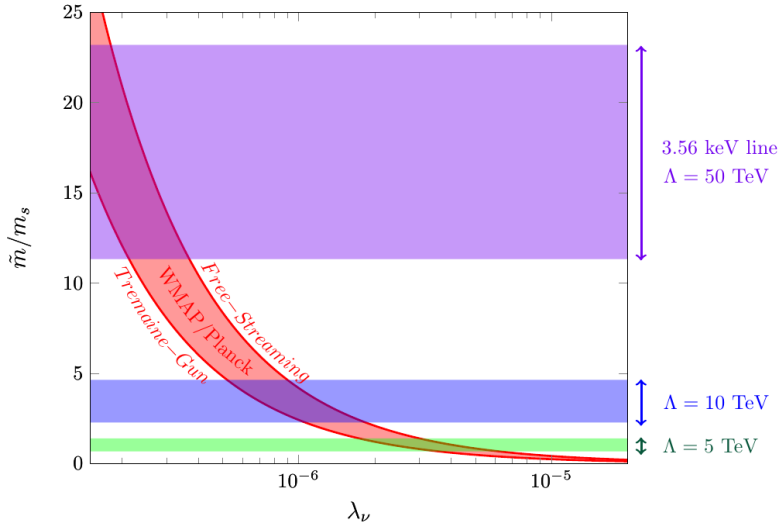

Figure 12: Constraints on the parameter space $(\tilde{m},\ \lambda_\nu)$, for $m_\phi = 500$ keV; considering cosmological constraints (relic abundance, free streaming and Tremaine-Gunn bounds) in the red/dark band and a 3.5 keV excess (blue/green region) for different values of the BSM scale Λ (see the text for details).

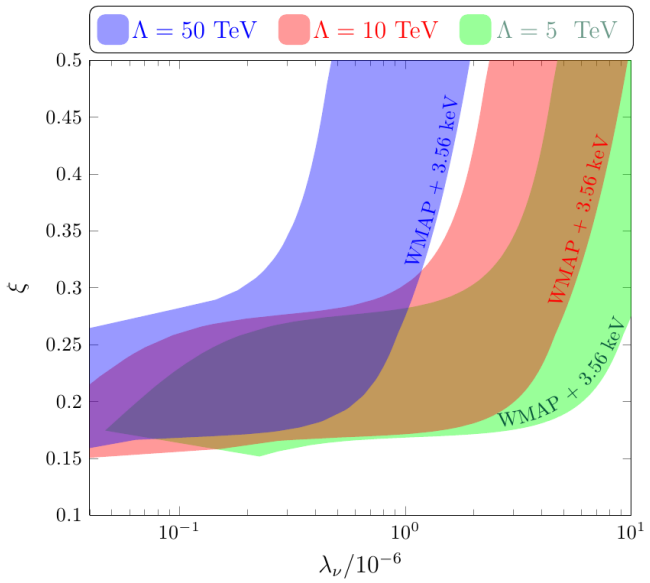

Figure 13: Hidden temperature factor ξ allowed by the flux measurement limits, as a function of the relic density value, for different values of the mass scale Λ.

of heavier fields could at the loop order give corrections to the tree level mass of dark matter, which would, after renormalization, not be as light as expected.

We hence give here an explicit example realizing the case A of Section 6.3.

Let us write a model containing a scalar σ and a pseudoscalar S, together with a (set of) fermion(s) ψ, with the lagrangian

$$\begin{aligned}\mathcal{L} &= \mathcal{L}_{kin} + \frac{\mu^2}{2}(\sigma^2+S^2) - \frac{\lambda}{4}(\sigma^2+S^2)^2 \\ &-\bar{\psi}(h_1\sigma + ih_2 S\gamma_5)\psi + \frac{\sigma}{\Lambda}F_{\mu\nu}F^{\mu\nu} \ . \end{aligned} \tag{6.5.1}$$

In this picture, the set of fermions ψ are part of the hidden sector, in particular they are singlets with respect to the Standard Model. By defining the complex field $\Phi = \frac{1}{\sqrt{2}}(\sigma + iS)$, we can then split the lagrangian (6.5.1) into two parts:

$$\begin{aligned}&\mathcal{L} = \mathcal{L}_0 + \mathcal{L}_1 \ , \text{where} \\ &\mathcal{L}_0 = \mathcal{L}_{kin} + \mu^2\Phi^\dagger\Phi - \lambda(\Phi^\dagger\Phi)^2 - (h_1\bar{\psi}_L\Phi\psi_R + \text{h.c.}) \ , \\ &\mathcal{L}_1 = i(h_1-h_2)\ S\ \bar{\psi}\gamma_5\psi + \frac{\sigma}{\Lambda}F_{\mu\nu}F^{\mu\nu} \ . \end{aligned} \tag{6.5.2}$$

One can here notice that the whole lagrangian is invariant under the vectorial transformation

$$U(1)_V \quad : \quad \psi \to e^{i\alpha}\psi \quad , \quad \Phi \to \Phi \ , \tag{6.5.3}$$

whereas $\mathcal{L}_0$ is also invariant under the axial transformation

$$U(1)_A \quad : \quad \psi \to e^{i\beta\gamma_5}\psi \quad , \quad \Phi \to e^{-2i\beta}\Phi \ . \tag{6.5.4}$$

The axial transformation is broken by $\mathcal{L}_1$ and is therefore an exact symmetry of the hidden sector lagrangian in the limit $h_1 = h_2$. The symmetry is broken additionally by the coupling to the photons.

At tree-level, S is massless since it is the (pseudo)Goldstone boson of the axial $U(1)_A$ symmetry. For $\mu^2 > 0$ there is a symmetry breaking vacuum, with $\langle\sigma\rangle = v$ and $v^2 = \frac{\mu^2}{\lambda}$. By expanding around the minimum one also finds at tree-level that

$$m_\phi^2 = 2\mu^2 \quad , \quad \tilde{m} = \sqrt{\frac{\lambda}{2}}\ m_\phi \ . \tag{6.5.5}$$

At the one-loop level, there is a quantum correction to the potential $V_1 = V_1(h_1^2\sigma^2 + h_2^2 S^2)$, which generates a mass for the pseudo-goldstone boson S, proportional to $m_S^2 \sim O(\frac{h_2^2-h_1^2}{16\pi^2})m_\phi^2$, which has a one-loop suppression with respect to the mediator mass ϕ. This model is an example of a UV embedding of case A of Section 6.3, in which one naturally expects $\tilde{m} \leq m_\phi$ and selects therefore natural regions in the parameter space in Section 6.3.

We thus showed that the hypothesis of Case A (heavy mediator) as well as the theoretical constraint $\tilde{m} \leq m_\phi$ both can naturally arise in a microscopic model with appropriate symmetries. The second point appears yet to be a more general feature of the model, since the mixing term $\tilde{m}$ is expected to be sourced by the same process giving masses to dark matter and to the mediator and hence to stand in a range of mass in between the masses of dark matter and of the mediator.

We have hence shown in detail that a keV scalar dark matter can be the main constituent of the matter of the universe, producing monochromatic X-ray signals that can be fitted with the recently claimed events of a 3.5 keV line in nearby clusters of galaxies. Moreover, we know that for a warm dark matter mass of order of a keV, free streaming produces a cutoff in the linear fluctuation power spectrum at a scale corresponding to dwarf galaxies and can fit observations for $m_s \gtrsim 1.5$ keV [212]. We have shown that astrophysical, collider and relic density constraints are more difficult to accommodate. They are however possible to satisfy for certain values of the mediator mass m_ϕ and scale Λ of the couplings between the mediator and the photon 300 keV $\lesssim m_\phi \lesssim$ 50 MeV and 5 TeV $\lesssim \Lambda \lesssim$ 1000 TeV. These values can conversely be considered as a prediction of our setup of keV dark matter models leading to X-ray monochromatic lines.

6.6 Conclusions

In this part we have reviewed several aspects of dark matter searches. The possible implication of a mediator, either heavy, or light, has been studied in details, in the context of interactions with the electroweak sector as well as the strong sector of the Standard Model. Possible signatures at the LHC have been described as well as interesting toy models being able to contain all together right handed neutrinos, light dark matter and axion like particles.

The latter spectator particles in our studies remain very interesting beyond standard model particle candidates. A myriad of experimental devices are indeed being developed to detect scalar particles interacting with the electromagnetic field. Furthermore sterile neutrinos are well motivated particles which remain hypothetical, but that can have plenty of phenomenological implications.

We also showed that, as pointed out recently by [217], the study of *pure* effective models – as it is often done in the literature – misses important quantitative effects. Indeed, we could reach a cross section in agreement with the analysis of XMM Newton data only through the building of a microscopic model with the exchange of a light scalar.

Of course, a wide field of unexplored paths remains to be explored, paths that have to be more and more constrained, in order to be able, one day, to make a strong statement about the existence and the features of dark matter.

Part III

Low Energy Supersymmetry

7 Introduction To Flavor Physics

7.1 The Flavour Structure of the Standard Model

Let us in this section introduce the basic tools for studying the flavour structure of Standard Model, providing the reader a minimal toolbox which will widely used in the following sections.

Any model of particle physics is being given during its construction a certain amount of – *a priori* – free parameters (masses, couplings). Yet, by the use of field redefinitions, one can get rid of some of them, and count how many fundamental parameters the theory actually contains. As an example let us emphasize the case of the quark sector. Among the components of the quark Yukawa matrices (or equivalently the mass matrices at low energies), which are taken to be arbitrary 3×3 complex matrices, there would a priori be 18 free parameters (9 real components, 9 complex phases). The quark sector containing up and down quarks would then contain some 36 free parameters. Yet a careful counting of the physical parameters, conserved by the symmetry of the SM Lagrangian shows that the quark sector should contain only six physical masses and four additional parameters : 3 mixing angles and one CP violating phase. Let us see in this section how these show up in the Standard Model. The experimental goal of flavour physics is to measure with good precision these four parameters.

7.2 The CKM Matrix

In order to work out where do the physical parameters show up, one has to play with the different symmetries of the Lagrangian in particular to reduce the number of components of the Yukawa matrices we introduced. In order to do so, let us write the quark interaction terms under the form

$$\mathcal{L}_{Yuk} = \bar{Q}^i_L(\mathbf{y_u})_{ij} u^j_R \tilde{H} + \bar{Q}^i_L(\mathbf{y_d})_{ij} d^j_R H + (\text{lepton term}) + h.c.\,, \tag{7.2.1}$$

where H is the Higgs SU(2) doublet and $\tilde{H}_\alpha \equiv \epsilon_{\alpha\beta} H_\beta$ its charge conjugate. The field Q^i are the left-handed quark doublets

$$Q^i_L = \begin{pmatrix} u^i_L \\ d^i_L \end{pmatrix}, \tag{7.2.2}$$

where the index i runs over the familiy indices, and the fields u_R, d_R are their right-handed counterparts. The Higgs field reaching its vev $\langle H \rangle = (0\,,\, v/\sqrt{2})^T$ after spontaneous symmetry breaking generates the mass terms for the quarks of the form

$$\mathcal{L}_{mass,\ q} = m^d_{ij} \bar{d}^i_L d^j_R + m^u_{ij} \bar{u}^i_L u^j_R + h.c.\,, \tag{7.2.3}$$

such that the Yukawa couplings are in one to one correspondence with the quark masses. Now in order to go in the basis where the mass matrices are diagonal, one simply has to rotate the

left-handed and right-handed fields by two different unitary matrices V_L and V_R respectively

$$\left\{ \begin{array}{rcl} q_L^i &=& (V_L^q)_j^i \, q'^j_L \\ \\ q_R^i &=& (V_R^q)_j^i \, q'^j_R \end{array} \right. \quad \Rightarrow \quad \hat{m}_{ij}^q = \left(V_L^{q\dagger}\right)_i^k \, m_{kl}^q \, (V_R^q)_j^l \, , \tag{7.2.4}$$

where the symbole q stands for either "up" or "down" quarks u, d. In this new basis, the Yukawas become diagonal, the mass eigenstate basis. Yet, on the other hand, the interaction terms with gauge bosons get mixed up in the flavour space since it transforms like

$$\mathcal{L}_{Wqq} = \frac{g}{\sqrt{2}} \bar{u}_L i\gamma_\mu d_L W^\mu \; \longrightarrow \frac{g}{\sqrt{2}} \bar{u}'_L i\gamma_\mu \left(V_L^{u\dagger} V_L^d\right) d'_L W^\mu \, . \tag{7.2.5}$$

We see here appearing the well known **CKM** matrix (introduced for three generations of quarks by Makoto Kobayashi and Toshihide Maskawa in 1973 [236] , adding one generation to the matrix previously introduced by Nicola Cabibbo [237]) defined by

$$V_{CKM} \equiv V_L^{u\dagger} V_L^d = \begin{pmatrix} V_{ud} & V_{us} & V_{ub} \\ V_{cd} & V_{cs} & V_{cb} \\ V_{td} & V_{ts} & V_{tb} \end{pmatrix} \, . \tag{7.2.6}$$

The study of the CKM matrix is then the key point for a good understanding of the flavour changing processes in the standard model. Yet, it is necessary to parametrize this matrix in terms of the few physical parameters the theory is built on. Indeed, as we announced earlier, the construction of such a unitary matrix can be parametrized in terms of only four real parameters, that cannot appear all in the same row. A possible parametrization is to use the mixing angle θ_{12}, θ_{13} and θ_{23} (θ_{12} being the famous Cabbibo angle in the limit of two generations) adding to these angles a phase δ providing the formulation

$$V_{CKM} = \begin{pmatrix} c_{12}c_{13} & s_{12}c_{13} & s_{13}e^{-i\delta} \\ -s_{12}c_{23} - c_{12}s_{23}s_{13}e^{i\delta} & c_{12}c_{23} - s_{12}s_{23}s_{13}e^{i\delta} & s_{23}c_{13} \\ s_{12}c_{23} - c_{12}s_{23}s_{13}e^{i\delta} & -c_{12}c_{23} - s_{12}s_{23}s_{13}e^{i\delta} & c_{23}c_{13} \end{pmatrix} \, , \tag{7.2.7}$$

where $c_{ij} = \cos\theta_{ij}$ and $s_{ij} = \sin\theta_{ij}$.

This exact parametrization is usually pretty difficult to handle, which is the reason why people elaborated approximated formulations. In an inductive manner, Wolfenstein hence proposed [238] a particular pattern to approximate the CKM matrix

$$|V_{CKM}| \sim \begin{pmatrix} 1 & \lambda & \lambda^3 \\ \lambda & 1 & \lambda^2 \\ \lambda^3 & \lambda^2 & 1 \end{pmatrix} \, , \tag{7.2.8}$$

where the parameter λ, taking its value from experimental measurements would be of order

$$\lambda \sim 0.22 \, . \tag{7.2.9}$$

Such a leading order value of the CKM elements could indeed come from a particular expression of its components in terms of four independant parameters, defining

$$s_{12} \;=\; \lambda = \frac{|V_{us}|}{\sqrt{|V_{us}|^2 + |V_{ud}|^2}} \, , \tag{7.2.10}$$

$$s_{23} \;=\; \lambda^2 A = \lambda \left| \frac{V_{cb}}{V_{us}} \right| \, , \tag{7.2.11}$$

and

$$s_{13}e^{i\delta} = A\lambda^3(\rho + i\eta) = V_{ub}^* \,. \tag{7.2.12}$$

This formulation can seem rather tedious at first sight but becomes incredibly smart while expanding the whole CKM matrix for small λ, giving

$$V_{CKM} \sim \begin{pmatrix} 1 - \frac{\lambda^2}{2} & \lambda & A\lambda^3(\rho - i\eta) \\ -\lambda & 1 - \frac{\lambda^2}{2} & A\lambda^2 \\ A\lambda^3(1 - \rho - i\eta) & -A\lambda^2 & 1 \end{pmatrix} + \mathcal{O}(\lambda^4) \,, \tag{7.2.13}$$

where one can easily recognize, looking at first 2 by 2 block matrix the Cabbibo mixing matrix.

7.2.1 Geometrical Formulation

The unitarity of the CKM matrix provides an elegant way to parametrize the latter in a geometrical way. Indeed the well known properties of unitary matrices

$$\sum_i V_{id} V_{is}^* = 0 \,, \tag{7.2.14}$$

provides several relations (3 for the rows, 3 for the columns) that can de seen as vectorial closure relations of triangles in the complex plane. For instance the relation

$$V_{ud} V_{ub}^* + V_{cd} V_{cb}^* + V_{td} V_{tb}^* = 0 \,, \tag{7.2.15}$$

has the particularity to involve three terms of the same order of magnitude λ^3 and can be rewritten

$$\frac{V_{ud} V_{ub}^*}{V_{cd} V_{cb}^*} + 1 + \frac{V_{td} V_{tb}^*}{V_{cd} V_{cb}^*} = 0 \,, \tag{7.2.16}$$

such that, in the (ρ, η) plane, one can represent the associated triangle under the form depicted in Fig. 1. Each of the CKM matrix element can then be constrained by flavour changing measurements as shown in Fig. 2.

7.3 Mass and Mixing Hierarchy

Understanding the hierarchy between the different fermion masses and mixings is a challenging task which has to be understood and motivated in order to build viable models of the Standard Model flavour structure. In this section we present an approach, introduced by Frogatt and Nielsen in 1979 [240] where this hierarchy can be generated by an additional abelian symmetry, spontaneously broken.

7.3.1 Abelian Models : The Froggatt–Nielsen Mechanism

The approach of Frogatt and Nielsen starts from the observation that, at leading order, one expects the up quark Yukawa matrix to be of the form

$$\mathbf{y_u} \sim \begin{pmatrix} 0 & 0 & 0 \\ 0 & 0 & 0 \\ 0 & 0 & 1 \end{pmatrix} \,, \tag{7.3.1}$$

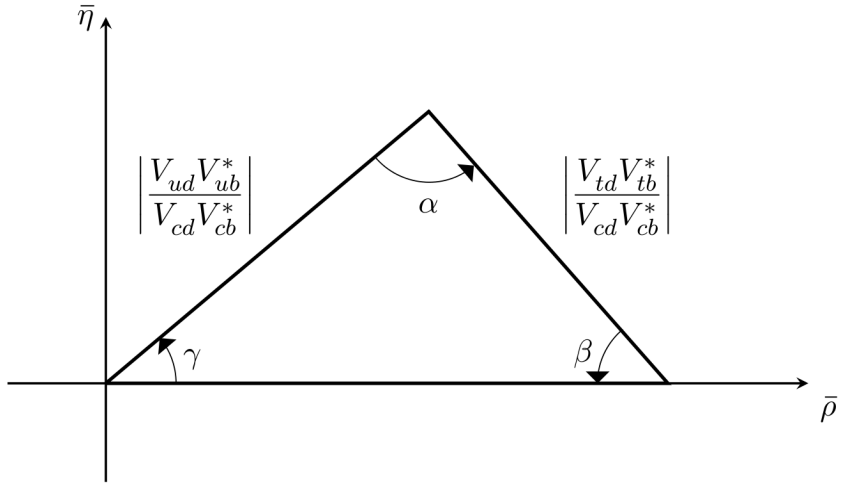

Figure 1: Geometrical representation of the unitarity relation (7.2.16) in the plane (ρ, η).

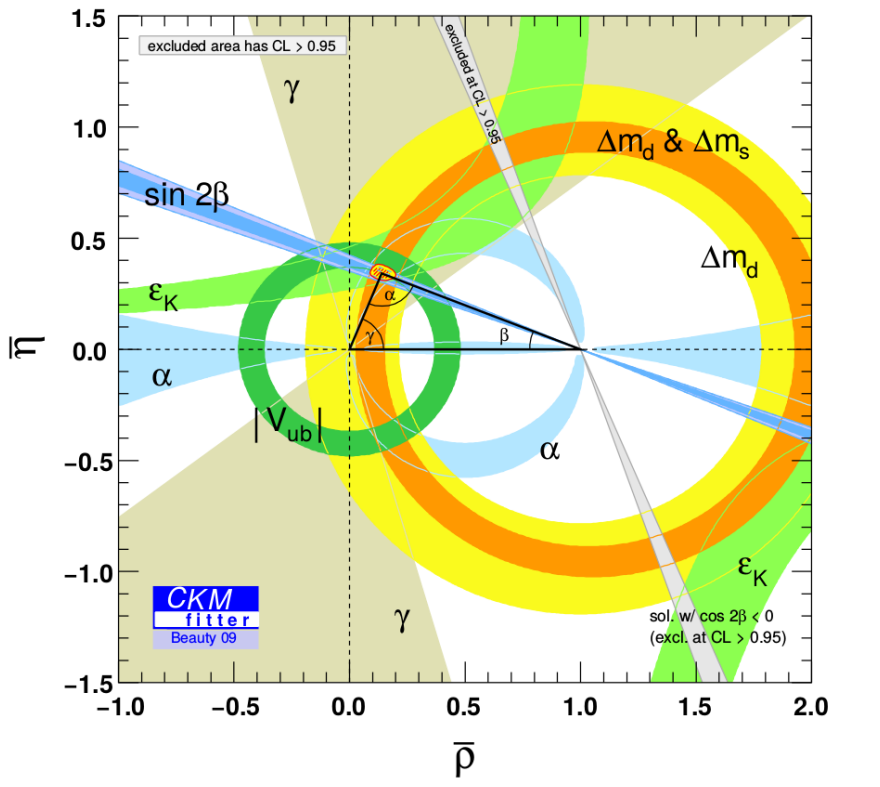

Figure 2: Summary of the experimental constraints on the CKM unitary triangle described in (7.2.16). Plot extracted from [239]

at the renormalizable level. The smallness of the light masses and mixing angles can then be interpreted as an expansion parameter ϵ coming from the mass suppression of higher dimensional operators involving an additional scalar field ϕ – called *flavon* – charged under an additional $U(1)$ symmetry and getting a vev through spontaneous symmetry breaking, leading to suppression factors of the form

$$\epsilon = \frac{\langle\phi\rangle}{\Lambda} \ll 1\,. \tag{7.3.2}$$

Here Λ can be the Planck scale or more generically the scale where Yukawa couplings are generated. Namely, at the renormalizable level, the lagrangian is assumed to contain the single interaction term

$$\mathcal{L}_{ren.} \supset (\mathbf{y_u})_{33}\bar{u}^t_L u^3_R \tilde{H} + h.c.\,, \tag{7.3.3}$$

meaning that the charges of these fields under this additional $U(1)$ satisfy

$$q_3 + u_3 - h = 0\,, \tag{7.3.4}$$

where q_3, u_3 and h denote the charges of the top quark, its right-handed counterpart and the higgs field, respectively, under the new abelian symmetry. The expansion parameter ϵ arises in the theory as soon as one introduces higher dimensional operators of the form

$$\begin{aligned}
\mathcal{L}_{hdo} &= (\mathbf{y_u})_{ij}\left(\frac{\phi}{\Lambda}\right)^{q_i+u_j-h} u^i_L u^j_R \tilde{H} + h.c. \qquad [\text{If } q_i+u_j-h>0] \\
&+ (\mathbf{y_u})_{ij}\left(\frac{\phi^\dagger}{\Lambda}\right)^{-(q_i+u_j-h)} \bar{u}^i_L u^j_R H + h.c. \quad [\text{If } q_i+u_j-h<0]\,,
\end{aligned} \tag{7.3.5}$$

where, for $(i,j) \neq (3,3)$, the charges summation satisfies $q_i + u_j - h$ can take different signs. Restricting to the case where $q_i + u_j - h > 0$, the effective Yukawa coupling becomes, after spontaneous symmetry breaknig of the $U(1)$ symmetry, of the form

$$(\mathbf{y^{eff}_u})_{ij} \equiv \epsilon^{q_i+u_j-h}(\mathbf{y_u})_{ij}\,, \tag{7.3.6}$$

which can be re-written, using Eq. (7.3.4), with charges relative to the top quark ones,

$$(\mathbf{y^{eff}_u})_{ij} = \epsilon^{(q_i-q_3)+(u_j-u_3)}(\mathbf{y_u})_{ij} \equiv \epsilon^{q_{i3}+u_{j3}}(\mathbf{y_u})_{ij}\,, \tag{7.3.7}$$

providing, assuming the initial Yukawa matrix was of order one, the general form for the up quark effective Yukawa matrix

$$\mathbf{y^{eff}_u} \approx \begin{pmatrix} \epsilon^{q_{13}+u_{13}} & \epsilon^{q_{13}+u_{23}} & \epsilon^{q_{13}} \\ \epsilon^{q_{23}+u_{13}} & \epsilon^{q_{23}+u_{23}} & \epsilon^{q_{23}} \\ \epsilon^{u_{13}} & \epsilon^{u_{23}} & 1 \end{pmatrix}\,. \tag{7.3.8}$$

The down quarks generation Yukawa matrix can now be easily written as follows

$$\mathbf{y^{eff}_d} \approx \begin{pmatrix} \epsilon^{q_{13}+d_{13}} & \epsilon^{q_{13}+d_{23}} & \epsilon^{q_{13}} \\ \epsilon^{q_{23}+d_{13}} & \epsilon^{q_{23}+d_{23}} & \epsilon^{q_{23}} \\ \epsilon^{d_{13}} & \epsilon^{d_{23}} & 1 \end{pmatrix} \times \epsilon^{q_3+d_3+h}\,. \tag{7.3.9}$$

In the simplest approximation where the charges are distributed in the reversed order than the masses hierarchy

$$\begin{aligned} q_1 > q_2 > q_3 \,, \\ u_1 > u_2 > u_3 \,, \\ d_1 > d_2 > d_3 \,, \end{aligned} \tag{7.3.10}$$

the latter matrices are close to be diagonal and the rotation matrices $V_{L,R}^{u,d}$ close to the identity matrix. The CKM matrix turns out to be given by the values of the charges q_i

$$V_{CKM} \approx \begin{pmatrix} 1 & \epsilon^{q_{12}} & \epsilon^{q_{13}} \\ \epsilon^{q_{12}} & 1 & \epsilon^{q_{23}} \\ \epsilon^{q_{13}} & \epsilon^{q_{23}} & 1 \end{pmatrix} . \tag{7.3.11}$$

The mass ratios are thus simply given by the relations

$$\frac{m_u}{m_t} \approx \epsilon^{q_{13}+u_{13}} \,, \quad \frac{m_c}{m_t} \approx \epsilon^{q_{23}+u_{23}} \,, \quad \frac{m_d}{m_b} \approx \epsilon^{q_{13}+d_{13}} \,, \quad \frac{m_s}{m_b} \approx \epsilon^{q_{23}+d_{23}} \,. \tag{7.3.12}$$

One simple possibility, elaborated in [241, 242], using an expansion parameter of the order the Cabbibo angle $\sin\theta_c \approx 0.22 \sim \epsilon$, is given by

$$\begin{aligned} (q_1, q_2, q_3) &= (3, 2, 0) \,, \\ (u_1, u_2, u_3) &= (5, 2, 0) \,, \\ (d_1, d_2, d_3) &= (1, 0, 0) \,, \end{aligned} \tag{7.3.13}$$

$$\tag{7.3.14}$$

giving the ratios

$$\frac{m_u}{m_t} \approx \epsilon^8 \,, \quad \frac{m_c}{m_t} \approx \epsilon^4 \,, \quad \frac{m_d}{m_b} \approx \epsilon^4 \,, \quad \frac{m_s}{m_b} \approx \epsilon^2 \,. \tag{7.3.15}$$

Such model provides a simple example for introducing a hierarchy in the flavour structure of the Standard model.

7.4 Flavor Changing Neutral Currents

Now that we have introduced how flavours can get mixed up in the standard model, we will in this section briefly review what are the major constraints coming from experiment and why, are Flavor Changing Neutral Currents (FCNCs) such important tests for building a viable phenomenological model.

7.4.1 Charged vs Neutral Currents

Let us make a short parenthesis making some purely phenomenological comments. Indeed let us look at particular flavour changing currents, from both the charged and neutral sides. Let us for instance consider two processes involving K hadrons and look at their decays into leptonic final states branching ratios. Namely

$$\mathrm{Br}(K^+ \to \mu^+\nu) = 64\% \,, \qquad \mathrm{Br}(K_L \to \mu^+\mu^-) = 7 \times 10^{-9} \,. \tag{7.4.1}$$

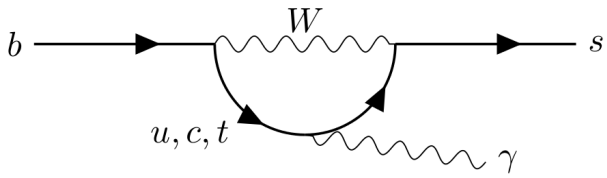

Figure 3: Process $b \to s\gamma$ generating flavour changing at the one loop order

In these two processes, flavour number is violated, whereas the first one involves a charged intermediate (charged current) while the second has a neutral one (neutral current). One immediately notices the huge difference of order of magnitude between these two different branching ratios. Indeed the neutral current process is strongly suppressed compared to the charged one. This is actually a generic phenomenological feature of the Standard Model. Looking at other flavour changing processes therefore confirms this first sight statement : The B and D mesons decays give

$$\mathrm{Br}(B^{\pm} \to D^{\pm} l \nu_l X) = 11\% \,, \qquad \mathrm{Br}(B^0 \to K^* l^+ l^-) \approx 10^{-6} \,, \tag{7.4.2}$$

and

$$\mathrm{Br}(D^{\pm} \to K^0 \mu^{\pm} \nu) = 9\% \,, \qquad \mathrm{Br}(D^0 \to K^{\pm} \pi^{\mp} \mu^{\pm} \mu^{\mp}) < 5 \times 10^{-4} \,. \tag{7.4.3}$$

The same pattern is thus generically observed in particle physics and constitutes a stringent constraint while building phenomenological models. That is, as a matter of fact, **FCNCs have to be strongly suppressed in any reasonable beyond the Standard Model example.**

We will in what follows describe some classical FCNC processes, and see how they are naturally suppressed in the Standard Model before plunging into supersymmetric considerations.

7.4.2 The GIM Mechanism : When the SM *Feels Fine*

At the tree level, only interaction involving mediation of a $W^{\pm}$ can generate flavour changing since the photon and the Z couple diagonally in the flavour space. FCNCs thus appear only at the loop level, but we will see here that it gets a suppression factor in addition to the simple loop factor. The typical flavour changing process at one loop, involving FCNC, is the process $b \to s\gamma$ depicted in Fig. 3.

Computing the amplitude of such a diagram makes appear the following quantity

$$\mathcal{M} \propto \sum_{i=u,c,t} V_{ib} V_{is}^* F\left(\frac{m_i^2}{m_W^2}\right) . \tag{7.4.4}$$

Where $F\left(\frac{m_i^2}{m_W^2}\right)$ arises from the precise calculation of the loop integral, and is expected to be of order one. The reader may notice, that weak couplings involving only left handed quarks would lead to a global factor of

$$q_\mu^\gamma \epsilon_\nu(q^\gamma) \left(\bar{u}(p_s) P_R \sigma^{\mu\nu} P_L u(p_b)\right) \,, \tag{7.4.5}$$

which would exactly vanish. One has to add, as a consequence, a chirality flip to make one of the quarks change its chirality during the process. Flipping the chirality of the heaviest quark $m_b \gg m_s$, and taking into account the mass suppression coming from the propagator of the W bosons as well as the loop factor gives an overall factor of the form

$$\mathcal{M} \propto \frac{g_2^2}{16\pi^2}\frac{m_b}{m_W^2}\sum_{i=u,c,t} V_{ib}V_{is}^* F\left(\frac{m_i^2}{m_W^2}\right). \tag{7.4.6}$$

Let us for a while make the simple assumption that all the internal quarks u, c, t are lighter than the W boson. This assumption turns out to be partially wrong, and we will see later on how one can generalize the following results in a more realistic formulation. Using this naive assumption, one can however expand the function F around zero

$$F\left(\frac{m_i^2}{m_W^2}\right) = F(0) + \frac{m_i^2}{m_W^2}F'(0) + \dots, \tag{7.4.7}$$

giving for the amplitude factor

$$\sum_{i=u,c,t} V_{ib}V_{is}^* F\left(\frac{m_i^2}{m_W^2}\right) = F(0)\left(\sum_{i=u,c,t} V_{ib}V_{is}^*\right) + \sum_{i=u,c,t} V_{ib}V_{is}^*\left(\frac{m_i^2}{m_W^2}\right)F'(0) + \dots. \tag{7.4.8}$$

The orthogonality of the CKM matrix hence ensures that the first term of the expansion (7.4.8) vanishes. One can furthermore write

$$V_{tb}V_{ts}^* = -\sum_{i=u,c} V_{ib}V_{is}^*, \tag{7.4.9}$$

which gives the final expression

$$\begin{aligned}\sum_{i=u,c,t} V_{ib}V_{is}^* F\left(\frac{m_i^2}{m_W^2}\right) &= -F'(0)\sum_{i=u,c} V_{ib}V_{is}^*\left(\frac{m_t^2 - m_i^2}{m_W^2}\right) + \dots, \\ &\approx -F'(0)\sum_{i=u,c} V_{ib}V_{is}^*\left(\frac{m_t^2}{m_W^2}\right), \\ &\approx -F'(0)\left(\lambda^4 + \lambda^2\right)\left(\frac{m_t^2}{m_W^2}\right).\end{aligned} \tag{7.4.10}$$

where powers of the mixing angle $\lambda \sim 0.22$ come from the Wolfenstein parametrization (7.2.8) of the CKM matrix. Therefore it turns out that, in addition to the suppression loop factor, comes the additional factor m_t^2/m_W^2 as well as a mixing angle suppression λ^2.

Obviously the assumption $m_t \ll m_W$ is now outdated since we know that $m_t \sim 2m_W$ and one could doubt of the validity of the latter result since the expansion (7.4.8) is now not relevant. This can be done writing simply by noting that the leading contribution to the function F comes from the top running in the loop, such that

$$F\left(\frac{m_t^2}{m_W^2}\right) \gg F\left(\frac{m_u^2}{m_W^2}\right),\ F\left(\frac{m_c^2}{m_W^2}\right), \tag{7.4.11}$$

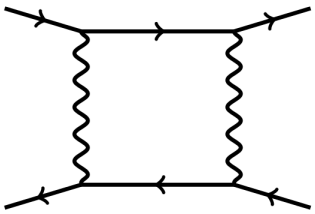

Figure 4: Schematic representation of a meson mixing loop process.

and the integral becomes roughly

$$\sum_{i=u,c,t} V_{ib}V_{is}^* F\left(\frac{m_i^2}{m_W^2}\right) \approx V_{tb}V_{ts}^* F\left(\frac{m_t^2}{m_W^2}\right) \sim \lambda^2 F\left(\frac{m_t^2}{m_W^2}\right) . \tag{7.4.12}$$

The function F being of order one, one gets the same suppression as stated in the old version. This is a peculiar feature of the Standard Model : The consideration of the complete set of quarks in the loops involved in FCNC processes, naturally leads to a suppression of the latter compared to charged current processes. This idea was first suggested by Glashow, Iliopoulos, and Maiani in [243] in a slightly different context, giving their name to a mechanism that is usually called the GIM mechanism.

7.4.3 Meson Mixing

Historically speaking, the GIM mechanism was proposed in another context than the $b \to s\gamma$ process, which was the case of meson mixing. Indeed one can imagine loop processes in which mesons can oscillate through a $\Delta F = 2$ flavour changing interaction, as depicted in Fig. 4.

Such oscillation were first studied in the case of the neutral Kaon K^0, the combination of a d quark and an s-antiquark oscillating with its counterpart $\bar{K}^0$ – s quark and d anti-quark. The diagram of this oscillation process is drawn in Fig. 5. Indeed, in this case the same argument can be used, using the CKM matrix unitarity to show that altogether, the quarks running in the loops provide a necessary compensation, rendering the associated FCNC highly suppressed in the Standard Model. Such proof was actually an argument at that time to claim for the existence of the c quark.

The Kaon system is one of the best precisely measured FCNC process in the standard model and hence turns out to be a major source of constraint for building beyond standard model theories. We will see in what follows that this is the case in particular in the context of the supersymmetric version of the Standard Model, the so called MSSM.

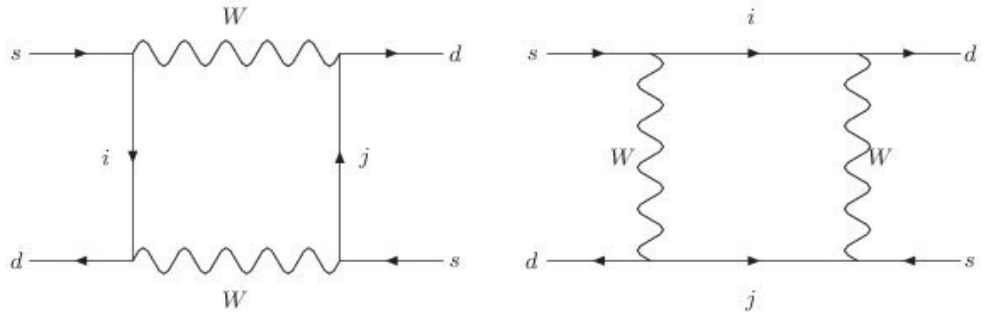

Figure 5: Processes inducing a Kaon oscillation in the Standard Model. The internal indices i, j run over the quarks u, c and t.

8 The Case of the Minimal Supersymmetric Standard Model

8.1 Generalities

The supersymmetric version of the Standard Model, in its minimal formulation, is probably the cleanest formulation of a phenomenological supersymmetric theory, although it suffers from theoretical and phenomenological problems that will not be detailed in the context of this work. Its particle content is summarized in Table 8.1 and 8.2.

Quarks and leptons supermultiplets are present in the model under three versions constituting the three different flavour families. A family index i = 1, 2, 3 can hence be affixed to the chiral supermultiplet names $(Q_i, u_i, \ldots)$ when needed, for example $(e_1, e_2, e_3) = (e, \mu, \tau)$. The superpotential of the MSSM is given by Yukawa terms as well as the μ term for the higgs doublets, namely

$$W_{MSSM} = \bar{U}\mathbf{y_u}QH_u - \bar{D}\mathbf{y_d}QH_d - \bar{e}\mathbf{y_e}LH_d + \mu H_u H_d\,, \tag{8.1.1}$$

To parametrize ones ignorance on the supersymmetry breaking process, one usually add to the lagrangian so called soft breaking terms (*soft* in the sense they have positive mass dimension) of the form

$$\begin{aligned}
\mathcal{L}_{soft}^{MSSM} &= -\frac{1}{2}\left(M_3\tilde{g}\tilde{g} + M_2\tilde{W}\tilde{W} + M_1\tilde{B}\tilde{B} + h.c.\right) \\
&- \left(\tilde{\bar{U}}\mathbf{a_u}\tilde{Q}H_u - \tilde{\bar{D}}\mathbf{a_d}\tilde{Q}H_d - \tilde{\bar{e}}\mathbf{a_e}\tilde{L}H_d + h.c.\right) \\
&- \tilde{Q}^\dagger\mathbf{m_Q^2}\tilde{Q} - \tilde{L}^\dagger\mathbf{m_L^2}\tilde{L} - \tilde{\bar{U}}\mathbf{m_{\bar{u}}^2}\tilde{\bar{U}}^\dagger - \tilde{\bar{D}}\mathbf{m_{\bar{d}}^2}\tilde{\bar{D}}^\dagger - \tilde{\bar{e}}\mathbf{m_{\bar{e}}^2}\tilde{\bar{e}}^\dagger \\
&- m_{H_u}^2 H_u^* H_u - m_{H_d}^2 H_d^* H_d - (b\; H_u H_d + h.c.)\;.
\end{aligned} \tag{8.1.2}$$

Here matrices $\mathbf{a_{u,d,e}}$ represent $(scalar)^3$ interaction matrices (in one-to-one correspondence with the Yukawa couplings) while the $\mathbf{m^2_{Q,\bar{u},\bar{d},\bar{e},L}}$ are hermitian mass matrices. The model contains

Names		Spin 0	Spin 1/2	$SU(3)_c, SU(2)_L, U(1)_Y$
Squarks, quarks (× 3 families)	Q	$(\tilde{u}_L, \tilde{d}_L)$	(u_L, d_L)	$(\mathbf{3}, \mathbf{2}, \frac{\mathbf{1}}{\mathbf{6}})$
	$\bar{U}$	$\tilde{u}_R^*$	u_R^c	$(\bar{\mathbf{3}}, \mathbf{1}, -\frac{\mathbf{2}}{\mathbf{3}})$
	$\bar{D}$	$\tilde{d}_R^*$	d_R^c	$(\bar{\mathbf{3}}, \mathbf{1}, \frac{\mathbf{1}}{\mathbf{3}})$
Sleptons, leptons (× 3 families)	L	$(\tilde{\nu}, \tilde{e}_L)$	(ν, e_L)	$(\mathbf{1}, \mathbf{2}, -\frac{\mathbf{1}}{\mathbf{2}})$
	$\bar{e}$	$\tilde{e}_R^*$	e_R^c	$(\bar{\mathbf{1}}, \mathbf{1}, \mathbf{1}$
Higgs, higgsinos	H_u	(H_u^+, H_u^0)	$(\tilde{H}_u^+, \tilde{H}_u^0)$	$(\mathbf{1}, \mathbf{2}, +\frac{\mathbf{1}}{\mathbf{2}})$
	H_d	(H_d^0, H_d^-)	$(\tilde{H}_d^0, \tilde{H}_d^-)$	$(\bar{\mathbf{1}}, \mathbf{2}, -\frac{\mathbf{1}}{\mathbf{2}})$

Table 8.1: Chiral supermultiplets in the Minimal Supersymmetric Standard Model. The spin-0 fields are complex scalars, and the spin-1/2 fields are left-handed two-component Weyl fermions.

Names	Spin 1/2	Spin 1	$SU(3)_c, SU(2)_L, U(1)_Y$
Gluino, gluon	$\tilde{g}$	g	$(\mathbf{8},\mathbf{1},\mathbf{0})$
Winos, W boson	$\tilde{W}^{\pm}\ \tilde{W}^0$	$W^{\pm}\ W^0$	$(\mathbf{1},\mathbf{3},\mathbf{0})$
Bino, B boson	$\tilde{B}^0$	B^0	$(\mathbf{1},\mathbf{1},\mathbf{0})$

Table 8.2: Gauge supermultiplets in the Minimal Supersymmetric Standard Model.

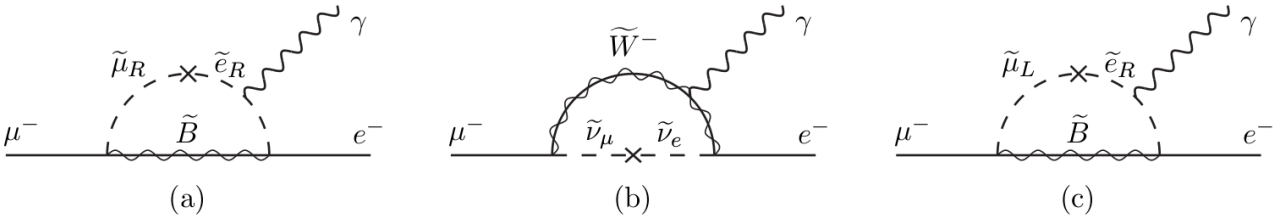

Figure 1: Example of diagrams contributing to the process $\mu^- \to e^-\gamma$ in models with lepton flavour violating soft supersymmetry breaking parameters (denoted by mass insertion symbols $\times$). Diagrams (a), (b), and (c) contribute to constraints on the off-diagonal elements of $\mathbf{m^2_{\tilde{e}}}$, $\mathbf{m^2_L}$, and $\mathbf{a_e}$, respectively.

furthermore Majorana masses for the gluinos M_1, M_2, M_3. All these masses parameters are introduced in order to break supersymmetry and we assume them to be of the order of a typical supersymmetry breaking mass scale

$$m_{soft} \gtrsim \text{TeV}\,. \tag{8.1.3}$$

Although the MSSM adds to the old fashion non-supersymmetric Standard Model in total about one hundred new free parameters, and hence render its phenomenological treatment more difficult, one can easily see that all these different couplings and new possible vertices introduce dangerous flavour mixing or CP violating processes, that are severely restricted by experiments. A typical example is the process $\mu^- \to e^-\gamma$, whose branching ratio is constrained by experiment [244, 245] to be lower than

$$\text{Br}(\mu^- \to e^-\gamma) < 1.2 \times 10^{-11}\,, \tag{8.1.4}$$

constraining, among others, the parameter $m^2_{\tilde{\mu}^*_R \tilde{e}_R} \equiv (\mathbf{m^2_{\tilde{e}}})_{12}$ to be very small, the numerical value depending on the particular scenario explored. Off-diagonal terms of the left-handed sleptons squared-mass matrix $\mathbf{m^2_L}$ also induce, as depicted in Fig 1 b, contributions to the $\mu^- \to e^-\gamma$ process, that is, the slepton squared-mass matrices must not have significant mixings for e_L , μ_L.

Note that the aforementioned process induced by supersymmetric interactions violates the flavour number conservation by $\Delta F = 1$. However there exists other strong constraints, in particular on the squarks squared-mass matrices, with the higher degree of violation $\Delta F = 2$. The strongest of these comes from the neutral kaon system $K^0 \leftrightarrow \bar{K}^0$ arising through box diagrams of the kind depicted in Fig. 2.

We will in what follows study in detail the constraints arising from the study of meson mixings in the MSSM, in the generalized case where Dirac gauginos are added to the standard MSSM.

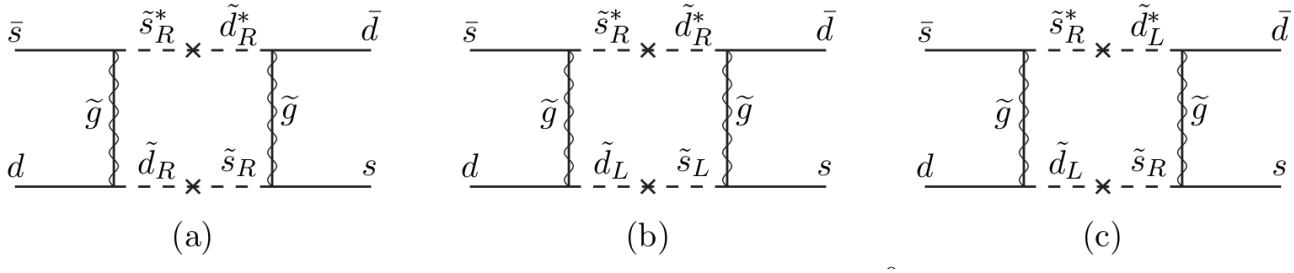

Figure 2: Among others, some of the diagrams contributing to the neutral kaon mixing $K^0 \leftrightarrow \bar{K}^0$ induced by the squarks mass insertion parameters (indicated by $\times$).

8.2 Constraining the MSSM with Dirac Gauginos

It has been known since the early days of low-energy supersymmetry that flavour-changing processes set severe constraints on the flavour structure of the superpartner spectrum in the MSSM. For example, the simplest models based on a single abelian flavoured gauge group that we have briefly reviewed in section 7.3.1 in the case of the Standard Model, although providing an approximate alignment mechanism for scalar mass matrices, still require scalar partners heavier than at least 100 TeV. Both collider and flavour constraints encourage us to search for non-minimal extensions with suppressed collider bounds and flavour-changing transitions. Supersymmetric extensions with a Dirac gaugino sector [246, 247, 248, 249, 250, 251, 252, 253, 254, 255, 256, 257, 258, 259, 260, 261, 262, 263, 264, 265, 266, 267, 268, 269, 270, 271, 272, 273, 274, 275, 276, 277, 278, 279, 280, 281, 282, 283, 284] enter precisely into this category.

Originally motivated by the preserved R-symmetry, which allows simpler supersymmetry breaking sectors [246, 247], and the possible connection with extra dimensions and $N = 2$ supersymmetry [251, 285], it was subsequently noticed that Dirac gaugino masses have many phenomenological advantages over their Majorana counterparts. For example, the Dirac mass is *supersoft* [286, 287, 250, 288], which naturally allows somewhat heavy gluinos compared to the squarks [289, 290, 291]. Furthermore, it was argued later on that in this case flavour-changing neutral current (FCNC) transitions are suppressed due to protection from the underlying R-symmetry that lead to a chirality flip suppression [253]. It was also proved that the collider signatures of superpartner production are suppressed compared to the MSSM case due to the heaviness of the Dirac gluino and the absence of several squark decay channels [292, 293, 294, 295]. We want, in what will follow to understand the most general bounds arising from flavour physics when we allow Dirac gaugino masses in addition to Majorana masses. This work was made in collaboration with E.Dudas, M. Goodsell and P. Tziveloglou and published in [296].

In recent years, very precise measurements of observables in flavour violation processes have been made [297] while the Standard Model contribution to some of these processes is now being known with reasonable accuracy [298]. This results in very strong restrictions on the flavour structure of theories beyond the SM. An exact theoretical computation of the neutral meson mixing systems is particularly difficult due to unresolved non-perturbative, strong-interaction effects. The general strategy is to compute the amplitude between the valence quarks in the full perturbative theory, then match the amplitude to an effective theory of four-fermion contact interactions. Contact with neutral meson mixing is achieved by estimating the matrix elements between initial and final states, typically by use of PCAC [299] and lattice QCD techniques.

8.2.1 Effective Hamiltonian

Within the context of MSSM, the dominant contribution to neutral meson mixing comes from gluino-squark box diagrams (see eg. fig. 2 for the Kaon system). Starting from the superfield lagrangian (where V^a is denoting the gluino superfield in what follows)

$$\begin{aligned}\mathcal{L}_{MSSM} &\supset \int d^4\theta\; Q^\dagger e^{2g_s V^a T^a} Q + \overline{D}^\dagger e^{-2g_s V^a T^{a*}} \overline{D} \\ &\supset -\sqrt{2} g_s \Big[\tilde{d}^*_{Lxi} T^a_{xy} \lambda^{a\alpha} d_{Lyi\alpha} - \tilde{d}_{Rxi} T^{a*}_{xy} \lambda^{a\alpha} d^c_{Ryi\alpha} \Big] + h.c.\,, \end{aligned} \tag{8.2.1}$$

we expand in the following the standard computation to include both Majorana and Dirac gluino masses. In particular

$$\begin{aligned}\mathcal{L} &\supset -\frac{1}{2}\left(M\lambda^a\lambda^a + M_\chi \chi^a\chi^a + 2 m_D \chi^a \lambda^a + h.c.\right) \\ &\quad -\sqrt{2} g_s \Big[\tilde{d}^*_{Lxi} T^a_{xy} \lambda^{a\alpha} d_{Lyi\alpha} - \tilde{d}_{Rxi} T^{a*}_{xy} \lambda^{a\alpha} d^c_{Ryi\alpha} \Big] + h.c.\,, \end{aligned} \tag{8.2.2}$$

where λ^a_α is the Majorana gaugino, χ^a_α its Dirac partner and T^a_{xy}, d_{Li}, $\tilde{d}_{Li}$ are the SU(3) generators, the quarks and the squarks of generation i respectively[1]. The mass matrix is diagonalized by performing an orthogonal transformation and then a phase shift to render the masses positive,

$$\begin{pmatrix} \lambda^a \\ \chi^a \end{pmatrix} = R \begin{pmatrix} \psi^a_1 \\ \psi^a_2 \end{pmatrix}. \tag{8.2.3}$$

In basis ψ_i, eq. (8.2.2) becomes

$$\begin{aligned}\mathcal{L}' \supset & -\frac{1}{2}\left(M_1 \psi^a_1 \psi^a_1 + M_2 \psi^a_2 \psi^a_2 + h.c.\right) \\ & - \sqrt{2} g_s \Big[\tilde{d}^*_{Lxi} T^a_{xy} (R_{11}\psi^{a\alpha}_1 + R_{12}\psi^{a\alpha}_2) d_{Lyi\alpha} - \tilde{d}_{Rxi} T^{a*}_{xy} (R_{11}\psi^{a\alpha}_1 + R_{12}\psi^{a\alpha}_2) d^c_{Ryi\alpha} \Big] + h.c. \end{aligned} \tag{8.2.4}$$

The four-fermion effective action is given by [301, 302]

$$\mathcal{H}_K = \sum_{i=1}^{5} C_i Q_i + \sum_{i=1}^{3} \tilde{C}_i \tilde{Q}_i\,, \tag{8.2.5}$$

where the conventionally chosen basis of the dimension six operators is (now in Dirac notation)

$$\begin{aligned} Q_1 &= \overline{d}_x \gamma^\mu P_L s_x\, \overline{d}_n \gamma_\mu P_L s_n\,, \\ Q_2 &= \overline{d}_x P_L s_x\, \overline{d}_n P_L s_n\,, \\ Q_3 &= \overline{d}_x P_L s_n\, \overline{d}_n P_L s_x\,, \\ Q_4 &= \overline{d}_x P_L s_x\, \overline{d}_n P_R s_n\,, \\ Q_5 &= \overline{d}_x P_L s_n\, \overline{d}_n P_R s_x\,, \end{aligned} \tag{8.2.6}$$

[1] Our conventions are the ones from [300].

$\tilde{Q}_{1,2,3}$ are the analogues of $Q_{1,2,3}$ through the exchange $L \leftrightarrow R$ and

$$\begin{aligned}
C_1 &= ig_s^4 W_{1K} W_{1L} \left(\frac{11}{36} |R_{1r}|^2 |R_{1q}|^2 \tilde{I}_4 + \frac{1}{9} M_r M_q R_{1r}^{*2} R_{1q}^2 I_4 \right) W_{K2}^\dagger W_{L2}^\dagger \,, \\
C_2 &= ig_s^4 \frac{17}{18} W_{4K} W_{4L} I_4 W_{K2}^\dagger W_{L2}^\dagger \, M_r M_q R_{1r}^2 R_{1q}^2 \,, \\
C_3 &= -ig_s^4 \frac{1}{6} W_{4K} W_{4L} I_4 W_{K2}^\dagger W_{L2}^\dagger \, M_r M_q R_{1r}^2 R_{1q}^2 \,, \\
C_4 &= ig_s^4 W_{1K} W_{4L} \left(\frac{7}{3} M_r M_q R_{1r}^{*2} R_{1q}^2 I_4 - \frac{1}{3} |R_{1r}|^2 |R_{1q}|^2 \tilde{I}_4 \right) W_{K2}^\dagger W_{L5}^\dagger \\
&\quad -ig_s^4 \frac{11}{18} W_{1K} W_{4L} \tilde{I}_4 W_{K5}^\dagger W_{L2}^\dagger \, |R_{1r}|^2 |R_{1q}|^2 \,, \\
C_5 &= ig_s^4 W_{1K} W_{4L} \left(\frac{1}{9} M_r M_q R_{1r}^{*2} R_{1q}^2 I_4 + \frac{5}{9} |R_{1r}|^2 |R_{1q}|^2 \tilde{I}_4 \right) W_{K2}^\dagger W_{L5}^\dagger \\
&\quad -ig_s^4 \frac{5}{6} W_{1K} W_{4L} \tilde{I}_4 W_{K5}^\dagger W_{L2}^\dagger \, |R_{1r}|^2 |R_{1q}|^2 \,,
\end{aligned} \tag{8.2.7}$$

$$\begin{aligned}
\tilde{C}_1 &= ig_s^4 W_{4K} W_{4L} \left(\frac{11}{36} |R_{1r}|^2 |R_{1q}|^2 \tilde{I}_4 + \frac{1}{9} M_r M_q R_{1r}^2 R_{1q}^{*2} I_4 \right) W_{K5}^\dagger W_{L5}^\dagger \,, \\
\tilde{C}_2 &= ig_s^4 \frac{17}{18} W_{1K} W_{1L} I_4 W_{K5}^\dagger W_{L5}^\dagger \, M_r M_q R_{1r}^{*2} R_{1q}^{*2} \,, \\
\tilde{C}_3 &= -ig_s^4 \frac{1}{6} W_{1K} W_{1L} I_4 W_{K5}^\dagger W_{L5}^\dagger \, M_r M_q R_{1r}^{*2} R_{1q}^{*2} \,.
\end{aligned} \tag{8.2.8}$$

where summation over $r, q = 1, 2$ and $K, L = 1, \ldots, 6$ is implied and the Feynman integrals $I_4 = I_4(M_r^2, M_q^2, m_K^2, m_L^2)$, $\tilde{I}_4 = \tilde{I}_4(M_r^2, M_q^2, m_K^2, m_L^2)$ are given by the expressions

$$\begin{aligned}
I_n(m_1^2, ..., m_{n-1}^2, m_n^2) &\equiv \int \frac{d^4p}{(2\pi)^4} \frac{1}{(p^2 - m_1^2)(p^2 - m_2^2)...(p^2 - m_{n-1}^2)(p^2 - m_n^2)} \\
&\equiv \frac{i}{16\pi^2 m_n^{2n-4}} f_n(x_1, x_2, ..., x_{n-1}) \\
\tilde{I}_n(m_1^2, ..., m_{n-1}^2, m_n^2) &\equiv \int \frac{d^4p}{(2\pi)^4} \frac{p^2}{(p^2 - m_1^2)(p^2 - m_2^2)...(p^2 - m_{n-1}^2)(p^2 - m_n^2)} \\
&\equiv \frac{i}{16\pi^2 m_n^{2n-6}} \tilde{f}_n(x_1, x_2, ..., x_{n-1})
\end{aligned}$$

with $x_i \equiv \frac{m_i^2}{m_n^2}$. Convenient expressions of the latters can be found in the appendix of [296]. The quantities W_{IJ} are the components of the unitary matrix that diagonalizes the down squark mass-squared matrix $m_{\tilde{d}}^2$ in a basis where the down quark mass matrix is diagonal. Matrix W is given in terms of the squark diagonalizing matrix Z and the quark diagonalizing matrices V_L, V_R by

$$W = \begin{pmatrix} V_L^\dagger Z_{LL} & V_L^\dagger Z_{LR} \\ V_R^\dagger Z_{RL} & V_R^\dagger Z_{RR} \end{pmatrix} . \tag{8.2.9}$$

In the simple case that the mass of the gaugino is Dirac-type ($M = M_\chi = 0$), we obtain $M_1 = M_2 = m_D$, $R_{11} = -iR_{12} = \frac{1}{\sqrt{2}}$, so that $\sum |R_{1r}|^2 |R_{1q}|^2 \tilde{I}_4 = \tilde{I}_4$ and $\sum M_r M_q R_{1r}^{*2} R_{1q}^2 I_4 =$

$\sum M_r M_q R_{1r}^2 R_{1q}^2 I_4 = \sum M_r M_q R_{1r}^{*2} R_{1q}^{*2} I_4 = 0$. The effective coefficients simplify to

$$\begin{aligned}
C_1 &= ig_s^4 \frac{11}{36} W_{1K} W_{1L} \tilde{I}_4 W_{K2}^\dagger W_{L2}^\dagger \,, \quad C_2 = 0 \,, \quad C_3 = 0 \,, \\
C_4 &= -ig_s^4 \frac{1}{3} W_{1K} W_{4L} \tilde{I}_4 W_{K2}^\dagger W_{L5}^\dagger - ig_s^4 \frac{11}{18} W_{1K} W_{4L} \tilde{I}_4 W_{K5}^\dagger W_{L2}^\dagger \,, \\
C_5 &= ig_s^4 \frac{5}{9} W_{1K} W_{4L} \tilde{I}_4 W_{K2}^\dagger W_{L5}^\dagger - ig_s^4 \frac{5}{6} W_{1K} W_{4L} \tilde{I}_4 W_{K5}^\dagger W_{L2}^\dagger \,, \\
\tilde{C}_1 &= ig_s^4 \frac{11}{36} W_{4K} W_{4L} \tilde{I}_4 W_{K5}^\dagger W_{L5}^\dagger \,, \quad \tilde{C}_2 = 0 \,, \quad \tilde{C}_3 = 0 \,,
\end{aligned} \tag{8.2.10}$$

The derivation of the effective action for the mixing between the other neutral mesons is the same as above. Therefore, the corresponding effective actions are given by simple substitution in the K, L indices of the W components :

$$\begin{aligned}
\mathcal{H}_{B_d} &= \mathcal{H}_K(s \to b, 2 \to 3, 5 \to 6) \,, \\
\mathcal{H}_{B_s} &= \mathcal{H}_K(d \to s, s \to b, 1 \to 2, 2 \to 3, 4 \to 5, 5 \to 6) \,, \\
\mathcal{H}_{D^0} &= \mathcal{H}_K(d \to u, s \to c, W \to W^u) \,.
\end{aligned} \tag{8.2.11}$$

8.2.2 Flavour-violation observables

We have seen in the previous section how one can parametrize the Kaons oscillation in terms of 8 operators that we have made explicit, as functions of Feynman integrals I_4, $\tilde{I}_4$, the rotation matrix R and the matrix W containing the information relative to diagonalization of the quarks and squarks mass matrices. We will now see how such parametrization can be constrained, using it to express observable quantities, that are to be directly constrained by experiment.

Flavour violation in the Kaon mixing system is typically parametrised by the real and imaginary part of the mixing amplitude. These two are related to the mass difference between K_L and K_S and the CP violating parameter as

$$\Delta m_K = 2\mathrm{Re}\langle K^0 | \mathcal{H}_K | \overline{K}^0 \rangle \,, \quad |\epsilon_K| = \left| \frac{\mathrm{Im}\langle K^0 | \mathcal{H}_K | \overline{K}^0 \rangle}{\sqrt{2} \Delta m_K} \right| \,, \tag{8.2.12}$$

which have both been experimentally measured with great accuracy [297]. Their size sets strict bounds on the amount of flavour violation allowed by new physics. In order to compute these observables we need to extract the hadronic matrix elements of the operators in (8.2.5). They are first derived in the Vacuum Saturation Approximation (VSA),

$$\begin{aligned}
\langle K^0 | Q_1 | \overline{K}^0 \rangle_{VSA} &= \frac{1}{3} m_K f_K^2 \,, \\
\langle K^0 | Q_2 | \overline{K}^0 \rangle_{VSA} &= -\frac{5}{24} \left(\frac{m_K}{m_s + m_d} \right)^2 m_K f_K^2 \,, \\
\langle K^0 | Q_3 | \overline{K}^0 \rangle_{VSA} &= \frac{1}{24} \left(\frac{m_K}{m_s + m_d} \right)^2 m_K f_K^2 \,, \\
\langle K^0 | Q_4 | \overline{K}^0 \rangle_{VSA} &= \left[\frac{1}{24} + \frac{1}{4} \left(\frac{m_K}{m_s + m_d} \right)^2 \right] m_K f_K^2 \,, \\
\langle K^0 | Q_5 | \overline{K}^0 \rangle_{VSA} &= \left[\frac{1}{8} + \frac{1}{12} \left(\frac{m_K}{m_s + m_d} \right)^2 \right] m_K f_K^2 \,.
\end{aligned} \tag{8.2.13}$$

Since only strong interactions are involved, we get identical expressions for the 'R-projection' version of the first three operators. The ratio of the exact over the VSA result for each of the five operators above is parametrized by the "bag" factors B_i, $i = 1, ..., 5$ (see later on, Tab. 8.3), that are typically extracted by numerical techniques. In comparing with the SM contribution, the usual parametrization used is

$$\frac{\mathrm{Re}\langle K^0|\mathcal{H}_K|\overline{K}^0\rangle}{\mathrm{Re}\langle K^0|\mathcal{H}_K^{SM}|\overline{K}^0\rangle} = C_{\Delta m_K}\,, \quad \frac{\mathrm{Im}\langle K^0|\mathcal{H}_K|\overline{K}^0\rangle}{\mathrm{Im}\langle K^0|\mathcal{H}_K^{SM}|\overline{K}^0\rangle} = C_{\epsilon_K}\,. \tag{8.2.14}$$

8.2.3 Flavour patterns

Now that we have specified our choice of parametrization and observables, as well as how to extract constraints on results obtained in the vacuum saturation approximation from general experimental measurement, one should find a way to express the hamiltonian in a simplified way in order to be able to conclude in some clear constraints on the model parameters. In order to do so, one may specify a particular choice of flavour pattern, in order to get rather simple expression of the factors from their general expression (8.2.7).

The stringent experimental bounds on flavour violation processes require that contributions from extensions of the Standard Model be highly suppressed. This is typically achieved by employing particular patterns for the flavour structure of the BSM theory. In the following we describe how flavour violation is parametrized along the study of different flavour patterns.

Degeneracy - mass insertion approximation

One way to suppress flavour violation is to assume that the masses of the squarks are almost degenerate,

$$m_I^2 = m_{\tilde{q}}^2 + \delta m_I^2\,, \tag{8.2.15}$$

where m_I^2 are the squark mass eigenvalues and δm_I^2 are small enough deviations from an "average" squark mass-squared $m_{\tilde{q}}^2$, $I = 1, ..., 6$. Expansion of the loop integrals in δm_I^2 and use of the unitarity of the W matrices delivers (for $I \neq J$, $L \neq N$)

$$W_{IK}W_{LM}I_4(m_K^2, m_M^2)W_{KJ}^\dagger W_{MN}^\dagger = m_{IJ}^2 m_{LN}^2 I_6(m_{\tilde{q}}^2, m_{\tilde{q}}^2, m_{\tilde{q}}^2, m_{\tilde{q}}^2) + ... \tag{8.2.16}$$

where m^2 is the squark squared mass matrix in the basis where the quark mass matrix is diagonal. Flavour violation in this scheme is parametrised by the small ratio of the off-diagonal elements m_{IJ}^2 over the average squark mass $\delta_{ij}^{L(R)L(R)} \equiv m_{\tilde{q}}^{-2} m^2_{i(i+3)\,j(j+3)}$.

Hierarchy

A slightly different notation is used in the case of hierarchical squark masses where the squarks of first and second generation are much heavier than those of the third so that their contribution to the box diagrams is negligible. Further below we will consider such flavour patterns, in the simpler case of absent left-right mixing. In this case, one can parametrize flavour violation processes by $\hat{\delta}_{ij}^L \equiv W_{i3}^L W_{3j}^{L\dagger}$, $\hat{\delta}_{ij}^R \equiv W_{i3}^R W_{3j}^{R\dagger}$, where W_{ij}^L and W_{ij}^R are the block diagonal matrices of (8.2.9). The reasoning behind this choice can be illustrated by the following example [303]. Let us assume that $\tilde{b}_L$ is much lighter than the other squarks. Then

$$W_{1K}W_{1L}I_4(m_K^2, m_L^2)W_{K2}^\dagger W_{L2}^\dagger \;\simeq\; (\hat{\delta}_{12}^L)^2\, I_4(m_{\tilde{b}_L}^2, m_{\tilde{b}_L}^2) \quad \text{where } (\hat{\delta}_{12}^L) = W_{13}^L W_{32}^{L\dagger}\,. \tag{8.2.17}$$

Alignment

An alternative to degeneracy or hierarchy for the suppression of flavour violating processes is to consider that the squark mass-squared matrix is simultaneously diagonalised with the quark mass matrix [304]. In this "alignment" flavour pattern, the suppression appears because $W^L_{ij} = V^{L\,\dagger}_{ik} Z^{LL}_{kj} \sim \delta_{ij}$ and $W^R_{ij} = V^{R\,\dagger}_{ik} Z^{RR}_{kj} \sim \delta_{ij}$. In this framework, we can take the squark masses to be of the same order $m_{\tilde{q}}$ but not degenerate. If we ignore left-right mixing, we obtain eg. for the left sector

$$W^L_{1i} W^L_{1j} I_4(m_i^2, m_j^2) W^{L\dagger}_{i2} W^{L\dagger}_{j2} \simeq (\tilde{\delta}^L_{12})^2 I_4(m^2_{\tilde{q}}, m^2_{\tilde{q}}) \quad \text{where } \tilde{\delta}^L_{12} = \max_k (W^L_{1k} W^{L\dagger}_{k2}) \tag{8.2.18}$$

and similarly for $\tilde{\delta}^R_{12}$.

8.3 Bounds in the mass insertion approximation

Now that we have set up the parametrization of the different observables and specify the possible flavour patterns, we will for a while concetrate on the case of near degenerate squarks, namely what we called the *mass insertion approximation*. In the following we present the bounds for representative points in the gluino parameter space (M, m_D, M_χ). Hierarchical and alignment flavour patterns will be discussed in section 8.4.

In the mass insertion approximation, coefficients (8.2.7) and (8.2.8) of the general effective action for the Kaon mixing system become

$$\begin{aligned}
C_1 &= -\frac{\alpha_s^2}{m^2_{\tilde{q}}} \left(\frac{11}{36} |R_{1r}|^2 |R_{1q}|^2 \tilde{f}_6 + \frac{1}{9} \sqrt{x_r x_q} R^{*2}_{1r} R^2_{1q} f_6 \right) (\delta^{LL}_{12})^2 \,, \\
C_2 &= -\frac{17}{18} \frac{\alpha_s^2}{m^2_{\tilde{q}}} \sqrt{x_r x_q} R^2_{1r} R^2_{1q} f_6 (\delta^{RL}_{12})^2 \,, \quad C_3 = \frac{1}{6} \frac{\alpha_s^2}{m^2_{\tilde{q}}} \sqrt{x_r x_q} R^2_{1r} R^2_{1q} f_6 (\delta^{RL}_{12})^2 \,, \\
C_4 &= -\frac{\alpha_s^2}{m^2_{\tilde{q}}} \Big[\Big(\frac{7}{3} \sqrt{x_r x_q} R^{*2}_{1r} R^2_{1q} f_6 - \frac{1}{3} |R_{1r}|^2 |R_{1q}|^2 \tilde{f}_6 \Big) \delta^{LL}_{12} \delta^{RR}_{12} - \frac{11}{18} |R_{1r}|^2 |R_{1q}|^2 \tilde{f}_6 \, \delta^{LR}_{12} \delta^{RL}_{12} \Big] \,, \\
C_5 &= -\frac{\alpha_s^2}{m^2_{\tilde{q}}} \Big[\Big(\frac{1}{9} \sqrt{x_r x_q} R^{*2}_{1r} R^2_{1q} f_6 + \frac{5}{9} |R_{1r}|^2 |R_{1q}|^2 \tilde{f}_6 \Big) \delta^{LL}_{12} \delta^{RR}_{12} - \frac{5}{6} |R_{1r}|^2 |R_{1q}|^2 \tilde{f}_6 \, \delta^{LR}_{12} \delta^{RL}_{12} \Big] \,, \\
\tilde{C}_1 &= -\frac{\alpha_s^2}{m^2_{\tilde{q}}} \left(\frac{11}{36} |R_{1r}|^2 |R_{1q}|^2 \tilde{f}_6 + \frac{1}{9} \sqrt{x_r x_q} R^2_{1r} R^{*2}_{1q} f_6 \right) (\delta^{RR}_{12})^2 \,, \\
\tilde{C}_2 &= -\frac{17}{18} \frac{\alpha_s^2}{m^2_{\tilde{q}}} \sqrt{x_r x_q} R^{*2}_{1r} R^{*2}_{1q} f_6 (\delta^{LR}_{12})^2 \,, \quad \tilde{C}_3 = \frac{1}{6} \frac{\alpha_s^2}{m^2_{\tilde{q}}} \sqrt{x_r x_q} R^{*2}_{1r} R^{*2}_{1q} f_6 (\delta^{LR}_{12})^2 \,.
\end{aligned} \tag{8.3.1}$$

In the expressions above, $x_k = M_k^2/m^2_{\tilde{q}}$ with M_k the gluino mass eigenstate and we have introduced for notation convenience, the definitions

$$\begin{aligned}
I_6(M_r^2, M_q^2, m^2_{\tilde{q}}, m^2_{\tilde{q}}, m^2_{\tilde{q}}, m^2_{\tilde{q}}) &= \frac{i}{16\pi^2 m^8_{\tilde{q}}} f_6(x_r, x_q, 1, 1, 1) = \frac{i f_6}{16\pi^2 m^8_{\tilde{q}}} \,, \\
\tilde{I}_6(M_r^2, M_q^2, m^2_{\tilde{q}}, m^2_{\tilde{q}}, m^2_{\tilde{q}}, m^2_{\tilde{q}}) &= \frac{i}{16\pi^2 m^6_{\tilde{q}}} \tilde{f}_6(x_r, x_q, 1, 1, 1) = \frac{i \tilde{f}_6}{16\pi^2 m^6_{\tilde{q}}} \,.
\end{aligned} \tag{8.3.2}$$

The bounds on $d \leftrightarrow s$ transitions from the Kaon system are proven to be the most restrictive and therefore we will focus on them, but a discussion about the comparison of bounds coming from other mesons can be found in the appendix C of [296]. We allow the SUSY contribution to Δm_K to be as large as the experimental bound; however, the contribution to ϵ_K is restricted by the SM calculation [298]. Our analysis takes into account NLO corrections to the effective Hamiltonian [305]; as for the parameter inputs, they can be found in Tab. 8.3 as well as the bag factors (see section 8.3) used for exploiting constraints on exact results by the use of calculations in the vacuum saturation approximation.

Parameter	Value	Ref.
$\alpha_s(M_Z)$	0.1184	[297]
f_K	0.1598 GeV	[297]
m_K	0.497672 GeV	[297]
$m_s(2\,\text{GeV})$	0.095 GeV	[297]
$m_d(2\,\text{GeV})$	0.0048 GeV	[297]
Δm_K^{exp}	$(3.484 \pm 0.006) \times 10^{-15}$ GeV	[297]
$\lvert\epsilon_K^{\text{exp}}\rvert$	$(2.228 \pm 0.011) \times 10^{-3}$	[297]
$\lvert\epsilon_K^{\text{SM}}\rvert$	$(2.04 \pm 0.19) \times 10^{-3}$	[298]

Parameter	Value
B_1	0.60
B_2	0.66
B_3	1.05
B_4	1.03
B_5	0.73

Table 8.3: Input used for Kaon bounds bag numbers [306].

8.3.1 Majorana gluino

In tables 8.4 and 8.5, we update the bounds on flavour violation parameters for the MSSM with a Majorana gluino, for an average gluino mass of 1.5 TeV and 2 TeV. Non vanishing $\delta^{L(R)L(R)}$ parameters are set for simplicity to a common value δ whose value saturating the 2σ deviation in ϵ_K^{SM} are indicated in the tables. The results turn out to be identical for $\text{Re}(\delta^2)$ and $c^2\text{Im}(\delta^2)$, with a coefficient of order $c \simeq 25$. As seen in the tables, the $K - \overline{K}$ system sets powerful constraints on the size of flavour violation.

$m_{\tilde{q}}$ [GeV]	$\delta^{LL} \neq 0$	$\delta^{LL} = \delta^{RR} \neq 0$	$\delta^{LR} = \delta^{RL} \neq 0$
750	0.211	0.002	0.004
1500	0.180	0.002	0.014
2000	0.157	0.003	0.008

Table 8.4: Majorana gluino bounds for $M_{\tilde{g}} = 1500\,\text{GeV}$. By δ^{AB} we denote $\sqrt{|\text{Re}\,(\delta_{12}^{AB})^2|}$ and $c\sqrt{|\text{Im}\,(\delta_{12}^{AB})^2|}$.

$m_{\tilde{q}}$ [GeV]	$\delta^{LL} \neq 0$	$\delta^{LL} = \delta^{RR} \neq 0$	$\delta^{LR} = \delta^{RL} \neq 0$
750	0.192	0.002	0.005
1500	0.374	0.003	0.011
2000	0.240	0.003	0.019

Table 8.5: Majorana gluino bounds for $M_{\tilde{g}} = 2000\,\text{GeV}$. By δ^{AB} we denote $\sqrt{|\text{Re}\,(\delta^{AB}_{12})^2|}$ and $c\sqrt{|\text{Im}\,(\delta^{AB}_{12})^2|}$.

8.3.2 Dirac gluino

As we have already mentioned, flavour violation for quasi-degenerate squarks is suppressed if the gluino is of Dirac type, especially in the large gluino mass limit. This is true both because of the absence of the chirality-flip processes and because we are allowed to increase a Dirac gluino mass over the squark masses without affecting naturalness as much as in the Majorana case. These properties lead to a significant relaxation of the bounds from Δm_K and ϵ_K, as seen in figure 3 for representative values of δ^{AB}.

However, despite the order of magnitude (or better) improvement over the Majorana case, the bounds on ϵ_K still require a relatively high flavour degeneracy or that the flavour violating masses in the squark matrix are almost real. For example, for a 6 TeV gluino and average squark mass of 1 TeV, $\sqrt{|\text{Im}\,(\delta^{LL}_{12})^2|}$ can be as high as $\sim 1\%$.

In section 8.4 we will explore flavour bounds on models with Dirac gauginos beyond the mass insertion approximation. We will see that there exist flavour models where a Dirac gluino can satisfy even the ϵ_K bounds for reasonable values of gluino and squark masses. We will also notice that in many other flavour models, Dirac gauginos do not enjoy the suppression of flavour violation with respect to Majorana ones that is seen here.

8.3.3 Fake gluino

The mass terms of eq. 8.2.2 allow for non-standard gluinos, when all M, m_D and M_χ are non-zero. One such scenario is when $M \gg M_\chi, m_D$ and corresponds to the interesting case of a light gluino with a suppressed squark - quark vertex, which we call "fake gluino". In section 8.5 we explore this possibility in more detail.

In this limit we obtain more relaxed bounds on flavour violation parameters with respect to MSSM with Majorana gluino. In order to illustrate the point, we consider

$$m_D = M_\chi = M/10\,. \tag{8.3.3}$$

Even for an order of magnitude difference between M and m_D, M_χ, we obtain no restrictions for the size of flavour violation from effective operator Q_1, where $\delta^{LL} \neq 0$, $\delta^{RR} = \delta^{LR} = \delta^{RL} = 0$. For other combinations, we obtain results given in tables 8.6 and 8.7.

In this case, the quark/squark coupling of the fake gluino is suppressed with respect to the standard one by $R_{12} \sim \frac{m_D}{M} = 0.1$ as can be seen in eq. (8.2.4). So if the contribution to the box diagram is dominated by the lighest eigenstate, we should expect the box diagram to be

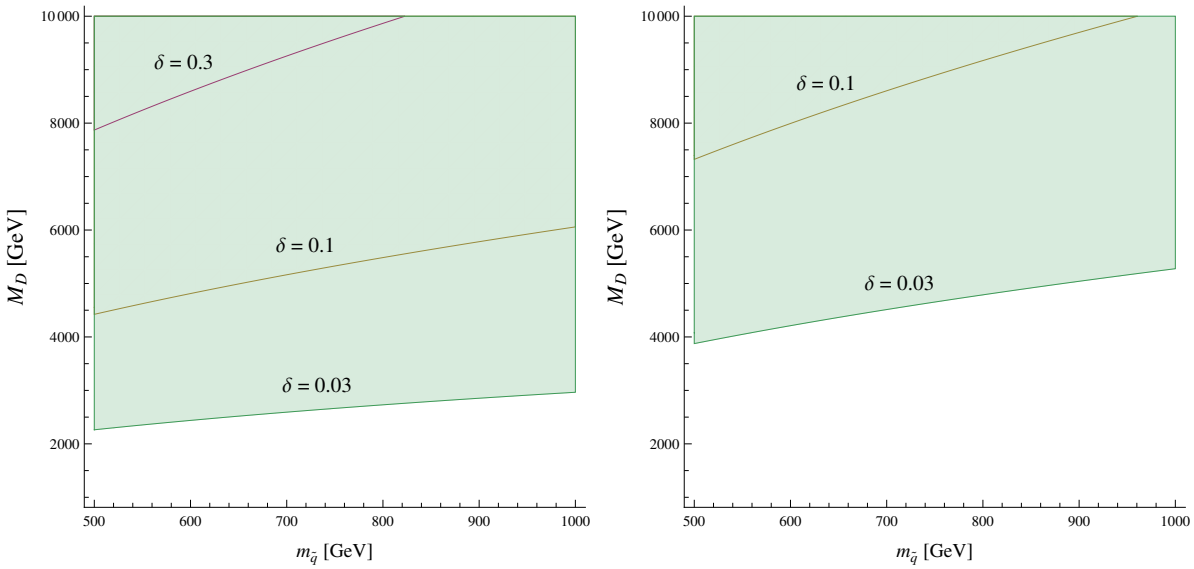

Figure 3: Contour plots in parameter space $m_{\tilde{q}}$ - m_D for purely Dirac gluino ($M = M_\chi = 0$). Left: $\delta^{LL} = \delta^{RR} = \delta$, $\delta^{LR} = \delta^{RL} = 0$. Right: $\delta^{LL} = \delta^{RR} = \delta^{LR} = \delta^{RL} = \delta$. Along the contours $\Delta m_K = \Delta m_K^{\rm exp}$ (for $\delta^{AB} = \sqrt{|{\rm Re}\,(\delta_{12}^{AB})^2|}$) and $\epsilon_K = \epsilon_K^{\rm exp}$ (for $\delta^{AB} = c\sqrt{|{\rm Im}\,(\delta_{12}^{AB})^2|}$).

$m_{\tilde{q}}$ [GeV]	$\delta^{LL} = \delta^{RR} \neq 0$	$\delta^{LR} = \delta^{RL} \neq 0$
750	0.013	0.028
1500	0.014	0.029
2000	0.014	0.030

Table 8.6: "Fake" gluino bounds for $M_{\tilde{g}} = 1500\,{\rm GeV}$. By δ^{AB} we denote $\sqrt{|{\rm Re}\,(\delta_{12}^{AB})^2|}$ and $c\sqrt{|{\rm Im}\,(\delta_{12}^{AB})^2|}$.

$m_{\tilde{q}}$ [GeV]	$\delta^{LL} = \delta^{RR} \neq 0$	$\delta^{LR} = \delta^{RL} \neq 0$
750	0.017	0.037
1500	0.018	0.038
2000	0.018	0.039

Table 8.7: "Fake" gluino bounds for $M_{\tilde{g}} = 2000\,{\rm GeV}$. By δ^{AB} we denote $\sqrt{|{\rm Re}\,(\delta_{12}^{AB})^2|}$ and $c\sqrt{|{\rm Im}\,(\delta_{12}^{AB})^2|}$.

suppressed by R_{12}^4 for the same lightest gluino mass, leading to bounds reduced by $R_{12}^2 \sim 0.01$. However, we observe from the bounds in tables 8.6 and 8.7 that the suppression is much less dramatic, of the order 0.1. The reason is that it is not the light but actually the *heavy* eigenstate that dominates the box integral!

This can be seen by comparing, for example, the loop integral contribution from the chirality-flip process

$$\sqrt{x_r x_q} R_{1r}^{*2} R_{1q}^2 f_6(x_r, x_q) \simeq x_1 f_6(x_1, x_1) + x_2 \left(\frac{x_2}{x_1}\right)^2 f_6(x_2, x_2) + 2\sqrt{x_1 x_2} \left(\frac{x_2}{x_1}\right) f_6(x_1, x_2)\,. \tag{8.3.4}$$

In the approximation mentioned above where, denoting by x the quantity $x \equiv M_{\tilde{g}}^2/m_{\tilde{q}}^2$, we get the hierarchy

$$\begin{aligned} x_2 &\simeq x\,, \\ x_1 &\simeq 100x\,, \end{aligned} \tag{8.3.5}$$

and one can introduce the dimensionless parameter

$$y \equiv \frac{x_2}{x_1} \ll 1\,. \tag{8.3.6}$$

In this case the chirality-flip process becomes

$$\sqrt{x_r x_q} R_{1r}^{*2} R_{1q}^2 f_6(x_r, x_q) \simeq \frac{x}{y} f_6(x/y, x/y) + x y^2 f_6(x, x) + 2xy\sqrt{y} f_6(x/y, x)\,, \tag{8.3.7}$$

where we have replaced $R_{11} \simeq 1$, $R_{12}^2 \simeq \frac{x_2}{x_1}$. Since $f_6(x/y, x) \sim y^2 \log y$, $f_6(x/y, x/y) \sim \frac{y^2}{6x^2}$, the dominant contribution comes from the heavy gluino term $x_1 f_6(x_1, x_1)$ and is given by

$$\sqrt{x_r x_q} R_{1r}^{*2} R_{1q}^2 f_6(x_r, x_q) \simeq \frac{1}{6x} \frac{M_D^2}{M^2}\,. \tag{8.3.8}$$

The parametric scaling of the *bound* on δ^{AB} is then

$$\frac{|\delta^{AB}_{\text{Majorana}}|}{|\delta^{AB}_{\text{fake gluino}}|} \sim \frac{M}{m_D} \tag{8.3.9}$$

which is much less than the naive scaling of $\frac{M^2}{m_D^2}$.

8.4 Beyond the mass insertion approximation

Having established in the previous section that the bounds from ϵ_K do not allow flavour-generic models at LHC-accesible energies even in the case of Dirac gaugino masses, we are led to the conclusion that it is likely that we either require an accidental suppression of the mixing between the first two generations or we must impose some additional structure on the squark mass matrices. It is therefore important to consider flavour models. However, in doing so we invariably find that the mass insertion approximation is no longer valid: in fact, it is hard to

find *any* models in which it would actually apply. Hence, in this section we shall investigate the consequences - and the general bounds - when we go beyond the mass insertion approximation in the context of Dirac gauginos.

One of the most important things that we find in the general case is that the much-vaunted suppression of $\Delta F = 2$ FCNC processes is in general much less marked; in fact, for certain specific cases the Majorana case is actually less suppressed! We explain this in section 8.4.1. In the remainder of the section we then discuss specific flavour models to illustrate the different types of behaviour. We shall consider:

- The simple case of non-degenerate but same order of magnitude squark masses, where *alignment* applies.
- A simple flavour model realising such a spectrum.
- The general case of an inverted hierarchy between the first two squark generations and the third, à la reference [303]. In addition to changing the gluino masses to Dirac type, we will update the bounds with the latest flavour data and also take into account the LHC bounds on squark and gaugino masses.
- Models where in addition to the first two generations of squarks, the third generation of *right-handed* squarks is also heavy. These models provide a minimum of extra coloured particles available to the LHC.
- A flavour model realising the above, as given in [307] but with Dirac gaugino masses. This model highly restricts the allowed flavour violation by imposing additional symmetries upon the first two generations.

In the following, we ignore left - right squark mixing and define $W^L_{ij} = W_{ij}$ and $W^R_{ij} = W_{i+3\,j+3}$ for $i, j \leqslant 3$. We also define

$$\tilde{f}^{AB} = W^A_{1i} W^B_{1j} \tilde{I}_4(m^2_D, m^2_{Ai}, m^2_{Bj}) W^{A\dagger}_{i2} W^{B\dagger}_{j2}\,, \tag{8.4.1}$$

where $A = L, R$. Then the effective action (8.2.5) can be written as

$$\mathcal{H}^{Dirac}_K = C_1 Q_1 + \tilde{C}_1 \tilde{Q}_1 + C_4 Q_4 + C_5 Q_5 \tag{8.4.2}$$

where the Dirac coefficients (8.2.10) are written as

$$C_1 = \frac{11}{36} i g_s^4 \tilde{f}^{LL}\,, \quad \tilde{C}_1 = \frac{11}{36} i g_s^4 \tilde{f}^{RR}\,, \quad C_4 = -\frac{1}{3} i g_s^4 \tilde{f}^{LR}\,, \quad C_5 = \frac{5}{9} i g_s^4 \tilde{f}^{LR} \tag{8.4.3}$$

8.4.1 Dirac versus Majorana

In reference [253], it was argued that the absence of chirality-flip processes in the case of Dirac gluinos leads to a suppression in the contribution to the box diagram by a factor $x \equiv M^2_{\tilde{g}}/m^2_{\tilde{q}}$ as the Dirac mass becomes larger than the squark masses. In the following we show that this is generally not true beyond mass insertion approximation and even when it is, the flavour bounds are often relaxed by a factor of few rather than being parametrically reduced.

This can be immediately seen by taking the large x limit in the loop functions that appear in the coefficients (8.2.7) of the general expression (8.2.5) for $\Delta F = 2$ FCNC processes. Taking for simplicity equal masses $m_{\tilde{q}}$ for the squarks in the loop, these functions are (see appendix A.3 of [296]):

$$M_{\tilde{g}}^2 I_4(M_{\tilde{g}}^2, M_{\tilde{g}}^2, m_{\tilde{q}}^2, m_{\tilde{q}}^2) \equiv \frac{i}{16\pi^2 m_{\tilde{q}}^2} x f_4(x) = \frac{i}{16\pi^2 m_{\tilde{q}}^2}\left[\frac{2x(x-1) - x(x+1)\ln(x)}{(1-x)^3}\right],$$
$$\tilde{I}_4(M_{\tilde{g}}^2, M_{\tilde{g}}^2, m_{\tilde{q}}^2, m_{\tilde{q}}^2) \equiv \frac{i}{16\pi^2 m_{\tilde{q}}^2} \tilde{f}_4(x) = \frac{i}{16\pi^2 m_{\tilde{q}}^2}\left[\frac{x^2 - 2x\ln(x) - 1}{(1-x)^3}\right]. \tag{8.4.4}$$

Function $\tilde{f}_4(x)$ appears in both Dirac and Majorana cases while $x f_4(x)$ appears only in the Majorana case, corresponding to the chirality-flip process. Notice that $x f_4(x)$ is always positive, and $\tilde{f}_4(x)$ always negative; moreover they have broadly similar values except near $x = 0$; for example $f_4(1) = 1/6, \tilde{f}_4(1) = -1/3$. As $x \to \infty$ the ratio between them tends to $-\ln(x) + 2$, which is not the aforementioned enhancement by a factor of x.

This can be understood in the following way. Following the reasoning of [253], integrating out the heavy gluino generates effective operators

$$\frac{1}{M_{\tilde{g}}} \tilde{d}_R^* \tilde{s}_L^* \overline{d}_R s_L\,, \qquad \frac{1}{M_{\tilde{g}}^2} \tilde{d}_L \partial_\mu \tilde{s}_L^* \overline{d}_L \gamma^\mu s_L\,, \tag{8.4.5}$$

the first of these being the chirality-flip process forbidden in the Dirac case. In the mass insertion approximation, the flavour changing loop diagram is then as in figure 4(a) and gives (Q_i refers to the four-fermion effective operators of sec. 8.2)

$$\mathcal{L}_{eff} \supset Q_i \frac{(m_{12}^2)^2}{M_{\tilde{g}}^2} \int d^4q \frac{1}{(q^2 - m_{\tilde{q}}^2)^4} \sim Q_i \frac{\delta_{12}^2}{M_{\tilde{g}}^2} \tag{8.4.6}$$

for the chirality-flip case and

$$\mathcal{L}_{eff} \supset Q_i \frac{(m_{12}^2)^2}{M_{\tilde{g}}^4} \int d^4q \frac{q^2}{(q^2 - m_{\tilde{q}}^2)^4} \sim Q_i \frac{m_{\tilde{q}}^2}{M_{\tilde{g}}^4} \delta_{12}^2 \tag{8.4.7}$$

in the same chirality case, in line with the claim in [253]. The insertion of operators of the form $m_{12}^2 \tilde{q}_1^* \tilde{q}_2$ as effective vertices is of course only valid in the limit $m_{12}^2 \ll m_{\tilde{q}}^2$; however, as we shall see below in section 8.4.2, the above behaviour of the integrands can also arise in certain cases beyond mass insertion approximation, where there is approximate unitarity of a submatrix of the squark rotations leading to cancellations between diagrams. However, in all other cases we instead have diagrams like that of figure 4(b), which gives

$$\mathcal{L}_{eff} \supset Q_i \frac{W_{12}^2}{M_{\tilde{g}}^2} \int^{M_{\tilde{g}}} d^4q \frac{1}{(q^2 - m_{\tilde{q}}^2)^2} \sim Q_i \frac{W_{12}^2}{M_{\tilde{g}}^2} \ln \frac{M_{\tilde{g}}^2}{m_{\tilde{q}}^2} \tag{8.4.8}$$

in the chirality-flip case and

$$\mathcal{L}_{eff} \supset Q_i \frac{W_{12}^2}{M_{\tilde{g}}^4} \int^{M_{\tilde{g}}} d^4q \frac{q^2}{(q^2 - m_{\tilde{q}}^2)^2} \sim Q_i \frac{W_{12}^2}{M_{\tilde{g}}^2} \tag{8.4.9}$$

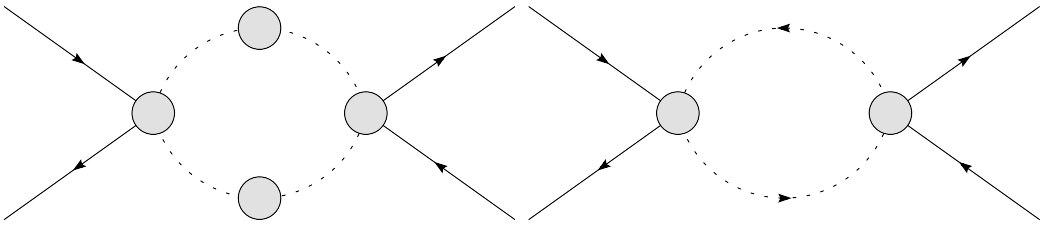

Figure 4: Loop diagrams in the effective theory where the gaugino has been integrated out. In figure (a) the mass insertions are shown, whereas in figure (b) the mass-insertion approximation is inappropriate.

in the same chirality case, where we needed to use the cutoff of $M_{\tilde{g}}$ in the integrals[2]. This is exactly the behaviour that we find born out in the amplitudes and explains why in generic flavour models the Dirac case will not provide a parametric suppression of the flavour-changing bounds.

The logarithmic, instead of a linear suppression for the Dirac amplitude has then striking consequences. In the case that the contribution from same-chirality and chirality-flip amplitudes is comparable for reasonable values of x, the flavour bounds on Dirac gluinos can be proven more strict than those on Majorana, because in the latter there can exist cancellations between the same- and flipped- chirality amplitudes. Let us consider the impact that this has on bounds, by taking the ratio between the value of the Wilson coefficients C_i for purely Majorana gauginos C_i^M and for purely Dirac C_i^D. For a given contribution to the integrand (i.e. for the same values of K, L) in equation (8.2.7) and taking for simplicity equal masses for the squarks in the loop (while neglecting left-right mixing) we find:

$$\begin{aligned}
\frac{C_1^M}{C_1^D} =& 1 + \frac{4}{11}\frac{x f_4(x,x,1)}{\tilde{f}_4(x,x,1)} = -\frac{4}{11}\ln(x) + \frac{19}{11} + \mathcal{O}(x^{-1}\ln^2(x)),\\
\frac{C_4^M}{C_4^D} =& 7\ln(x) - 13 + \mathcal{O}(x^{-1}\ln^2(x)),\\
\frac{C_5^M}{C_5^D} =& -\frac{1}{5}\ln(x) + \frac{7}{5} + \mathcal{O}(x^{-1}\ln^2(x)).
\end{aligned} \tag{8.4.10}$$

For arbitrarily large values of x the Majorana case will have a larger contribution, but for reasonable values, up to $x = \mathcal{O}(100)$, only C_4 is actually enhanced compared to the Dirac case (for C_1 we would require gluinos about 40 times heavier than squarks to obtain a relative suppression).

Finally, we note that the cancellation between the amplitudes can also be relevant when the linear enhancement of the chirality-flip contribution applies, i.e. when f^{AB} and $\tilde{f}^{AB}$ are proportional to $\overset{(\sim)}{I}_6$. This is the case when squarks are quasi-degenerate but also in certain cases beyond the mass insertion approximation for very particular squark matrix configurations as

[2]Note that if we define $m^2_{\tilde{q}_K} = m^2_{\tilde{q}}(1+\delta_K)$, sum the integrals of the above form (8.4.8) and (8.4.9) over $W_{1K}W^*_{2K}W_{1L}W^*_{2L}$ we and expand to leading order in δ_K we recover (8.4.6) and (8.4.7).

we shall find below. In this case, for moderate values of x the cancellation plays a role:

$$\begin{aligned}
\frac{C_1^M}{C_1^D} &\to 1 + \frac{4}{11}\frac{x f_6(x,x,1)}{\tilde{f}_6(x,x,1)} = \frac{1}{11}(47 - 2x - 12\ln(x)) + \mathcal{O}(x^{-1}\ln^2(x)),\\
\frac{C_4^M}{C_4^D} &\to \frac{7x}{2} - 62 + 21\ln x + \mathcal{O}(x^{-1}\ln^2(x)),\\
\frac{C_5^M}{C_5^D} &\to \frac{1}{10}(28 - x - 6\ln x) + \mathcal{O}(x^{-1}\ln^2(x))
\end{aligned} \tag{8.4.11}$$

We observe that the Majorana contribution is smaller than the Dirac for $C_1(x \lesssim 5)$ and $C_5(x \lesssim 15)$ while the Dirac is only suppressed by a factor of 10 for $C_1(x \simeq 50)$ and $C_5(x \simeq 100)$.

8.4.2 Alignment

In the previous section we examined how flavour constraints in the mass insertion approximation are affected by a generalized gluino spectrum. However, flavour models often do not lead to a near degeneracy of the squarks' masses but to different flavour patterns such as alignment or hierarchy, as mentioned in section 8.2.3. Moreover, one expects non-degeneracy to arise from running: there will always be a split between at least the first two generations and the third due to the larger Yukawa couplings. It therefore makes sense to consider models that can suppress flavour constraints even without requiring degeneracy of the squarks' masses.

Alignment in the left sector

Alignment is typically obtained in flavour models of additional horizontal $U(1)$ symmetries [241, 241]. In a minimal representative of such models there is only one horizontal $U(1)$ symmetry, under which the quark superfields are charged with charges X as

$$X[Q_i] = (3,2,0)\,, \qquad X[\overline{U}_i] = (3,1,0)\,, \qquad X[\overline{D}_i] = (3,2,2)\,. \tag{8.4.12}$$

If we neglect D-term contributions to the squark masses, the order of magnitude structure of the squark mass matrices (before any quark rotations) is[3]

$$m^2_{\tilde{d}_L} \sim m_F^2 \begin{pmatrix} 1 & \epsilon & \epsilon^3 \\ \epsilon & 1 & \epsilon^2 \\ \epsilon^3 & \epsilon^2 & 1 \end{pmatrix}, \qquad m^2_{\tilde{d}_R} \sim m_F^2 \begin{pmatrix} 1 & \epsilon & \epsilon \\ \epsilon & 1 & 1 \\ \epsilon & 1 & 1 \end{pmatrix}, \tag{8.4.13}$$

where ϵ is a small number, the parameter of $U(1)$ symmetry breaking. Throughout this section, $\epsilon = \lambda$, where $\lambda \simeq 0.22$ is the Cabibbo angle. In this flavour model, the quark diagonalizing matrices have the same structure

$$V_L^d \sim \begin{pmatrix} 1 & \epsilon & \epsilon^3 \\ \epsilon & 1 & \epsilon^2 \\ \epsilon^3 & \epsilon^2 & 1 \end{pmatrix}, \qquad V_R^d \sim \begin{pmatrix} 1 & \epsilon & \epsilon \\ \epsilon & 1 & 1 \\ \epsilon & 1 & 1 \end{pmatrix}, \tag{8.4.14}$$

and the squark diagonalizing matrices (in the basis where the quarks are diagonal) are approximated by $W^L \sim V_L^{d\dagger}$ and $W^R \sim V_R^{d\dagger}$. Therefore, with this particular choice of $U(1)$ charges, the left-squarks sector exhibits alignment while the right-squarks sector does not.

[3] In all flavour abelian models in what follows, $\sim$ means order of magnitude only and not a precise number.

We can estimate flavour violation in Δm_K in the leading order in ϵ, by focusing on

$$\begin{aligned}\tilde{f}^{LR} &= \epsilon^2\Big[(m^2_{R1}-m^2_{R2})\left(\tilde{I}_5(m^2_{L1},m^2_{R1},m^2_{R2})-\tilde{I}_5(m^2_{L2},m^2_{R1},m^2_{R2})\right)\,,\\ &\quad +(m^2_{L2}-m^2_{L1})\tilde{I}_5(m^2_{L1},m^2_{L2},m^2_{R3})\Big]+\mathcal{O}(\epsilon^4)\;\sim\;\frac{i}{16\pi^2}\frac{\epsilon^2}{m^2_{\tilde{q}}}\tilde{f}_5(x)\,,\end{aligned} \tag{8.4.15}$$

$$\begin{aligned}\tilde{f}^{LL} &= \epsilon^2(m^2_{L1}-m^2_{L2})^2\tilde{I}_6(m^2_D,m^2_{L1},m^2_{L2})+\mathcal{O}(\epsilon^4)\;\sim\;\frac{i}{16\pi^2}\frac{\epsilon^2}{m^2_{\tilde{q}}}\tilde{f}_6(x)\,,\\ \tilde{f}^{RR} &= \epsilon^2\Big[\sum_i\tilde{I}_4(m^2_{Ri},m^2_{Ri})-2\tilde{I}_4(m^2_{R1},m^2_{R2})-2\tilde{I}_4(m^2_{R1},m^2_{R3})+2\tilde{I}_4(m^2_{R2},m^2_{R3})\Big]\\ &\quad+\mathcal{O}(\epsilon^4)\;\sim\;\frac{i}{16\pi^2}\frac{\epsilon^2}{m^2_{\tilde{q}}}\tilde{f}_4(x)\,,\end{aligned} \tag{8.4.16}$$

where $x = m_D^2/m_{\tilde{q}}^2$ and in approximating, we have required that all squark masses are of the same order $m_{\tilde{q}}$ but not degenerate. In the limit of Dirac gluinos much heavier than $m_{\tilde{q}}$ we obtain

$$\frac{\langle K^0|H_{eff}|\overline{K}^0\rangle}{\Delta m_K(\text{exp})}\simeq\left(\frac{\alpha_s}{0.1184}\right)^2\left(\frac{15\text{ TeV}}{m_D}\right)^2 e^{2i\phi_K}\,, \tag{8.4.17}$$

which is much too large: in order to meet the bounds from ϵ_K we would need $m_D \sim \mathcal{O}(100)$ TeV. Here, we might have expected Dirac gaugino masses to soften the bounds with respect to Majorana masses. However, this is not the case. Since the strongest constraint comes from operator $\tilde{Q}_1$, according to equation (8.4.10) we have a bound about 5 times *stronger* for Dirac masses than Majorana ones when $x = 100$.

Alignment in both left and right sectors

As we have seen above, since the constraints are severe for Kaon mixing, models that suppress the elements W_{12}^L and W_{12}^R are then most attractive (since $\tilde{f}^{AB}$ obtains largest contribution from $W_{11}^A W_{12}^{A\dagger} \sim W_{12}^A$ and $W_{21}^A W_{22}^{A\dagger} \sim W_{21}^A$). However, retrieving the correct form for the CKM matrix leads to large flavour rotation for the up-quark matrix. Therefore, apart from checking that B-meson constraints are satisfied, one must as well consider constraints from D-meson mixing.

Since both down and up squark sectors are involved in the following discussion, we restore the corresponding superscripts in the W matrices, so that $W_{ij}^{q_A}$ is the matrix that diagonalizes the A-handed squarks in the q-type sector, with $A = L, R$ and $q = u, d$.

Defining $\langle W_{ij}^q\rangle \equiv \sqrt{W_{ij}^{q_L}W_{i,j}^{q_R}}$ we can place approximate bounds in this framework

$$\begin{aligned}&W_{12}^{d_L}, W_{12}^{d_R} \lesssim 2\times10^{-3}\,, && \langle W_{12}^d\rangle \lesssim 4\times10^{-4}\,,\\ &W_{13}^{d_L}, W_{13}^{d_R} \lesssim 0.1\,, && \langle W_{13}^d\rangle \lesssim 0.2\,,\\ &W_{23}^{d_L}, W_{23}^{d_R} \lesssim 0.4\,, && \langle W_{23}^d\rangle \lesssim 0.5\,,\\ &W_{21}^{u_L}, W_{21}^{u_R} \lesssim 0.03\,, && \langle W_{21}^u\rangle \lesssim 0.04\,,\end{aligned} \tag{8.4.18}$$

where all of these should be multiplied by $\left(\frac{m_{\tilde{q}}}{2\text{ TeV}}\right)\sqrt{\left|\frac{1/3}{\tilde{f}_4(x)}\right|}$. The constraints[4] in the left column of (8.4.18) come from operators of the type $Q_1, \tilde{Q}_1$, whereas the ones in the right column come from Q_4, Q_5.

Of these bounds, it is the D-meson constraint that proves problematic for alignment models, as typically suppressing the W_{12}^d element will require $W_{21}^u \sim \lambda$. However, the problem is not particularly severe: it can either be remedied by having somewhat heavy first two generations, or by allowing a small degeneracy between the first two generations.

To explore this, consider as a representative example a model with two abelian symmetries $U(1)_1 \times U(1)_2$ under which the quark superfields have charges [241]

Q	$\overline{D}$	$\overline{U}$
$(3,0)$	$(-1,2)$	$(-1,2)$
$(0,1)$	$(4,-1)$	$(1,0)$
$(0,0)$	$(0,1)$	$(0,0)$

(8.4.19)

Other examples of models with alignment can be found eg in [308, 309]. The symmetry breaking parameters, coming from flavon fields of charges $(-1,0)$ and $(0,-1)$, are $\epsilon_1 \sim \lambda$ and $\epsilon_2 \sim \lambda^2$ respectively. The diagonalising matrices are given by

$$W_{ij}^{d_L} \sim \begin{pmatrix} 1 & \lambda^5 & \lambda^3 \\ \lambda^5 & 1 & \lambda^2 \\ \lambda^3 & \lambda^2 & 1 \end{pmatrix}, \qquad W_{ij}^{d_R} \sim \begin{pmatrix} 1 & \lambda^7 & \lambda^3 \\ \lambda^7 & 1 & \lambda^4 \\ \lambda^3 & \lambda^4 & 1 \end{pmatrix},$$
$$W_{ij}^{u_L} \sim \begin{pmatrix} 1 & \lambda & \lambda^3 \\ \lambda & 1 & \lambda^2 \\ \lambda^3 & \lambda^2 & 1 \end{pmatrix}, \qquad W_{ij}^{u_R} \sim \begin{pmatrix} 1 & \lambda^6 & \lambda^5 \\ \lambda^6 & 1 & \lambda \\ \lambda^5 & \lambda & 1 \end{pmatrix}, \tag{8.4.20}$$

which are generically challenged by the bounds given above via D-meson mixing. However, those bounds are derived under the assumption that the amplitude is well dominated by a single contribution. We find that, in practice, they are overly conservative. Indeed, in order for this to be the case there has to actually be a substantial hierarchy between the squark masses, and then since there is a minimum mass for the second generation via LHC bounds we will find that the model will be less constrained than feared. Considering this model, the constraint essentially comes from the Q_1 operator for D-meson mixing. Moreover, if we were to suppress the amplitude by $\mathcal{O}(\lambda^2)$ then we would easily meet the constraints; hence we must only suppress the leading order contribution in λ, which we find to be:

$$\begin{aligned} \tilde{f}^{LL} &= \lambda^2\left[\tilde{I}_4(m_{L1}^2, m_{L1}^2) + \tilde{I}_4(m_{L2}^2, m_{L2}^2) - 2\tilde{I}_4(m_{L1}^2, m_{L2}^2)\right] + \mathcal{O}(\lambda^4) \\ &= \lambda^2(m_{L1}^2 - m_{L2}^2)^2\tilde{I}_6(m_{L1}^2, m_{L2}^2) + \mathcal{O}(\lambda^4). \end{aligned} \tag{8.4.21}$$

Clearly if the first two generations are quasi-degenerate then this will vanish sufficiently to satisfy the constraints. Indeed, particular UV models could have them degenerate up to $\mathcal{O}(\lambda^2)$ [310, 311, 312, 313, 314, 315], which would give a much greater suppression of the FCNC

[4]These approximate bounds include bag factors but no NLO corrections (no magic numbers) (in plots we include all available data including magic numbers).

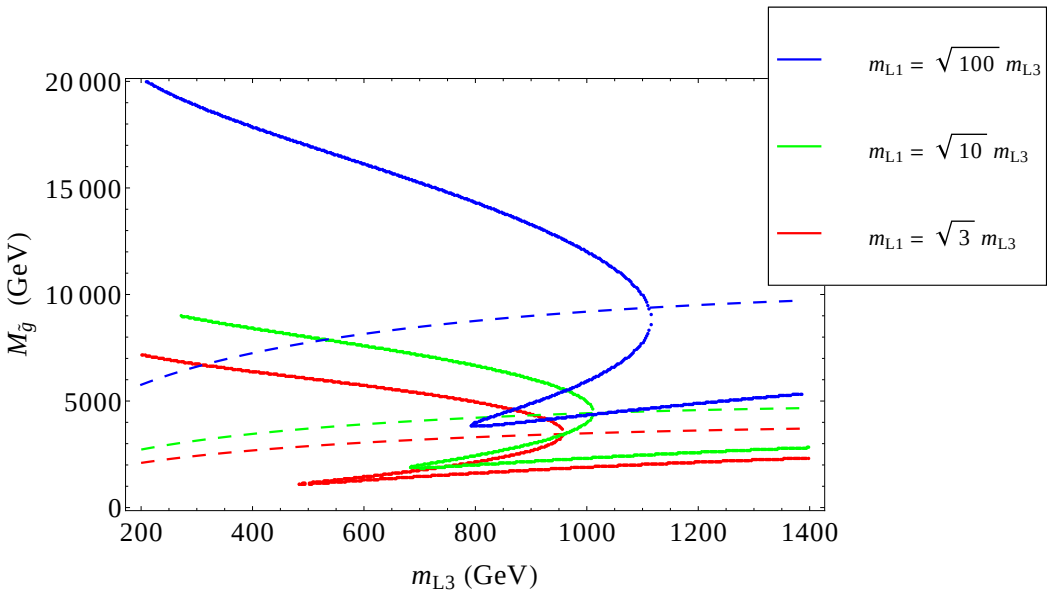

Figure 5: Constraints on the model described in section 8.4.2. The dashed lines correspond to exactly Dirac gauginos, while the solid lines are purely Majorana. We take the same hierarchies for up- and down-type squarks, with $m^2_{L1} = 1.5m^2_{L2} = 3m^2_{L3}$ for the red plots; $m^2_{L1} = 5m^2_{L2} = 10m^2_{L3}$ for the green curves and $m^2_{L1} = 25m^2_{L2} = 100m^2_{L3}$ for the blue.

processes than necessary to avoid current bounds. However, it is actually not necessary to have so much degeneracy; for example taking $m^2_{L1} = 3m^2_{L3}, m^2_{L2} = 2m^2_{L3}$ and taking $m_D = m_{L2}$ the amplitude is suppressed by a factor of 0.02 compared to simply taking $\tilde{f}_4(1)$, which is enough to satisfy the bounds for squark at gluino masses of $\mathcal{O}(2$ TeV).

To illustrate this, we show plots in figure 5 of the allowed lightest squark mass versus gaugino mass for this model with randomly chosen entries of the above form. In order to harden the bounds we must introduce a large hierarchy between the squark masses. We take three different hierarchies: $m^2_{L1} = 1.5m^2_{L2} = 3m^2_{L3}$, $m^2_{L1} = 5m^2_{L2} = 10m^2_{L3}$ and $m^2_{L1} = 25m^2_{L2} = 100m^2_{L3}$ (the same hierarchies for both up- and down-type squarks) and calculate the bounds showing the gluino mass against the *lightest* squark mass using NLO corrections and taking into account all $\Delta F = 2$ constraints. In practice, the D-meson constraint is dominant: we insist that $|\Delta m_{D^0}|$ is less than the experimental value of 7.754×10^{-15} GeV (since this is approximately three standard deviations from zero, and moreover the standard model value is known to much less accuracy).

The results of figure 5 agree with our discussion in the end of sec. 8.4.1. The cancellation between the chirality-flip and the same chirality process suppresses the contribution in the Majorana case for moderate x even if the enhancement over the Dirac case is linear in x. Since the flavour bounds for $m_{L3} \gtrsim 0.8 \div 1\,$TeV are obeyed already at low x, a Majorana gluino is less contrained than a Dirac one. Another feature of this model is that, due to the suppression in the unitary rotations, the main FCNC effects come from the first two generations, even if they are heavier than the third one. Hence, one should bear in mind that the relevant squark mass for the loop diagrams is heavier than the m_{L3} shown on the abscissa.

8.4.3 Inverted hierarchy

Decoupling the first two generations

A particularly attractive scenario in light of the strong LHC bounds on the first two generations of squarks and the desire for "natural supersymmetry" is to have an inverted hierarchy, where the first two generations of squarks are substantially heavier than the third. This can be simply accommodated in flavour models, as we shall discuss below.

One approach, following [303], is to decouple the first two generations. In this case, the effective action is given by (8.4.2) with $\tilde{f}^{AB}$ of (8.4.1) given by

$$\tilde{f}^{AB} = \hat{\delta}^A_{12}\,\hat{\delta}^B_{12}\,\tilde{I}_4(m^2_D, m^2_{A3}, m^2_{B3}) \tag{8.4.22}$$

in the inverted hierarchy limit, as we have described in sec. 8.2.3. Here m_{L3}, m_{R3} are the masses of the 'left-handed' and 'right-handed' sbottoms. The reader should be careful with the "hat" notation however: since $\hat{\delta}^A_{12} \equiv W^A_{13}\overline{W}^A_{23}$ we expect the $\hat{\delta}^A_{12}$ to be small, coming from two small rotations rather than (in the generic case) one - indeed if the rotations come from the squark mass-squared matrices $M^2_{A\,ij}$ themselves (rather than from quark rotations) so that $W^A_{13} \simeq -M^2_{A\,13}/m^2_{A1}$ then we expect $\hat{\delta}^A_{12} < m^2_{A3}/m^2_{A1}$.

For $m^2_D \gg m^2_{L3}, m^2_{R3}$ we find

$$\frac{\langle K^0|H_{eff}|\overline{K}^0\rangle}{\Delta m_K(\text{exp})} = 3\times 10^3 \times \left(\frac{\alpha_s}{0.1184}\right)^2 \left(\frac{2000\,\text{GeV}}{m_D}\right)^2 \left(0.3(\hat{\delta}^L_{12})^2 + 0.3(\hat{\delta}^R_{12})^2 - 2.6\,\hat{\delta}^L_{12}\hat{\delta}^R_{12}\right) \tag{8.4.23}$$

and hence

$$\sqrt{|\text{Re}(\hat{\delta}^L_{12})^2|} < 3\times 10^{-2}\left(\frac{m_D}{2000\text{ GeV}}\right), \quad \sqrt{|\text{Im}(\hat{\delta}^L_{12})^2|} < 9\times 10^{-4}\left(\frac{m_D}{2000\text{ GeV}}\right), \tag{8.4.24}$$

which are not much weaker than the limits from [303] despite the larger gaugino mass and the change from Majorana to Dirac gauginos. The reason is that the flavour data have been updated and the limits scale only inversely proportional to the gaugino mass, since there is no further suppression of the Dirac case relative to the Majorana case, as described in section 8.4.1. In fact, since the limits are derived from the constraints on $C_1, \tilde{C}_1$ without the mass insertion approximation, for moderate values of the ratio of gluino to third generation squark masses, the Dirac version of this model is actually more constrained than the Majorana one.

Including the first two generations

The above discussion assumed that we could completely decouple the first two generations. However, we know that we cannot make them arbitrarily massive compared to the third generation without the two-loop RGEs leading either to tachyons or substantial fine-tuning to avoid them. Typically a factor of $m_1/m_3 \sim 10-15$ is the maximum that is allowed. Given this, we must still worry about flavour-changing effects from the first two generations.

For example, let us suppose that the heavy eigenstates are not degenerate, but have masses $m_1 \leqslant m_2$. In the limit where m_1 is much larger than m_D, one of the contributions to $\tilde{f}^{LR}$ of (8.4.1) can be written as

$$-16\pi^2 i\tilde{f}^{LR} \sim \frac{W^L_{12}W^R_{12}}{m^2_1}\,.$$

Under the reasonable assumption that there are no accidental cancellations between the different contributions, for $m_1 \sim 10\,\text{TeV}$ the constraint from ϵ_K requires $W_{12}^L W_{12}^R \lesssim 10^{-6}$ which is clearly highly restrictive for any flavour model. Therefore we must impose restrictions upon the heavy squarks.

Let us determine the condition for neglecting the contribution from the first two generations in the approximation that the first two generations of left- and right-handed squarks are degenerate to leading order with masses m_{L1}, m_{R1} respectively, with the third generation masses m_{L3}, m_{R3}. Then, there are corrections $\delta_{12}^A m_1^2$, $\delta_{13}^A m_1^2$, $\delta_{23}^A m_1^2$ to the off-diagonal elements of the squark mass-squared matrix, with δ_{ij}^A defined similar to the mass insertion approximation flavour parameter described in sec. 8.2.3: $\delta_{ij}^A = m_1^{-2}(m_{ij}^A)^2$, $A = L, R$. In this case, eq. (8.4.1) is expressed as

$$\begin{aligned}\tilde{f}^{AB} \;\simeq\; & \hat{\delta}_{12}^A\,\hat{\delta}_{12}^B\,\tilde{I}_4(m_{A3}^2, m_{B3}^2) \\ & + \delta_{12}^A\,\hat{\delta}_{12}^B\,m_{A1}^2\,\frac{\partial}{\partial m_{A1}^2}\left[\tilde{I}_4(m_{A1}^2, m_{B3}^2) - \tilde{I}_4(m_{A1}^2, m_{B1}^2)\right] + (A \leftrightarrow B) \\ & + \delta_{12}^A\delta_{12}^B\,m_{A1}^2\,m_{B1}^2\,\frac{\partial^2\tilde{I}_4(m_{A1}^2, m_{B1}^2)}{\partial m_{A1}^2\partial m_{B1}^2}\,, \end{aligned} \tag{8.4.25}$$

where we have neglected subleading terms in $\hat{\delta}_{12}^{A,B}$. If we further take $m_{A1} = m_{B1} = m_1$, $m_{A3} = m_{B3} = m_3$, then this simplifies to

$$\begin{aligned}-16\pi^2 i\tilde{f}^{AB} \;=\; & \hat{\delta}_{12}^A\hat{\delta}_{12}^B\frac{1}{m_3^2}\tilde{f}_4(\frac{m_D^2}{m_3^2}) + \delta_{12}^A\delta_{12}^B\frac{1}{m_1^2}\tilde{f}_6(\frac{m_D^2}{m_1^2}) \\ - \; & \left[\delta_{12}^A\,\hat{\delta}_{12}^B\frac{1}{m_1^2}\tilde{f}_5(\frac{m_D^2}{m_1^2}, \frac{m_3^2}{m_1^2}) + (A \leftrightarrow B)\right], \end{aligned} \tag{8.4.26}$$

where

$$\tilde{f}_5(\frac{m_D^2}{m_1^2}, \frac{m_3^2}{m_1^2}) = \log\frac{m_D^2}{m_1^2} + \frac{2m_D^4 - 3m_D^2m_3^2 + m_3^4(1 + \log\frac{m_3^2}{m_D^2})}{(m_3^2 - m_D^2)^2} + \mathcal{O}(m_1^{-2})\,. \tag{8.4.27}$$

Assuming that $m_D \ll m_1$, in order to neglect the contribution of the first two generations we require $\delta_{12} \lesssim \hat{\delta}_{12}\frac{m_1}{m_3}$. Since, as explained above, we expect $\frac{m_1}{m_3} \lesssim 10 \div 15$, we see that only certain flavour models will actually allow this.

Concrete Realizations

In order to realise a model with heavy first two generations of squarks with suppressed mixing between them, we could consider models with a large D-term for an extra abelian gauged flavour symmetry under which only the first two generations are charged, and obtain a natural supersymmetric spectrum [316, 317]. These D-term contributions were argued to be naturally generated (at least) in effective string models [318, 319], to be positive and, in certain circumstances, to be dominant over the F-term contributions. It is then clear from (7.3.13) that precisely because the first generations of *fermions* are lighter than the third one, the corresponding scalars are *predicted to be heavier*. While such models would be one approach to realizing the scenario of the previous subsection, there is currently no extant example that

solves the FCNC problem of mixing between the first two generations (owing to the need to have degeneracy between them).

Another class of flavour models adds extra (non abelian) symmetry between the first two generations [320, 321, 322, 323, 324, 325, 326]. In this case, we can effectively take the squark mass matrix to be diagonal, with flavour-changing processes only induced by the quark rotations combined with the (possibly small) non-degeneracies in the squark matrix (of course, if the squarks were degenerate then the super-GIM mechanism would lead to vanishing of the flavour-changing effects).

Taking the model of [307] for $m^2_{L1} = m^2_{L2} = m^2_1 \gg m^2_{L3}$, $m^2_{R1} = m^2_{R2} = m^2_1 \simeq m^2_{R3}$ as an illustrative example of this scenario (see appendix B.2 of [296] for more details), we have approximately

$$\tilde{f}^{LR} \simeq \frac{i}{16\pi^2} W^L_{13} W^{L\dagger}_{32} W^R_{13} W^{R\dagger}_{32} \frac{m^2_1 - m^2_{3R}}{m^4_1} \tilde{f}_5(\frac{m^2_D}{m^2_1}, \frac{m^2_{L3}}{m^2_1}) \,, \tag{8.4.28}$$

where $\tilde{f}_5$ is given in (8.4.27) and the diagonalizing matrices are given in terms of parameters of the model:

$$W^L_{13} W^{L\dagger}_{32} W^R_{13} W^{R\dagger}_{32} = -s^2_d \frac{m_d}{m_s} |V^d_{23}|^2 e^{-2i\tilde{\alpha}_{12}} \,, \tag{8.4.29}$$

with s_d and V^d_{23} that take values $s^2_d \simeq 0.2$ and $V^d_{23} \simeq 0.04$ in the best fit of one of the models in [307].

The bounds on Δm_K are easily satisfied by this model, so we focus directly on the bounds on ϵ_K. We obtain, allowing $C_{\epsilon_K} \in [0.66, 1.73]$ at 99% confidence level:

$$\begin{aligned} \frac{|\Delta\epsilon_K|}{|\epsilon_K(SM)|0.73} \simeq & \frac{4.25}{0.73 \times 2.04 \times 10^{-3}} \frac{1}{3} \frac{m_K f^2_K}{m^2_1 \sqrt{2} \Delta m_K(\text{exp})} |V^d_{23}|^2 \frac{m_d}{m_s} s^2_d \sin 2\tilde{\alpha}_{12} \frac{|m^2_{\tilde{d}_R} - m^2_{\tilde{b}_R}|}{m^2_1} \tilde{f}_5 \\ = & 0.07 \times \left(\frac{|V^2_{23}|}{0.04}\right)^2 \left(\frac{s^2_d}{0.2}\right) \left(\frac{\sin 2\tilde{\alpha}_{12}}{\sqrt{3}/2}\right) \left(\frac{|m^2_{\tilde{d}_R} - m^2_{\tilde{b}_R}|}{1 \text{ TeV}^2}\right) \left(\frac{10 \text{ TeV}}{m^2_1}\right)^2 \left(\frac{\tilde{f}_5}{1.1}\right) \end{aligned} \tag{8.4.30}$$

where we have used $m_D = 2$ TeV, $m_{L3} = m_{\tilde{b}_L} = 1$ TeV, $m_1 = 10$ TeV to evaluate $\tilde{f}_5$. The results from [307] are compatible with the 95% confidence level bound $C_{\epsilon_K} \in [0.77, 1.41]$ and we show the comparison in figure 6.

In this model, the Dirac gluino offers an improvement by roughly a factor of four over the Majorana case. Again, this is in agreement with sec. 8.4.1 since the dominant contribution comes from C_4 where the chirality-flip process adds to the same-chirality one instead of cancelling it.

8.5 A Diversion: how to fake a gluino

We saw previously that large suppression of FCNC and production of coloured particles can be obtained in two different ways:

- Large Dirac mass $m_D \gg M, M_\chi$, due to the underlying R-symmetry, in the mass insertion approximation.
- Large Majorana mass $M \gg m_D, M_\chi$, due to small couplings of the light "fake gaugino" fermion to quarks/squarks.

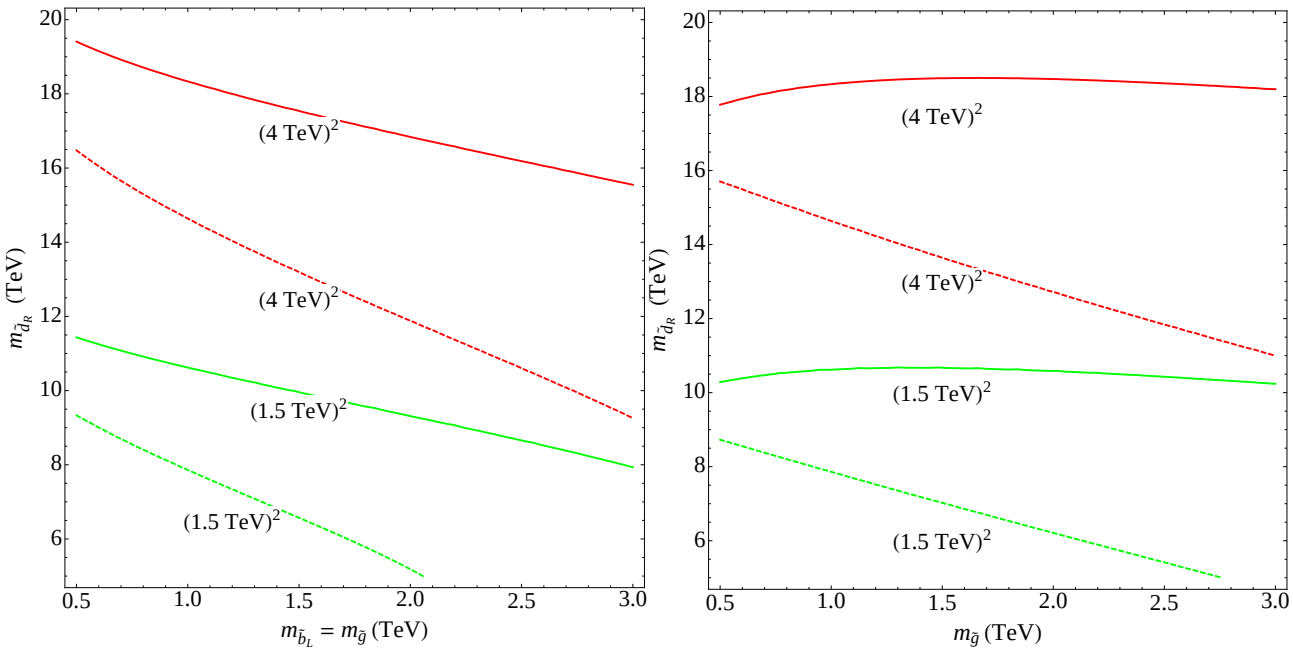

Figure 6: Contour plots for the model of section 8.4.3. Along the contour, $|\Delta\epsilon_K| = \Delta\epsilon_K(exp)$. The dashed lines correspond to exactly Dirac gauginos, while the solid lines are purely Majorana, as in the original model of [307]. In the left plot, the left-handed sbottom mass is set equal to that of the gluino; in the right plot, the left-handed sbottom is fixed at 1 TeV. The two lines correspond to $m^2_{\tilde{d}_R} - m^2_{\tilde{b}_R} = (1.5, 4 \text{ TeV})^2$. The remaining parameters are chosen as $|V^d_{23}| = 0.04, \sin(\alpha_{12}) = 0.5$ and $s^2_d = 0.2$.

The second case can be realized in two distinct ways.
i) We can have a scenario with a very moderate hierarchy and without a see-saw mass: we can take for example $M_\chi \sim$ TeV, $M \sim 10$ TeV, 1 TeV $\lesssim m_{\tilde{q}} \lesssim 5$ TeV and an arbitrarily small Dirac mass. In particular, we need only consider the gluino as being so heavy (the other gauginos could be somewhat lighter). In this case, all of the masses would be generated by F-term supersymmetry-breaking. The Dirac mass is then automatically suppressed, as can be checked by writing explicitly the Dirac mass term with the help of a chiral spurion superfield. Alternatively, there can be also a small D-term which would explain the smallness of the Dirac mass. Here $R_{12}^{\tilde{g}} \sim m_D/M$, so the mixing between the gauginos and the fake gaugino could be almost arbitrarily small.
ii) A second way is by having a large, intermediate scale gluino mass. A theoretical motivation for this case is gauge coupling unification. According to [327], MSSM with additional adjoint chiral fields leads to a good unification of couplings at the string scale for adoint masses around 10^{12} GeV. In the case they considered, the low-energy effective theory is just the MSSM. From the gauge unification viewpoint however, we can switch the masses of the gauginos/gluinos with those of the chiral adjoint fermions, keeping the scalar adjoint masses heavy. This switch will not affect gauge coupling unification at one-loop, whereas it will significantly change phenomenology, which we call "fake split SUSY" for obvious reasons in what follows. In this section we therefore consider in more detail this scenario and comment on its qualitative phenomenological consequences.

Case i) is clearly easy to justify. Before discussing phenomenological implications, let elaborate more about case ii). The obvious question is the stability of the hierarchy $M \gg m_D, M_\chi$ under radiative corrections through diagrams of the form represented in Fig. 7. For this, we need to consider the effective theory when we integrate out the gauginos and the adjoint scalars. The adjoint fermion χ (the "fake gaugino") has no tree-level renormalisable couplings to the squarks and sleptons, but it does couple via the gauge current to the gaugino λ and the adjoint scalar Σ: the relevant terms are

$$\mathcal{L} \supset -\left(\frac{M}{2}\lambda^a\lambda^a + \frac{M_\chi}{2}\chi^a\chi^a + \frac{1}{2}B_\Sigma\Sigma^a\Sigma^a + i\sqrt{2}gf^{abc}\overline{\Sigma}^a\lambda^b\chi^c + h.c.\right) - m_\Sigma^2\Sigma^a\overline{\Sigma}^a$$
$$-(m_D\Sigma^a + \overline{m_D}\overline{\Sigma}^a)^2 - (m_D\lambda^a\chi^a + c.c.). \qquad (8.5.1)$$

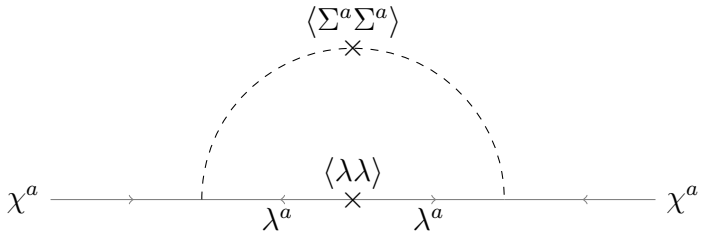

Figure 7: Loop diagram generating corrections to the bare majorana mass M_χ. Symbols $\times$ denote mass insertions for the adjoint scalar Σ and the gluino λ.

On the second line we included the terms coming from the Dirac gaugino mass term, which necessarily also generates the term $(m_D\Sigma^a + \overline{m_D}\overline{\Sigma}^a)^2$. We do not absorb these into m_Σ, B_Σ

because these corrections are RGE invariant and therefore apply at any renormalisation scale [286, 287, 288]. Instead we define

$$\hat{B}_\Sigma \equiv B_\Sigma + 2m_D^2 \ , \ \hat{m}_\Sigma^2 \equiv m_\Sigma^2 + 2|m_D|^2. \tag{8.5.2}$$

Since we are making the logical assumption that the adjoint scalars are at least as massive as the other scalars in the theory, we can integrate them out along with the gaugino λ: at one loop we generate a term M_χ given by

$$M_\chi = 2g^2 C_2(G)\hat{B}_\Sigma M \int \frac{d^4p}{(2\pi)^4} \frac{p^2}{(p^2+m_D^2)^2 + M^2p^2)((p^2+\hat{m}_\Sigma^2)^2 - \hat{B}_\Sigma^2)} \ , \tag{8.5.3}$$

which gives to leading order in $B_\Sigma/m_\Sigma^2, m_D/M$

$$M_\chi = \frac{2C_2(G)g^2}{16\pi^2} \times \begin{cases} \frac{\hat{B}_\Sigma}{M}\left(1 - \log\frac{M^2}{\hat{m}_\Sigma^2}\right) & M \gg \hat{m}_\Sigma \ , \\ \frac{\hat{B}_\Sigma}{\hat{m}_\Sigma^2} M & \hat{m}_\Sigma \gtrsim M. \end{cases} \tag{8.5.4}$$

This clearly prevents an arbitrary hierarchy between M and M_χ. We might consider simply ignoring $\hat{B}_\Sigma$; however, it will always have a D-term contribution from the Dirac mass, so that without tuning we can say $|\hat{B}_\Sigma| \gtrsim |m_D|^2$. More honestly, one should check if there can be a symmetry preventing the generation of such a term. Indeed this is the case: If we rotate under $U(1)_F$ the adjoint superfield Σ then this prevents both M_χ and B_Σ, but also prevents the Dirac mass m_D. However, if we break this symmetry with the vev of a field ϕ such that $\phi/M_{\rm high} \equiv \epsilon$ then we generate

$$m_D \sim \epsilon M \quad , \quad M_\chi \sim \epsilon^2 M \quad , \quad B_\Sigma \sim \epsilon^2 M^2 \sim m_D^2 \tag{8.5.5}$$

and thus the above contribution is irrelevant: the see-saw (and direct) masses for the "fake" gluino are of order m_D^2/M where the scale is controlled by the parameter ϵ. We also note that since this hierarchy is protected by the approximate symmetry, it is not affected by renormalisation group running from above the SUSY-breaking scale[5]

$$\begin{aligned} \delta M_\chi &\sim \epsilon^2 \frac{g_s^2}{16\pi^2} M \, , \\ \delta B_\Sigma &\sim M M_\chi \frac{g^2}{16\pi^2} \log\left(\frac{\Lambda}{M}\right) \sim \epsilon^2 \frac{g^2}{16\pi^2} M^2 \log\left(\frac{\Lambda}{M}\right). \end{aligned} \tag{8.5.6}$$

Taking $M \sim m_{\tilde{q}} \sim m_\Sigma \sim 10^{12}$ GeV and assuming that the "fake" gluino mass is of order $M_\chi \sim 1$ TeV, this fixes the parameter ϵ to be of order 10^{-4} (so that we could take $\langle\phi\rangle \sim M, M_{\rm high} \sim M_{\rm GUT}$). Hence we get the following masses

$$M \sim 10^{12}{\rm GeV} \gtrsim m_\Sigma \quad \gg \quad m_D, \ \sqrt{B_\Sigma} \sim 10^8{\rm GeV} \quad \gg \quad M_\chi \sim 1{\rm TeV} \ . \tag{8.5.7}$$

If the switch of masses is also performed for the wino/bino $\leftrightarrow$ fake wino/bino, the resulting low-energy effective theory in this case is different compared to standard split SUSY. Indeed,

[5] In terms of the parameter $\hat{B}_\Sigma$ defined in (8.5.2), we find $\delta\hat{B}_\Sigma \sim (MM_\chi - m_D^2)\frac{g^2}{16\pi^2}\log\left(\frac{\Lambda}{M}\right)$.

we should consider whether there are any light higgsinos remaining in the spectrum: in split SUSY, there is an R-symmetry that protects the mass of the higgsinos, whereas we have broken this, and we would expect the higgsinos to obtain a mass through diagrams similar to the one considered above:

$$\mu \simeq \frac{1}{4} 2 g_Y^2 M B_\mu \tilde{I}_4(m_h^2, m_H^2, M_{\tilde{B}^1}^2, M_{\tilde{B}^2}^2) + \frac{3}{4} 2 g_2^2 M B_\mu \tilde{I}_4(m_h^2, m_H^2, M_{\tilde{W}^1}^2, M_{\tilde{W}^2}^2) \ , \tag{8.5.8}$$

where $M_{\tilde{B}^i}, M_{\tilde{W}^i}$ with $i = 1, 2$ are the masses for the bino and wino eigenstates respectively (before electroweak symmetry breaking) and m_h (m_H) are the light (heavy) mass parameters in the Higgs sector,

$$m_h^2 \simeq \frac{m_{h_u}^2 m_{h_d}^2 - B_\mu^2}{m_{h_u}^2 + m_{h_d}^2} \quad , \quad m_H^2 \simeq m_{h_u}^2 + m_{h_d}^2 \ . \tag{8.5.9}$$

In writing (8.5.8) we neglected M_χ in the loop. In this case, a more compact form for the integrals is, for example

$$\tilde{I}_4(m_h^2, m_H^2, M_{\tilde{W}^1}^2, M_{\tilde{W}^2}^2) = \int \frac{d^4p}{(2\pi)^4} \frac{p^2}{(p^2 + m_h^2)(p^2 + m_H^2)[(p^2 + m_D^2)^2 + M_{\tilde{W}}^2 p^2]}. \tag{8.5.10}$$

Whereas the general expression is rather involved, in the limit $M \gg m_H$ and (for simplicity) with equal gaugino mass parameters for $SU(2)$ and $U(1)$ factors $M_{\tilde{W}} = M_{\tilde{B}} \simeq M$, it simplifies to

$$\mu \simeq \frac{g_Y^2 + 3 g_2^2}{32\pi^2} \frac{B_\mu}{M - m_H^2/M} \log \frac{m_H^2}{M^2} \ . \tag{8.5.11}$$

However, this can be repaired in a similar fashion: we can suppose that the Higgs fields are charged under the same $U(1)$ symmetry that the adjoints are charged under. This would suppress the μ and B_μ terms, and also prevent any superpotential couplings between the adjoints and the higgsinos. We would have $\mu \sim \epsilon^2 M, B_\mu \sim \epsilon^2 M^2$ so we would have $B_\mu \gg |\mu|^2$ and the heavy Higgs scalars would be parametrically heavier than the electroweak scale. In this scenario we effectively take infinite $\tan\beta$ and require the down-quark and lepton Yukawa couplings non-holomorphic and generated in the high-energy theory (see e.g. [328, 266]).

Then, in split SUSY the effective lagrangian contains higgs/higgsino/gaugino couplings

$$\mathcal{L}_{\text{eff}} \supset -\frac{H^\dagger}{\sqrt{2}} (\tilde{g}_u \sigma^a \tilde{W}^a + \tilde{g}'_u \tilde{B}) \ \tilde{H}_u - \frac{H^T \epsilon}{\sqrt{2}} (-\tilde{g}_d \sigma^a \tilde{W}^a + \tilde{g}'_d \tilde{B}) \ \tilde{H}_d. \tag{8.5.12}$$

In usual split SUSY, $\tilde{g}_u = g \sin\beta, \tilde{g}_d = g \cos\beta, \tilde{g}'_u = g' \sin\beta, \tilde{g}'_d = g' \cos\beta$; however, in our case these couplings will be strongly suppressed by the fake gaugino/bino compositions R_{12}, R'_{12}. If the adjoint superpotential couplings $W \supset \lambda_S H_d S H_u + 2\lambda_T H_d T H_u$ had not been suppressed, then they would have provided couplings of the same form. Instead, the absence of such couplings at low-energy could be therefore a signature of a remote $N = 2$ supersymmetric sector, instead of a more conventional split SUSY spectrum.

Finally, in the absence of couplings $\lambda_{S,T}$, the model has difficulties to accomodate a good dark matter candidate, due to the small couplings of the fake electroweakinos to quarks and leptons.

8.5.1 Phenomenological consequences

In the context of split SUSY, where squarks are very heavy compared to the gluino, one striking experimental signature is the long lifetime of the gluino and associated displaced vertices or (for even heavier squarks) gluino stability. Indeed the lifetime of the gluino could be sufficiently long to propagate on macroscopic distances in detectors [329, 330, 331]. This lifetime, in the standard split SUSY context, can be estimated in an approximate manner according to [331] as follows

$$\tau_{\tilde{g}} = \frac{4 \text{ sec}}{N} \times \left(\frac{m_{\tilde{q}}}{10^9 \text{GeV}}\right)^4 \times \left(\frac{1 \text{ TeV}}{M}\right)^5 , \tag{8.5.13}$$

where N is a quantity varying with M and $m_{\tilde{q}}$ but of order une for our range of masses.

As we saw in the previous sections, the fake gluino couplings are altered by the diagonalisation of the gluino mass matrix and contain a tiny contribution of the original gluino gauge coupling, proportional to $R^{\tilde{g}}_{12} \sim m_D/M$. In case i) above, the mixing between the gauginos and the fake gaugino could be almost arbitrarily small by having $m_D \ll$ TeV, meaning that the fake gluino could still have displaced vertices without requiring large mass scales. Particularly interesting is the case where the usual gluinos are not accessible (they are heavier than say 5 TeV), whereas some of the squarks are. Displaced vertices /long lifetime for the fake gluino with light squarks would be a direct probe of a high-energy $N = 2$ supersymmetric spectrum. Pair production of faked gluinos in this case lead to displaced vertices, since although some squarks could be light, their small couplings to the fake gluino suppresses such processes. On the other hand, direct squark production is possible, but subsequent squark decays to quarks/neutralinos go dominantly through the Higgsino components and corresponding Yukawas couplings. They are therefore unsuppressed only for third generation squarks (and eventually third generation sleptons if similar arguments are applied to the other gauginos). Of course, the heavier the usual gluino, the bigger the fine-tuning needed in order to keep a squark to be light. Some fine-tuning, moderate for gluino mass below 10 TeV or so, is unavoidable for such a scenario to be realized in nature. However, its very different phenomenological implications could be worth further study.

In case ii) above, the fake gluino couplings to quarks/squarks are proportional to $g_s R_{12} \simeq g_s \frac{m_D}{M} \sim \epsilon$ and encodes the small gluino composition of the lightest fermion octet. According to our numerical choice of masses we get $R_{12} \sim \epsilon \sim 10^{-4}$. This affects therefore the fake gluino lifetime, which has to be modified according to

$$\tau_\chi = \frac{4 \times 10^{28} \text{ sec}}{N} \times \left(\frac{10^{-4}}{R^{\tilde{g}}_{12}}\right)^2 \left(\frac{10^{-4}}{R^{\chi^0}_{12}}\right)^2 \times \left(\frac{m_{\tilde{q}}}{10^{12}\text{GeV}}\right)^4 \times \left(\frac{1 \text{ TeV}}{M_\chi}\right)^5 \sim 10^{21} \text{ years} \tag{8.5.14}$$

where we define $R^{\tilde{g}}$ and $R^{\chi^0}_{12}$ to be the rotation matrices for the gluino and neutralino respectively. For the scales given, this lifetime is hence longer than the age of the universe, and so we should make sure that fake gluinos are not produced in the early universe[6].

We could also consider different moderate hierarchies with interesting low-energy implications. For example, let us suppose that $M_\chi \sim m_D \sim$ TeV and gluino and squark masses $M \sim m_{\tilde{q}} \sim 100$ TeV, while the higgsinos remain light; in split SUSY gluino decays are prompt inside the detector, but in our "fake split SUSY" case, now $R^{\tilde{g}}_{12} \sim 10^{-2}$ and we can take $R^{\chi^0}_{12} \sim 1$.

[6]For more discussion of this issue we refer the reader to [332]

The gluino propagation length is increased by a factor of 10^4 and the vertex starts to become displaced. Although the squarks are still very heavy, they could produce testable CP violating FCNC effects in the Kaon system (ϵ_K).

8.6 Conclusions

In this third part, we introduced the flavour structure of the standard model of particle physics. We reviewed briefly how things turn bad while going in a supersymmetric formulation when looking at FCNC processes like the Kaon oscillation system. We saw that flavour physics sets severe constraints on supersymmetric models of flavour. In models in which the scale of mediation of supersymmetry breaking is similar or higher than the scale of flavour symmetry breaking, fermion masses and mixing hierarchies are correlated with the flavour structure of superpartners. In the MSSM constructing a fully successful flavour model of this type is difficult and usually requires the simultaneous presence of several ingredients like abelian and non-abelian symmetries. At first sight, flavour models with Dirac gauginos are simpler to build, due to the flavour suppression argued in the literature in their R-symmetric pure Dirac limit, for gluinos heavier than squarks. In this last part, we found that this suppression is only strong in the near-degeneracy (mass insertion approximation) limit, whereas in most flavour models this approximation is not valid.

We analyzed the simplest Dirac flavour models with abelian symmetries realising various degrees of alignment of fermion and scalar mass matrices and for non-abelian symmetries realising a natural supersymmetric spectrum with heavy first two generations. We found only a moderate improvement in the flavour constraints over the MSSM case. We also showed in an explicit example in section 8.4.2 that due to cancellations in the Majorana case, it is even possible that a Dirac model is for some parts of the parameter space more constrained than its MSSM cousin.

We also considered generalised Lagrangians with both Majorana and Dirac masses, by not imposing an R-symmetry in the UV. We considered, in particular, the case in which the gluino Majorana mass is very large compared to that of the chiral octet fermion and the Dirac mass $M \gg M_\chi, m_D$. This led to the scenario dubbed "fake gluino" in which the light adjoint fermions are not the $N = 1$ partners of the gauge fields, but the other fermions in the $N = 2$ gauge multiplets. In this case, couplings of the light "fake gluino" to quarks are suppressed parametrically by the ratio m_D/M. This leads to a potentially new exotic phenomenology in which squarks can be light and accessible experimentally, while the light adjoint fermions can be long-lived and generate displaced vertices or escape detection. Experimental discovery of a squark and simultaneously of long-lived light gluinos would be spectacular evidence of such a spectrum. An extreme case with heavy gluinos and light adjoint fermions is obtained by pushing a Majorana gluino mass and squark masses to an intermediate scale $M \sim 10^{12}$ GeV, which leads to good gauge coupling unification. The outcome is similar in spirit to split supersymmetry, with however light adjoint fermion couplings to quarks and (for electroweakinos) to higgs/higgsino which are highly suppressed compared to split supersymmetry.

9 Conclusion

We have gone through this work along the timeline of the Universe History focusing on three major topics that are the Inflationary period, the dark matter relic density production and detection, and finally the question of flavor changing constraints on low energy supersymmetric theories.

We studied in particular the intimate link that shows up between the breaking of supersymmetry in the Minkowski vacuum and the successful achievement of a large field inflation scenario. We saw that combining these two concepts in a single supergravity model imposes bounds on the gravitino mass depending strongly on the kind of model – with or without stabilizer – used to produce effective chaotic inflation. Furthermore we saw that in some cases supersymmetry breaking non decoupling effects of integrating out heavy fields can be required to be the major source of energy for driving inflation during 60 e-folds.

Letting aside supersymmetric theories for a while we investigated the possibility that dark matter could interact with our visible sector through the exchange of a *mediator* particle. The latter mediator has been imagined to couple to the Standard Model particles through higher dimensional effective operators. We considered the case of a Z' interacting through dimension six operators to the strong SU(3) sector, as well as an axion like particle interacting with the photons. The work released showed the possibility to include relatively light mediators, although only satisfying direct and indirect detection constraints thanks to the use of non renormalizable – and hence suppressed by a large energy scale – operators. In order to explain with our models the presence of the recently detected 3.5 keV line, we made in addition a prediction for the existence of an axion like particle with a mass of order $m \sim$ MeV, which may be detected in the next generations axion like particle detection experiments.

Finally we explored, back into supersymmetric theories how the presence of Dirac Gauginos could either reinforce or relax constraints coming from flavor changing neutral currents on the minimal supersymmetric standard model. We saw that going beyond the naive assumption of nearly degenerate squark masses can lead to even more restrictive constraints on the model. We defined in the case of heavy Majorana mass compared to the Dirac one, the concept of *fake gluino*, allowing experimentally accessible squarks and long-lived light gluinos which could lead to displaced vertices detectable in future collider experiments.

Although dealing with various themes, this thesis encompasses fundamental questions of both cosmology and particle physics beyond the Standard Model. Indeed a better understanding of the early times of the Universe requires a strong knowledge on the particle content of our world, especially in order to interpret properly the observations we are able to have access to on earth experiments. The models exposed propose original scenarios among which a few experimental signatures could be detected in the future years, learning us hopefully better what our Universe is actually truly made of.

Bibliography

[1] **ATLAS** Collaboration, G. Aad *et al.*, "Observation of a new particle in the search for the Standard Model Higgs boson with the ATLAS detector at the LHC," *Phys.Lett.* **B716** (2012) 1–29, arXiv:1207.7214 [hep-ex].

[2] **CMS** Collaboration, S. Chatrchyan *et al.*, "Observation of a new boson at a mass of 125 GeV with the CMS experiment at the LHC," *Phys.Lett.* **B716** (2012) 30–61, arXiv:1207.7235 [hep-ex].

[3] **WMAP** Collaboration, E. Komatsu *et al.*, "Five-Year Wilkinson Microwave Anisotropy Probe (WMAP) Observations: Cosmological Interpretation," *Astrophys.J.Suppl.* **180** (2009) 330–376, arXiv:0803.0547 [astro-ph].

[4] **Supernova Cosmology Project** Collaboration, M. Kowalski *et al.*, "Improved Cosmological Constraints from New, Old and Combined Supernova Datasets," *Astrophys.J.* **686** (2008) 749–778, arXiv:0804.4142 [astro-ph].

[5] C. W. Misner, "Mixmaster universe," *Phys.Rev.Lett.* **22** (1969) 1071–1074.

[6] E. Lifshitz and I. Khalatnikov, "Investigations in relativistic cosmology," *Adv.Phys.* **12** (1963) 185–249.

[7] G. Ellis and S. Hawking, "The Cosmic black body radiation and the existence of singularities in our universe," *Astrophys.J.* **152** (1968) 25.

[8] A. D. Linde, "Chaotic Inflation," *Phys.Lett.* **B129** (1983) 177–181.

[9] K. Freese, J. A. Frieman, and A. V. Olinto, "Natural inflation with pseudo - Nambu-Goldstone bosons," *Phys.Rev.Lett.* **65** (1990) 3233–3236.

[10] G. F. Smoot, C. Bennett, A. Kogut, E. Wright, J. Aymon, *et al.*, "Structure in the COBE differential microwave radiometer first year maps," *Astrophys.J.* **396** (1992) L1–L5.

[11] **Planck** Collaboration, P. Ade *et al.*, "Planck 2015 results. XIII. Cosmological parameters," arXiv:1502.01589 [astro-ph.CO].

[12] D. H. Lyth, "What would we learn by detecting a gravitational wave signal in the cosmic microwave background anisotropy?," *Phys.Rev.Lett.* **78** (1997) 1861–1863, arXiv:hep-ph/9606387 [hep-ph].

[13] S. Dimopoulos, S. Kachru, J. McGreevy, and J. G. Wacker, "N-flation," *JCAP* **0808** (2008) 003, arXiv:hep-th/0507205 [hep-th].

[14] A. A. Starobinsky, "The Perturbation Spectrum Evolving from a Nonsingular Initially De-Sitte r Cosmology and the Microwave Background Anisotropy," *Sov.Astron.Lett.* **9** (1983) 302.

[15] L. Kofman, A. D. Linde, and A. A. Starobinsky, "Inflationary Universe Generated by the Combined Action of a Scalar Field and Gravitational Vacuum Polarization," *Phys.Lett.* **B157** (1985) 361–367.

[16] B. Whitt, "Fourth Order Gravity as General Relativity Plus Matter," *Phys.Lett.* **B145** (1984) 176.

[17] T. Futamase and K.-i. Maeda, "Chaotic Inflationary Scenario in Models Having Nonminimal Coupling With Curvature," *Phys.Rev.* **D39** (1989) 399–404.

[18] D. Salopek, J. Bond, and J. M. Bardeen, "Designing Density Fluctuation Spectra in Inflation," *Phys.Rev.* **D40** (1989) 1753.

[19] N. Makino and M. Sasaki, "The Density perturbation in the chaotic inflation with nonminimal coupling," *Prog.Theor.Phys.* **86** (1991) 103–118.

[20] R. Fakir, S. Habib, and W. Unruh, "Cosmological density perturbations with modified gravity," *Astrophys.J.* **394** (1992) 396.

[21] E. Komatsu and T. Futamase, "Complete constraints on a nonminimally coupled chaotic inflationary scenario from the cosmic microwave background," *Phys.Rev.* **D59** (1999) 064029, arXiv:astro-ph/9901127 [astro-ph].

[22] L. Kofman and S. Mukohyama, "Rapid roll Inflation with Conformal Coupling," *Phys.Rev.* **D77** (2008) 043519, arXiv:0709.1952 [hep-th].

[23] F. L. Bezrukov and M. Shaposhnikov, "The Standard Model Higgs boson as the inflaton," *Phys.Lett.* **B659** (2008) 703–706, arXiv:0710.3755 [hep-th].

[24] E. J. Copeland, A. R. Liddle, D. H. Lyth, E. D. Stewart, and D. Wands, "False vacuum inflation with Einstein gravity," *Phys.Rev.* **D49** (1994) 6410–6433, arXiv:astro-ph/9401011 [astro-ph].

[25] M. Dine, L. Randall, and S. D. Thomas, "Supersymmetry breaking in the early universe," *Phys.Rev.Lett.* **75** (1995) 398–401, arXiv:hep-ph/9503303 [hep-ph].

[26] P. Binetruy and G. Dvali, "D term inflation," *Phys.Lett.* **B388** (1996) 241–246, arXiv:hep-ph/9606342 [hep-ph].

[27] C. Wieck and M. W. Winkler, "Inflation with Fayet-Iliopoulos Terms," *Phys.Rev.* **D90** no. 10, (2014) 103507, arXiv:1408.2826 [hep-th].

[28] E. Halyo, "Hybrid inflation from supergravity D terms," *Phys.Lett.* **B387** (1996) 43–47, arXiv:hep-ph/9606423 [hep-ph].

[29] S. Antusch, M. Bastero-Gil, S. F. King, and Q. Shafi, "Sneutrino hybrid inflation in supergravity," *Phys.Rev.* **D71** (2005) 083519, arXiv:hep-ph/0411298 [hep-ph].

[30] V. N. Senoguz and Q. Shafi, "New inflation, preinflation, and leptogenesis," *Phys.Lett.* **B596** (2004) 8–15, arXiv:hep-ph/0403294 [hep-ph].

[31] M. Bastero-Gil, S. King, and Q. Shafi, "Supersymmetric Hybrid Inflation with Non-Minimal Kahler potential," *Phys.Lett.* **B651** (2007) 345–351, arXiv:hep-ph/0604198 [hep-ph].

[32] M. Kawasaki, M. Yamaguchi, and T. Yanagida, "Natural chaotic inflation in supergravity," *Phys.Rev.Lett.* **85** (2000) 3572–3575, arXiv:hep-ph/0004243 [hep-ph].

[33] M. Yamaguchi and J. Yokoyama, "New inflation in supergravity with a chaotic initial condition," *Phys.Rev.* **D63** (2001) 043506, arXiv:hep-ph/0007021 [hep-ph].

[34] P. Brax and J. Martin, "Shift symmetry and inflation in supergravity," *Phys.Rev.* **D72** (2005) 023518, arXiv:hep-th/0504168 [hep-th].

[35] R. Kallosh and A. D. Linde, "O'KKLT," *JHEP* **0702** (2007) 002, arXiv:hep-th/0611183 [hep-th].

[36] R. Kallosh and A. Linde, "New models of chaotic inflation in supergravity," *JCAP* **1011** (2010) 011, arXiv:1008.3375 [hep-th].

[37] R. Kallosh, A. Linde, and T. Rube, "General inflaton potentials in supergravity," *Phys.Rev.* **D83** (2011) 043507, arXiv:1011.5945 [hep-th].

[38] R. Kallosh and A. D. Linde, "Testing String Theory with CMB," *JCAP* **0704** (2007) 017, arXiv:0704.0647 [hep-th].

[39] A. Linde, M. Noorbala, and A. Westphal, "Observational consequences of chaotic inflation with nonminimal coupling to gravity," *JCAP* **1103** (2011) 013, arXiv:1101.2652 [hep-th].

[40] C. Savage, K. Freese, and W. H. Kinney, "Natural Inflation: Status after WMAP 3-year data," *Phys.Rev.* **D74** (2006) 123511, arXiv:hep-ph/0609144 [hep-ph].

[41] L. O'Raifeartaigh, "Spontaneous Symmetry Breaking for Chiral Scalar Superfields," *Nucl.Phys.* **B96** (1975) 331.

[42] J. Polonyi, "Generalization of the Massive Scalar Multiplet Coupling to the Supergravity," *Hungary Central Inst Res - KFKI-77-93 (77,REC.JUL 78) 5p* (1977) .

[43] W. Buchmuller, E. Dudas, L. Heurtier, and C. Wieck, "Large-Field Inflation and Supersymmetry Breaking," *JHEP* **1409** (2014) 053, arXiv:1407.0253 [hep-th].

[44] R. Kallosh, A. Linde, K. A. Olive, and T. Rube, "Chaotic inflation and supersymmetry breaking," *Phys.Rev.* **D84** (2011) 083519, arXiv:1106.6025 [hep-th].

[45] K. Nakayama, F. Takahashi, and T. T. Yanagida, "Gravitino Problem in Supergravity Chaotic Inflation and SUSY Breaking Scale after BICEP2," *Phys.Lett.* **B734** (2014) 358–363, arXiv:1404.2472 [hep-ph].

[46] L. E. Ibanez and I. Valenzuela, "BICEP2, the Higgs Mass and the SUSY-breaking Scale," *Phys.Lett.* **B734** (2014) 354–357, arXiv:1403.6081 [hep-ph].

[47] E. Palti and T. Weigand, "Towards large r from [p, q]-inflation," *JHEP* **1404** (2014) 155, arXiv:1403.7507 [hep-th].

[48] A. Hebecker, S. C. Kraus, and L. T. Witkowski, "D7-Brane Chaotic Inflation," *Phys.Lett.* **B737** (2014) 16–22, arXiv:1404.3711 [hep-th].

[49] L. Alvarez-Gaume, C. Gomez, and R. Jimenez, "Minimal Inflation," *Phys.Lett.* **B690** (2010) 68–72, arXiv:1001.0010 [hep-th].

[50] L. Alvarez-Gaume, C. Gomez, and R. Jimenez, "Phenomenology of the minimal inflation scenario: inflationary trajectories and particle production," *JCAP* **1203** (2012) 017, arXiv:1110.3984 [astro-ph.CO].

[51] I. Antoniadis, E. Dudas, S. Ferrara, and A. Sagnotti, "The Volkov-Akulov-Starobinsky supergravity," *Phys.Lett.* **B733** (2014) 32–35, arXiv:1403.3269 [hep-th].

[52] S. Ferrara, A. Kehagias, and A. Riotto, "The Imaginary Starobinsky Model," *Fortsch.Phys.* **62** (2014) 573–583, arXiv:1403.5531 [hep-th].

[53] S. Ferrara, A. Kehagias, and A. Riotto, "The Imaginary Starobinsky Model and Higher Curvature Corrections," *Fortsch.Phys.* **63** (2015) 2–11, arXiv:1405.2353 [hep-th].

[54] R. Kallosh and A. D. Linde, "Landscape, the scale of SUSY breaking, and inflation," *JHEP* **0412** (2004) 004, arXiv:hep-th/0411011 [hep-th].

[55] A. Linde, Y. Mambrini, and K. A. Olive, "Supersymmetry Breaking due to Moduli Stabilization in String Theory," *Phys.Rev.* **D85** (2012) 066005, arXiv:1111.1465 [hep-th].

[56] E. Dudas, A. Linde, Y. Mambrini, A. Mustafayev, and K. A. Olive, "Strong moduli stabilization and phenomenology," *Eur.Phys.J.* **C73** no. 1, (2013) 2268, arXiv:1209.0499 [hep-ph].

[57] R. Kallosh, A. Linde, B. Vercnocke, and T. Wrase, "Analytic Classes of Metastable de Sitter Vacua," *JHEP* **1410** (2014) 11, arXiv:1406.4866 [hep-th].

[58] **Supernova Cosmology Project** Collaboration, S. Perlmutter *et al.*, "Measurements of Omega and Lambda from 42 high redshift supernovae," *Astrophys.J.* **517** (1999) 565–586, arXiv:astro-ph/9812133 [astro-ph].

[59] **Supernova Search Team** Collaboration, A. G. Riess *et al.*, "Observational evidence from supernovae for an accelerating universe and a cosmological constant," *Astron.J.* **116** (1998) 1009–1038, arXiv:astro-ph/9805201 [astro-ph].

[60] J. M. Maldacena and C. Nunez, "Supergravity description of field theories on curved manifolds and a no go theorem," *Int.J.Mod.Phys.* **A16** (2001) 822–855, arXiv:hep-th/0007018 [hep-th].

[61] G. Gibbons, "ASPECTS OF SUPERGRAVITY THEORIES,".

[62] B. de Wit, D. Smit, and N. Hari Dass, "Residual Supersymmetry of Compactified D=10 Supergravity," *Nucl.Phys.* **B283** (1987) 165.

[63] S. Kachru, R. Kallosh, A. D. Linde, and S. P. Trivedi, "De Sitter vacua in string theory," *Phys.Rev.* **D68** (2003) 046005, arXiv:hep-th/0301240 [hep-th].

[64] W. Buchmuller, E. Dudas, L. Heurtier, A. Westphal, C. Wieck, *et al.*, "Challenges for Large-Field Inflation and Moduli Stabilization," *JHEP* **1504** (2015) 058, arXiv:1501.05812 [hep-th].

[65] S. B. Giddings, S. Kachru, and J. Polchinski, "Hierarchies from fluxes in string compactifications," *Phys.Rev.* **D66** (2002) 106006, arXiv:hep-th/0105097 [hep-th].

[66] S. Gukov, C. Vafa, and E. Witten, "CFT's from Calabi-Yau four folds," *Nucl.Phys.* **B584** (2000) 69–108, arXiv:hep-th/9906070 [hep-th].

[67] T. R. Taylor and C. Vafa, "R R flux on Calabi-Yau and partial supersymmetry breaking," *Phys.Lett.* **B474** (2000) 130–137, arXiv:hep-th/9912152 [hep-th].

[68] G. Curio, A. Klemm, D. Lust, and S. Theisen, "On the vacuum structure of type II string compactifications on Calabi-Yau spaces with H fluxes," *Nucl.Phys.* **B609** (2001) 3–45, arXiv:hep-th/0012213 [hep-th].

[69] E. Witten, "Nonperturbative superpotentials in string theory," *Nucl.Phys.* **B474** (1996) 343–360, arXiv:hep-th/9604030 [hep-th].

[70] J. J. Blanco-Pillado, R. Kallosh, and A. D. Linde, "Supersymmetry and stability of flux vacua," *JHEP* **0605** (2006) 053, arXiv:hep-th/0511042 [hep-th].

[71] F. Marchesano, G. Shiu, and A. M. Uranga, "F-term Axion Monodromy Inflation," *JHEP* **1409** (2014) 184, arXiv:1404.3040 [hep-th].

[72] T. W. Grimm, "Axion Inflation in F-theory," *Phys.Lett.* **B739** (2014) 201–208, arXiv:1404.4268 [hep-th].

[73] L. E. Ibáñez and I. Valenzuela, "The inflaton as an MSSM Higgs and open string modulus monodromy inflation," *Phys.Lett.* **B736** (2014) 226–230, arXiv:1404.5235 [hep-th].

[74] R. Blumenhagen, D. Herschmann, and E. Plauschinn, "The Challenge of Realizing F-term Axion Monodromy Inflation in String Theory," *JHEP* **1501** (2015) 007, arXiv:1409.7075 [hep-th].

[75] A. Hebecker, P. Mangat, F. Rompineve, and L. T. Witkowski, "Tuning and Backreaction in F-term Axion Monodromy Inflation," *Nucl.Phys.* **B894** (2015) 456–495, arXiv:1411.2032 [hep-th].

[76] L. E. Ibanez, F. Marchesano, and I. Valenzuela, "Higgs-otic Inflation and String Theory," *JHEP* **1501** (2015) 128, arXiv:1411.5380 [hep-th].

[77] I. García-Etxebarria, T. W. Grimm, and I. Valenzuela, "Special Points of Inflation in Flux Compactifications," arXiv:1412.5537 [hep-th].

[78] L. Covi, M. Gomez-Reino, C. Gross, J. Louis, G. A. Palma, *et al.*, "de Sitter vacua in no-scale supergravities and Calabi-Yau string models," *JHEP* **0806** (2008) 057, arXiv:0804.1073 [hep-th].

[79] L. Covi, M. Gomez-Reino, C. Gross, J. Louis, G. A. Palma, *et al.*, "Constraints on modular inflation in supergravity and string theory," *JHEP* **0808** (2008) 055, arXiv:0805.3290 [hep-th].

[80] E. Dudas, "Three-form multiplet and Inflation," *JHEP* **1412** (2014) 014, arXiv:1407.5688 [hep-th].

[81] A. Mazumdar, T. Noumi, and M. Yamaguchi, "Dynamical breaking of shift-symmetry in supergravity-based inflation," *Phys.Rev.* **D90** no. 4, (2014) 043519, arXiv:1405.3959 [hep-th].

[82] W. Buchmuller, C. Wieck, and M. W. Winkler, "Supersymmetric Moduli Stabilization and High-Scale Inflation," *Phys.Lett.* **B736** (2014) 237–240, arXiv:1404.2275 [hep-th].

[83] V. Balasubramanian, P. Berglund, J. P. Conlon, and F. Quevedo, "Systematics of moduli stabilisation in Calabi-Yau flux compactifications," *JHEP* **0503** (2005) 007, arXiv:hep-th/0502058 [hep-th].

[84] S. C. Davis and M. Postma, "SUGRA chaotic inflation and moduli stabilisation," *JCAP* **0803** (2008) 015, arXiv:0801.4696 [hep-ph].

[85] R. Kallosh and T. Wrase, "Emergence of Spontaneously Broken Supersymmetry on an Anti-D3-Brane in KKLT dS Vacua," *JHEP* **1412** (2014) 117, arXiv:1411.1121 [hep-th].

[86] O. Lebedev, H. P. Nilles, and M. Ratz, "De Sitter vacua from matter superpotentials," *Phys.Lett.* **B636** (2006) 126–131, arXiv:hep-th/0603047 [hep-th].

[87] M. Cicoli, J. P. Conlon, A. Maharana, and F. Quevedo, "A Note on the Magnitude of the Flux Superpotential," *JHEP* **1401** (2014) 027, arXiv:1310.6694 [hep-th].

[88] D. Chialva and A. Mazumdar, "Super-Planckian excursions of the inflaton and quantum corrections," *Mod.Phys.Lett.* **A30** no. 03n04, (2015) 1540008, arXiv:1405.0513 [hep-th].

[89] S. Talaganis, T. Biswas, and A. Mazumdar, "Towards understanding the ultraviolet behavior of quantum loops in infinite-derivative theories of gravity," arXiv:1412.3467 [hep-th].

[90] W. Buchmuller, V. Domcke, and K. Schmitz, "The Chaotic Regime of D-Term Inflation," *JCAP* **1411** no. 11, (2014) 006, arXiv:1406.6300 [hep-ph].

[91] W. Buchmuller and K. Ishiwata, "Grand Unification and Subcritical Hybrid Inflation," *Phys.Rev.* **D91** no. 8, (2015) 081302, arXiv:1412.3764 [hep-ph].

[92] X. Dong, B. Horn, E. Silverstein, and A. Westphal, "Simple exercises to flatten your potential," *Phys.Rev.* **D84** (2011) 026011, arXiv:1011.4521 [hep-th].

[93] N. Kaloper, A. Lawrence, and L. Sorbo, "An Ignoble Approach to Large Field Inflation," *JCAP* **1103** (2011) 023, arXiv:1101.0026 [hep-th].

[94] S. Dubovsky, A. Lawrence, and M. M. Roberts, "Axion monodromy in a model of holographic gluodynamics," *JHEP* **1202** (2012) 053, arXiv:1105.3740 [hep-th].

[95] N. Kaloper and A. Lawrence, "Natural chaotic inflation and ultraviolet sensitivity," *Phys.Rev.* **D90** no. 2, (2014) 023506, arXiv:1404.2912 [hep-th].

[96] L. McAllister, E. Silverstein, A. Westphal, and T. Wrase, "The Powers of Monodromy," *JHEP* **1409** (2014) 123, arXiv:1405.3652 [hep-th].

[97] E. Silverstein and A. Westphal, "Monodromy in the CMB: Gravity Waves and String Inflation," *Phys.Rev.* **D78** (2008) 106003, arXiv:0803.3085 [hep-th].

[98] L. McAllister, E. Silverstein, and A. Westphal, "Gravity Waves and Linear Inflation from Axion Monodromy," *Phys.Rev.* **D82** (2010) 046003, arXiv:0808.0706 [hep-th].

[99] M. Dodelson, X. Dong, E. Silverstein, and G. Torroba, "New solutions with accelerated expansion in string theory," *JHEP* **1412** (2014) 050, arXiv:1310.5297 [hep-th].

[100] A. Einstein, "On the Foundations of the Generalized Theory of Relativity and the Theory of Gravitation," *Phys.Z.* **15** (1914) 176–180.

[101] E. Dudas, L. Heurtier, and Y. Mambrini, "Generating X-ray lines from annihilating dark matter," *Phys.Rev.* **D90** (2014) 035002, arXiv:1404.1927 [hep-ph].

[102] E. Dudas, L. Heurtier, Y. Mambrini, and B. Zaldivar, "Extra U(1), effective operators, anomalies and dark matter," *JHEP* **1311** (2013) 083, arXiv:1307.0005 [hep-ph].

[103] J. Oort, "The force exerted by the stellar system in the direction perpendicular to the galactic plane and some related problems," *Bull. Astron. Inst. Netherlands* **6** (1932) 249.

[104] K. Begeman, A. Broeils, and R. Sanders, "Extended rotation curves of spiral galaxies: Dark haloes and modified dynamics," *Mon.Not.Roy.Astron.Soc.* **249** (1991) 523.

[105] V. C. Rubin and J. Ford, W. Kent, "Rotation of the Andromeda Nebula from a Spectroscopic Survey of Emission Regions," *Astrophys.J.* **159** (1970) 379–403.

[106] J. F. Navarro, C. S. Frenk, and S. D. White, "The Structure of cold dark matter halos," *Astrophys.J.* **462** (1996) 563–575, arXiv:astro-ph/9508025 [astro-ph].

[107] A. Einstein, "Covariance Properties of the Field Equations of the Theory of Gravitation Based on the Generalized Theory of Relativity," *Z.Math.Phys.* **63** (1914) 215–225.

[108] F. Dyson, A. Eddington, and C. Davidson, "A determination of the deflection of light by the sun's gravitational field, from observations made at the total eclipse of May 29, 1919," *Mem. R. Astron. Soc.* **62** (1920) 291.

[109] D. Clowe, A. Gonzalez, and M. Markevitch, "Weak lensing mass reconstruction of the interacting cluster 1E0657-558: Direct evidence for the existence of dark matter," *Astrophys.J.* **604** (2004) 596–603, arXiv:astro-ph/0312273 [astro-ph].

[110] **Chandra Telescope** Collaboration, "http://chandra.harvard.edu /photo/2006/1e0657/ ; http://chandra.harvard.edu /press/06releases/press082106.html,".

[111] P. Langacker, "The Physics of Heavy Z' Gauge Bosons," *Rev.Mod.Phys.* **81** (2009) 1199–1228, arXiv:0801.1345 [hep-ph].

[112] T. G. Rizzo, "Z' phenomenology and the LHC," arXiv:hep-ph/0610104 [hep-ph].

[113] M. Carena, A. Daleo, B. A. Dobrescu, and T. M. Tait, "Z' gauge bosons at the Tevatron," *Phys.Rev.* **D70** (2004) 093009, arXiv:hep-ph/0408098 [hep-ph].

[114] E. Salvioni, G. Villadoro, and F. Zwirner, "Minimal Z-prime models: Present bounds and early LHC reach," *JHEP* **0911** (2009) 068, arXiv:0909.1320 [hep-ph].

[115] E. Salvioni, A. Strumia, G. Villadoro, and F. Zwirner, "Non-universal minimal Z' models: present bounds and early LHC reach," *JHEP* **1003** (2010) 010, arXiv:0911.1450 [hep-ph].

[116] M. Cvetic and P. Langacker, "Implications of Abelian extended gauge structures from string models," *Phys.Rev.* **D54** (1996) 3570–3579, arXiv:hep-ph/9511378 [hep-ph].

[117] M. Cvetic and P. Langacker, "New gauge bosons from string models," *Mod.Phys.Lett.* **A11** (1996) 1247–1262, arXiv:hep-ph/9602424 [hep-ph].

[118] M. Cvetic, D. A. Demir, J. Espinosa, L. Everett, and P. Langacker, "Electroweak breaking and the mu problem in supergravity models with an additional U(1)," *Phys.Rev.* **D56** (1997) 2861, arXiv:hep-ph/9703317 [hep-ph].

[119] D. Ghilencea, L. Ibanez, N. Irges, and F. Quevedo, "TeV scale Z-prime bosons from D-branes," *JHEP* **0208** (2002) 016, arXiv:hep-ph/0205083 [hep-ph].

[120] P. Anastasopoulos, "Anomalous U(1)'s, Chern-Simons couplings and the Standard Model," *Fortsch.Phys.* **55** (2007) 633–638, arXiv:hep-th/0701114 [hep-th].

[121] C. Coriano, N. Irges, and E. Kiritsis, "On the effective theory of low scale orientifold string vacua," *Nucl.Phys.* **B746** (2006) 77–135, arXiv:hep-ph/0510332 [hep-ph].

[122] P. Anastasopoulos, F. Fucito, A. Lionetto, G. Pradisi, A. Racioppi, *et al.*, "Minimal Anomalous U(1)-prime Extension of the MSSM," *Phys.Rev.* **D78** (2008) 085014, arXiv:0804.1156 [hep-th].

[123] C. Coriano, N. Irges, and S. Morelli, "Stuckelberg axions and the effective action of anomalous Abelian models. 1. A Unitarity analysis of the Higgs-axion mixing," *JHEP* **0707** (2007) 008, arXiv:hep-ph/0701010 [hep-ph].

[124] N. Irges, C. Coriano, and S. Morelli, "Stuckelberg Axions and the Effective Action of Anomalous Abelian Models 2. A SU(3)C x SU(2)W x U(1)Y x U(1)B model and its signature at the LHC," *Nucl.Phys.* **B789** (2008) 133–174, arXiv:hep-ph/0703127 [HEP-PH].

[125] C. Coriano, M. Guzzi, and S. Morelli, "Unitarity Bounds for Gauged Axionic Interactions and the Green-Schwarz Mechanism," *Eur.Phys.J.* **C55** (2008) 629–652, arXiv:0801.2949 [hep-ph].

[126] J. Kumar, A. Rajaraman, and J. D. Wells, "Probing the Green-Schwarz Mechanism at the Large Hadron Collider," *Phys.Rev.* **D77** (2008) 066011, arXiv:0707.3488 [hep-ph].

[127] I. Antoniadis, A. Boyarsky, S. Espahbodi, O. Ruchayskiy, and J. D. Wells, "Anomaly driven signatures of new invisible physics at the Large Hadron Collider," *Nucl.Phys.* **B824** (2010) 296–313, arXiv:0901.0639 [hep-ph].

[128] Y. Mambrini, "A Clear Dark Matter gamma ray line generated by the Green-Schwarz mechanism," *JCAP* **0912** (2009) 005, arXiv:0907.2918 [hep-ph].

[129] M. Goodsell, J. Jaeckel, J. Redondo, and A. Ringwald, "Naturally Light Hidden Photons in LARGE Volume String Compactifications," *JHEP* **0911** (2009) 027, arXiv:0909.0515 [hep-ph].

[130] G. Shiu, P. Soler, and F. Ye, "Millicharged Dark Matter in Quantum Gravity and String Theory," *Phys.Rev.Lett.* **110** no. 24, (2013) 241304, arXiv:1302.5471 [hep-th].

[131] M. Cvetic, J. Halverson, and H. Piragua, "Stringy Hidden Valleys," *JHEP* **1302** (2013) 005, arXiv:1210.5245 [hep-ph].

[132] B. Kors and P. Nath, "A Supersymmetric Stueckelberg U(1) extension of the MSSM," *JHEP* **0412** (2004) 005, arXiv:hep-ph/0406167 [hep-ph].

[133] D. Feldman, Z. Liu, and P. Nath, "The Stueckelberg Z-prime Extension with Kinetic Mixing and Milli-Charged Dark Matter From the Hidden Sector," *Phys.Rev.* **D75** (2007) 115001, arXiv:hep-ph/0702123 [HEP-PH].

[134] D. Feldman, B. Kors, and P. Nath, "Extra-weakly Interacting Dark Matter," *Phys.Rev.* **D75** (2007) 023503, arXiv:hep-ph/0610133 [hep-ph].

[135] E. Dudas, Y. Mambrini, S. Pokorski, and A. Romagnoni, "(In)visible Z-prime and dark matter," *JHEP* **0908** (2009) 014, arXiv:0904.1745 [hep-ph].

[136] E. Dudas, Y. Mambrini, S. Pokorski, and A. Romagnoni, "Extra U(1) as natural source of a monochromatic gamma ray line," *JHEP* **1210** (2012) 123, arXiv:1205.1520 [hep-ph].

[137] C. Weniger, "A Tentative Gamma-Ray Line from Dark Matter Annihilation at the Fermi Large Area Telescope," *JCAP* **1208** (2012) 007, arXiv:1204.2797 [hep-ph].

[138] C. Jackson, G. Servant, G. Shaughnessy, T. M. Tait, and M. Taoso, "Higgs in Space!," *JCAP* **1004** (2010) 004, arXiv:0912.0004 [hep-ph].

[139] C. Jackson, G. Servant, G. Shaughnessy, T. M. Tait, and M. Taoso, "Gamma-ray lines and One-Loop Continuum from s-channel Dark Matter Annihilations," *JCAP* **1307** (2013) 021, arXiv:1302.1802 [hep-ph].

[140] L. Landau, "On the angular momentum of a two-photon system," *Dokl.Akad.Nauk Ser.Fiz.* **60** (1948) 207–209.

[141] X. Chu, T. Hambye, T. Scarna, and M. H. Tytgat, "What if Dark Matter Gamma-Ray Lines come with Gluon Lines?," *Phys.Rev.* **D86** (2012) 083521, arXiv:1206.2279 [hep-ph].

[142] **Planck** Collaboration, P. Ade *et al.*, "Planck 2013 results. XVI. Cosmological parameters," *Astron.Astrophys.* **571** (2014) A16, arXiv:1303.5076 [astro-ph.CO].

[143] **WMAP** Collaboration, G. Hinshaw *et al.*, "Nine-Year Wilkinson Microwave Anisotropy Probe (WMAP) Observations: Cosmological Parameter Results," *Astrophys.J.Suppl.* **208** (2013) 19, arXiv:1212.5226 [astro-ph.CO].

[144] D. Hooper, C. Kelso, and F. S. Queiroz, "Stringent and Robust Constraints on the Dark Matter Annihilation Cross Section From the Region of the Galactic Center," *Astropart.Phys.* **46** (2013) 55–70, arXiv:1209.3015 [astro-ph.HE].

[145] **Fermi-LAT** Collaboration, M. Ackermann *et al.*, "Constraints on the Galactic Halo Dark Matter from Fermi-LAT Diffuse Measurements," *Astrophys.J.* **761** (2012) 91, arXiv:1205.6474 [astro-ph.CO].

[146] **Fermi-LAT** Collaboration, A. Drlica-Wagner, "Constraints on Dark Matter and Supersymmetry from LAT Observations of Dwarf Galaxies," arXiv:1210.5558 [astro-ph.HE].

[147] A. Egorov and E. Pierpaoli, "Constraints on dark matter annihilation by radio observations of M31," *Phys.Rev.* **D88** no. 2, (2013) 023504, arXiv:1304.0517 [astro-ph.CO].

[148] G. Belanger, F. Boudjema, P. Brun, A. Pukhov, S. Rosier-Lees, *et al.*, "Indirect search for dark matter with micrOMEGAs2.4," *Comput.Phys.Commun.* **182** (2011) 842–856, arXiv:1004.1092 [hep-ph].

[149] Y. Bai, P. J. Fox, and R. Harnik, "The Tevatron at the Frontier of Dark Matter Direct Detection," *JHEP* **1012** (2010) 048, arXiv:1005.3797 [hep-ph].

[150] P. J. Fox, R. Harnik, J. Kopp, and Y. Tsai, "LEP Shines Light on Dark Matter," *Phys.Rev.* **D84** (2011) 014028, arXiv:1103.0240 [hep-ph].

[151] H. M. Lee, M. Park, and V. Sanz, "Interplay between Fermi gamma-ray lines and collider searches," *JHEP* **1303** (2013) 052, arXiv:1212.5647 [hep-ph].

[152] Y. Mambrini and B. Zaldivar, "When LEP and Tevatron combined with WMAP and XENON100 shed light on the nature of Dark Matter," *JCAP* **1110** (2011) 023, arXiv:1106.4819 [hep-ph].

[153] **ATLAS** Collaboration, "Search for New Phenomena in Monojet plus Missing Transverse Momentum Final States using 10fb-1 of pp Collisions at sqrts=8 TeV with the ATLAS detector at the LHC,". http://inspirehep.net/record/1230004/files/ATLAS-CONF-2012-147.pdf.

[154] **CMS** Collaboration, "Search for new physics in monojet events in pp collisions at sqrt(s)= 8 TeV,". http://inspirehep.net/record/1230233/files/EXO-12-048-pas.pdf.

[155] P. Anastasopoulos, M. Bianchi, E. Dudas, and E. Kiritsis, "Anomalies, anomalous U(1)'s and generalized Chern-Simons terms," *JHEP* **0611** (2006) 057, arXiv:hep-th/0605225 [hep-th].

[156] **XENON100** Collaboration, E. Aprile *et al.*, "Dark Matter Results from 225 Live Days of XENON100 Data," *Phys.Rev.Lett.* **109** (2012) 181301, arXiv:1207.5988 [astro-ph.CO].

[157] **LUX** Collaboration, D. Akerib *et al.*, "First results from the LUX dark matter experiment at the Sanford Underground Research Facility," *Phys.Rev.Lett.* **112** (2014) 091303, arXiv:1310.8214 [astro-ph.CO].

[158] **Fermi-LAT** Collaboration, M. Ackermann *et al.*, "Dark matter constraints from observations of 25 Milky Way satellite galaxies with the Fermi Large Area Telescope," *Phys.Rev.* **D89** (2014) 042001, arXiv:1310.0828 [astro-ph.HE].

[159] **Fermi-LAT** Collaboration, M. Ackermann *et al.*, "Search for gamma-ray spectral lines with the Fermi large area telescope and dark matter implications," *Phys.Rev.* **D88** (2013) 082002, arXiv:1305.5597 [astro-ph.HE].

[160] G. A. Gómez-Vargas, M. A. Sánchez-Conde, J.-H. Huh, M. Peiró, F. Prada, *et al.*, "Constraints on WIMP annihilation for contracted dark matterin the inner Galaxy with the Fermi-LAT," *JCAP* **1310** (2013) 029, arXiv:1308.3515 [astro-ph.HE].

[161] A. Kusenko, "Sterile neutrinos: The Dark side of the light fermions," *Phys.Rept.* **481** (2009) 1–28, arXiv:0906.2968 [hep-ph].

[162] E. W. Kolb, D. J. Chung, and A. Riotto, "WIMPzillas!," arXiv:hep-ph/9810361 [hep-ph].

[163] L. J. Hall, K. Jedamzik, J. March-Russell, and S. M. West, "Freeze-In Production of FIMP Dark Matter," *JHEP* **1003** (2010) 080, arXiv:0911.1120 [hep-ph].

[164] J. McDonald, "Thermally generated gauge singlet scalars as selfinteracting dark matter," *Phys.Rev.Lett.* **88** (2002) 091304, arXiv:hep-ph/0106249 [hep-ph].

[165] X. Chu, T. Hambye, and M. H. Tytgat, "The Four Basic Ways of Creating Dark Matter Through a Portal," *JCAP* **1205** (2012) 034, arXiv:1112.0493 [hep-ph].

[166] C. E. Yaguna, "An intermediate framework between WIMP, FIMP, and EWIP dark matter," *JCAP* **1202** (2012) 006, arXiv:1111.6831 [hep-ph].

[167] X. Chu, Y. Mambrini, J. Quevillon, and B. Zaldivar, "Thermal and non-thermal production of dark matter via Z'-portal(s)," *JCAP* **1401** no. 01, (2014) 034, arXiv:1306.4677 [hep-ph].

[168] A. Goudelis, Y. Mambrini, and C. Yaguna, "Antimatter signals of singlet scalar dark matter," *JCAP* **0912** (2009) 008, arXiv:0909.2799 [hep-ph].

[169] Y. Mambrini, K. A. Olive, J. Quevillon, and B. Zaldivar, "Gauge Coupling Unification and Nonequilibrium Thermal Dark Matter," *Phys.Rev.Lett.* **110** no. 24, (2013) 241306, arXiv:1302.4438 [hep-ph].

[170] L. Dugger, T. E. Jeltema, and S. Profumo, "Constraints on Decaying Dark Matter from Fermi Observations of Nearby Galaxies and Clusters," *JCAP* **1012** (2010) 015, arXiv:1009.5988 [astro-ph.HE].

[171] E. Bulbul, M. Markevitch, A. Foster, R. K. Smith, M. Loewenstein, *et al.*, "Detection of An Unidentified Emission Line in the Stacked X-ray spectrum of Galaxy Clusters," *Astrophys.J.* **789** (2014) 13, arXiv:1402.2301 [astro-ph.CO].

[172] A. Boyarsky, O. Ruchayskiy, D. Iakubovskyi, and J. Franse, "Unidentified Line in X-Ray Spectra of the Andromeda Galaxy and Perseus Galaxy Cluster," *Phys.Rev.Lett.* **113** (2014) 251301, arXiv:1402.4119 [astro-ph.CO].

[173] A. Boyarsky, J. Franse, D. Iakubovskyi, and O. Ruchayskiy, "Checking the dark matter origin of 3.53 keV line with the Milky Way center," arXiv:1408.2503 [astro-ph.CO].

[174] T. Jeltema and S. Profumo, "Reply to Two Comments on "Dark matter searches going bananas the contribution of Potassium (and Chlorine) to the 3.5 keV line"," arXiv:1411.1759 [astro-ph.HE].

[175] E. Bulbul, M. Markevitch, A. R. Foster, R. K. Smith, M. Loewenstein, *et al.*, "Comment on "Dark matter searches going bananas: the contribution of Potassium (and Chlorine) to the 3.5 keV line"," arXiv:1409.4143 [astro-ph.HE].

[176] A. Boyarsky, J. Franse, D. Iakubovskyi, and O. Ruchayskiy, "Comment on the paper "Dark matter searches going bananas: the contribution of Potassium (and Chlorine) to the 3.5 keV line" by T. Jeltema and S. Profumo," arXiv:1408.4388 [astro-ph.CO].

[177] T. E. Jeltema and S. Profumo, "Discovery of a 3.5 keV line in the Galactic Center and a Critical Look at the Origin of the Line Across Astronomical Targets," arXiv:1408.1699 [astro-ph.HE].

[178] A. Boyarsky, O. Ruchayskiy, and M. Shaposhnikov, "The Role of sterile neutrinos in cosmology and astrophysics," *Ann.Rev.Nucl.Part.Sci.* **59** (2009) 191–214, arXiv:0901.0011 [hep-ph].

[179] H. Ishida, K. S. Jeong, and F. Takahashi, "7 keV sterile neutrino dark matter from split flavor mechanism," *Phys.Lett.* **B732** (2014) 196–200, arXiv:1402.5837 [hep-ph].

[180] K. N. Abazajian, "Resonantly Produced 7 keV Sterile Neutrino Dark Matter Models and the Properties of Milky Way Satellites," *Phys.Rev.Lett.* **112** no. 16, (2014) 161303, arXiv:1403.0954 [astro-ph.CO].

[181] F. Bezrukov and D. Gorbunov, "Relic Gravity Waves and 7 keV Dark Matter from a GeV scale inflaton," *Phys.Lett.* **B736** (2014) 494–498, arXiv:1403.4638 [hep-ph].

[182] T. Tsuyuki, "Neutrino masses, leptogenesis, and sterile neutrino dark matter," *Phys.Rev.* **D90** no. 1, (2014) 013007, arXiv:1403.5053 [hep-ph].

[183] K. P. Modak, "3.5 keV X-ray Line Signal from Decay of Right-Handed Neutrino due to Transition Magnetic Moment," *JHEP* **1503** (2015) 064, arXiv:1404.3676 [hep-ph].

[184] D. J. Robinson and Y. Tsai, "Dynamical framework for KeV Dirac neutrino warm dark matter," *Phys.Rev.* **D90** no. 4, (2014) 045030, arXiv:1404.7118 [hep-ph].

[185] H. Ishida and H. Okada, "3.55 keV X-ray Line Interpretation in Radiative Neutrino Model," arXiv:1406.5808 [hep-ph].

[186] T. Higaki, K. S. Jeong, and F. Takahashi, "The 7 keV axion dark matter and the X-ray line signal," *Phys.Lett.* **B733** (2014) 25–31, arXiv:1402.6965 [hep-ph].

[187] J. Jaeckel, J. Redondo, and A. Ringwald, "3.55 keV hint for decaying axionlike particle dark matter," *Phys.Rev.* **D89** (2014) 103511, arXiv:1402.7335 [hep-ph].

[188] H. M. Lee, S. C. Park, and W.-I. Park, "Cluster X-ray line at 3.5 keV from axion-like dark matter," *Eur.Phys.J.* **C74** (2014) 3062, arXiv:1403.0865 [astro-ph.CO].

[189] M. Cicoli, J. P. Conlon, M. C. D. Marsh, and M. Rummel, "3.55 keV photon line and its morphology from a 3.55 keV axionlike particle line," *Phys.Rev.* **D90** (2014) 023540, arXiv:1403.2370 [hep-ph].

[190] J. P. Conlon and F. V. Day, "3.55 keV photon lines from axion to photon conversion in the Milky Way and M31," *JCAP* **1411** no. 11, (2014) 033, arXiv:1404.7741 [hep-ph].

[191] K. Babu and R. N. Mohapatra, "7 keV Scalar Dark Matter and the Anomalous Galactic X-ray Spectrum," *Phys.Rev.* **D89** (2014) 115011, arXiv:1404.2220 [hep-ph].

[192] N. Chen, Z. Liu, and P. Nath, "3.5 keV galactic emission line as a signal from the hidden sector," *Phys.Rev.* **D90** no. 3, (2014) 035009, arXiv:1406.0687 [hep-ph].

[193] J.-C. Park, S. C. Park, and K. Kong, "X-ray line signal from 7 keV axino dark matter decay," *Phys.Lett.* **B733** (2014) 217–220, arXiv:1403.1536 [hep-ph].

[194] K.-Y. Choi and O. Seto, "X-ray line signal from decaying axino warm dark matter," *Phys.Lett.* **B735** (2014) 92–94, arXiv:1403.1782 [hep-ph].

[195] S. P. Liew, "Axino dark matter in light of an anomalous X-ray line," *JCAP* **1405** (2014) 044, arXiv:1403.6621 [hep-ph].

[196] K. Nakayama, F. Takahashi, and T. T. Yanagida, "Anomaly-free flavor models for Nambu–Goldstone bosons and the 3.5keV X-ray line signal," *Phys.Lett.* **B734** (2014) 178–182, arXiv:1403.7390 [hep-ph].

[197] C. Kolda and J. Unwin, "X-ray lines from R-parity violating decays of keV sparticles," *Phys.Rev.* **D90** (2014) 023535, arXiv:1403.5580 [hep-ph].

[198] N. E. Bomark and L. Roszkowski, "3.5 keV x-ray line from decaying gravitino dark matter," *Phys.Rev.* **D90** (2014) 011701, arXiv:1403.6503 [hep-ph].

[199] B. Dutta, I. Gogoladze, R. Khalid, and Q. Shafi, "3.5 keV X-ray line and R-Parity Conserving Supersymmetry," *JHEP* **1411** (2014) 018, arXiv:1407.0863 [hep-ph].

[200] S. Demidov and D. Gorbunov, "SUSY in the sky or a keV signature of sub-GeV gravitino dark matter," *Phys.Rev.* **D90** (2014) 035014, arXiv:1404.1339 [hep-ph].

[201] Z. Kang, P. Ko, T. Li, and Y. Liu, "Natural X-ray Lines from the Low Scale Supersymmetry Breaking," *Phys.Lett.* **B742** (2015) 249–255, arXiv:1403.7742 [hep-ph].

[202] R. Krall, M. Reece, and T. Roxlo, "Effective field theory and keV lines from dark matter," *JCAP* **1409** (2014) 007, arXiv:1403.1240 [hep-ph].

[203] C. El Aisati, T. Hambye, and T. Scarnà, "Can a millicharged dark matter particle emit an observable γ-ray line?," *JHEP* **1408** (2014) 133, arXiv:1403.1280 [hep-ph].

[204] J. M. Cline, Y. Farzan, Z. Liu, G. D. Moore, and W. Xue, "3.5 keV x rays as the "21 cm line" of dark atoms, and a link to light sterile neutrinos," *Phys.Rev.* **D89** (2014) 121302, arXiv:1404.3729 [hep-ph].

[205] H. M. Lee, "Magnetic dark matter for the X-ray line at 3.55 keV," *Phys.Lett.* **B738** (2014) 118–122, arXiv:1404.5446 [hep-ph].

[206] F. S. Queiroz and K. Sinha, "The Poker Face of the Majoron Dark Matter Model: LUX to keV Line," *Phys.Lett.* **B735** (2014) 69–74, arXiv:1404.1400 [hep-ph].

[207] R. Allahverdi, B. Dutta, and Y. Gao, "keV Photon Emission from Light Nonthermal Dark Matter," *Phys.Rev.* **D89** (2014) 127305, arXiv:1403.5717 [hep-ph].

[208] C.-W. Chiang and T. Yamada, "3.5 keV X-ray line from nearly-degenerate WIMP dark matter decays," *JHEP* **1409** (2014) 006, arXiv:1407.0460 [hep-ph].

[209] S. Baek, P. Ko, and W.-I. Park, "The 3.5 keV X-ray line signature from annihilating and decaying dark matter in Weinberg model," arXiv:1405.3730 [hep-ph].

[210] D. P. Finkbeiner and N. Weiner, "An X-Ray Line from eXciting Dark Matter," arXiv:1402.6671 [hep-ph].

[211] H. Okada and T. Toma, "3.55 keV X-ray Line Signal from Excited Dark Matter in Radiative Neutrino Model," *Phys.Lett.* **B737** (2014) 162–166, arXiv:1404.4795 [hep-ph].

[212] M. R. Lovell, C. S. Frenk, V. R. Eke, A. Jenkins, L. Gao, *et al.*, "The properties of warm dark matter haloes," *Mon.Not.Roy.Astron.Soc.* **439** no. 1, (2014) 300–317, arXiv:1308.1399 [astro-ph.CO].

[213] M. T. Frandsen, F. Sannino, I. M. Shoemaker, and O. Svendsen, "X-ray Lines from Dark Matter: The Good, The Bad, and The Unlikely," *JCAP* **1405** (2014) 033, arXiv:1403.1570 [hep-ph].

[214] J. Goodman, M. Ibe, A. Rajaraman, W. Shepherd, T. M. Tait, *et al.*, "Constraints on Dark Matter from Colliders," *Phys.Rev.* **D82** (2010) 116010, arXiv:1008.1783 [hep-ph].

[215] H. Dreiner, M. Huck, M. Krämer, D. Schmeier, and J. Tattersall, "Illuminating Dark Matter at the ILC," *Phys.Rev.* **D87** no. 7, (2013) 075015, arXiv:1211.2254 [hep-ph].

[216] K. Cheung, P.-Y. Tseng, Y.-L. S. Tsai, and T.-C. Yuan, "Global Constraints on Effective Dark Matter Interactions: Relic Density, Direct Detection, Indirect Detection, and Collider," *JCAP* **1205** (2012) 001, arXiv:1201.3402 [hep-ph].

[217] M. Papucci, A. Vichi, and K. M. Zurek, "Monojet versus the rest of the world I: t-channel models," *JHEP* **1411** (2014) 024, arXiv:1402.2285 [hep-ph].

[218] T. Lin, H.-B. Yu, and K. M. Zurek, "On Symmetric and Asymmetric Light Dark Matter," *Phys.Rev.* **D85** (2012) 063503, arXiv:1111.0293 [hep-ph].

[219] S. Galli, F. Iocco, G. Bertone, and A. Melchiorri, "Updated CMB constraints on Dark Matter annihilation cross-sections," *Phys.Rev.* **D84** (2011) 027302, arXiv:1106.1528 [astro-ph.CO].

[220] M. Pospelov, A. Ritz, and M. B. Voloshin, "Secluded WIMP Dark Matter," *Phys.Lett.* **B662** (2008) 53–61, arXiv:0711.4866 [hep-ph].

[221] M. Kleban and R. Rabadan, "Collider bounds on pseudoscalars coupling to gauge bosons," arXiv:hep-ph/0510183 [hep-ph].

[222] G. Raffelt, "Stars as laboratories for fundamental physics," *Chicago : University of Chicago Press* (1996) .

[223] J. Hewett, H. Weerts, R. Brock, J. Butler, B. Casey, *et al.*, "Fundamental Physics at the Intensity Frontier," arXiv:1205.2671 [hep-ex].

[224] R. Essig, R. Harnik, J. Kaplan, and N. Toro, "Discovering New Light States at Neutrino Experiments," *Phys.Rev.* **D82** (2010) 113008, arXiv:1008.0636 [hep-ph].

[225] D. Cadamuro and J. Redondo, "Cosmological bounds on pseudo Nambu-Goldstone bosons," *JCAP* **1202** (2012) 032, arXiv:1110.2895 [hep-ph].

[226] A. Ringwald, "Exploring the Role of Axions and Other WISPs in the Dark Universe," *Phys.Dark Univ.* **1** (2012) 116–135, arXiv:1210.5081 [hep-ph].

[227] E. Dwek and F. Krennrich, "The Extragalactic Background Light and the Gamma-ray Opacity of the Universe," *Astropart.Phys.* **43** (2013) 112–133, arXiv:1209.4661 [astro-ph.CO].

[228] C. Boehm, T. Ensslin, and J. Silk, "Can Annihilating dark matter be lighter than a few GeVs?," *J.Phys.* **G30** (2004) 279–286, arXiv:astro-ph/0208458 [astro-ph].

[229] S. Das and K. Sigurdson, "Cosmological Limits on Hidden Sector Dark Matter," *Phys.Rev.* **D85** (2012) 063510, arXiv:1012.4458 [astro-ph.CO].

[230] J. L. Feng, H. Tu, and H.-B. Yu, "Thermal Relics in Hidden Sectors," *JCAP* **0810** (2008) 043, arXiv:0808.2318 [hep-ph].

[231] M. Drewes, "The Phenomenology of Right Handed Neutrinos," *Int.J.Mod.Phys.* **E22** (2013) 1330019, arXiv:1303.6912 [hep-ph].

[232] J. Kopp, P. A. N. Machado, M. Maltoni, and T. Schwetz, "Sterile Neutrino Oscillations: The Global Picture," *JHEP* **1305** (2013) 050, arXiv:1303.3011 [hep-ph].

[233] K. Sigurdson, "Hidden Hot Dark Matter as Cold Dark Matter," arXiv:0912.2346 [astro-ph.CO].

[234] A. Boyarsky, J. Lesgourgues, O. Ruchayskiy, and M. Viel, "Lyman-alpha constraints on warm and on warm-plus-cold dark matter models," *JCAP* **0905** (2009) 012, arXiv:0812.0010 [astro-ph].

[235] S. Tremaine and J. Gunn, "Dynamical Role of Light Neutral Leptons in Cosmology," *Phys.Rev.Lett.* **42** (1979) 407–410.

[236] M. Kobayashi and T. Maskawa, "CP Violation in the Renormalizable Theory of Weak Interaction," *Prog.Theor.Phys.* **49** (1973) 652–657.

[237] N. Cabibbo, "Unitary Symmetry and Leptonic Decays," *Phys.Rev.Lett.* **10** (1963) 531–533.

[238] L. Wolfenstein, "Parametrization of the Kobayashi-Maskawa Matrix," *Phys.Rev.Lett.* **51** (1983) 1945.

[239] **CKMfitter Group** Collaboration, J. C. et al., "Dark matter constraints from observations of 25 Milky Way satellite galaxies with the Fermi Large Area Telescope," *Eur. Phys. J. C* **41** (2005) 1–131, arXiv:hep-ph/0406184.

[240] C. Froggatt and H. B. Nielsen, "Hierarchy of Quark Masses, Cabibbo Angles and CP Violation," *Nucl.Phys.* **B147** (1979) 277.

[241] M. Leurer, Y. Nir, and N. Seiberg, "Mass matrix models: The Sequel," *Nucl.Phys.* **B420** (1994) 468–504, arXiv:hep-ph/9310320 [hep-ph].

[242] E. Dudas, S. Pokorski, and C. A. Savoy, "Yukawa matrices from a spontaneously broken Abelian symmetry," *Phys.Lett.* **B356** (1995) 45–55, arXiv:hep-ph/9504292 [hep-ph].

[243] S. L. Glashow, J. Iliopoulos, and L. Maiani, "Weak Interactions with Lepton-Hadron Symmetry," *PRD* **2** (Oct, 1970) 1285–1292.

[244] **MEGA Collaboration** Collaboration, M. B. et al., "Dark matter constraints from observations of 25 Milky Way satellite galaxies with the Fermi Large Area Telescope," *Phys. Rev. Lett.* **83** (1999) 1521, arXiv:hep-ex/9905013.

[245] **MEGA Collaboration** Collaboration, M. B. et al., "Dark matter constraints from observations of 25 Milky Way satellite galaxies with the Fermi Large Area Telescope," *Phys. Rev. D* **65** (2002) 112002, arXiv:hep-ex/0111030.

[246] P. Fayet, "MASSIVE GLUINOS," *Phys.Lett.* **B78** (1978) 417.

[247] J. Polchinski and L. Susskind, "Breaking of Supersymmetry at Intermediate-Energy," *Phys.Rev.* **D26** (1982) 3661.

[248] L. Hall and L. Randall, "U(1)-R symmetric supersymmetry," *Nucl.Phys.* **B352** (1991) 289–308.

[249] A. E. Nelson, N. Rius, V. Sanz, and M. Unsal, "The Minimal supersymmetric model without a mu term," *JHEP* **0208** (2002) 039, arXiv:hep-ph/0206102 [hep-ph].

[250] P. J. Fox, A. E. Nelson, and N. Weiner, "Dirac gaugino masses and supersoft supersymmetry breaking," *JHEP* **0208** (2002) 035, arXiv:hep-ph/0206096 [hep-ph].

[251] I. Antoniadis, A. Delgado, K. Benakli, M. Quiros, and M. Tuckmantel, "Splitting extended supersymmetry," *Phys.Lett.* **B634** (2006) 302–306, arXiv:hep-ph/0507192 [hep-ph].

[252] I. Antoniadis, K. Benakli, A. Delgado, and M. Quiros, "A New gauge mediation theory," *Adv.Stud.Theor.Phys.* **2** (2008) 645–672, arXiv:hep-ph/0610265 [hep-ph].

[253] G. D. Kribs, E. Poppitz, and N. Weiner, "Flavor in supersymmetry with an extended R-symmetry," *Phys.Rev.* **D78** (2008) 055010, arXiv:0712.2039 [hep-ph].

[254] S. D. L. Amigo, A. E. Blechman, P. J. Fox, and E. Poppitz, "R-symmetric gauge mediation," *JHEP* **0901** (2009) 018, arXiv:0809.1112 [hep-ph].

[255] A. E. Blechman, "R-symmetric Gauge Mediation and the Minimal R-Symmetric Supersymmetric Standard Model," *Mod.Phys.Lett.* **A24** (2009) 633–646, arXiv:0903.2822 [hep-ph].

[256] T. Plehn and T. M. Tait, "Seeking Sgluons," *J.Phys.* **G36** (2009) 075001, arXiv:0810.3919 [hep-ph].

[257] K. Benakli and M. Goodsell, "Dirac Gauginos in General Gauge Mediation," *Nucl.Phys.* **B816** (2009) 185–203, arXiv:0811.4409 [hep-ph].

[258] G. Belanger, K. Benakli, M. Goodsell, C. Moura, and A. Pukhov, "Dark Matter with Dirac and Majorana Gaugino Masses," *JCAP* **0908** (2009) 027, arXiv:0905.1043 [hep-ph].

[259] K. Benakli and M. Goodsell, "Dirac Gauginos and Kinetic Mixing," *Nucl.Phys.* **B830** (2010) 315–329, arXiv:0909.0017 [hep-ph].

[260] S. Choi, J. Kalinowski, J. Kim, and E. Popenda, "Scalar gluons and Dirac gluinos at the LHC," *Acta Phys.Polon.* **B40** (2009) 2913–2922, arXiv:0911.1951 [hep-ph].

[261] K. Benakli and M. Goodsell, "Dirac Gauginos, Gauge Mediation and Unification," *Nucl.Phys.* **B840** (2010) 1–28, arXiv:1003.4957 [hep-ph].

[262] S. Choi, D. Choudhury, A. Freitas, J. Kalinowski, J. Kim, *et al.*, "Dirac Neutralinos and Electroweak Scalar Bosons of N=1/N=2 Hybrid Supersymmetry at Colliders," *JHEP* **1008** (2010) 025, arXiv:1005.0818 [hep-ph].

[263] L. M. Carpenter, "Dirac Gauginos, Negative Supertraces and Gauge Mediation," *JHEP* **1209** (2012) 102, arXiv:1007.0017 [hep-th].

[264] G. D. Kribs, T. Okui, and T. S. Roy, "Viable Gravity-Mediated Supersymmetry Breaking," *Phys.Rev.* **D82** (2010) 115010, arXiv:1008.1798 [hep-ph].

[265] S. Abel and M. Goodsell, "Easy Dirac Gauginos," *JHEP* **1106** (2011) 064, arXiv:1102.0014 [hep-th].

[266] R. Davies, J. March-Russell, and M. McCullough, "A Supersymmetric One Higgs Doublet Model," *JHEP* **1104** (2011) 108, arXiv:1103.1647 [hep-ph].

[267] K. Benakli, M. D. Goodsell, and A.-K. Maier, "Generating mu and Bmu in models with Dirac Gauginos," *Nucl.Phys.* **B851** (2011) 445–461, arXiv:1104.2695 [hep-ph].

[268] J. Kalinowski, "Higgs bosons of R-symmetric supersymmetric theories," *PoS* **EPS-HEP2011** (2011) 265.

[269] C. Frugiuele and T. Gregoire, "Making the Sneutrino a Higgs with a $U(1)_R$ Lepton Number," *Phys.Rev.* **D85** (2012) 015016, arXiv:1107.4634 [hep-ph].

[270] H. Itoyama and N. Maru, "D-term Dynamical Supersymmetry Breaking Generating Split N=2 Gaugino Masses of Mixed Majorana-Dirac Type," *Int.J.Mod.Phys.* **A27** (2012) 1250159, arXiv:1109.2276 [hep-ph].

[271] H. Itoyama and N. Maru, "D-term Triggered Dynamical Supersymmetry Breaking," *Phys.Rev.* **D88** no. 2, (2013) 025012, arXiv:1301.7548 [hep-ph].

[272] H. Itoyama and N. Maru, "126 GeV Higgs Boson Associated with D-term Triggered Dynamical Supersymmetry Breaking," *Symmetry* **7** no. 1, (2015) 193–205, arXiv:1312.4157 [hep-ph].

[273] K. Rehermann and C. M. Wells, "Weak Scale Leptogenesis, R-symmetry, and a Displaced Higgs," arXiv:1111.0008 [hep-ph].

[274] E. Bertuzzo and C. Frugiuele, "Fitting Neutrino Physics with a $U(1)_R$ Lepton Number," *JHEP* **1205** (2012) 100, arXiv:1203.5340 [hep-ph].

[275] R. Davies, "Dirac gauginos and unification in F-theory," *JHEP* **1210** (2012) 010, arXiv:1205.1942 [hep-th].

[276] R. Argurio, M. Bertolini, L. Di Pietro, F. Porri, and D. Redigolo, "Holographic Correlators for General Gauge Mediation," *JHEP* **1208** (2012) 086, arXiv:1205.4709 [hep-th].

[277] R. Fok, G. D. Kribs, A. Martin, and Y. Tsai, "Electroweak Baryogenesis in R-symmetric Supersymmetry," *Phys.Rev.* **D87** no. 5, (2013) 055018, arXiv:1208.2784 [hep-ph].

[278] R. Argurio, M. Bertolini, L. Di Pietro, F. Porri, and D. Redigolo, "Exploring Holographic General Gauge Mediation," *JHEP* **1210** (2012) 179, arXiv:1208.3615 [hep-th].

[279] C. Frugiuele, T. Gregoire, P. Kumar, and E. Ponton, "'L=R' - $U(1)_R$ as the Origin of Leptonic 'RPV'," *JHEP* **1303** (2013) 156, arXiv:1210.0541 [hep-ph].

[280] C. Frugiuele, T. Gregoire, P. Kumar, and E. Ponton, "'L=R' – $U(1)_R$ Lepton Number at the LHC," *JHEP* **1305** (2013) 012, arXiv:1210.5257 [hep-ph].

[281] K. Benakli, M. D. Goodsell, and F. Staub, "Dirac Gauginos and the 125 GeV Higgs," *JHEP* **1306** (2013) 073, arXiv:1211.0552 [hep-ph].

[282] S. Chakraborty and S. Roy, "Higgs boson mass, neutrino masses and mixing and keV dark matter in an $U(1)_R-$ lepton number model," *JHEP* **1401** (2014) 101, arXiv:1309.6538 [hep-ph].

[283] C. Csaki, J. Goodman, R. Pavesi, and Y. Shirman, "The $m_D - b_M$ problem of Dirac gauginos and its solutions," *Phys.Rev.* **D89** no. 5, (2014) 055005, arXiv:1310.4504 [hep-ph].

[284] K. Benakli, M. Goodsell, F. Staub, and W. Porod, "Constrained minimal Dirac gaugino supersymmetric standard model," *Phys.Rev.* **D90** no. 4, (2014) 045017, arXiv:1403.5122 [hep-ph].

[285] I. Antoniadis, K. Benakli, A. Delgado, M. Quiros, and M. Tuckmantel, "Split extended supersymmetry from intersecting branes," *Nucl.Phys.* **B744** (2006) 156–179, arXiv:hep-th/0601003 [hep-th].

[286] I. Jack and D. Jones, "Nonstandard soft supersymmetry breaking," *Phys.Lett.* **B457** (1999) 101–108, arXiv:hep-ph/9903365 [hep-ph].

[287] I. Jack and D. Jones, "Quasiinfrared fixed points and renormalization group invariant trajectories for nonholomorphic soft supersymmetry breaking," *Phys.Rev.* **D61** (2000) 095002, arXiv:hep-ph/9909570 [hep-ph].

[288] M. D. Goodsell, "Two-loop RGEs with Dirac gaugino masses," *JHEP* **1301** (2013) 066, arXiv:1206.6697 [hep-ph].

[289] C. Brust, A. Katz, S. Lawrence, and R. Sundrum, "SUSY, the Third Generation and the LHC," *JHEP* **1203** (2012) 103, arXiv:1110.6670 [hep-ph].

[290] M. Papucci, J. T. Ruderman, and A. Weiler, "Natural SUSY Endures," *JHEP* **1209** (2012) 035, arXiv:1110.6926 [hep-ph].

[291] A. Arvanitaki, M. Baryakhtar, X. Huang, K. van Tilburg, and G. Villadoro, "The Last Vestiges of Naturalness," *JHEP* **1403** (2014) 022, arXiv:1309.3568 [hep-ph].

[292] M. Heikinheimo, M. Kellerstein, and V. Sanz, "How Many Supersymmetries?," *JHEP* **1204** (2012) 043, arXiv:1111.4322 [hep-ph].

[293] G. D. Kribs and A. Martin, "Supersoft Supersymmetry is Super-Safe," *Phys.Rev.* **D85** (2012) 115014, arXiv:1203.4821 [hep-ph].

[294] G. D. Kribs and N. Raj, "Mixed Gauginos Sending Mixed Messages to the LHC," *Phys.Rev.* **D89** no. 5, (2014) 055011, arXiv:1307.7197 [hep-ph].

[295] G. D. Kribs and A. Martin, "Dirac Gauginos in Supersymmetry – Suppressed Jets + MET Signals: A Snowmass Whitepaper," arXiv:1308.3468 [hep-ph].

[296] E. Dudas, M. Goodsell, L. Heurtier, and P. Tziveloglou, "Flavour models with Dirac and fake gluinos," *Nucl.Phys.* **B884** (2014) 632–671, arXiv:1312.2011 [hep-ph].

[297] **Particle Data Group** Collaboration, J. Beringer *et al.*, "Review of Particle Physics (RPP)," *Phys.Rev.* **D86** (2012) 010001.

[298] **UTfit Collaboration** Collaboration, A. e. a. Bevan, "Marcella Bona, talk at UK Flavor Workshop '13.,".

[299] S. Adler and R. Dashen, "Current Algebras and Applications to Particle Physics," *Benjamin, New York.* (1998) .

[300] M. Drees, R. Godbole, and P. Roy, "Theory and phenomenology of sparticles: An account of four-dimensional N=1 supersymmetry in high energy physics," *Hackensack, USA: World Scientific* (2004) 555 p.

[301] J. S. Hagelin, S. Kelley, and T. Tanaka, "Supersymmetric flavor changing neutral currents: Exact amplitudes and phenomenological analysis," *Nucl.Phys.* **B415** (1994) 293–331.

[302] F. Gabbiani, E. Gabrielli, A. Masiero, and L. Silvestrini, "A Complete analysis of FCNC and CP constraints in general SUSY extensions of the standard model," *Nucl.Phys.* **B477** (1996) 321–352, arXiv:hep-ph/9604387 [hep-ph].

[303] G. F. Giudice, M. Nardecchia, and A. Romanino, "Hierarchical Soft Terms and Flavor Physics," *Nucl.Phys.* **B813** (2009) 156–173, arXiv:0812.3610 [hep-ph].

[304] Y. Nir and N. Seiberg, "Should squarks be degenerate?," *Phys.Lett.* **B309** (1993) 337–343, arXiv:hep-ph/9304307 [hep-ph].

[305] M. Ciuchini, V. Lubicz, L. Conti, A. Vladikas, A. Donini, *et al.*, "Delta M(K) and epsilon(K) in SUSY at the next-to-leading order," *JHEP* **9810** (1998) 008, arXiv:hep-ph/9808328 [hep-ph].

[306] C. Allton, L. Conti, A. Donini, V. Gimenez, L. Giusti, *et al.*, "B parameters for Delta S = 2 supersymmetric operators," *Phys.Lett.* **B453** (1999) 30–39, arXiv:hep-lat/9806016 [hep-lat].

[307] E. Dudas, G. von Gersdorff, S. Pokorski, and R. Ziegler, "Linking Natural Supersymmetry to Flavour Physics," *JHEP* **1401** (2014) 117, arXiv:1308.1090 [hep-ph].

[308] O. Gedalia, J. F. Kamenik, Z. Ligeti, and G. Perez, "On the Universality of CP Violation in Delta F = 1 Processes," *Phys.Lett.* **B714** (2012) 55–61, arXiv:1202.5038 [hep-ph].

[309] I. Galon, G. Perez, and Y. Shadmi, "Non-Degenerate Squarks from Flavored Gauge Mediation," *JHEP* **1309** (2013) 117, arXiv:1306.6631 [hep-ph].

[310] E. Dudas, S. Pokorski, and C. A. Savoy, "Soft scalar masses in supergravity with horizontal U(1)-x gauge symmetry," *Phys.Lett.* **B369** (1996) 255–261, arXiv:hep-ph/9509410 [hep-ph].

[311] Y. Kawamura and T. Kobayashi, "Soft scalar masses in string models with anomalous U(1) symmetry," *Phys.Lett.* **B375** (1996) 141–148, arXiv:hep-ph/9601365 [hep-ph].

[312] E. Dudas, C. Grojean, S. Pokorski, and C. A. Savoy, "Abelian flavor symmetries in supersymmetric models," *Nucl.Phys.* **B481** (1996) 85–108, arXiv:hep-ph/9606383 [hep-ph].

[313] L. E. Ibanez and G. G. Ross, "Fermion masses and mixing angles from gauge symmetries," *Phys.Lett.* **B332** (1994) 100–110, arXiv:hep-ph/9403338 [hep-ph].

[314] P. Binetruy and P. Ramond, "Yukawa textures and anomalies," *Phys.Lett.* **B350** (1995) 49–57, arXiv:hep-ph/9412385 [hep-ph].

[315] P. Binetruy, S. Lavignac, and P. Ramond, "Yukawa textures with an anomalous horizontal Abelian symmetry," *Nucl.Phys.* **B477** (1996) 353–377, arXiv:hep-ph/9601243 [hep-ph].

[316] A. G. Cohen, D. Kaplan, and A. Nelson, "The More minimal supersymmetric standard model," *Phys.Lett.* **B388** (1996) 588–598, arXiv:hep-ph/9607394 [hep-ph].

[317] A. E. Nelson and D. Wright, "Horizontal, anomalous U(1) symmetry for the more minimal supersymmetric standard model," *Phys.Rev.* **D56** (1997) 1598–1604, arXiv:hep-ph/9702359 [hep-ph].

[318] P. Binetruy and E. Dudas, "Gaugino condensation and the anomalous U(1)," *Phys.Lett.* **B389** (1996) 503–509, arXiv:hep-th/9607172 [hep-th].

[319] G. Dvali and A. Pomarol, "Anomalous U(1) as a mediator of supersymmetry breaking," *Phys.Rev.Lett.* **77** (1996) 3728–3731, arXiv:hep-ph/9607383 [hep-ph].

[320] M. Dine, R. G. Leigh, and A. Kagan, "Flavor symmetries and the problem of squark degeneracy," *Phys.Rev.* **D48** (1993) 4269–4274, arXiv:hep-ph/9304299 [hep-ph].

[321] A. Pomarol and D. Tommasini, "Horizontal symmetries for the supersymmetric flavor problem," *Nucl.Phys.* **B466** (1996) 3–24, arXiv:hep-ph/9507462 [hep-ph].

[322] R. Barbieri, G. Dvali, and L. J. Hall, "Predictions from a U(2) flavor symmetry in supersymmetric theories," *Phys.Lett.* **B377** (1996) 76–82, arXiv:hep-ph/9512388 [hep-ph].

[323] R. Barbieri, L. J. Hall, and A. Romanino, "Consequences of a U(2) flavor symmetry," *Phys.Lett.* **B401** (1997) 47–53, arXiv:hep-ph/9702315 [hep-ph].

[324] N. Craig, M. McCullough, and J. Thaler, "The New Flavor of Higgsed Gauge Mediation," *JHEP* **1203** (2012) 049, arXiv:1201.2179 [hep-ph].

[325] N. Craig, M. McCullough, and J. Thaler, "Flavor Mediation Delivers Natural SUSY," *JHEP* **1206** (2012) 046, arXiv:1203.1622 [hep-ph].

[326] F. Brümmer, M. McGarrie, and A. Weiler, "Light third-generation squarks from flavour gauge messengers," *JHEP* **1404** (2014) 078, arXiv:1312.0935 [hep-ph].

[327] C. Bachas, C. Fabre, and T. Yanagida, "Natural gauge coupling unification at the string scale," *Phys.Lett.* **B370** (1996) 49–51, arXiv:hep-th/9510094 [hep-th].

[328] L. E. Ibanez, "Hierarchical Suppression of Radiative Quark and Lepton Masses in Supersymmetric GUTs," *Phys.Lett.* **B117** (1982) 403.

[329] M. Toharia and J. D. Wells, "Gluino decays with heavier scalar superpartners," *JHEP* **0602** (2006) 015, arXiv:hep-ph/0503175 [hep-ph].

[330] J. L. Hewett, B. Lillie, M. Masip, and T. G. Rizzo, "Signatures of long-lived gluinos in split supersymmetry," *JHEP* **0409** (2004) 070, arXiv:hep-ph/0408248 [hep-ph].

[331] P. Gambino, G. Giudice, and P. Slavich, "Gluino decays in split supersymmetry," *Nucl.Phys.* **B726** (2005) 35–52, arXiv:hep-ph/0506214 [hep-ph].

[332] K. Benakli, L. Darmé, M. D. Goodsell, and P. Slavich, "A Fake Split Supersymmetry Model for the 126 GeV Higgs," *JHEP* **1405** (2014) 113, arXiv:1312.5220 [hep-ph].